Identification of novel susceptibility genes for diabetes-related traits in a backcross of obese NZO with lean C3H mice

Inaugural-Dissertation

zur Erlangung des Doktorgrades
der Mathematisch-Naturwissenschaftlichen Fakultät
der Heinrich-Heine-Universität Düsseldorf

vorgelegt von

Tanja Schallschmidt
aus Köln

Düsseldorf, Juni 2018

Aus dem Institut für Klinische Biochemie und Pathobiochemie
des Deutschen Diabetes-Zentrums,
Leibniz-Zentrum für Diabetesforschung
der Heinrich-Heine-Universität Düsseldorf

Gedruckt mit der Genehmigung der
Mathematisch-Naturwissenschaftlichen Fakultät der
Heinrich-Heine-Universität Düsseldorf

Berichterstatter:

1. Prof. Dr. Hadi Al-Hasani

2. Prof. Dr. Michael Feldbrügge

Tag der mündlichen Prüfung: 08.10.2018

Summary

Genetic predisposition plays a key role in the development of metabolic diseases such as type 2 diabetes mellitus (T2DM). Until today, genome-wide association studies (GWAs) and familial linkage analyses in humans led to the identification of more than 100 gene variants potentially associated with the pathogenesis of T2DM. Nevertheless, it is estimated that these variants account only for a maximum of 20 % of the total heritable component of this disease, indicating that there is an obvious need for additional strategies aiming to detect causal genetic determinants. Mouse models share a large part of their genome with humans and thus have become an essential complementary tool for the identification of novel disease genes and signaling pathways. The genetic predisposition to develop obesity and/ or T2DM differs widely between the diverse mouse inbred strains; therefore they bear the potential to discover novel genotype-phenotype correlations.

To identify new susceptibility loci for T2DM, a novel crossbreeding approach of obese and T2DM-susceptible New Zealand Obese (NZO) with lean and T2DM-resistant C3HeB/FeJ mice was conducted in this study. Subsequent whole-genome linkage scan of the N2(NZOxC3H) population revealed a novel quantitative trait locus (QTL) for blood glucose- (12 cM, logarithm of the odds (LOD) 13.3) and plasma insulin levels (17 cM, LOD 4.8) on proximal chromosome 7. This locus was designated as *Cdp7-prox* (C3H diabetes protector on proximal chromosome 7). Already at early stages of age, homozygous *Cdp7-prox*$^{NZO/NZO}$ allele carriers developed hyperglycaemia progressing into severe pancreatic β-cell failure as indicated by the loss of plasma insulin and body weight at later stages of age. By contrast, heterozygous *Cdp7-prox*$^{NZO/C3H}$ allele carriers were widely protected from T2DM. The onset of hyperglycaemia in the risk allele carriers was independent from the body weight, indicating that *Cdp7-prox* acts directly on pancreatic β-cell function. Introgression of the critical C3H fragment into the genetic NZO background by generating recombinant congenic strains (RCS) and metabolic phenotyping validated the phenotype observed in the N2 population. By contrast, introgression of the same C3H fragment into a C57BL/6J genetic background yielded a different phenotype, presumable due to the contribution of additional background-specific modifier genes. By a combined approach of gene expression- and haplotype analysis, the critical QTL region between 27 and 47 Mb including 776 annotated genes was narrowed down to a limited number of candidates. Two candidate genes (*Pop4* and *Atp4a*) were shown to affect glucose-stimulated insulin secretion *in vitro* using cultivated murine β-cells (*MIN6* cells). Another gene, *Nudt19,* was able to inhibit fatty acid β-oxidation in culivated liver (*Hepa 1-6*) cells. The gene *Klk1b22* represents the only candidate gene whose expression was detectable exclusively in one genotype (C3H). In the future, a potential causal relationship of the candidate genes with the *Cdp7-prox* locus will to be determined and the underlying molecular pathways will be functionally analyzed.

Zusammenfassung

Die genetische Prädisposition spielt eine entscheidende Rolle bei der Entstehung von Stoffwechselerkrankungen wie Typ-2-Diabetes mellitus (T2DM). In genomweiten Assoziationsstudien (GWAS) und familiären Kopplungsstudien konnten bis heute bereits mehr als 100 Genvarianten identifiziert werden, die potenziell mit der Pathogenese des T2DM assoziiert sind. Dennoch schätzt man, dass diese Gene nur für maximal 20 % der genetischen Gesamtkomponente der Krankheit verantwortlich sind. Dies zeigt deutlich, dass zusätzliche Strategien für die Identifizierung neuer Risikogene erforderlich sind. Aufgrund der starken Übereinstimmung mit dem menschlichen Genom sind Mausmodelle zu einem wichtigen komplementären Werkzeug für die Identifizierung neuer Krankheitsgene und Signalwege geworden. Die verschiedenen Maus-Inzuchtstämme unterscheiden sich stark in ihrer genetischen Prädiposition für die Entwicklung von Adipositas und/ oder T2DM und eignen sich daher für die Entdeckung neuer Genotyp-Phänotyp Korrelationen.

Mit dem Ziel der Identifizierung neuer Suszeptibilitätsloci für T2DM, wurde im Rahmen dieser Arbeit eine neue Kreuzung zwischen adipösen, T2DM-anfälligen *New Zealand Obese* (NZO)- und schlanken, T2DM-resistenten C3H Mäusen durchgeführt. In der anschließenden genomweiten Kopplungsanalyse der N2(NZOxC3H) Population wurde ein neuartiger QTL (*Quantitative Trait Locus*) für Blutglukose (12 cM; *logarithm of the odds* (LOD) 13,3) und Plasma-Insulin (17 cM; LOD 4,8) auf dem proximalen Bereich des Chromosoms 7 identifiziert. Dieser Genlocus wurde *Cdp7-prox* (*C3H diabetes protector on proximal chromosome 7*) benannt. Bereits im jungen Alter entwickelten die homozygoten *Cdp7-prox*$^{NZO/NZO}$-Allel-Träger eine Hyperglykämie mit fortschreitendem Verlust der pankreatischen β-Zellen, was anhand des niedrigen Plasma-Insulin-Spiegels, sowie dem einsetzenden Gewichtsverlust im späteren Alter deutlich wurde. Im Gegensatz dazu waren die heterozygoten *Cdp7-prox*$^{NZO/C3H}$-Allel-Träger weitgehend vor der Entwicklung eines T2DM geschützt. Die Entstehung der Hyperglykämie in den Risiko-Allel-Trägern war unabhängig vom Körpergewicht, was nahelegt, dass *Cdp7-prox* unmittelbar auf die Funktion der β-Zellen des Pankreas wirkt. Infolge der Introgression des kritschen C3H-Fragments auf einen genetischen NZO-Hintergrund, durch die Erzeugung und metabolische Charakterisierung rekombinant kongener Stämme (RCS), konnte der Phänotyp der N2-Population validiert werden. Im Gegensatz dazu bewirkte die Introgression desselben C3H-Fragments auf einen genetischen C57BL/6J-Hintergrund einen anderen Phänotyp, was vermutlich auf den Einfluss weiterer Hintergrund-spezifischer Modifikationsgene zurückzuführen ist. Mit Hilfe eines kombinierten Ansatzes aus Genexpressions- und Haplotypen-Analyse konnte der kritische QTL-Bereich zwischen 27 und 47 Mb mit 776 annotierten Genen auf eine begrenzte Anzahl von Kandidaten eingegrenzt werden. Für zwei der Kandidatengene (*Pop4* und *Atp4a*) konnte eine Wirkung auf die Glukose-stimulierte Insulinsekretion *in vitro*, mit Hilfe von kultivierten murinen

β-Zellen (*MIN6*), nachgewiesen werden. Für das Gen *Nudt19* konnte ein inhibierender Effekt auf die Fettsäureoxidation in kultivierten Leberzellen (*Hepa 1-6*) gezeigt werden. Das Gen *Klk1b22* stellt das einzige Kandidatengen dar, dessen Expression ausschließlich in einem Genotyp (C3H) nachgewiesen werden konnte. In zukünftigen Analysen soll ein potenzieller kausaler Zusammenhang der Kandidatengene mit dem *Cdp7-prox*-Locus ermittelt, und die zugrunde liegenden molekularen Signalwege funktionell untersucht werden.

Table of Contents

1 Introduction

1.1 Diabetes mellitus

1.1.1 Definition and classification

Diabetes mellitus is a chronic metabolic disorder with rapidly increasing numbers of affected people in the last years. Since 1980, the global prevalence of diabetes has almost quadrupled to nearly half a billion today (International Diabetes Federation, 2017; World Health Organization, 2016). The disease is characterized by a chronically elevated blood glucose level, which triggers the onset of several further complications leading over the time to serious damages of various organs, including the heart, blood vessels, eyes, kidneys, and nerves (World Health Organization, 2016). According to the WHO global report on diabetes from 2016, the disease is today one of the leading causes of death. In 2012, 1.5 million deaths have been reported as the consequence of diabetes. In total, diabetes and its complications are estimated to consume about 12 % of health budgets (International Diabetes Federation, 2015).

In the second report from the WHO in 1980, the disease was firstly classified into different subclasses. Besides Gestational diabetes and several rare types, the predominantly classes are type 1- and type 2 diabetes. Type 1 diabetes mellitus (T1DM), previously also known as insulin-dependent or juvenile-onset diabetes, accounts for 5-10 % of diabetes. The onset of T1DM results from a cellular-mediated autoimmune destruction of the insulin-secreting pancreatic β-cells, which leads to an absolute deficiency of insulin secretion (International Diabetes Federation, 2017; World Health Organization, 2016). For this reason, people with T1DM are dependent on the daily administration of insulin to ensure a balanced glucose homeostasis. Today four different autoantibodies against insulin, glutamic acid decarboxylase (GAD), the protein tyrosine phosphatase IA-2, and/or zinc transporter 8 have been identified that can be detected prior to clinical diagnosis of T1DM (Bonifacio, 2015). However, the underlying mechanisms triggering this destructive immune response are still largely unknown, but a combination of genetic- and environmental factors, such as viral infection, toxins or some dietary factors seem to be involved (You and Henneberg, 2016).

In contrast, type 2 diabetes mellitus (T2DM), previously also named non-insulin-dependent or adult-onset diabetes, occurs as a result of the cell´s ineffective use of insulin. T2DM is the most prevalent form accounting for approximately 90 % of all cases of diabetes worldwide. In addition to more than 400 million individuals worldwide diagnosed with T2DM today, numerous diseases have not been diagnosed. Due to an often asymptomatic development especially in the earliest stages, it is

estimated that up to one half of all cases remain undiagnosed (Beagley et al., 2014; International Diabetes Federation, 2017).

1.1.2 Obesity and the pathophysiology of type 2 diabetes mellitus (T2DM)

Overweight is defined as a body mass index (BMI) (weight in kg / height in m^2) of 25 or more, obesity as a BMI of more than 29.9 kg/m^2 (World Health Organization, 2016). Obesity arises from a genetic predisposition in combination with different environmental factors, including excessive caloric intake, insufficient physical activity, the intrauterine environment, socioeconomic status or medications (Goodarzi, 2017). It is estimated, that obesity accounts for about 90 % to the risk of developing T2DM (Hossain et al., 2007). Due to the close link between obesity and T2DM, the association of both is often summarized with the word “diabesity” (Chadt et al., 2014; Kahn et al., 2006). Besides T2DM, obesity is further strongly associated with the development of hypercholesterinaemia, hyperlipidemia and hypertension. The combination of these complications is referred to as the metabolic syndrome (Kesaniemi et al., 1992). A main cause for the pathophysiology connecting obesity and T2DM is likely the insulin resistance, a state in which the efficiency of glucose uptake into peripheral insulin-sensitive tissues (liver, skeletal muscle and adipose tissue) is reduced. However, only a relatively small fraction of individuals with obesity and insulin resistance develop T2DM (Chadt et al., 2014; Kahn et al., 2006). This is due to the pancreatic islet´s capacity to increase insulin secretion to compensate for the reduced efficiency of insulin action, thus ensuring the maintenance of the glucose homeostasis (Kahn et al., 1993; Polonsky et al., 1988). Moreover, the release of insulin inhibits the output of glucose from the liver into the bloodstream, thereby contributing to balanced blood glucose levels. As a consequence of a progressive insulin secretion to cope for increasing insulin resistance, a combination of different factors, including glucotoxicity, inflammation and ectopic fat storage finally leads to the failure of the pancreatic β-cells. As a result, an absolute deficiency of insulin secretion becomes manifest at final stages of the disease which in turn leads to a dysfunctional uptake of glucose into the peripheral tissues, causing a chronic state of hyperglycaemia (Fig. 1).

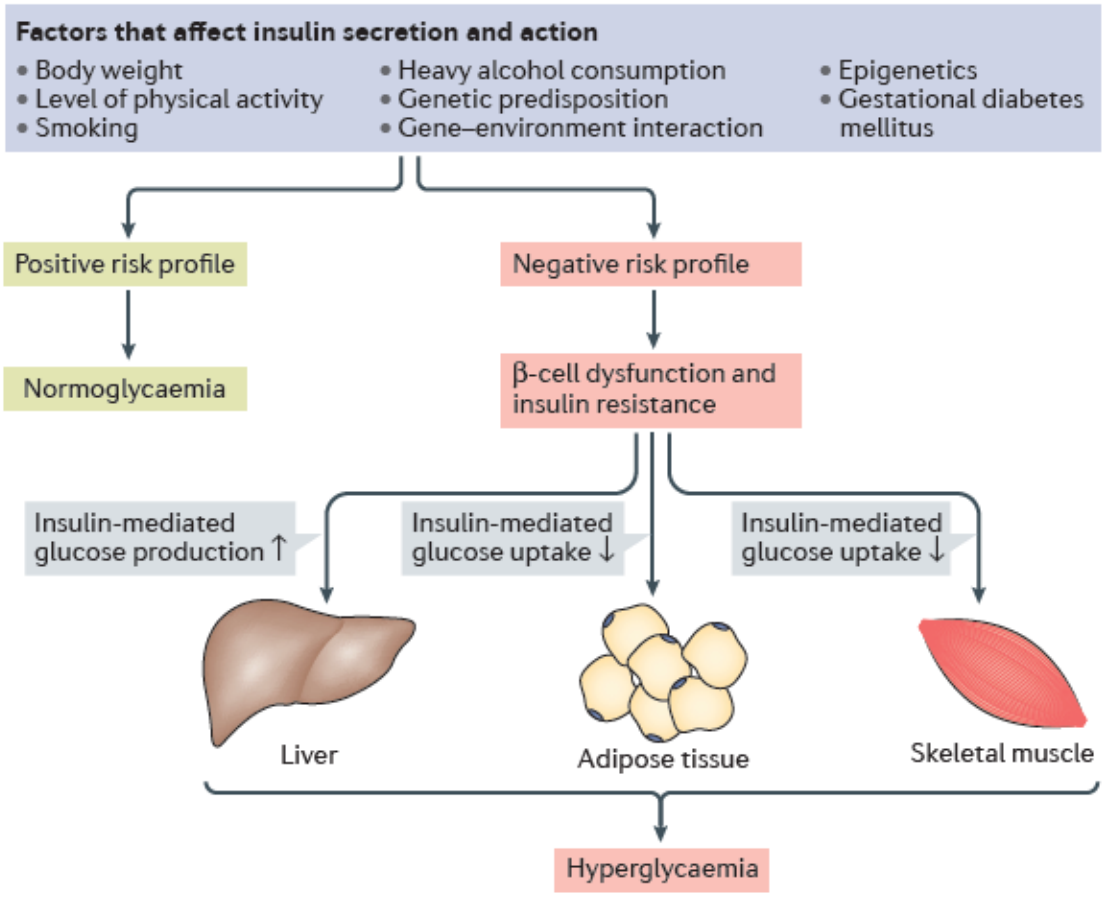

Figure 1: Pathophysiology of T2DM. Different factors, including environmental-, genetic- and epigenetic factors initiate the pathophysiology of the disease. In most individuals, a healthy blood glucose level can be maintained by the action of insulin, which is secreted from the pancreatic β-cells and mediates the uptake of glucose into the skeletal muscle and adipose tissue as well as the inhibition of glucose production from the liver. As a consequence of the failure of the pancreatic β-cells, these processes become gradually impaired leading to the accumulation of circulating glucose in the blood (Zheng et al., 2018).

It is generally accepted that the risk of developing T2DM is mainly due to visceral fat depots, whereas subcutaneous fat depots are contrarily associated with a beneficial impact on metabolism (Fujioka et al., 1987; Hamdy et al., 2006; Krotkiewski et al., 1983; Neeland et al., 2012). However, the molecular mechanisms underlying the progression of obesity into insulin resistance and hyperglycaemia are still not well understood und controversially discussed. In general, three major different hypotheses have been emerged during the last decades (Chadt et al., 2014).

The prevalent “lipid overflow hypothesis” also known as “adipose tissue expandability hypothesis” assumes that the adipose tissue has a limited capacity for expansion to cope with nutritional overload (Unger, 2003a). Once the maximal capacity is reached, the adipose tissue fails to appropriately accommodate lipids leading to the leakage / spillover into other peripheral tissues involved in the metabolic homeostasis, including liver, skeletal muscle and the pancreas (Tan and

Vidal-Puig, 2008; Zwick et al., 2018). Since these organs are not specialized for the storage of larger amounts of fat, the release of lipid metabolites (such as ceramides or secondary messengers (e.g. diacylglycerol)) exerts toxic effects in these tissues leading to disturbed insulin signaling that triggers insulin resistance (Rosen and Spiegelman, 2014; Stinkens et al., 2015). The hypothesis that the expansion ability of the adipose tissue is crucial for the prevention of such lipotoxic effects is supported by several studies on lipodystrophy in human and animal models. Thus, the loss of adipose tissue in these individuals is associated with metabolic complications including T2DM, hypertriglyceridemia and hepatic steatosis, similar features as observed in the metabolic syndrome (Brown and Gorden, 2015; Moitra et al., 1998). The molecular factors determining the adipose tissue´s expansion capacity are not well understood, but the properties of its extracellular matrix and angiogenic capacity have been implicated (Hardy et al., 2012). With the progression of insulin resistance into T2DM, the peripheral organs and the pancreatic islets become exposed to toxic levels of glucose (glucotoxicity) as well as lipids (lipotoxicity). The accumulation of triglycerides in the pancreatic islets is considered as a primary cause for β-cell death (Unger, 2003b). This is attributed to lipotoxicity in the pancreatic islets, including endoplasmic reticulum (ER) stress, impairment in mitochondrial function, the generation of reactive oxygen species (ROS), de novo synthesis of de ceramides, and inadequate autophagy (Sharma and Alonso 2014). The New Zealand Obese (NZO) mouse represents a popular polygenetic model for obesity-driven T2DM in humans (Kluge et al., 2012; Ortlepp et al., 2000). The relatively early onset of obesity and T2DM usually progresses into severe β-cell failure at later stages of the disease (Junger et al., 2002; Lange et al., 2006). In the course of the disease, a progressive loss of glucose transporters (Chankiewitz et al., 2006) and the transcription factor v-maf musculoaponeurotic fibrosarcoma oncogene family, protein A (avian) (MafA) (Jurgens et al., 2007), which activates insulin gene expression, can be observed. Interestingly, upon carbohydrate-free high fat diet these mice develop obesity in combination with insulin resistance; however, they seem to be protected from β-cell destruction and subsequent hyperglycaemia. In contrast, upon carbohydrate and fat rich diet, the disease rapidly progresses into β-cell failure and T2DM in these mice, suggesting that an additive toxicity from an overflow of carbohydrates is required for the onset of hyperglycaemia (Dreja et al., 2010; Kluth et al., 2011).

The second “inflammation hypothesis” proposes that the adipose tissue promotes systemic inflammation by secreting inflammatory adipokines from infiltrated macrophages. This idea is supported by the observation that the amount of macrophages in the adipose tissue correlates positively with the BMI as well as with the adipocytes size, both representing main characteristics of obesity. The cytokines and chemokines produced from the adipose tissue macrophages (such as TNF-α, MCP-1, Il-1. Il-6 or TLR4) activate intracellular pathways that promote the onset of insulin resistance and T2DM (Ouchi et al., 2011; Pereira and Alvarez-Leite, 2014; Thomas and Apovian,

2017). Moreover, these inflammatory signals impair endoplasmic reticulum function and promote JNK (c-Jun N-terminal kinases) activation in insulin-sensitive tissues (Hotamisligil, 2008). Activated JNK, in particular the JNK1 isoform, plays a key role in the inhibition of insulin action by the phosphorylation of the insulin receptor substrate-1.

The third "adipokine hypothesis" is based on the concept that the adipose tissue functions as an endocrine organ which secrets several hormones and molecules involved in metabolism and immunity (Grant and Dixit, 2015). Well studied adipokines include adiponectin, leptin, resistin, tumor necrosis factor α (TNFα) and monocyte chemotactic protein-1 (MCP-1). With the expansion of the adipocytes the levels of released inflammatory markers increases, which promotes the development of insulin resistance and subsequent T2DM (Trayhurn and Wood, 2005). Interestingly, adipocytes express numerous factors that are involved in immunity. In addition to that, adipocytes express several receptors for immune cells, including interleukin 6 (IL-6) receptor, the toll-like receptor (TLR) family, and TNFα receptor, indicating that they are responsive to immunomodulating factors (Schaffler and Scholmerich, 2010).

1.1.3 Criteria and biomarkers for T2DM

T2DM is typically diagnosed by determination of fasting blood glucose-, glycated hemoglobin A1c (HbA1c) levels (Peters et al., 1996), or oral glucose tolerance test (OGTT). Blood glucose levels above 126 mg/dL (7 mmol/L) after an eight hour fasting period and HbA1c concentrations above 6.5 % (48 mmol/mol) are defined as criteria for T2DM (American Diabetes Association, 2018). In the OGTT a standard dose of glucose (usually 75 g) is ingested and the blood glucose concentration is measured two hours afterwards to determine the efficiency of insulin action that mediates the uptake of glucose into the peripheral tissues. By definition, a blood glucose value more than 200 mg/dL (11.1 mmol/L) two hours after the glucose administration is considered as a further criterion for diabetes (American Diabetes Association, 2018).

In addition to the classical methods that serve for the diagnosis of the disease, several further parameters have been proposed to estimate the risk for the development of T2DM prior its onset. In common T2DM, hyperglycaemia occurs as a result of increasing insulin resistance. The hyperinsulinemic euglycemic glucose clamp technique is widely considered as the gold standard method for evaluating insulin resistance (DeFronzo et al., 1979). During this experiment insulin is constantly infused through a peripheral vein, to reach a state of hyperinsulinemia. In parallel, glucose is infused in a variable rate to maintain a stable euglycemic blood glucose level. The glucose infusion rate (GIR) is adjusted by observing the development of blood glucose levels during the whole experiment. Since the GIR is directly dependent on the insulin-mediated glucose uptake by the

peripheral tissues, it represents a measure for the insulin sensitivity. However, this test is expensive and time-consuming and therefore extremely impractical when large scale studies are involved. The insulin tolerance test (ITT) represents an alternative, however less sensitive method to investigate the sensitivity of the insulin receptors in the different metabolic peripheral tissues. The ITT was originally designed to analyze the activity of the hypothalamic–pituitary–adrenal (HPA) axis in response to insulin-induced hypoglycaemia (Plumpton and Besser, 1969) and was subsequently adapted to measure insulin sensitivity in humans (Akinmokun et al., 1992). Similar to the OGTT, this test consists in the measurement of blood glucose levels before and at defined time point(s) after the administration of insulin. Based on the relative drop of blood glucose levels in response to insulin, the insulin sensitivity can be quantified. Further well-established biomarkers for insulin resistance include body composition, insulin, C-peptide (Torn, 2003), HDL-cholesterol (Abu-Qamar and Wilson, 2007), triglycerides (Herder et al., 2011), fetuin-A (Stefan et al., 2008), adiponectin and inflammatory markers (Swellam et al., 2009). Early detection of precursors for T2DM is crucial in order to allow the use strategies that may prevent the onset of the disease, such as dietary changes and increased physical activity (Tuomilehto et al., 2001). In addition, the detection of early alterations in the metabolic homeostasis is beneficial to explore the etiological pathways that trigger the onset of T2DM (Floegel et al., 2013). Metabolites have been proposed as more useful biomarkers than the above described conventional biomarkers, as they reflect end products of metabolic pathways and therefore more rapidly physiological dysfunctions (Adamski, 2016; Roberts et al., 2014). Nowadays advanced high-throughput analytical techniques allow the simultaneous analysis of numerous metabolites. The resulting metabolic profile, which is also referred to as the metabolome, provides a valuable picture of the whole organism's metabolic status (Nicholson and Wilson, 2003). A large number of studies have made use of metabolomics to explore the pathogenesis of T2DM and its related risk factors (Gonzalez-Franquesa et al., 2016; Guasch-Ferre et al., 2016). The most prominent metabolic shifts during the development of obesity and T2DM were observed for the levels of branched-chain amino acids (BCAAs, includes valine, leucine and isoleucine) (Menni et al., 2013; Palmer et al., 2015) and blood acylcarnitines (Mai et al., 2013; Mihalik et al., 2010). A constant activation of the mTOR signaling pathway, which uncouples the insulin receptor from insulin receptor substrate, has been proposed as the underlying mechanism connecting increased BCAAs levels with the development of insulin resistance (Tanti and Jager, 2009). Acylcarnitines are synthesized by the enzyme carnitine palmitoyltransferase 1 (CPT1) which mediates the transport of fatty acids into the mitochondrial matrix (Indiveri et al., 2011). These acylcarnitines are transported across the inner mitochondrial membrane into the mitochondrion, where they are converted back into free carnitine and long-chain acyl-CoAs by the enzyme CTP2. Subsequently, acyl-CoA undergoes fatty acid oxidation (FAO) for the production of ATP in the tricarboxylic acid (TCA) cycle. Deficiencies in the mitochondrial

FAO, which is strongly linked to insulin resistance (Koves et al., 2008), causes elevated levels of acylcarnitines. For this reason, the measurement of acylcarnitine levels can be directly utilized as biomarker for insulin resistance (Ramos-Roman et al., 2012; Schooneman et al., 2013). Moreover, in newborn screenings acylcarnitine levels serve for the detection of genetic metabolic disorders (Lehotay et al., 2011).

1.2 Genetic aspects of T2DM

In 1992, Froguel and colleagues bought the first evidence for genetically-driven T2DM through familial linkage analysis of French pedigrees with early-onset, non-auto-immune, non-obese diabetes that was also called maturity-onset diabetes of the young (MODY) (Froguel et al., 1992). The onset of MODY was shown to result from a mutation in GCK (encoding glucokinase), which is a key regulatory enzyme of insulin secretion in the pancreatic β-cells. The discovery of the GCK mutation further served as the first demonstration that the onset of T2DM was directly caused by relative insulin deficiency without prior development of insulin resistance. The subsequent discovery of 27 further monogenetic gene variants causing neonatal diabetes and/or MODY (Bonnefond and Froguel, 2015) has shed important light on the pathophysiology of the disease, in particular on the role of insulin secretion. However, common T2DM in humans is a complex polygenic disease, which is driven by the interplay of several hundred gene variants and their interaction with the environment. The heritability of T2DM which mainly reflects the heritability of obesity as the main driver of the disease, was evidenced in several twin and family studies. However, estimations on the genetic contribution vary between 25 % and 85 % in different studies (Kaprio et al., 1992; Newman et al., 1987; Poulsen et al., 1999; Poulsen et al., 2005; Schousboe et al., 2003; Willemsen et al., 2015). Individuals with one parent suffering from T2DM have a risk of 40 % to develop T2DM; this risk is increased to 70 % if both parents are affected (Köbberling and Tillil, 1982). First degree relatives of people with T2DM have a 3-fold increased risk for developing the disease compared to individuals without diabetic family members (Florez et al., 2003). Furthermore, the concordance rate in monozygotic twins is estimated with 70 % compared to only 20-30 % in dizygotic twins (Kaprio et al., 1992). However, it has to be mentioned that not all observed familial associations can entirely be attributed to genetic factors, but are most likely further influenced by epigenetic factors, which can generate inherited risk over generations (Van Baak et al., 2018).

The completion of the Human Genome Project (Venter et al., 2001), the International HapMap Project (International HapMap, 2003), advances in high-throughput genotyping technologies and the development of new powerful bioinformatic tools offered new opportunities to search for novel

genetic determinants. The year 2007 bought the first wave of human genome-wide association studies (GWAs), in which phenotypic data from a natural unrelated population are usually correlated with hundreds of thousands of single nucleotide polymorphisms (SNPs) to search for associations. The first GWAs, conducted in a French cohort, led to the discovery of the genes SLC30A8 and HHEX and confirmed the already described association of the TCF7L2 gene with T2DM (Grant et al., 2006; Sladek et al., 2007). Subsequently, several further GWAs were published that confirmed these associations and identified further T2DM-associated genes in Europeans. Most of these studies combined the data from different cohorts to increase the statistical power, a strategy which was later named meta-analysis. The first obesity-susceptibility gene identified by GWAs is FTO, which was detected in three independent studies in 2007 (Frayling et al., 2007; Hinney et al., 2007; Scuteri et al., 2007). Many successive GWAs in non-European cohorts confirmed the association between SNPs in the first intron of FTO with BMI (Fawwad et al., 2016; Keaton et al., 2014; Monda et al., 2013), indicating that FTO has a global impact on obesity. However, the expression of FTO in the adipose tissue did not correlate with the SNPs that were found in the different GWAs (Kloting et al., 2008), leading to the hypothesis that the association with obesity is due to an altered expression of IRX3 (Smemo et al., 2014), a gene which is located directly next to FTO. Until today, the molecular pathway connecting FTO with obesity is not validated. This example reflects the difficulties from many GWAs of connecting SNPs that map in a non-coding region with single genes. Indeed, 80 % of all T2DM-associated SNPs that were found until today map in non-coding regions. For this reason, scientists have selected genes with the closest location to the SNP, without verification of the linkage or any functional evidence (Bonnefond and Froguel, 2015). Until today, GWAs contributed with more than 100 candidate genes for obesity and T2DM (Dorajoo et al., 2015; McCarthy, 2010; Nettleton et al., 2013; Prasad and Groop, 2015; Visscher et al., 2012), thereby providing valuable insights into the genetic basis of T2DM. Nevertheless, with exception of the SNPs that mapped in protein altering variants, such as PPARG6 (Altshuler et al., 2000), KCNJ11-ABCC8 (Gloyn et al., 2003), SLC30A8 (Sladek et al., 2007), and GCKR9 (Dupuis et al., 2010), the underlying mechanism connecting these genes with T2DM remain to be evidenced (Gaulton et al., 2015).

1.3 Mouse models in the research of T2DM

During the last decades animal models, in particular mice that share 99 % of the genome with humans (Peters et al., 2007) have become a popular additional tool for the identification of candidate genes for T2DM and their related pathways (Kleinert et al., 2018). Mice are the most widely used animal models to study metabolic disorders (European Commission, 2013). This can in large parts be attributed to the availability of numerous well-established molecular genetic tools that

allow the engineering of mutations, from single nucleotide- to full chromosomal exchanges (Kleinert et al., 2018). In contrast to humans, all kinds of tissues can be relatively easily collected for the analysis of gene expression or functional assays. In addition to standardized methods, researchers can nowadays profit from free-available genome and phenome databases that have been developed over the last decades and are continuously improved. Moreover, the ability to control the environment and short generation times in combination with large litter sizes represent further advantages that emphasize the utility of mouse models over human studies.

Inbred mouse strains, which are generated by brother-sister breeding to produce identical genomes, are nowadays commonly used in the research for different human diseases. Most of these inbred strains originated from one of the four subspecies of the house mouse (*Mus musculus*) that diverged approximately one million years ago: the *domesticus* subspecies (developed in Western Europe), the *musculus* subspecies (developed in Eastern Europe, Russia, and Northern China, the *castaneus* subspecies (developed in Southeast Asia and Southern China) and the *molossinus* subspecies, which is a hybrid of the *castaneus* and *musculus* subspecies from Japan. An intensive haplotype analysis based on the use of SNPs validated that most of nowadays used inbred strains have derived from a limited number of founders, primarily of the *domesticus* and *musculus* subspecies (Wade et al., 2002). More than 100 years ago, inbred strains were originally bred and selected for 'fancy' characteristics like extraordinary coat color or neurological features. The observation that some of these features resembled symptoms of human diseases led to the idea of using these strains for the research of human diseases. The Jackson Laboratory, which harbors more than 2000 different inbred strains today, was founded by Clarence Cook Little in 1929 (Paigen, 2003). The different inbred strains differ in their susceptibility towards obesity and T2DM and their response to environmental factors like diet, thereby providing genetic diversity similar to the human population. Moreover, most of the underlying gene variants for the different phenotypes of these strains have not been identified so far (Clee and Attie, 2007), making them to valuable resources for the discovery of new disease genes. Until today, many spontaneous mutations have occurred and preserved as valuable mouse models. Prominent examples represent the discoveries of the genes for leptin and its receptor. A spontaneous mutation in the gene which codes for the leptin hormone led to overt obesity in *ob/ob* mice, whereas a mutation in the leptin receptor caused diabetes in *db/db* mice (Chua et al., 1996; Coleman, 1978; Ingalls et al., 1950). The *fat* mutation in the gene *carboxypeptidase E* (*Cpe*), the *tubby* mutation, and the ectopic expression induced by the *yellow* (*y*) allele of the *agouti* (*Ay*) gene are further examples for spontaneous mutations associated with development of obesity and severe insulin resistance (Bultman et al., 1992; Coleman and Eicher, 1990; Naggert et al., 1995; Noben-Trauth et al., 1996). Furthermore, numerous inbred strains are available, in which the development of T2DM is not due to a single gene mutation, but similar as in

humans the result of a complex interplay of hundreds of genes. Popular examples for polygenetic-driven T2DM represent the two strains New Zealand Obese (NZO) and TALLYHO which both mimic the metabolic characteristics of the human disease, indicating that the underlying molecular mechanisms are similar as in humans.

1.3.1 New Zealand obese mouse (NZO)

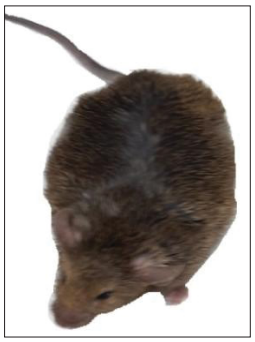

Figure 2: New Zealand Obese Mouse

The Zealand Obese strain (NZO) was brought to New Zealand from an outbred stock of the Imperial Cancer Research Fund Laboratories in London. Along with the two strains New Zealand Black (NZB) and New Zealand White (NZW) the strain was initially selected by Dr. Franz Bielschowsky for agouti coat colour. After then generations of breeding, the mice started to develop obesity and were subsequently bred separately as NZO mice (Bielschowsky and Bielschowsky, 1953; Bielschowsky and Goodall, 1970; Haskell et al., 2002). Nowadays, the NZO strain is frequently used in research as a model for spontaneous polygenetic obesity and T2DM. Both genders develop impaired glucose tolerance and obesity, however, subsequent T2DM progressing into pancreatic islet failure is limited to the males, whereas the females benefit from the protective influence of the hormone estrogen (Lubura et al., 2015; Vogel et al., 2013). In response to high fat diet (HFD) consumption male NZO mice develop all features of the metabolic syndrome, including hyperglycaemia, hyperinsulinemia, hypercholesterinaemia, hyperlipidemia, and hypertension leading to the destruction of the β-cells at final stages of the disease (Joost, 2010; Joost and Schurmann, 2014; Jurgens et al., 2007; Jurgens et al., 2006; Kluth et al., 2011). Usually, the first symptoms of obesity and hyperglycaemia can be observed already within the first weeks of life, indicating a strong genetic predisposition (Veroni et al., 1991). Therefore, NZO mice have been utilized in several studies as a polygenetic model for obesity-driven T2DM in humans (Andrikopoulos et al., 2016; Chadt et al., 2008; Giesen et al., 2003; Kluge et al., 2000; Kluth et al., 2015; Leiter et al., 1998; Plum et al., 2000; Reifsnyder et al., 2000; Reifsnyder and Leiter, 2002; Scherneck et al., 2009; Taylor et al., 2001; Vogel et al., 2009). Almost on each chromosome of this strain associations with obesity and T2DM could already be detected (Reifsnyder et al., 2000). However, only for some of these associations the underlying genes could have been identified, indicating that the NZO genome bears many further diabetes-promoting (or protective) gene variants that still need to be identified. Interestingly, a mutation in the leptin receptor could be found, which however seems not to be play a major role for the onset of T2DM as the related diabetes-resistant NZB strain shares this mutation. In addition, genome-wide association studies with this strain could not discover linkage with T2DM-related traits in this region so far (Kluge et al., 2000; Plum et al., 2000). However, it is possible that the mutation

contributes to the observed leptin resistance and the progression of T2DM through the interaction with further genes (Igel et al., 1997; Kluge et al., 2000).

1.3.2 C3HeB/FeJ mouse

Figure 3: C3HeB/FeJ mouse
(www.jax.org)

In 1920, the C3H parent strain was developed by LC Strong for mammary tumour studies from the cross of a Bagg albino female with a DBA male (Heston and Vlahakis, 1971). The high incidence of tumours observed in the C3H strain was caused by an exogenous mouse mammary tumor virus (MMTV) transmitted through the mother's milk (Outzen et al., 1985). The C3H/HeJ substrain that has arisen from the progenitor strain was passed to Jackson Laboratories in 1947 (Lyon et al., 1996). One year later, Feketein developed the C3HeB/FeJ strain (Fig. 3) by transferring fertilized C3H/HeJ ova to C57BL/6 foster mothers. Today, four different C3H substrains (C3H/HeJ, C3H/HeOuJ, C3HeB/FeJ and C3H/HeSnJ) that are now free of exogenous MMTV are available at the Jackson Laboratory. Even though the C3HeB/FeJ strain shares the same genetic background with the more widely used C3H/HeJ strain, some mutations have become differentially fixed in the two substrains. The probably most prominent one is the mutation of the lipopolysaccharide response locus (in the toll-like receptor 4 gene, *Tlr4*^{lps}). This mutation confers an endotoxin resistance in C3H/HeJ mice, whereas C3HeB/FeJ mice with the normal variant are endotoxin sensitive (Poltorak et al., 1998).

In contrast to NZO and other obese mouse models, C3H mice are lean and relatively resistant towards the development of hyperglycaemia. However, compared to C57BL/6J mice and other lean inbred strains they show mild features of the metabolic syndrome, as they exhibit relatively high body fat content in combination with high plasma glucose, cholesterol, and triglyceride levels (Champy et al., 2008). On the other hand, as seen during a glucose tolerance test both C3H/FeJ and C3H/HeJ mice are more glucose tolerant compared to C57BL/6J mice which seems to be due to their capacity to increase insulin secretion (Champy et al., 2008; Kaku et al., 1988; Kayo et al., 2000; Toye et al., 2005). Moreover, C3H/HeJ mice were shown to be protected from the β-cell toxic effects of streptozotocin, possibly as the result of a single gene mutation (Kaku et al., 1989; Rossini et al., 1977). Morphological analysis of the C3H/HeJ pancreas revealed an increased β-cell mass, derived from relatively few islets of large size compared to the C57BL/6J pancreas (Bock et al., 2005). A genome-wide linkage analysis in an intercrosss population generated from the breeding of C57BL/6 and with C3H/HeJ mice revealed associations with improved glucose tolerance on chromosomes 2 and 13 (Kayo et al., 2000). In contrast to that, another linkage analysis in an intercross population generated from the breeding of BKS.Cg-m+/+Lepr(db) and C3H/HeJ, revealed a C3H allele on chromosome 13 associated with impaired glucose tolerance (Moritani et al., 2006).

1.3.3 C57BL/6J mouse

Figure 4: C57BL/6J mouse (www.jax.org)

The C57BL/6J strain (Fig. 4) was generated by Little in 1921 from a cross of females no. 57 with males no. 52 from Lathrop's stock. The C57BL/6J strain is the most widely used inbred strain serving as reference in diabetes- and other disease studies. It is the most often used background strain for congenics and the generation of mutations. From all inbred strains, the genome from C57BL/6J was the first one that has been sequenced. Compared to mouse models of overt T2DM, such as NZO and TALLYHO, the strain is largely protected from β-cell failure and T2DM. However, in response to a HFD the males are susceptible for the development of obesity in combination with glucose intolerance, hyperinsulinemia, and islet hypertrophy, whereas the females seem to be protected from these HFD-induced metabolic changes (Pettersson et al., 2012). The Jackson Laboratory provides phenotyping data from C57BL/6J males fed a 60 % HFD (Diet-Induced Obesity (DIO) C57BL/6J Mice) compared to C57BL/6J males on normal standard-diet (The Jackson Laboratory, 2018b). These data demonstrate the development of obesity, mild hyperglycaemia, hyperinsulinemia, glucose intolerance together with increases in HDL cholesterol and triglyceride levels in C57BL/6J mice in response to the diet. The scientific literature provides several further studies showing a susceptibility to diet-induced obesity and hyperglycaemia in this mouse strain compared with other lean inbred strains (Collins et al., 2004; Rebuffe-Scrive et al., 1993; Surwit et al., 1995; Surwit et al., 1988). Surwit and his colleagues showed a 50 % -increase in fasting blood glucose and a more than 10-fold increase in plasma insulin levels in C57BL/6J mice fed a fat- and carbohydrate enriched diet. In contrast to that, A/J mice used in the same study showed only marginal changes in blood glucose levels and only a 2.6-fold increase of plasma insulin levels in response to the same diet (Surwit et al., 1995). Upon chow-diet, C57BL/6J mice were shown to be least glucose tolerant compared to C3H and several other lean inbred strains (Champy et al., 2008; Kaku et al., 1989) which seems to be due to deficiencies in the insulin secretion (Ahren and Pacini, 2002). Toye and colleagues showed that islets from C57BL/6J failed to respond to intermediate glucose levels (10 mM), due to an incomplete closure of K_{ATP} channels (Toye et al., 2005). Investigations on the pancreatic architecture revealed a relatively low islet- and β-cell mass (Bock et al., 2005), which could contribute to the relatively high sensitivity to the β-cell toxic effects of streptozotocin in C57BL/6J mice compared to C3H and other strains (Cardinal et al., 1998; Kaku et al., 1989).

1.4 Identification of novel susceptibility genes for obesity and T2DM

1.4.1 Quantitative trait locus (QTL) analysis and positional cloning

Most traits affecting human diseases, including T2DM (e.g. body weight, blood glucose, and plasma insulin levels) are quantitative in nature. In addition to the influence from environmental- and epigenetic factors, these so called quantitative traits are strongly regulated by the interaction of many genomic regions, referred to as quantitative trait loci (QTL). The identification of such a QTL is the first step of positional cloning, a strategy which allows the localization of a disease gene based on the knowledge of its approximate chromosomal location (Brockmann and Neuschl, 2012) (Fig. 5).

In mouse genetics, the detection of a QTL is initiated by the crossbreeding of two mouse strains that differ in the phenotype of interest. The offspring from this cross (F1) are then crossed either to one of the parental strains to generate a backcross (N2)-, or to each other to produce an intercross (F2) population. As a result of genetic recombination events, each mouse from the N2- or F2 population inherits a unique combination of parental alleles. However, there are important differences between the two populations. When a heterozygous F1 animal is crossed with one homozygous parental strain, the offspring can be either homozygous for the parental genotype or heterozygous (50 % probability for each genotype). For this reason, only dominant acting genes can be detected in a N2 population. In contrast to that, when F1 mice are crossed to each other, the offspring can have all three genotypes: heterozygous (50 % probability), homozygous for one parental allele or homozygous for the other parental allele (each 25 % probability). The generation of a F2 generation has a higher degree of power if the aim of the research consists in the receipt of a “general picture”, meaning the number of QTLs segregating and estimates on their additive and dominant effects. On the other hand, if the aim consists in the detection of dominant acting QTL, a N2 is more useful as it requires only about half of the animals of an F2 population (Darvasi, 1998). Usually, a few hundred N2- or F2 mice are generated to increase the statistical power for the subsequent *in silico* linkage analysis, in which phenotypic data are correlated with genetic markers (nowadays mostly informative single nucleotide polymorphisms (SNPs)) spread over the whole genome (Lander and Kruglyak, 1995; Lander and Botstein, 1989). The genetic linkage analysis is based on the observation that genes that reside physically close on a chromosome remain linked during meiosis. The typical unit used to calculate genetic linkage is centimorgan (cM), whereupon 1 cM corresponds to 1 % recombination frequency. The recombination frequency ranges from 0 % for genes being perfectly linked to 50 % corresponding to genes being perfectly unlinked (Griffiths et al., 2000). In the QTL analysis the recombination frequency between a QTL and the genetic markers is estimated at each position in the genome. The linkage of a QTL with a genetic marker implies that individuals with another genotype for this marker have different mean values of the quantitative trait. The LOD (logarithm of the odds)

score is used as a statistical measure for the genotype-phenotype correlation. Usually, appropriate computer programs are able to calculate a significance threshold for the LOD-score to evaluate the significance of a QTL.

The genomic regions that are revealed in the linkage analysis are usually relatively large containing, depending on the density of the region, several hundred genes. Furthermore, the linkage analysis does not provide any hints on the target tissue or the molecular function, for this reason the identification of causal genes requires additional strategies. A conventional strategy is the introgression of the QTL into the genomic background of a reference strain, usually with contrary phenotype, with the help of recombinant congenic strains (RCS). The replication of the phenotype in another genomic background serves as the ultimate evidence for the linkage. Furthermore, by the generation of sublines that carry different fragment sizes of the QTL, the candidate region can be narrowed down. In addition, RCS can be used for a deeper phenotyping of the QTL, thereby providing a relevant picture of the cellular and the molecular function of the causal gene. The integration of additional strategies, including gene expression- and sequence studies, allow the identification of strain-specific gene variants as potential candidates for the QTL (Brockmann and Neuschl, 2012).

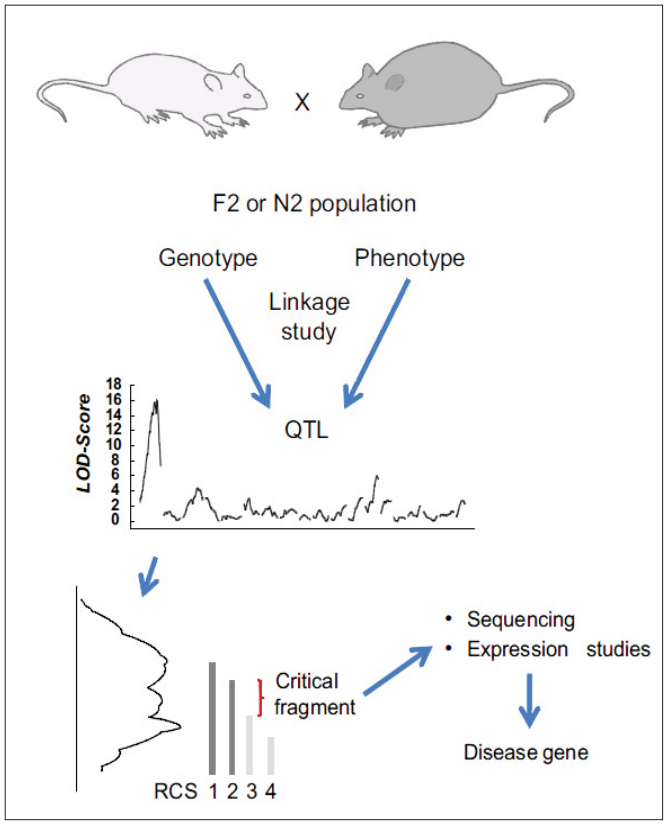

Figure 5: Strategy of positional cloning for the identification of novel candidate genes for obesity and T2DM. Quantitative trait locus (QTL) analysis is initiated by the crossbreeding of two strains differing in the phenotype of interest. The subsequent linkage analysis results in the detection of potential QTLs by *in silico* phenotype-genotype correlation. The introgression of the QTL into a reference strain by the use of recombinant congenic mouse strains (RCS) allows a deeper characterization and enables narrowing down the critical region. Gene expression- and sequencing studies can be used for the identification of candidate genes (Schwenk et al., 2013). LOD= logarithm of the odds

By positional cloning, several diabetes key modifier genes could have been successfully identified. A backcross population generated from the breeding of obese NZO with lean SJL (Swiss Jim Lambert) mice exhibited linkage with diet-induced obesity on chromosome 5 (*Nob1*) (Kluge et al., 2000). Subsequent generation of recombinant congenic strains carrying the critical region on a C57BL/6J reference background in combination with gene expression- and sequence analyses finally resulted in the detection of *Tbc1d1* as the causal gene for the QTL (Chadt et al., 2008). The Sequence analysis discovered a deletion in the variant from SJL, which led to a loss-of-function of the protein. This mutation protected the animals from fat gain by mediating a metabolic shift from glucose to fat oxidation (Chadt et al., 2008; Dokas et al., 2013). In addition to that, another research group independently confirmed the role of *Tbcd1* in human insulin action (Dash et al., 2009). Furthermore, in the same outcross population a major QTL for blood glucose (*Nidd/SJL*) could be detected on chromosome 4 (Plum et al., 2000). With the help of similar strategies, *Zfp69* was found as the causal

gene variant (Scherneck et al., 2009), being involved in the regulation of lipid distribution between different organs, more specifically leading to an excessive fat accumulation in the liver (Chung et al., 2015; Scherneck et al., 2009). In accordance with these findings, the human orthologue of *Zfp69* (ZNF642) was shown to be upregulated in human adipose tissue of type 2 diabetic subjects. Another prominent example for successful disease gene identification by positional cloning represents the discovery of *Ifi202b*, a member of the Ifi200 family of interferon inducible transcriptional modulators (Vogel et al., 2012). The discovery was initiated by the generation of a F2 population from the cross of obese NZO with lean C57BL/6J mice resulting in the detection of *Nob3*, a major QTL for obesity and hyperglycaemia on chromosome 1 (Vogel et al., 2009). An extensive gene expression profiling of the critical region exposed an expression deficiency of *Ifi202b* in C57BL/6J mice, resulting from a sequence deletion. The mutation was shown to cause obesity and insulin resistance by inducing the expression of adipogenic genes, such as *11β-Hsd1* (Vogel et al., 2017; Vogel et al., 2012).

Numerous further diabetes modifier genes could have been identified in murine outcross populations using comparable approaches (Andrikopoulos et al., 2016; Bhatnagar et al., 2011; Clee et al., 2006; Dokmanovic-Chouinard et al., 2008; Joost and Schurmann, 2014; Kebede and Attie, 2014; Wang et al., 2012).

1.4.2 Candidate gene approaches after QTL discovery

Since 1990, more than 2300 QTLs for different traits were detected in murine outcross populations generated from different inbred strains (The Jackson Laboratory, 2018a) but only for about 1 % the causal genes could have been identified (Flint et al., 2005). The main reason why most of the QTL studies failed to proceed to the molecular characterization was attributed to the small effects sizes of most of the identified QTLs (Flint et al., 2005; Lynch and Walsh, 1992). Even for QTLs with large effect sizes, the identification of the causative genes only based on the imprecise knowledge of their chromosomal position remains highly challenging. For this reason, in particular during the last decade a lot of afford was put on the development and improvement of new resources, making gene discovery more tractable for researchers.

1.4.2.1 Recombinant congenic strains (RCS)

Recombinant congenic strains (RCS) represent a powerful tool to narrow down the candidate region of a QTL and for the functional characterization of the locus. A RCS is a mouse line that harbours a genetic region from another strain. It is generated by repeated backcrossing of mice selected for the chromosomal region of interest with the desired reference strain (Demant and Hart, 1986). In theory, with each backcross the percentage of the reference genome is increased by 50 % (75 % after one, 87.5 % after two, 93.75 % after three backcrosses and so on). For this reason, several backcrosses are

necessary to produce a genetic background that is identical to the genome of reference strain with the only difference in the region of interest (Groot et al., 1992). The use of an approach called “speed congenics” can substantially accelerate this process. This approach includes the genome-wide genotyping of the potential breeding animals with the help of molecular markers (e.g. SNPs) to determine the real genomic background from the reference strain. Subsequently, mice with maximal genomic background can be selected, thereby reducing the number of required backcrosses (Markel et al., 1997). RCS breeding typically starts with the introgression of the QTL together with the full chromosome into a reference strain, resulting in a recombinant consomic strain. A major advantage of the use of RCS is that the background genomic variance can be substantially reduced; consequently phenotypic differences between the genotypes can be reliably attributed to the region of interest as the only difference in the genome. Provided that the phenotype observed in the initial N2- or F2 population can be replicated, congenic and consomic mice serve as ultimate evidence for the linkage. In addition, depending on the effect size of the QTL, a relatively low number of animals are sufficient to recover the phenotype. This allows the execution of extensive and time-consuming experiments that can help with the identification of the target tissue and the molecular function of the causative gene(s). Subsequently, RCS with smaller fragments of the chromosome are generated to narrow down the candidate region based on the recovery of the phenotype. As a result, the candidate region can be reduced to little megabase pairs including only a handful of genes (Brockmann and Neuschl, 2012; Darvasi, 1997).

1.4.2.2 Gene expression profiling

Gene expression profiling of the candidate regions is another useful approach helping with the identification of the causative genes. Advances in high-throughput expression technologies, such as genome-wide microarrays, allow a fast identification of genes that are differentially regulated in tissues of the parental mouse strains or RCS. This approach is based on the assumption that the observed phenotypic distinctions are reflected by differences in the mRNA abundance of the causative gene(s). Numerous QTL studies have made use of this approach leading to the identification of the causative genes (Andrikopoulos et al., 2016; Chadt et al., 2008; Dokmanovic-Chouinard et al., 2008; Scherneck et al., 2009; Vogel et al., 2012).

An expanded form of expression profiling represents the expression QTL (eQTL) analysis, in which mRNA transcript abundances are used as phenotypic traits and mapped to the genome in a linkage analysis (Solberg Woods, 2014). By eQTL analysis, the genomic regulators of the mRNA expression from candidate genes can be identified (Rockman and Kruglyak, 2006). In this approach the choice of the tissue is of fundamental importance since many genes show tissue specific alterations (Petretto et al., 2006). Expression QTLs are typically distinguished into two categories. The majority of eQTLs

are *cis*-acting, meaning that they map to the location of their coding gene. On the other hand, eQTLs that do not co-localize with their coding gene but map to a region far away (for instance on another chromosome) are referred to as *trans*-acting eQTLs. The detection of *trans*-eQTLs that do not reside within an identified physiological QTL can be used as a mean to exclude candidate genes for a physiological QTL, thereby narrowing down the number of candidate (Bao et al., 2007; Hubner et al., 2005; Schadt et al., 2003). On the other hand, *cis*-eQTLs that co-localize with a physiological QTL share a genetic origin with the physiological QTL, therefore they present plausible candidates. In addition, the mRNA transcript levels can be investigated for potential correlations with the physiological traits and tested for causality (Schadt et al., 2005). Indeed, the co-localization of an eQTL with the physiological QTL, accompomied by correlation between the expression- and phenotypic data, suggests strong evidence for a potential connection between both traits (Doss et al., 2005). With the help of this strategy, several causal genes could have been successfully identified in murine and human studies (Chen et al., 2008; Doss et al., 2005; Parker et al., 2016; Tsaih et al., 2014; Tu et al., 2012; Yang et al., 2009).

1.4.2.3 Haplotype analysis

Another useful strategy for the identification of candidate genes is the haplotype analysis of the parental inbred strains (Browning and Browning, 2011b). This approach makes use of the observation that phenotypic distinctions that are typically mapped in the QTL analysis are almost exclusively due to loci inherited from different ancestral progenitors rather than new mutations (Frazer et al., 2004). Haplotypes are genomic regions in an organism containing polymorphisms that are dependently inherited from one parent. Since haplotypes are likely to be inherited in a cluster of alleles for many generations, these regions are less susceptible for recombination and thus mutations compared to other regions in the genome. Nowadays, the availability of the genomic sequence from many inbred strains allows the comparative analysis of haplotype patterns between different mouse strains. By the use of a dense SNP panel or other genetic markers these patterns can be matched to determine regions that are identical by descent (IBDs, genomic regions that are identical between individuals due to descent from a common ancestor without recombination). Based on the hypothesis that IBD regions are unlikely to contain mutations and are therefore unlikely to cause phenotypic variations (Browning and Browning, 2011b; Grupe et al., 2001; Wiltshire et al., 2003), many QTL studies have successfully used this approach to identify candidate genes in regions that genetically differ between the used inbred strains (Liu et al., 2007; Manenti et al., 2004; Park et al., 2003; Vogel et al, 2018; Wang et al., 2004).

In general, it is useful to combine the different candidate gene approaches to reduce the number of candidates, thereby substantially facilitating and accelerating the process of gene discovery (Flint et al., 2005; Liu et al., 2007). However, none of the above presented approaches is sufficient for the functional evidence of a gene. Therefore, final steps of gene discovery require appropriate cell models for the knockdown or overexpression of a candidate genes followed by functional *in vitro* assays (Abiola et al., 2003). Finally, mice genetically modified for the gene of interest are necessary for the ultimate proof of the function *in vivo*. In addition to that, studies that show a similar role of the human variant are desirable to underscore its relevance in the human disease.

1.5 Aim of the study

Despite the immense progress from the last decade in the development of novel high-throughput genotyping technologies, the emerging and improvement of genome- and phenome databases, in combination with advancement in novel bioinformatic tools to assist the data analysis, the current knowledge on genetic factors account only for about 15- 20 % of the total heritable component of the disease (Morris et al., 2012; Schwenk et al., 2013; Tsaih et al., 2014). The overall aim of this study consisted in the identification of further, yet unknown candidate genes for obesity- and T2DM, with the help of mouse genetic approaches. Hence, the first aim of this work was the detection of novel quantitative trait loci (QTLs) in a backcross population generated from the crossbreeding between obese NZO with lean C3HeB/FeJ mice. For this purpose, an *in silico* linkage analysis was conducted by correlating the collected metabolic data from the backcross population to a genome-wide panel of informative SNP markers. This analysis exhibited the most significant association with blood glucose levels and plasma insulin on proximal chromosome 7, this locus was named *Cdp7-prox* (C3H diabetes protector on proximal chromosome 7). As a consequence, the second aim of this project consisted in the identification of potential causative genes for *Cdp7-prox*. For this purpose, different approaches, including the generation of recombinant congenic strains (RCS), gene expression profiling, and haplotype-analysis were used.

2. Material and Methods

2.1 Material

2.1.1 Mouse strains

Table 1: **Mouse strains**

Mouse strain	Supplier
NZO/Hl	Lieselotte Herberg (Herberg and Coleman, 1977), DDZ Düsseldorf
C3HeB/FeJ	Helmholtz Center Munich
C57BL/6J	Charles River Laboratories, Sulzfeld, Germany

2.1.2 Mouse diets

Table 2: Mouse diets

Diet	Supplier	Protein (gm %/ kcal %)	Carbohydrate (gm %/ kcal %)	Fat (gm %/ kcal %)
Standard diet (#V1126 M-Z Extrudat)	ssniff, Soest, Germany	22.1 /36.0	53.3 / 53	4.4 / 11.0
High-fat diet with 45 % calories from fat (#D12451)	Research Diets Inc., New Brunswick, NJ, USA	24.0 / 20.0	41.0 / 35.0	24.0 / 45.0
High-fat diet with 60 % calories from fat (#D12492)	Research Diets Inc., New Brunswick, NJ, USA	26.2 /20.0	26.3 / 20.0	34.9 / 60.0

2.1.3 Murine cell lines

Table 3: Cell lines

Cell line	Origin
MIN6	Murine pancreatic β-cell line originated from a transgenic C57BL/6 mouse insulinoma (Miyazaki et al., 1990). Cells were provided by Prof. Dr. Baltrusch (University of Rostock)
Hepa 1-6	Murine liver cell line originated from a C57BL/6J tumor (BW7756) (Darlington et al., 1980). Cells were provided by Prof. Dr. Belgardt (DDZ Düsseldorf) / Prof Dr. Lammert (University of Düsseldorf)

2.1.4 siRNA- and plasmid-DNA oligonucleotides

Table 4: siRNA oligonucleotides. For each target, a pool of four single siRNAs (SMART pool, provided from Dharmacon) was used.

Target Gene	Sequence 5`→ 3`	Ordering number/ product name (Dharmacon)
Atp4a	#1 CCUGCGUGAUCAAUGGUAU #2 CUAACAUCUUCAACUUCAU #3 GUCUCAUCUAUGGUUUGAC #4 CCAUGAACUUUCCGAGUAG	E-046922-00-0005, Accell Mouse Atp4a (11944) siRNA SMART pool
Fxyd3	#1 CUUUCUACUAUGAUUGGUA #2 UUAUAGUCCUUAUGAGUGG #3 CUCAUUUGUGCAGGGAUUC #4 GCAGGCUCUUUGUUCAGUU	E-042089-00-005, Accell Mouse Fxyd3 (17178) siRNA SMART pool
Hspb6	#1 CCAUCAGUCCCCAAUAAAU #2 CUGCCAUUCUCUAAGGUCA #3 CUUGUAACCUGUGUAGAAU #4 CUUUCAGACUUAAAACUCC	E-058255-00-0005, Accell Mouse Hspb6 (243912) siRNA SMART pool
Nudt19	#1 CUUUUAACUUCUGAUGGCA #2 CUCUGCUCUGUAUAGAUUU #3 CCUGUGUCAUGUGUGUUUU #4 GCAAAGUCCUUAACCGAGU	E-040466-00-0005, Accell Mouse Nudt19 (110959) siRNA SMART pool
Pop4	#1 GCCGUGAUCUUGGAAUAUU #2 CCAUAGAAAUUGAUGACUU #3 GGAUUAACCUUGGGUCAUC #4 CUAUUAUUUCAGUCACGAA	E-062084-00-0005, Accell Mouse Pop4 (66161) siRNA SMART pool
Zfp420	#1 CGAAUAGACUUUAAUCAUC #2 GCAUUAUCAUUAAGAAAUC #3 CUGUGAUAUAGAAGGUCUU #4 UCUGCAAGCCUGUUGAUUU	E-055191-00-0005, Accell Mouse Zfp420 (233058) siRNA SMART pool
Non-target (used for transfection of Hepa 1-6 cells)	UAGCGACUAAACACAUCAAUU	D-001210-01, siGENOME Non-Targeting Control siRNAs

For the electroporation of MIN6 cells, the AllStars Negative Control siRNA (#1022076) from Qiagen was used, whose sequence is confidential.

Table 5: Plasmid-DNA

Plasmid name	Supplier
pEGFP-N1	CLONTECH (# 6085-1)
Nudt19 Mouse Tagged ORF Clone	Origene (# MR224694)
pcDNA3-FLAG-Klk1b22	Designed in the own working group

2.1.5 Synthetical oligonucleotides and TaqMan probes

Primer sequences were designed with the help of the online Primer-Blast tool from NCBI (Tab. 14) and synthesized by Eurogentec (Seraing, Belgium). Before use, the stock solution was diluted 1:10 in nuclease free water (final concentration: 10 nM). Fwd: Forward, Rev: Reverse, bp= base pairs

Table 6: qPCR primer

Primer	Sequence (5'→3')	Product length (bp)	Exon-Exon span (bp)
2200002J24Rik	Fwd: CCCCAGCGAAGGATTACCTC Rev: GCTTCCCGGGTCTTAAGGG	100	321/322
Actb	Fwd: CCACCATGTACCCAGGCATT Rev: AGGGTGTAAAACGCAGCTCA	253	1093/1094
Atp4a	Fwd: GGTTAATAGGAAGGATGCCCG Rev: CAGTCGCTGACAACTCTCCA	120	2045/2046
B230322F03Rik	Fwd: GTCAGGGTCATTCTCGCCC Rev: CCTATACAGGCAACAGGCCA		
Cox7a1	Fwd: TCTTCCAGGCCGACAATGAC Rev: GCCCAGCCCAAGCAGTATAA	127	247/248
Fxyd3	Fwd: ACAGAAACCCAGTCACCGCC Rev: AGTTCAAGCCCACCTTCAGAG	123	77/78
Gpi1	Fwd: GTACATCACCAAGTCCGGGG Rev: ATCATCTTGGTGCCTTGGTGG	120	1272/ 1273
Hamp	Fwd: ACATTGCGATACCAATGCAGAAG Rev: AGGATGTGGCTCTAGGCTATG	129	193/194
Hamp2	Fwd: AGCCACCACACAAGTCCTTA Rev: AGTCTGTCTCATCTGTTGCTGG	145	136/137
Hspb6	Fwd: CTCTTTGACCAGCGTTTCGG Rev: CATCCAGCAGCACGGAAAAA	157	231/232
Kcnk6	Fwd: TGCTTGTCACAGCGTACCTC Rev: GATCGGGCAGCAAGATGAGT	114	757/758
Klk1b22	Fwd: GCCTCCTGAGTCTCCCTTACA Rev: TGTGTCCATCAAGCTCCATCC	127	653/654
Klk1b4	Fwd: CGATGTGCAGGAGCTGGGAA Rev: TGTCAAAGAGCCGCATGTCT	218	255/256
Nudt19	Fwd: CTACCAGTGGTTGTCCCCAT Rev: TGATGGGCGATCCGAACAAA	148	775/776
Pop4	Fwd: CGATGTGCAGGAGCTGGGAA Rev: TGTCAAAGAGCCGCATGTCT	218	255/256
Rhpn2	Fwd: CACCTCAGTTCACCCTGGAC Rev: GGTTTGTGGCGACCTTCAGA	234	291/292
Spint2	Fwd: AGACGTCCACGAGAACACCA Rev: GGCCTTCGGGACACAGTATT	145	466/467
Tbp	Fwd: GCGGCACTGCCCATTTATTT Rev: GGCGGAATGTATCTGGCACA	236	
Tmem147	Fwd: TGTCATGGAGACCTTCGTCC Rev: GGTTCGCCAACACCTGAGAT	159	665/666
Tyrobp	Fwd: GTGGGAGGATTAAGTCCCGTA Rev: ACAATCCCAGCCAGTACACC	92	112/113
Zfp30	Fwd: GGTGGAGCCGAGATCTGGAA Rev: CCAAAAGGGAGTCTTCGGGG	135	423/424
Zfp420	Fwd: TCACGAGAGGGTTGTGTCTGG Rev: ACATCCCTGATTTCTCAAACTTCC	169	127/128
Zfp715	Fwd: TGTCAAAGAGCCGCATGTCT Rev: TCGAGTGTTACTTCGCTGGC	140	672/673
Zfp940	Fwd: GGAAGCCAGTTAGAAGCCGT Rev: GAGCCCGAGAAAGATTGGGA	128	152/153

The expression of the gene *Actn4* was analysed by TaqMan® Gene Expression Assay (ID: Mm00502489_m1, Thermo Fisher Scientific, Darmstadt, Germany)

2.1.6 SNP maker

All SNP markers (KASP by design assay mix) for genotyping were purchased from LGC genomics (LGC group, Teddington, United Kingdom). The full list of all used SNP markers is shown in the supplement (Suppl. Tab. 10-12).

2.1.7 Reaction kits

2.1.7.1 Reaction kits for molecular biological analysis

Table 7: Kits for molecular biological analysis

Kit	Application	Supplier
GoScript® Reverse Transcription System	cDNA synthesis	Promega, Madison, USA
GoTaq® qPCR Master Mix	qPCR	Promega, Madison, USA
Invisorb® Genomic DNA Kit II	DNA isolation	STRATEC Molecular GmbH, Berlin, Germany
KASP V4.0 2X Master mix, high Rox	Genotying	LGC group, Teddington, United Kingdom
RNAse free DNAse Set	RNA isolation	QIAGEN, Hilden, Germany
RNeasy Mini Kit	RNA isolation	QIAGEN, Hilden, Germany
TaqMan™ Gene Expression Master Mix	qPCR	Thermo Fisher Scientific, Darmstadt, Germany

2.1.7.2 Reaction kits for biochemical analysis

Table 8: Kits for biochemical analysis

Kit	Application	Supplier
Cholesterol Liquicolor kit	Plasma cholesterol determination	Human Diagnostics, Wiesbaden, Germany
Glucose Liquicolor kit	Plasma- and tissue glycogen determination	Human Diagnostics, Wiesbaden, Germany
Insulin ELISA (Mouse)	Insulin determination from pancreas and MIN6 cells	DRG, Marburg, Germany

Kit	Application	Supplier
Insulin ELISA Ultrasensitive (Mouse)	Plasma insulin determination	DRG, Marburg, Germany
Mouse C-Peptide ELISA Kit	Plasma C-peptide determination	CrystalChem, Chicago, USA
NEFA standard	Plasma free fatty acid determination	Wako Chemicals, Neuss, Germany
NEFA-HR (2) R1 set	Plasma free fatty acid determination	Wako Chemicals, Neuss, Germany
NEFA-HR (2) R2 set	Plasma free fatty acid determination	Wako Chemicals, Neuss, Germany
Pierce™ BCA Protein Assay kit	Total protein determination	Thermo Fisher Scientific, Darmstadt, Germany
Triglycerides (TRIGS) GPO-PAP kit	Plasma- and tissue triglyceride determination	RANDOX Laboratories Ltd. (Ardmore, UK)

For the electroporation of the MIN6 cells, the SF Cell Line 4D-Nucleofector® Kit (Lonza, Cologne, Germany) was used.

2.1.8 Cell media, buffer and solutions

Table 9: Cell culture media, buffers and solutions

Name	Ingredients / Supplier
Acid ethanol	0.18 M HCl in 75 % ethanol
Anticoagulant	25 mL 0.5 M EDTA, 92 mg aprotinin dissolved in 21 mL saline (0.15 M), 4 mL heparin (10.000 U/mL), 21.6 mg diprotin A
Dulbecco's Modified Eagle Medium (DMEM), high glucose and low glucose	Thermo Fisher Scientific, Darmstadt, Germany
CMRL medium without L-glutamine and HEPES	Thermo Fisher Scientific, Darmstadt, Germany
Dulbecco's Phosphate Buffered Saline (DPBS)	Thermo Fisher Scientific, Darmstadt, Germany
Fetal bovine serum	Biochrom, Berlin, Germany
Hepa 1-6 cultivation medium	10 % heat-inactivated FBS, 1 % penicillin / streptomycin, 1.12 % 1M HEPES, 1 % GlutaMAX, 1 % 100 mM sodiumpyruvate, 0.35 % 50 mM β-Mercaptoethanol in DMEM (high glucose)
KRH (Krebs-Ringer-HEPES) buffer	15 mM HEPES, 5 mM KCl, 120 mM NaCl, 24 mM $NaHCO_3$, 1 mM $MgCl_2$, 2 mM $CaCl_2$, add before use: 1 mg/mL BSA

Name	Ingredients / Supplier
Lysis buffer	20 mM Tris, 150 mM NaCl, 1 mM EDTA, 1 mM EGTA, 1% Triton X-100
Opti-MEM I Reduced Serum Medium	Thermo Fisher Scientific, Darmstadt, Germany
Pancreatic islet medium	15 % FBS, 0.1 % 50 mM β-Mercaptoethanol, 1 % penicillin/streptomycin, 0.5 % 1.11 M glucose, 2 % $NaHCO_3$ solution (7.5 %) in CMRL medium without L-glutamine and HEPES
Radioactive FAO buffer	47 µM ^{14}C-palmitic acid, 56.2 µM fatty acid free BSA, 9 µM L-Carnitine
Sodium acetate buffer	0.12 M Sodium acetate solved in distilled H_2O, pH 4.8
Trypsin-EDTA solution	Sigma-Aldrich, Steinheim, Germany
Penicillin/ Streptomycin	Thermo Fisher Scientific, Darmstadt, Germany

2.1.9 Chemicals

Table 10: Chemicals

Chemical / Solution	Supplier
Acetic acid (min. 99.8 %)	Kmf Laborchemie, Lohmar, Germany
Chloroform (pure)	AppliChem, Darmstadt, Germany
Deoxynucleoside triphosphates (dNTPs)	Promega, Madison, USA
D-Glucose ($C_6H_{12}O_6$)	Sigma-Aldrich, Steinheim, Germany
Dimethylsulfoxide (DMSO)	AppliChem, Darmstadt, Germany
EDTA	Roth, Karlsruhe, Germany
Ethanol (absolute, pure)	AppliChem, Darmstadt, Germany
FCCP	Sigma Aldrich, Steinheim, Germany
Hexanucleotide primer	Roche, Mannheim, Germany
Histopaque-1077	Sigma Aldrich, Steinheim, Germany
Hydrochloric acid (HCl) (37 %)	Roth, Karlsruhe, Germany
Insulin Actrapid® HM Penfill®	Novo Nordisk Pharma GmbH, Mainz, Germany
Isoflurane	Piramal Healthcare, Morpeth, UK

Chemical / Solution	Supplier
Isopentane	Merck, Darmstadt, Germany
Isopropanol (≥ 99. 5 %)	AppliChem, Darmstadt, Germany
Liberase TL Research Grade	Roche, Mannheim, Germany
Lipofectamine 2000	Thermo Fisher Scientific, Darmstadt, Germany
Lipofectamine RNAimax	Thermo Fisher Scientific, Darmstadt, Germany
^{14}C-palmitic acid	Perkin Elmer (Waltham, USA)
Methanol (≥99.9 %)	Carl Roth, Karlsruhe, Germany
Potassium hydroxide (KOH)	Merck, Darmstadt, Germany
QIAzol® reagent	QIAGEN, Hilden, Germany
Random primer	Roche Diagnostics, Mannheim, Germany
Rotiszint® eco plu	Roth, Karlsruhe, Germany
Sodium chloride (NaCl)	Roth, Karlsruhe, Germany
Sodium sulfate (Na_2SO_4)	Merck, Darmstadt, Germany
TRIzol® reagent	Thermo Fisher Scientific, Darmstadt, Germany

2.1.10 Disposables

Table 11: Disposables

Material	Supplier
Cellstar® Multiwell Platten	Oehmen, Essen, Germany
Combitips advanced®	Eppendorf, Hamburg, Germany
CRYO tubes 1.8 mL	Thermo Fisher Scientific, Darmstadt, Germany
Disposable scalpels # 12 +22	BBraun, Melsungen, Germany
Glucose test stripes Contour Next	Bayer HealthCare, Leverkusen, Germany
MaXtract High Density	QIAGEN, Hilden, Germany
MicroAmp® Fast Optical 96-well reaction plates	Applied Biosystems, Foster City, USA
MicroAmp® Optical adhesive film	Applied Biosystems, Foster City, USA
Microvette CB 300 µL Lithium-Heparin	Sarstedt, Nümbrecht, Germany
PCR-Plates (FrameStar® 384-Well)	4titude, Berlin, Germany

Material	Supplier
Plastic Petri dish 10 cm	Greiner Bio One, Kremsmünster, Austria
QIAshreder	QIAGEN, Hilden, Germany
Rotilabo microtest plates (96 well)	Carl Roth, Karlsruhe, Germany
Rotilabo®-aluminium foils	Carl Roth, Karlsruhe, Germany
Scintillation bottles with cup, 20 mL	Ratiolab, Dreieich, Germany
Scintillation vials 5 mL	Carl Roth, Karlsruhe, Germany
Stainless steel beads (5 mm)	Qiagen, Hilden, Germany
Sterican® needle G24x1" / ø 0,55 x 25 mm	BBraun, Melsungen, Germany
Sterican® needle G26x1" / ø 0,45 x 25 mm	BBraun, Melsungen, Germany
Syringe Omnifix® 1 mL	BBraun, Melsungen, Germany
Tissue culture flask 75 + 150 cm^3	Oehmen, Essen, Germany
Tissue culture test plates 6, 12, 48-wells	Oehmen, Essen, Germany
Whatman cellulose chromathography paper	Sigma Aldrich, Steinheim, Germany
Whatman Protein Saver 903™ Cards	GE Healthcare Bio-Sciences Corp., Chalfont St Giles, UK

2.1.11 Equipment

Table 12: Equipment

Device / Instrument	Supplier
4D-Nucleofector™ System	Lonza, Cologne, Germany
Agilent 2100 Bioanalyzer	Agilent Technologies, Waldbronn, Germany
Cell dissociation sieve	Sigma Aldrich, Steinheim, Germany
Centrifuge GPKR	Beckman Coulter, Krefeld, Germany
Centrifuge Megafuge 1.0	Heraeus, Hanau, Germany
Compact centrifuge SPROUT™	Biozym Scientific, Hessisch Oldendorf, Germany
Concentrator 5301 (Vacuum centrifuge)	Eppendorf, Wesseling-Berzdorf, Germany
Cooling table centrifuge 5425 R	Eppendorf, Hamburg, Germany
Electronic scale	Sartorius, Göttingen, Germany

Device / Instrument	Supplier
FeedTime	TSE-Systems, Bad Homburg, Germany
HERAcell 240i CO_2 Incubator	Thermo Fisher Scientific, Darmstadt, Germany
IKA® Vortex 4 basic	IKA®-Werke, Staufen, Germany
iMark™ Microplate reader	Bio-Rad, Munich, Germany
Infinite® 200 PRO Series Multimode Reader	Tecan Trading AG, Männedorf, Switzerland
LS 600LL Liquid Scintillation Counter	Beckman Coulter, Krefeld, Germany
Mastercycler	Eppendorf, Hamburg, Germany
Motic microscope AE2000	VWR International, Langenfeld, Germany
Multipipette® E3	Eppendorf, Hamburg, Germany
NanoDrop 2000	Thermo Fisher Scientific, Darmstadt, Germany
Neubauer chamber improved assistent	VWR International, Langenfeld, Germany
NMR	EchoMRI, Houston, USA
Overhead Shaker REAX 2	Heidolph Instruments, Schwabach, Germany
PCR Plate Spinner	VWR, Radnor, USA
QuantStudio 7 Flex	Applied Biosystems, Foster City, USA
Shaking waterbath	Köttermann, Uetze/Hänigsen, Germany
Speed Vac	Eppendorf, Hamburg, Germany
StepOnePlus™ System	Applied Biosystems, Foster City, USA
Stereomicroscope SMZ1500	Nikon Instruments, Amsterdam, Netherlands
Thermomixer ® comfort	Eppendorf, Hamburg, Germany
TissueLyser II	Qiagen, Hilden, Germany
Uniprep-Gyrator	UniEquip, Planegg, Germany
Vortex Genie 2	Scientific Industries, New York, USA
Water-jet vacuum pump	Ditabis, Pforzheim, Germany

2.1.12 Software

Table 13: Software

Software	Application	Supplier
4D v16.1	Animal documentation	4D SAS
Endnote X7	Literature research	Thomson Reuters
Excel 2010	Statistical analysis	Microsoft Office
GraphPad Prism 5 and 7	Statistical analysis	Graph Pad
Quantstudio Real-Time PCR Software	qPCR analysis	Applied Biosystems, Foster City, USA
R version i386 3.3.2	QTL analysis	R Development Core Team
StepOne software v2.3	qPCR / genotyping analysis	Applied Biosystems, Foster City, USA

2.1.13 Online Databases

Table 14: Online Databases

Database	Application	Online link
NCBI GenBank, PubMed	Literature research	https://www.ncbi.nlm.nih.gov/pubmed
NCBI GenBank, Primer-Blast	Primer design	https://www.ncbi.nlm.nih.gov/tools/primer-blast
PrimerBank	Primer design	https://pga.mgh.harvard.edu/primerbank/
Sanger SNP-Datenbank	Haplotype analysis	https://www.sanger.ac.uk/sanger/Mouse_SnpViewer

2.2 Methods

2.2.1 Animal experiments

2.2.1.1 Breeding strategy

2.2.1.1.1 Generation of the N2(NZOxC3H) population

NZO/Hl females were bred with C3HeB/FeJ males for the generation of the F1 generation. Subsequently, males from the F1 generation were backcrossed with female NZO mice to produce the N2(NZOxC3H) generation (Fig. 10). In total, 329 males and 310 females were generated.

2.2.1.1.2 Generation of the RCS NZO.C3H-*Cdp7*con and B6.C3H-*Cdp7*con

To generate RCS carrying full chromosome 7 on a genetic NZO or C57BL/6J background, respectively, a N2 generation was generated as described above (2.2.1.1.1). Subsequently, three/ four further backcrosses between males carrying heterozygous alleles for chromosome 7 (NZO.C3H-*Cdp7*con$^{NZO/C3H}$ and B6.C3H-*Cdp7*con$^{B6/C3H}$) with NZO or C57BL/6J females respectively, were performed to generate a N5/ N6 generation (Fig. 20A+B). The percentage of the genomic background from the reference strains (NZO and C57BL/6J) was determined in the N2 and N3 generation. For this purpose, a genome-wide panel of informative SNP marker (107 for NZO.C3H-*Cdp7*con and 101 for B6.C3H-*Cdp7*con) with a distance of 10-30 Mb between each marker was used. In NZO.C3H-*Cdp7*con mice, a genomic NZO background of 82.5 % in the N2, and 91.5 % in the N3 generation was determined. In B6.C3H-*Cdp7*con mice, a 77 % genomic B6 background was calculated in the N2-, and 87 % in the N3 generation (Fig. 20C). In order to produce homozygous C3H alleles on chromosome 7, intercrosses (brother-sister mating) were conducted in the N5 and N6 generation of NZO.C3H-*Cdp7*con-, and in the N6 generation of B6.C3H-*Cdp7*con mice. Homozygous N5F1 and N6F1 siblings with identical genotype were again intercrossed, resulting in the generation of homozygous offspring (N5F2-N5F3 and N6F2), which were phenotyped.

2.2.1.2 General animal maintenance

All experiments were in accordance with the National Institutes of Health guidelines for the care and use of laboratory animals and were approved by the Ethics Committee of the State Ministry of Agriculture, Nutrition and Forestry (State of North Rhine-Westphalia, Germany). All mice were housed at two to six mice per cage (Macrolon type III) at a constant temperature of 22 °C and a 12-h light-dark cycle (lights on at 6 a.m.). Animals had free access to food and water *ad libitum*. At 3 weeks of age, the animals were separated from their breeding cages and experimental mice were subsequently fed at high-fat diet (HFD). The parental strains, the N2(NZOxC3H) population and

RCS.NZO.C3H-*Cdp7*con mice received a diet with 45 kcal % from fat, whereas RCS.B6.C3H.*Cdp7*con mice received a diet with 60 kcal % from fat (Tab. 2).

2.2.1.3 Metabolic characterization

2.2.1.3.1 Determination of body weight and body composition

The body weight was determined with an electronic scale (Tab. 12) and the body composition was analysed with a nuclear magnetic resonance (NMR) spectrometer (Tab. 12).

2.2.1.3.2 Determination of BMI

For the determination of the BMI, the final body length was measured during isoflurane-anesthesia using millimeter paper before sacrificing of the mice. Subsequently, the BMI was calculated by dividing the weight (in g) by the height (in cm^2) of the mouse.

2.2.1.3.3 Determination of blood glucose levels and T2DM-prevalence

For the determination of blood glucose levels, the tail tip was pricked with a sterile scalpel (Tab. 11) and one droplet of blood was placed on a glucose test strip (Tab. 11). The T2DM-prevalence was determined by the percentage of diabetic animals (blood glucose > 300 mg/dL at least three times in a row).

2.2.1.3.4 Fasting/ refeeding

For the measurement of blood parameters (blood glucose, plasma insulin, NEFA and triglycerides) at fasted state, the mice were fasted for 16 hours overnight. Next morning, the tail tip was cut with a sterile scalpel to measure fasting blood glucose levels and tail blood was collected in lithium and heparin coated tubes (Tab. 11). Subsequently, the tubes were centrifuged at 9391 x g for 5 min and 4 °C and the plasma was transferred into new reaction tubes. To measure the same parameters at refed state, food was given to the cages. After two hours of refeeding, blood glucose levels were measured and further blood samples were collected in two different vials for each mouse (each approx. 40 µL). For the analysis of insulin levels one tube was centrifuged at 9391 x g for 5 min and 4 °C, whereas the other tube for the analysis of FFA and triglycerides was centrifuged for 5 min and 4 °C at lower speed (2348 x g) to avoid the separation of the fat from the plasma. The plasma was stored at -80 °C until further processing.

2.2.1.3.5 Metabolomic profile

For the generation of a metabolic profile the tail tip from 10-weeks-old N2 mice was cut with a sterile scalpel and whole blood was dropped (Ø 3 mm) on whatman filter paper (Tab. 11). The filter papers were dried for at least three hours and stored at -80 °C until the analysis. Subsequently, the concentrations of the different metabolites were analysed by liquidchromatography-tandem mass spectrometry (LC-MS/MS) (Burkhardt et al., 2015) by Prof. Dr. Ute Ceglarek and colleagues at the University Hospital of Leipzig.

2.2.1.3.6 Intraperitoneal glucose tolerance test (i.p. GTT)

According the same principle as in humans, for the intraperitoneal glucose tolerance test (i.p. GTT) the mice were injected with a high dose of glucose (2g/ kg) to test the efficiency of insulin action. Prior the injection, the animals were fasted overnight for 16- (RCS.NZO.C3H-*Cdp7*con) or six hours (RCS.B6.C3H-*Cdp7*con). Subsequently, the tail tip was cut with a sterile scalpel for the measurement of basal blood glucose levels (0 min). Furthermore, tail blood was collected in lithium and heparin coated tubes (Tab. 11) for the measurement of insulin levels. After glucose injection, further blood samples were collected after 15, 30, 60, 120 and 240 min for the measurement of blood glucose- and plasma insulin levels. The tubes were centrifuged at for 5 min 9391 x g and 4 °C and the plasma was stored at -80 °C until the measurement of insulin levels (2.2.4.1).

2.2.1.3.7 Intraperitoneal insulin tolerance test (i.p. ITT)

The intraperitoneal insulin tolerance test (i.p. ITT) was used to evaluate the insulin sensitivity of the mice. For this purpose, RCS.NZO.C3H-*Cdp7*con animals were fasted overnight for six hours, whereas RCS.B6.C3H-*Cdp7*con mice were not fasted before the test. Blood glucose levels were measured before (0 min) and at 15, 30, and 60 min after the injection of insulin (1 Unit/ kg body weight).

2.2.1.3.8 Sacrificing and tissue harvest

All mice were fasted overnight for six hours before they were sacrificed for the collection of the blood and tissues. Before sacrificing, fasting blood glucose levels were measured for all mice. In addition, the body length was measured during isoflurane-anesthesia for all N2 mice for the determination of the BMI (2.2.1.3.2). During isoflurane-anesthesia, parental- and N2 mice were sacrificed by cardiac puncture by the use of EDTA-coated syringes. The blood was transferred into a 1.5 mL reaction tube and was then centrifuged for 10 min at 9391 x g and 4 °C. RCS mice were euthanized by decapitation and the blood was collected in a 2 mL reaction tube prepared with 75 µL of anticoagulant (Tab. 9), followed by centrifugation for 10 min at 4000 g and 4 °C. All plasma samples and tissues, which were immediately frozen in liquid nitrogen, were stored at -80 °C until

further processing. For future immunohistochemically studies, the hind limb muscles TA (*Tibialis anterior*), EDL (*Extensor digitorum longus*) and *Soleus* from all N2 mice were snap-frozen in 2-methylbutane at -160 °C to minimize freezing artefacts. For this purpose, a custom-made copper cylinder was placed in a Dewar filled with liquid nitrogen and covered with 2-methylbutane. The muscles were frozen in 2-methylbutane and subsequently transferred into cold cryotubes, followed by their storage at -80°C.

2.2.1.3.9 Pancreatic islet isolation

Prior the isolation of the pancreatic islets the mice were fasted overnight for six hours. After decapitation, the abdomen was opened and the *papilla duodeni* major was blocked with a bulldog clamp. For the perfusion of the pancreas, 3 mL of diluted collagenase (0.18 mg/ mL DMEM) (Tab. 10) was injected into the *ductus choledochus*. After dissection, the inflated pancreas was stored on ice in a 50 mL falcon until it was shaked at 37 °C in a waterbath for 18 min to activate the collagenase. Afterwards, the falcon was filled with DMEM containing 15 % FCS to stop the reaction. After shaking by hand, the pancreas was centrifuged (900 rcf for 3 min at RT) and the pellet was resuspended in 10 mL DMEM. Subsequently, the suspension was passed throw a tissue sieve (mesh size: 380 µm) into a new falcon tube. After another centrifugation step (900 rcf for 3 min at RT) the pellet was resuspended in 10 mL Histopaque-1077 (Tab. 10) and covered with 13 mL of DMEM. After a centrifugation of 25 min at 1200 rcf (brake deactivated), two phases appeared which were subsequently transferred into a new falcon tube. After filling the tube with DMEM and another centrifugation step (900 rcf for 3 min at RT), the pellet was resuspended in 10 mL islet medium (Tab. 9) and transferred to a 10 cm disposable petri dish. Finally, the islets were checked under the microscope and picked to a new petri dish with 10 mL islet medium (Tab 9). Until the lysis in TRIzol® reagent at the next day for subsequent RNA isolation (2.2.2.4), the islets were cultivated at 37 °C and 5 % CO_2.

2.2.2 Molecular biological methods

2.2.2.1 DNA isolation from mouse tail tips

After weaning, the tail tip (~2 mm) from each mouse was cut and transferred to a reaction tube for subsequent DNA isolation prior genotyping. For this purpose, the Invisorb® Genomic DNA Kit II (Tab. 7) was used according to the manufacturer`s instructions. The DNA concentration was determined photometrically (2.2.2.6).

2.2.2.2 Genotyping by Kompetitive Allele Specific PCR (KASP)

All mice were genotyped using the KASP (Kompetitive Allele Specific PCR) technique developed by the company LGC Genomics (LGC group, Teddington, United Kingdom). The N2(NZOxC3H) animals were genotyped within the company by the use of 115 informative SNPs selected in a distance of 10-30 Mb on each chromosome (Suppl. Tab. 10). Genotyping of the RCS was executed in-house by the use of KASP assays (Suppl. Tab. 11+12) and KASP master mix (Tab. 7) purchased from LGC Genomics according to manufacturer's manual.

The KASP technique is based on a universal FRET (fluorescence resonant energy transfer) cassette reporter system which allows an accurate bi-allelic discrimination of the analysed SNPs. One of the cassettes is labeled with FAM™ dye (520 nm emission) and the other with HEX™ (556 nm emission) or VIC™ dye (554 nm emission). Two genotype specific primers (one for each of the SNP alleles) are used, each of them carrying a unique tail sequence that corresponds to one of the two FRET cassettes. During the PCR the two primers compete for the binding with the template DNA, but only one of the primers carries the correct corresponding base to the SNP and is therefore able to bind. Subsequently, its tail is incorporated into the PCR product, resulting in the generation of a complementary sequence which is able to bind to the corresponding FRET cassette. Consequently, the cassette becomes unquenched allowing it to emit fluorescence. As the reaction continues, the fluorescence increases. At the end of the PCR, the fluorescent signal can be read and translated to a genotype. If the animal is homozygous for one SNP marker, only one fluorescence signal (either from the FAM™ or the HEX™/VIC™ dye) can be detected. By contrast, if the animal is heterozygous both of the primers bind resulting in the generation of a mixed fluorescence signals.

The following components were added to each reaction 96-well:

Table 15: Pipetting scheme for the KASP

Reagent	Volume [µL/well]
DNA (5 ng/µL)	5
2x KASP Master mix (High Rox)	5
KASP Assay Mix (Primer)	0.14
Total volume	10.14

The amplification was conducted under the following conditions using the StepOnePlus™-PCR System:

Table 16: Thermocycler settings for the KASP

Step	Temperature	Time	Number of cycles
Hot-start activation	94 °C	15 min	1 x
Touchdown	94 °C	20 sec	10 x
	61-55 °C	60 sec	
	(dropping 0.6 °C per cycle)		
Amplification	94 °C	20 sec	26 x
	55 °C	60 sec	
Read stage	30 °C	60 sec	1 x

2.2.2.3 RNA isolation from mouse liver and quadriceps muscle

For RNA preparation, approx. 30 mg of pulverized liver- and quadriceps was homogenized in 500 µl of TRIzol® reagent (Tab. 10) together with a stainless steel bead (Tab. 11) with the help of the TissueLyser II (5 min at 25 Hz) (Tab. 12). After incubation for 5 min at RT the homogenates were centrifuged for 10 min at 12,000 x g and 4 °C and the supernatant was transferred into a new reaction tube. Afterwards, 100 µL of chloroform was added to each sample, followed by inversion for approx. 15 sec and subsequent incubation for 2-3 min at RT. In the next centrifugation step (4 °C and 12,000 x g for 15 min) the RNA was separated from the phenol-chloroform phase into an upper aqueous phase, which was then carefully transferred into a new reaction tube. Afterwards, 250 µL of 100 % Isopropanol was added followed by incubation for 10 min at RT. The RNA was precipitated by centrifugation for 10 min at 12,000 x g and 4 °C. The supernatant was carefully discarded and the RNA pellet was washed in 500 µL of ethanol (75 % v/v) (5 min centrifugation at 7500 x g and 4 °C). Afterwards, the open tube was incubated for 30 min at RT in order to dry the pellet. Finally, the pellet was resuspended in RNAse-free water (100 µL for liver and 30 µL for quadriceps muscle) and then incubated for 5 min at 55 °C in a heating block (300 rpm) to completely dissolve the RNA pellet. The RNA concentration was measured photometrically (2.2.2.6) and all samples were stored at -80°C.

2.2.2.4 RNA isolation from mouse fat tissue and isolated pancreatic islets

For RNA preparation from fat (approx. 100 mg gWAT and BAT) and isolated pancreatic islets (approx. 100 islets), 500 µL of QIAzol® reagent (Tab. 10) and a stainless steel bead were added to the samples, followed by homogenization in the TissueLyser II (5 min at 25 Hz). After 5 min incubation at RT the homogenate was transferred to a QiaShredder-column (Tab. 11) and centrifuged for 2 min at 18,407x g. The flow-through was transferred to MaXtract-tubes (Tab. 11) together with 100 µL of

chloroform. After inversion for 15 sec and subsequent incubation (2-3 min) at room temperate, the tubes were centrifuged for 15 min at 12,000 x g and 4 °C. Afterwards, the RNA-containing aqueous phase was transferred to a new reaction tube and 300 µL of ethanol (100 %) was added. After mixing by pipetting up and down, the mixture was transferred to columns, which are included in the miRNeasy Mini Kit (Tab. 7). Subsequently, the RNA was isolated using further components from the miRNeasy Mini Kit according to the manufacturer`s instructions. The concentration of the RNA was measured photometrically (2.2.2.6) and the samples were frozen at -80 °C.

2.2.2.5 RNA isolation from cultivated cells

To isolate RNA from cultivated cells (MIN6 and Hepa 1-6), cells were washed with PBS, before TRIzol® reagent (Tab. 10) was added. After detaching by pipetting several times up and down, the cells were transferred in a total volume of 500 µL into a new reaction tube and 100 µL of chloroform was added. After inversion (15 sec) and a short incubation (2-3 min) at RT, the tubes were centrifuged for 15 minutes at 12,000 x g and 4 °C and the aqueous phase was transferred to new reaction tubes. Afterwards, 250 µL of 100 % Isopropanol was added followed by incubation for 10 min at RT. The precipitation of the RNA was achieved by centrifugation for 10 min at 12,000 x g and 4°C. The RNA pellet was washed twice in 500 µL of ethanol (75 % v/v) (5 min centrifugation at 7500 x g and 4°C) and the open tube was incubated for 30 min at RT to dry the pellet. An additional incubation step of the open tubes in the heating block (5 min, 55 °C, 300 rmp) was included to ensure a proper drying of the pellet. Finally, the pellet was resuspended in 20 µL RNAse-free water, followed by another incubation in the heating block (5 min, 55 °C, and 300 rpm) to completely dissolve the RNA pellet. The RNA concentration was measured photometrically (2.2.2.6) and all samples were stored at -80°C.

2.2.2.6 Determination of DNA and RNA concentrations

The concentrations of isolated RNA and DNA samples were determined photometrically in the Nanodrop (Tab. 12) at a wavelength of 260 nm.

2.2.2.7 cDNA synthesis

For the transcription of the RNA into complementary DNA (cDNA), a reaction mix with RNA (2 µg from mouse tissues and 500 ng from cultivated cells and pancreatic islets), dNTPs (25 mM, Tab. 10) and hexanucleotide primers (12.5 mmol, Tab.10) was used. This reaction mix was incubated for 5 min at 65 °C to allow the annealing of the primers to the RNA template. After incubation for 1 min on ice and short spinning, the reverse transcriptase (Tab. 7) was added together with the corresponding buffer and $MgCl_2$ (25 mM) to the reaction. Subsequently, the cDNA-synthesis was conducted in a PCR cycler (Tab. 12) under the following conditions.

Table 17: Thermocycler settings for the cDNA synthesis

Step	Temperature	Duration
Annealing	25 °C	5 min
Elongation	42 °C	60 min
Enzyme-inactivation	70 °C	15 min
Hold	4 °C	∞

2.2.2.8 Quantitative Real-time PCR (qPCR)

The quantitative Real-time PCR (qPCR) serves for the quantification of gene expression by the use of a fluorescence reporter molecule, which is able to intercalate into the DNA. With each amplification cycle, the fluorescence intensity increases proportionally. The cycle, in which the fluorescence intensity noticeable exceeds the background fluorescence, is defined as the cycle of threshold (Ct). This value can be inversely correlated to the amount mRNA/cDNA in the starting material. The higher the amount of mRNA in the analysed sample, the lower the number of cycles needed to exceed the background fluorescence, the lower the Ct-value. In this work the GoTaq® qPCR Master Mix (Tab. 7), which uses BRYT® Green as fluorescence reporter, was used. For the qPCR reaction, 5 µL 2x GoTaq® qPCR Master Mix (containing 20 µL CXR reference dye per mL), 0.5 µL of each primer (10 nM, Tab. 6) and 4 µL of cDNA (10 ng from liver, quadriceps, BAT and gWAT (1:40 dilution) and 5 ng from cells and pancreatic islets (1:20 dilution)) was added to each reaction well (total volume of 10 µL). Afterwards, the plates were sealed with an optical clear film (Tab. 11) and briefly centrifuged. The qPCRs for all genes from 6-weeks-old parental tissues as well as from cells were conducted in the StepOnePlusTM-PCR System (Tab. 12). The qPCRs for all genes from 21-weeks-old parental- and all RCS tissues were executed in the QuantStudio 7 Flex PCR System (Tab. 12). The following protocol was used for the reaction in both machines:

Table 18: Thermocycler settings for the qPCR

Step	Temperature	Duration	Number of Cycles
Hot start	95 °C	2 min	1 x
Denaturation	95 °C	15 sec	40 x
Annealing/Extension	60 °C	60 sec	
Dissociation (melt analysis)	60-95 °C	75 sec	1 x

Finally, gene expression was quantified using the $2^{-\Delta\Delta CT}$ method (Livak and Schmittgen, 2001).

2.2.2.9 Microarray analysis

For the microarray analysis, RNA was isolated from liver, skeletal muscle (quadriceps), gonadal white adipose tissue (gWAT), brown adipose tissue (BAT) and pancreatic islets of the parental strains at 6 weeks of age (2.2.2.3 and 2.2.2.4). The RNA integrity was determined using an Agilent 2100 Bioanalyzer (Tab. 12). Samples with RIN values > 8 were selected for genome-wide expression analysis using an Affymetrix-Chip (GeneChip® Mouse Genome 430A 2.0 Array). The analysis was conducted by Dr. Birgit Knebel (Institute for Clinical Biochemistry and Pathobiochemistry, German Diabetes Center, Düsseldorf) and statistically analysed by Dr. Axel Rasche (Max Planck Institute for Molecular Genetics, Berlin).

2.2.3 Cell biological methods

2.2.3.1 Cultivation and dissemination of MIN6 and Hepa 1-6 cells

Both murine cell lines MIN6 and Hepa 1-6 were constantly cultivated at 37 °C with 5 % CO_2 in respective cultivation medium (Tab. 9). At approx. 90 % confluence, cells were detached by adding trypsin (Tab. 9) and approx. one third to one fifth (depending on the cell density) was seeded to a new cultivation flask. For the GSIS- assay, further cells were seeded into 12-wells plates (100,000 cells each well), and into 48-well plates (30,000 cells each well) for the FAO assay. For this purpose, cells were trypsinized and centrifuged for 5 min at 1000 rpm (Centrifuge GPKR, Tab. 12). After resuspension in 10 mL of cultivation medium the cells were counted with the help of a Neubauer chamber (Tab. 12).

For cryoconservation, cells were trypsinized and centrifuged for 5 min at 1000 rpm (Centrifuge GPKR, Tab. 12). The pellet was resuspended in cultivation medium containing 20 % FCS and 10 % DMSO. The cells were aliquoted ($1x10^6$ cells each tube) into appropriate cryopreservation tubes (Tab. 11) and frozen in a tank filled with isopropanol (100 %) at -80 °C overnight. At the next day, cells were transferred into liquid nitrogen where they were stored until recultivation.

2.2.3.2 Transfection of cells

2.2.3.2.1 Lipofection of Hepa 1-6 cells

Lipofection makes use of synthetic cationic lipids for the delivery of nucleic acids, such as plasmid DNA and siRNA, into living cells. This is mediated by the interaction of these lipids with the negatively charged nucleic acids to form so called lipoplexes and their subsequent fusion with the anionic plasma membrane. As a result, the nucleic acids cross into the cytoplasm of the cell where they can be used for replication or expression (Felgner *et al*. 1987).

For the siRNA-mediated knockdown of *Nudt19* in Hepa 1-6 cells in 48-well format, 1.5 µL of Lipofectamine® RNAiMAX reagent (Tab. 10) was added to 50 µL of Opti-MEM® (Tab. 9). Another reaction tube was prepared with 50 µL of Opti-MEM® and 1 µL siRNA (50 µM, Tab. 4). Subsequently, both mixtures were combined and incubated for 10 min at RT to allow the formation of lipoplexes. Meanwhile, cells were washed with 500 µL of PBS and provided with 400 µL of fresh cultivation medium. After adding of the lipoplexes, cells were incubated at 37 °C and 5 % CO_2 and the medium was removed after 24 hours. Subsequently, cells were incubated in cultivation medium at 37 °C and 5 % CO_2 until the start of the assay.

For the plasmid-DNA -mediated overexpression of *Nudt19* in Hepa 1-6 cells in 48-well format, 1.5 µL Lipofectamine® 2000 (Tab. 10) was added to 50 µL of Opti-MEM®. In a second tube, 0.5 µg Plasmid-DNA (Tab. 5) was added to 50 µL of Opti-MEM®, both mixtures were combined and incubated for 10 min at RT. Meanwhile, cells were washed with PBS and provided with cultivation medium free from FCS and antibiotics. The DNA-lipid complex was added and cells were subsequently cultivated at 37 °C and 5 % CO_2. The medium was removed after 5 hours and the cells were further incubated in normal cultivation medium until the start of the assay.

2.2.3.2.2 Electroporation of MIN6 cells

The electroporation method uses high-voltage pulses to permeabilize the membrane of a cell, allowing the entry of nucleic acids into the cytoplasm (Wong and Neumann, 1982).

For the knockdown or overexpression of candidate genes, MIN6 cells were electroporated with siRNA- or plasmid-DNA oligonucleotides (Tab. 4+5) using the SF Cell Line 4D-Nucleofector® kit (2.1.7) in combination with the 4D-Nucleofector™ system (Tab. 12). The Cells were eletroporated according the Amaxa™ 4D-Nucleofector™ protocol for SH-SY5Y cells provided from Lonza (bio.lonza.com/go/op/290). For this purpose, cells were trypsinized and centrifuged for 5 min at 1000 rpm (Centrifuge GPKR, Tab. 12). The pellet was resuspended in 1 mL of cultivation medium and $2x10^6$ cells were transferred to a reaction tube. This tube was centrifuged (90 x g for 10 min), after washing with PBS, the pellet was resuspended in 100 µL Nucleofector™ solution. After adding of 300 nM siRNA or 2 µg of plasmid-DNA, respectively, the solution was transferred into 100 µL Nucleocuvette™ vessels and electroporated with the 4D-Nucleofector™ system using the pre-set program CA-137. In addition to the electroporation of different oligonucleotides, cells were further electroporated in Nucleofector™ solution without any oligonucleotides serving as not-treated controls in each experiment. After electroporation, cells were incubated for 5 min in the Nucleocuvette™ vessels and then resuspended in pre-warmed medium using the supplied pipettes. The cells were added to the wells which were prepared with 1 mL pre-warmed medium. Two million cells from each cuvette were

split into six 12-wellls; three of the wells were used for the assay (technical triplicates) and the other three for RNA-isolation (2.2.2.5) to confirm the knockdown efficiency. Until the experiment, cells were cultivated at 37 °C and 5 % CO_2 and the medium was changed one day after the electroporation.

2.2.3.3 Glucose-stimulated insulin secretion (GSIS) assay in MIN6 cells

The Glucose-stimulated insulin secretion (GSIS) assay was executed two days after the electroporation of siRNA (2.2.3.2.2). For this purpose, MIN6 cells (cultivated in 12-wells plates) were washed for three times with 500 µL of KRH puffer (Tab. 9), which was freshly prepared with BSA (1 mg/ mL). After starvation for one hour at 37 °C and 5 % CO_2 in glucose-free KRH buffer, the medium was removed and 500 µL KRH buffer with 25 mM glucose was added. During the glucose stimulation, cells were incubated for two hours at 37 °C and 5 % CO_2. After both incubations, 200 µL from the supernatant was transferred into a reaction tube and centrifuged at 4°C for 5 min at 1000 x g. Subsequently, 100 µL from the supernatant was collected and stored at -20 °C until the determination of the insulin concentration (2.2.4.1). The remaining medium was aspirated and 300 µL of lysis buffer (Tab. 9) was added to the cells. The lysate was transferred into a reaction tube and vortexed for 10 min in a gyrator (Tab. 12). Finally, cells were centrifuged (10 min at maximal speed and 4 °C) and the supernatant was collected and stored at -20 °C until determination of the protein content by BCA kit (Tab. 8).

2.2.3.4 Fatty acid β-oxidation (FAO) assay in Hepa 1-6 cells

The fatty acid β-oxidation (FAO) assay in Hepa 1-6 cells (cultivated in 48-well plates) was executed two days after lipofection (2.2.3.2.1). For this purpose, cells were washed three times with cultivation medium (Tab. 9) and the control compound FCCP (100 µM, Tab. 10) was added to the wells containing 400 µL cultivation medium. Moreover, Whatman-filters (Tab. 11) of 2 cm^2 size were added to the neighbouring empty wells as represented in Figure 6. After adding 50 µL NaoH (1M) to each filter, the medium was supplemented with 50 µl freshly prepared radioactive FAO buffer (Tab. 9) to reach the following concentrations of required components in each well: 0.3 µCi ^{14}C-palmitic acid, 6.24 mM fatty acid-free BSA, and 1 mM L-Carnitin. Control wells were directly stopped by adding 400 µL of 1 M HCL. Subsequently, the plate was quickly placed into a custom-made silicon-sealed oxidation chamber and incubated for four hours at 37 °C and 5 % CO_2 to allow the β-oxidation of ^{14}C-palmitate. Afterwards, the medium and filters were transferred to a new 48-well plate according the same layout. 400 µL of 1 M HCL was given to the medium to allow the release of $^{14}CO_2$ which was subsequently trapped from the NaOH soaked filter papers. The plate was again placed into the oxidation chamber and incubated at 37 °C and 5 % CO_2 overnight. The cells which remained

in the other 48-well plate were washed with PBS, detached in 100 µL lysis puffer (Tab. 9) and transferred to a reaction tube. The lysate was centrifuged for 10 min at 15,871 x g and 4 °C and the supernatant was stored at -20 °C until determination of the protein content by BCA kit (Tab. 8). At the next day, the plate was removed from the oxidation chamber and the filters were transferred to scintillation vials (Tab. 11) prepared with 4 mL scintillation fluid (Tab. 10) and the amount of $^{14}CO_2$ was measured in a β-counter (Tab. 12). Scintillation vials only filled with scintillation fluid served as negative controls, whereas 50 µL of radioactive FAO buffer (Tab. 9) was added to positive control vials.

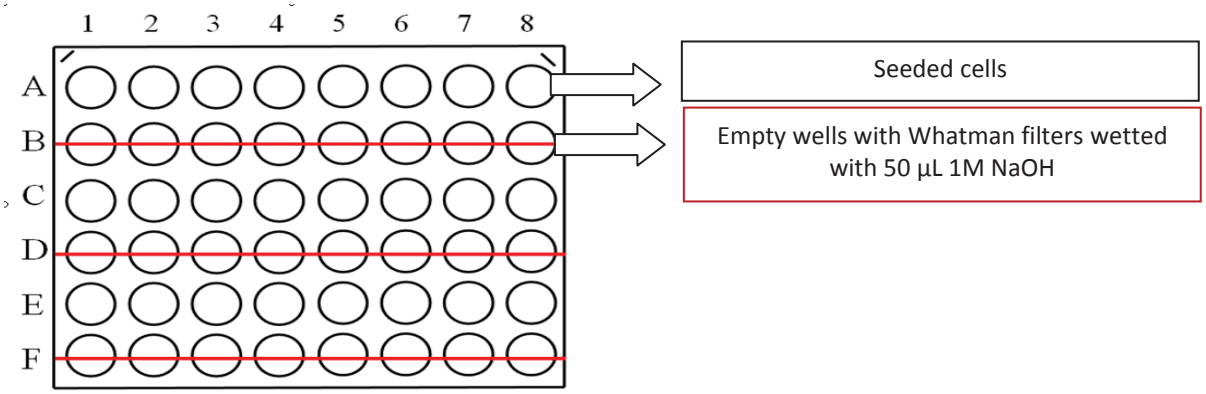

Figure 6: Layout for the fatty acid β-oxidation (FAO) assay in Hepa 1-6 cells. Cells were seeded in 48-well plates and every second raw was left empty for the preparation with NaOH soaked Whatman filters. Each well was connected to its subjacent well to allow the gas exchange between the two wells.

2.2.4 Biochemical methods

2.2.4.1 Analysis of plasma parameters

Plasma levels of insulin, C-peptide, free fatty acids, triglycerides, and total cholesterol were measured using the respective colorimetric kits listed in Table 8 according to the manufacturer's instructions.

2.2.4.2 Analysis of tissue parameters

2.2.4.2.1 Determination of total pancreatic insulin levels

For the measurement of the total pancreatic insulin content, the snap-frozen pancreas was transferred to a 2 mL reaction tube with 1 mL ice-cold acid ethanol solution (Tab. 9) together with a stainless steel bead (Tab. 11) and homogenized (5 min at 30 Hz) in the TissueLyser II (Tab. 12). The homogenate was rotated horizontally overnight at 4 °C and centrifuged the next morning for 15 min

at 4000 rcf and 4 °C. The supernatant was transferred to a new reaction tube and stored at -20 °C until determination of the insulin- and protein concentration with the respective kits (Tab. 8).

2.2.4.2.2 Determination of glycogen levels in liver and quadriceps muscle

For the measurement of glycogen content in liver- and quadriceps tissue, the protocol from Suzuki and colleagues (Suzuki et al., 2001) was used. For this purpose, approx. 40 mg of frozen pulverized tissue was homogenized for 30 min at 100 °C in 300 µL of KOH (wt/vol). Afterwards, the samples were washed with 100 µL of 1 M Na_2SO_4 and 800 µl of ethanol (100 %), followed by incubation for 2-3 min at 100 °C. After centrifugation (15 min at maximal speed and 4 °C), the pellet was washed three times in 200 µL H_2O with the help of a gyrator (Tab. 12). Afterwards, the pellet was dried for 10 min in a vacuum-centrifuge (Tab. 12) and then dissolved in 200 µL of sodium acetate buffer (Tab. 9), supplemented with 0.3 mg/mL Amyloglucosidase (Sigma-Aldrich, Steinheim, Germany) to enable the hydrolysis of glycogen to glucose. To initiate the enzymatic reaction, the solution was incubated for three hours at 40 °C. After short spinning, the supernatant was collected for the measurement of the glycogen concentration using the colorimetric glucose liquicolor kit (Tab. 8) according to the manufacturer's instructions.

2.2.4.2.3 Determination of triglyceride levels in liver and quadriceps muscle

For the determination of the triglyceride concentration, approx. 40 mg of frozen pulverized liver and quadriceps tissue was homogenized in 1.5 mL cold chloroform/methanol mixture (2:1 vol/vol) with a steel bead in the TissueLyser II (Tab. 12) at 25 Hz for 5 min. The homogenate was rotated horizontally for 2 hours at RT to allow the dissolution of all lipids. After adding 200 µL of dH_2O, the solution was mixed and centrifuged at 3.381 x g for 15 min to allow the phase separation. Afterwards, 250 µL of the lower organic phase was collected in a new reaction tube and dried for 1 hour in a vacuum-centrifuge (Tab. 12). Finally, the triglyceride fraction was resuspended in chloroform and quantified using the Triglyceride (TRIGS) GPO-PAP kit (Tab. 8) according to the manufacturer's protocol.

2.2.5 Haplotype analysis

SNPs were purchased from the Sanger Welcome Trust Institute Database (Tab. 14). As the sequence from the C3HeB/FeJ substrain is not listed in the database, the sequence from the closely related substrain C3HeB/HeJ was used for the haplotype analysis. Intervals of 250 kbp were selected for the count of polymorphic SNPs between the NZO/Hl and C3HeB/HeJ. A threshold of 200 SNPs /window was chosen for the distinction into IBD- or non-IBD regions. For the determination of the total SNP number, SNPs were compared to those annotated for C57BL/6J, which is used as reference in the database.

2.2.6 Statistical analysis

2.2.6.1 QTL analysis

By the use of the software *AntMap* 1.1 a chromosomal map was generated, which displays the distances between the genetic SNP markers with the unit centimorgan (cM). The distributions of the phenotypic data from the N2(NZOxC3H) population were tested for normality by the use of the D'Agostino-Pearson omnibus test. All data sets that were not normally distributed were logarithmized (log_2). The QTL analysis was executed by the use of the R/qtl 1.40-8 package (Broman and Sen 2009) of R (version i386 3.3.2). Single-QTL genome scans were performed by interval mapping with the Expectation-maximization (EM) algorithm (Lander and Botstein 1989). The results of this the QTL scans were represented with the logarithm of odds (LOD) scores, which were calculated with the help of the Haley-Knott -method. The significance threshold ($p< 0.05$) for linkage was estimated by 100 permutations (Lander and Kruglyak 1995). For the expression QTL (eQTL) analysis, mRNA expression levels ($2^{-\Delta CT}$) from the N2(NZOxC3H) population were used as quantitative traits and mapped to the genome in a non-parametric linkage analysis as described above.

2.2.6.2 Test for equality of distribution and significance

The distributions of phenotypic data from the N2(NZOxC3H) population were tested for normality with the Pearson omnibus test. Statistical significance was reported by two-tailed student´s t-test or one/ two-way analysis of variance (ANOVA) followed by post hoc Bonferroni test as appropriate. Differences were considered significant when $p< 0.05$. Values are presented as means ± SEM. Statistical analysis was conducted by GraphPad Prism 7. The significance threshold in the QTL analysis was calculated by a 100 permutation test by the use of the R/qtl 1.40-8 package (Broman and Sen 2009) of R (version i386 3.3.2).

2.2.6.3 Linear regression analysis

To estimate the relationship between the mRNA data from the N2(NZOxC3H) population with the metabolic traits, the p-value and coefficient of determination (r^2) was calculated by linear regression using the software GraphPad Prism 5.

3 Results

3.1 Metabolic characterization of the parental strains and the male F1 generation

Males and females of the parental mouse strains C3H and NZO, and males from the F1 generation were phenotyped on a HFD with 45 % calories from fat by measuring basic metabolic features. The different susceptibilities of the parental strains for the development of obesity and T2DM become evident in the following figures.

3.3.1 Blood glucose levels

Figure 7 illustrates the development of blood glucose levels. In total, 24 from 35 NZO males (69 %) exceeded the T2DM-treshold of 300 mg/dL during the experiment. In contrast, even after 17 weeks on HFD (20 weeks of age) C3H males were able to maintain blood glucose levels constantly below 190 mg/dL (Fig. 7A). On average, NZO males started to develop hyperglycaemia at the age of 6 weeks (NZO 310 ± 15 mg/dL, C3H 169 ± 4 mg/dL, $p<0.001$). The strongest differences in glycaemia between NZO and C3H mice were observed at week 14, when NZO mice exhibited 207 mg/dL higher mean blood glucose levels (NZO 367 ± 32 mg/dL, C3H 160 ± 8 mg/dL, $p<0.001$). As expected, the mean blood glucose levels from the F1 (first filial) males were generally intermediate to the values measured for NZO and C3H mice. However, the T2DM-prevalence was similar between F1- (72 %) and NZO males (69 %).

Similar to the males, strong differences in blood glucose were observed between NZO and C3H females (Fig. 7B). The differences in glycaemia started to reach statistical significance at the age of 15 weeks (NZO 214 ± 18 mg/dL, C3H 125 ± 5 mg/dL, $p<0.001$). The strongest differences were measured at 19 weeks of age, when NZO females exhibited on average 101 mg/dL higher blood glucose levels compared to C3H females (NZO 223 ± 21 mg/dL, C3H 122 ± 3 mg/dL, $p<0.001$). In total, two out of twelve NZO females (17 %) exceeded the T2DM-treshold of 300 mg/dL, but none of the C3H females.

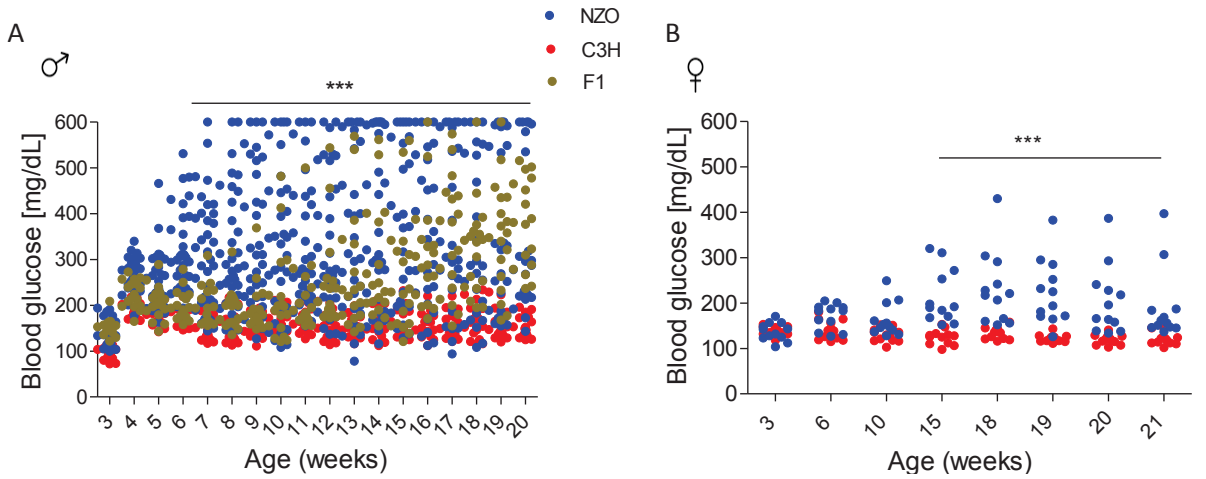

Figure 7: Development of blood glucose levels in the parental strains and the male F1 generation. Blood glucose levels were measured weekly for the parental- and F1 males (A) and at weeks 3, 6, 10, 15, 18-21 for the parental females (B). Dots represent single animals. NZO: 24-35 males and 12 females, C3H: 18 males and 12 females, F1 (NZOxC3H): 18 males. 2-way-ANOVA followed by Bonferroni's multiple comparisons test, ***p<0.001

3.3.2 Body weight and body composition

After weaning at 3 weeks of age, NZO males gained already 6.5 grams more compared C3H males (NZO 15.1 ± 0.5 g, C3H 8.7 ± 0.3 g, p<0.001) (Fig. 8 A). These differences in body weight increased further upon HFD. Thus, at 20 weeks of age NZO mice gained on average 18 grams more than C3H mice (NZO 62.1 ± 2.3 g, C3H 44.0 ± 0.4 g, p<0.001), most of it due to increases in body fat (week 15 of age: NZO 22.5 ± 1.2 g, C3H 10.7 ± 0.3 g, p<0.001) (Fig. 8C). In addition, NZO mice gained more lean mass compared to C3H mice with the strongest differences (6.5 g) at week 10 (NZO 31.5 ± 0.3 g, C3H 25.0 ± 0.3 g, p<0.001) (Fig. 8E). Moreover, an increased body length at 21 weeks of age (NZO 12.2 ± 0.1 cm, C3H 11.2 ± 0.1 cm, p<0.001) further contributes to the observed differences in the body weight. As expected, the data for body weight and body composition from the F1 generation were intermediate to the values measured in NZO and C3H.

Similar differences in regard to the body weight development were observed for the females. Whereas both strains had the same body weight after weaning, significant differences were observed starting from week 6, when NZO females already gained on average 10.6 grams more compared to C3H females (NZO 32.3 ± 0.8 g, C3H 21.7 ± 0.6 g, p<0.001). These differences gradually increased with age; at 21 weeks of age NZO females gained on average 24.3 grams more than C3H mice (NZO 67.7 ± 2.1 g, C3H 43.4 ± 1.4 g, p<0.001) (Fig. 8B). Similar to the males, the increase of body weight in the NZO females was mainly due to an increase of fat mass (week 15 of age: NZO 32.2 ± 1.2 g, C3H 14.2 ± 0.9 g, p<0.001) (Fig. 8D), whereas lean mass (week 15 of age: NZO 25.8 ± 0.4 g, C3H 22.5 ± 0.6 g, p<0.001) (Fig. 8E) and body lenght (week 21 of age: NZO 11.7 ± 0.1 cm, C3H 11.3 ± 0.1 cm, p<0.001) were only slightly increased.

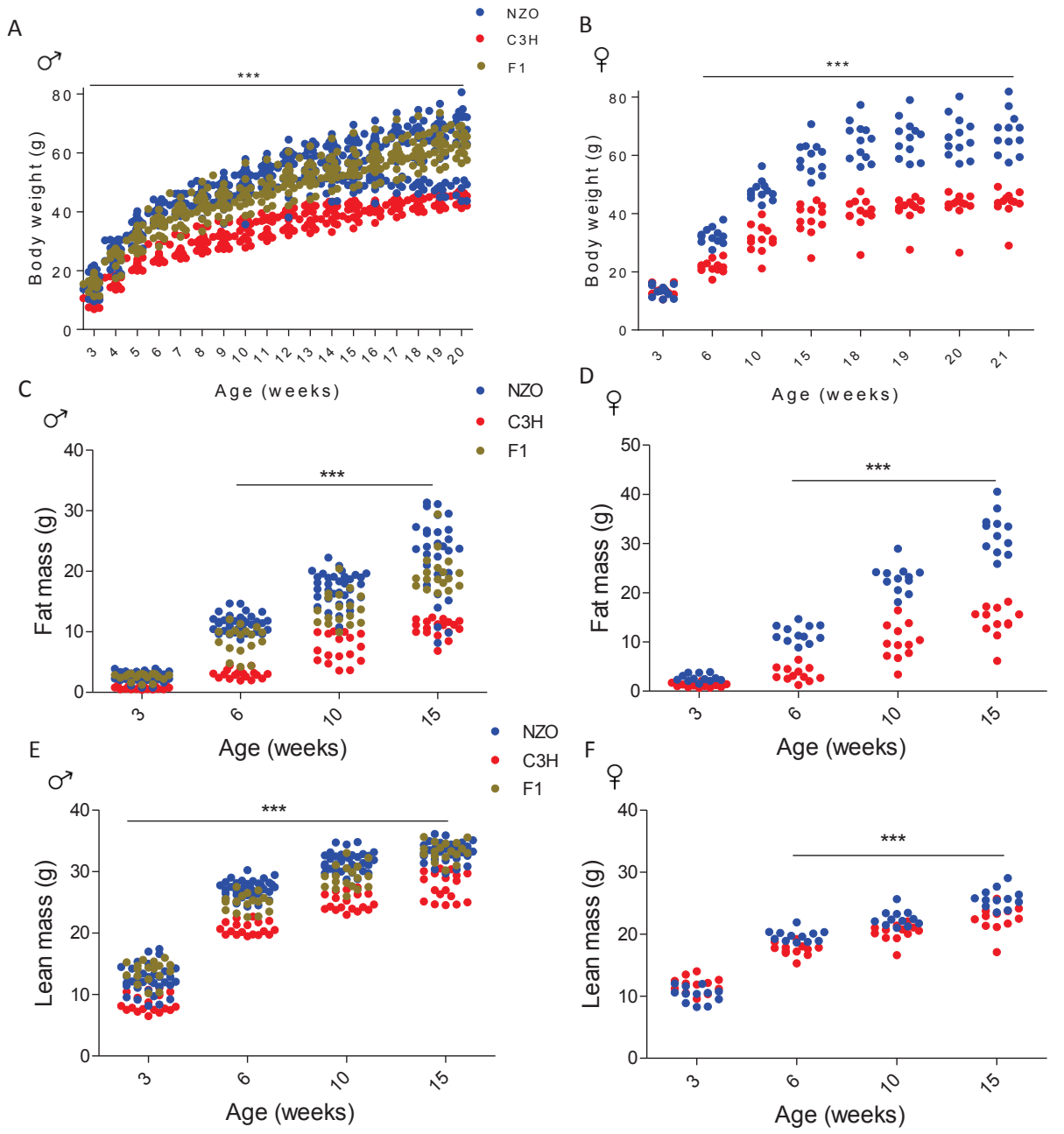

Figure 8: Development of body weight and body composition in the parental strains and the male F1 generation. Body weight was measured weekly for the parental- and F1 males (A) and at weeks 3, 6, 10, 15, 18-21 for the parental females (B). Fat mass (C: males, D: females) and lean mass (E: males, F: females) were measured via NMR at weeks 3, 6, 10 and 15. Dots represent single animals. NZO: 24-35 males and 12 females, C3H: 18 males and 12 females, F1 (NZOxC3H): 18 males. 2-way-ANOVA followed by Bonferroni's multiple comparisons test, ***p< 0.001

3.3.3 Plasma insulin- and total pancreatic insulin levels

The males were sacrificed at 21- and the females at 22 weeks of age for the analysis of further plasma- and tissue parameters. Among the males, 16 h-fasting plasma insulin levels at 8 weeks of age were on average 4-fold higher in NZO- compared to C3H males (NZO 1.0 ± 0.13 µg/L, C3H 0.23 ± 0.04 µg/L, p<0.001) mice (Fig. 9A). In contrast, at the age of 21 weeks, 6 h-fasting plasma insulin levels showed high variability in both male strains (NZO 6.2 ± 1.1 µg/L, C3H 4.9 ± 0.7 µg/L, Fig. 9B), whereas total pancreatic insulin levels were about 3-fold lower in the obese strain (NZO 11.3 ± 2.1 µg/mg, C3H 32.8 ± 3.2 µg/mg, p<0.001) (Fig. 9D). Among the females, plasma insulin levels were 2-fold higher in NZO (NZO 9.9 ± 1.5 µg/L, C3H 4.7 ± 0.8 µg/L, p=0.0095) (Fig. 9C), which was accompanied by a tendency towards higher levels of total pancreatic insulin compared to the lean strain (NZO 40 ± 6.6 µg/mg, C3H 26.6 ± 1.9 µg/mg, p=0.073) (Fig. 9E).

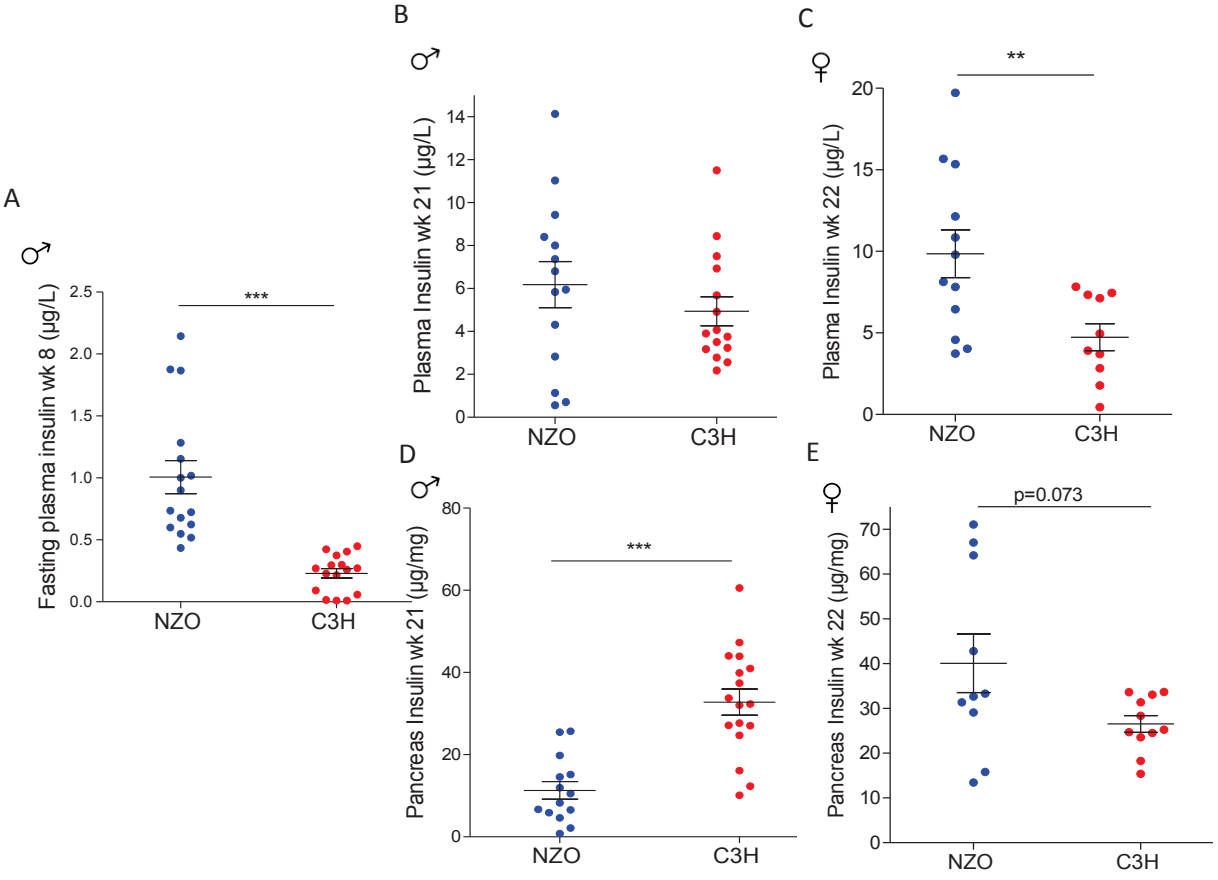

Figure 9: Plasma insulin- and total pancreatic insulin levels in the parental strains. For the males, 16 h-fasting-plasma insulin levels (A) were measured at 8 weeks of age, 6 h-fasting plasma insulin (B) and total pancreatic insulin (D) at 21 weeks of age. For the females, 6 h-fasting plasma insulin levels (C) and total pancreatic insulin levels (E) were measured at 22 weeks of age. Insulin levels were measured by ELISA. For total pancreatic insulin measurement, the snap-frozen pancreas was homogenized in acid ethanol and insulin levels were normalized to the total protein content, determined by BCA. Dots represent single animals. NZO: 14-16 males and 10-12 females, C3H: 16-17 males and 10-11 females. Unpaired t-test, two-tailed, **p<0.01, ***p<0.001. wk= week

3.2 Metabolic characterization of the N2(NZOxC3H) population

3.2.1 Generation of the backcross population

In order to generate the backcross (N2(NZOxC3H)) population males from the F1 generation, produced from the breeding of C3H males with NZO females, were backcrossed with NZO females (Fig. 10). In contrast to the F1 generation, in which each mouse is genetically identical (heterozygous), each mouse from the backcross population carries a different combination of parental alleles and therefore represents a genetic individual. In total, 310 females and 329 males were generated.

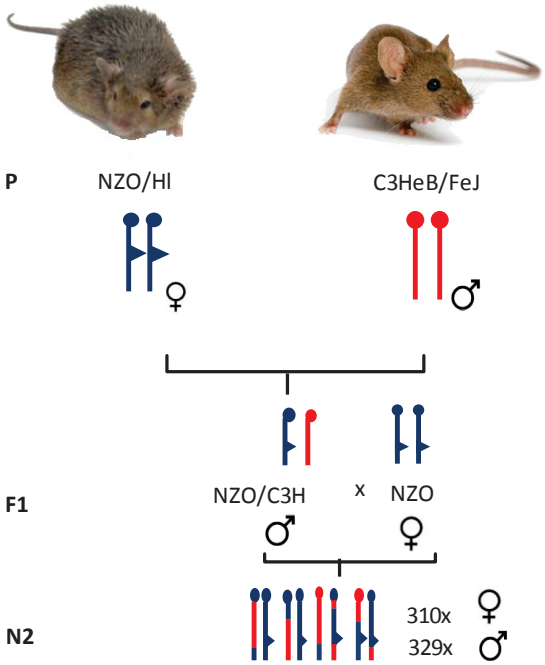

Figure 10: Generation of the N2(NZOxC3H) population. The two mouse strains NZO/HI and C3HeB/FeJ were bred to generate a F1 generation. Males from the F1 generation were backcrossed with NZO females for the generation of the N2(NZOxC3H) population consisting of 310 females and 329 males. P= Parental generation, F1= first filial generation, N2= backcross generation

3.2.2 Phenotyping of the backcross population

After weaning at 3 weeks of age, all N2(NZOxC3H) mice were fed a HFD with 45 % calories from fat. The mice were phenotyped according the schedule in Figure 11. Measured phenotypes included body weight, body length, and body composition, as well as blood glucose levels at different stages and times (fasted, refed, random), and final plasma insulin. Moreover, targeted metabolomic profiling was performed with blood samples at week 10 (see 2.2.1.3.5 and Suppl. Tab. 3). In females, blood glucose and body weight were measured every four weeks (instead of every week) and the fasting-refeeding experiment as well as the metabolic profile was not conducted for the females.

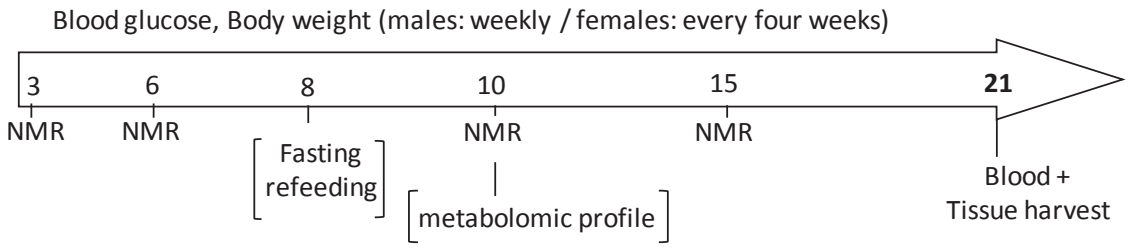

Figure 11: Phenotyping schedule for the N2(NZOxC3H) population. Blood glucose and body weight was measured weekly for the males and monthly for the females. The body composition was measured by nuclear magnetic resonance spectroscopy (NMR) at weeks 3, 6, 10, and 15. For the males, a fasting-refeeding experiment was executed at week 8 and a metabolic profile was created with blood samples collected at week 10. All animals were sacrificed at 21 weeks of age for the collection of the blood and tissues.

3.2.2.1 Blood glucose, body weight and body composition

In total, 329 males and 310 females were phenotyped for several obesity- and T2DM-associated traits. As expected, the N2 population showed a large variation in metabolic phenotypes. In comparison with the female N2 population, the male N2 population exhibited on average higher blood glucose levels (week 20 of age: males 349 ± 9 mg/dL, females 194 ± 4 mg/dL) (Fig. 12A) accompanied by a higher body weight (week 20 of age: males 67.7 ± 0.6 g, females 60.9 ± 0.6 g) (Fig. 12B). The differences in body weight between the sexes were mainly due to differences in the lean mass (week 15 of age: males: 32.4 ± 0.1 g, females: 24.9 ± 0.1 g) (Fig. 12D), whereas the fat mass was rather higher in the females (week 15 of age: males 23.9 ± 0.3 g, females 26.9 ± 0.4 g) (Fig. 12C). The N2 males further exhibited a higher relative lean mass content (lean mass divided by body weight) (week 15 of age: males 55 ± 0.3 %, females 47 ± 0.2 %), whereas the the females had a higher relative fat mass content (fat mass divided by body weight) (week 15 of age: males 39 ± 0.4 %, females 49 ± 0.3 %). Moreover, the T2DM-prevalence (males 71 %, females 11 %) as well as the mortality rate (males 18 %, females 1 %) was clearly higher in the males, compared to the females of the N2 population.

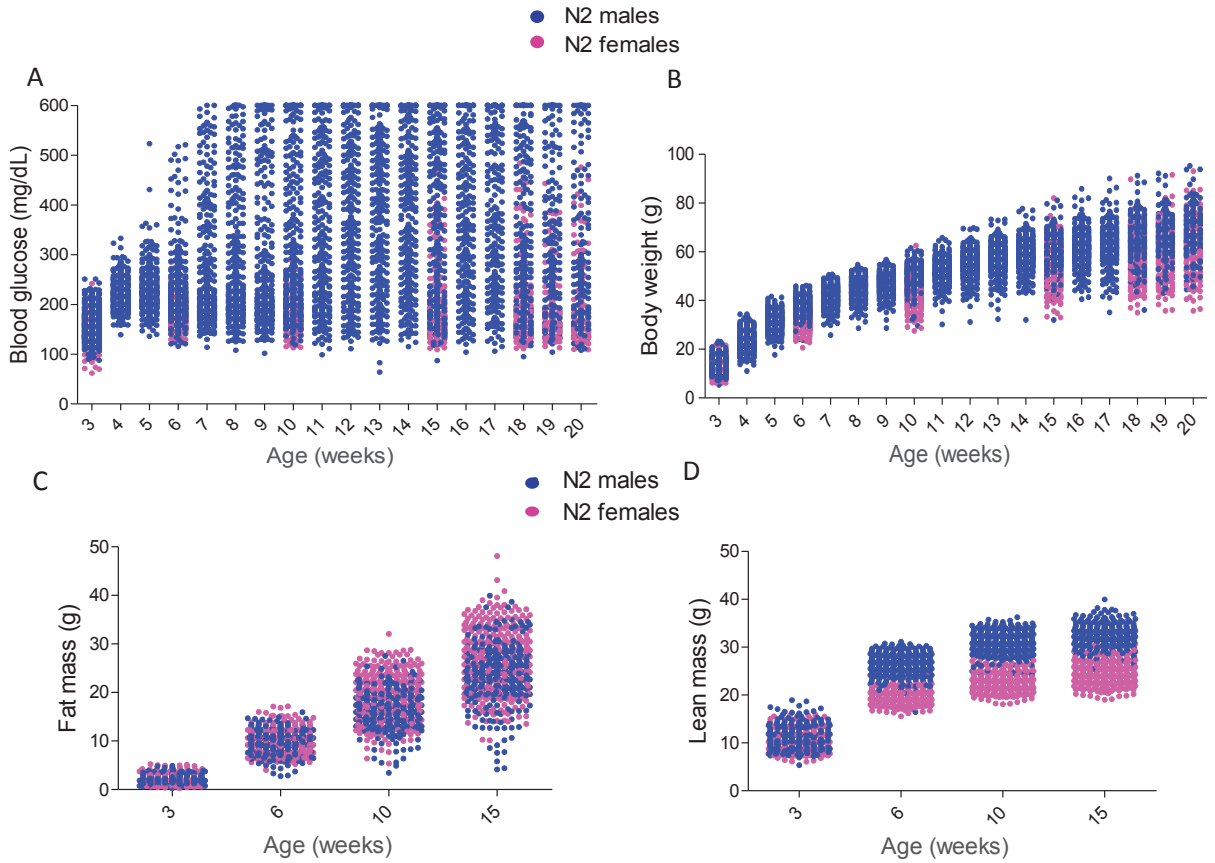

Figure 12: Metabolic characterization of the males and females from the N2(NZOxC3H) population. Body weight (A) and blood glucose levels (B) were measured weekly for the males (blue dots) and at weeks 3, 6, 10, 15, 18- 20 for the females (violet dots). Fat mass (C) and lean mass (D) were measured via NMR at weeks 3, 6, 10, and 15. n=258 - 329 males and 308- 310 females.

3.3 Genome-wide linkage analysis of the N2(NZOxC3H) population

For the genome-wide linkage analysis, all genotypes (115 informative SNP markers covering all 19 murine autosomes (Suppl. Tab. 10, Fig. 13)) and collected phenotypes (Fig. 11) from each N2(NZOxC3H) mouse (329 males and 310 females) were combined to search for novel obesity- and T2DM- associated QTLs. In total, 90 significant (LOD >3) QTLs were detected, 62 of them in the male- and 28 in the female N2 population (Suppl. Tab. 8 + 9).

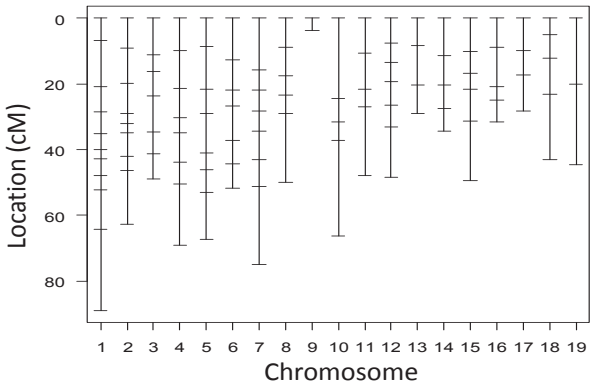

Figure 13: Genetic map for the linkage analysis of the N2(NZOxC3H) population. 115 SNPs (represented with the vertical lines) distributed over all 19 murine autosomes were genotyped in each N2 animal.

3.3.1 Linkage analysis for blood glucose, body weight and plasma insulin in the male N2(NZOxC3H) population

Figure 14 visualizes the results of the genome-wide linkage analysis from the male N2(NZOxC3H) population for the traits blood glucose and body weight (weeks 3-20) as well as plasma insulin at 21 weeks of age. The calculated LOD scores for all murine autosomes are plotted over the time, whereupon significant associations ($p < 0.05$) are highlighted in red (Fig. 14A+B) or indicated with the horizontal line (Fig. 14C) Analogue figures for all further traits which were measured in the male N2(NZOxC3H) population are shown in the supplement (Suppl. Fig. 1). The strongest associations with blood glucose levels (Fig. 14A) were found on chromosomes 4 (max. LOD 6.5 at 44 cM, week 20 of age), 7 (max. LOD 13.3 at 12 cM, week 10 of age) and 15 (max. LOD 6.6 at 13 cM, weeks 15 of age).

Further significant QTLs for blood glucose (LOD > 4) were detected on chromosomes 5 (max. LOD 6.7 at 34 cM, week 7 of age), 6 (max. LOD 5.1 at 52 cM, week 12 of age), 14 (max. LOD 4.4 at 24 cM, week 9 of age), 18 (max. LOD 4.3 at 12 cM, week 3 of age), 8 (max. LOD 4.3 at 11 cM, week 10 of age) and 16 (max. LOD 4.2 at 28 cM, week 10 of age).

The development of body weight (Fig. 14B) revealed to be regulated by mainly two chromosomes, namely 4 (max. LOD 8.4 at 30.2 cM, week 19 of age) and 7 (max. LOD 7.4 at 17 cM, week 17 of age). Another significant QTL for body weight with a LOD score above 4 was found on chromosome 16 (max. LOD 4.1 at 1 cM, week 6 of age).

The linkage analysis for plasma insulin levels at 21 weeks of age (Fig. 14C) exhibited two strong QTLs on chromosomes 4 (max. LOD 4.1 at 44 cM) and 7 (max. LOD 4.8 at 17 cM).

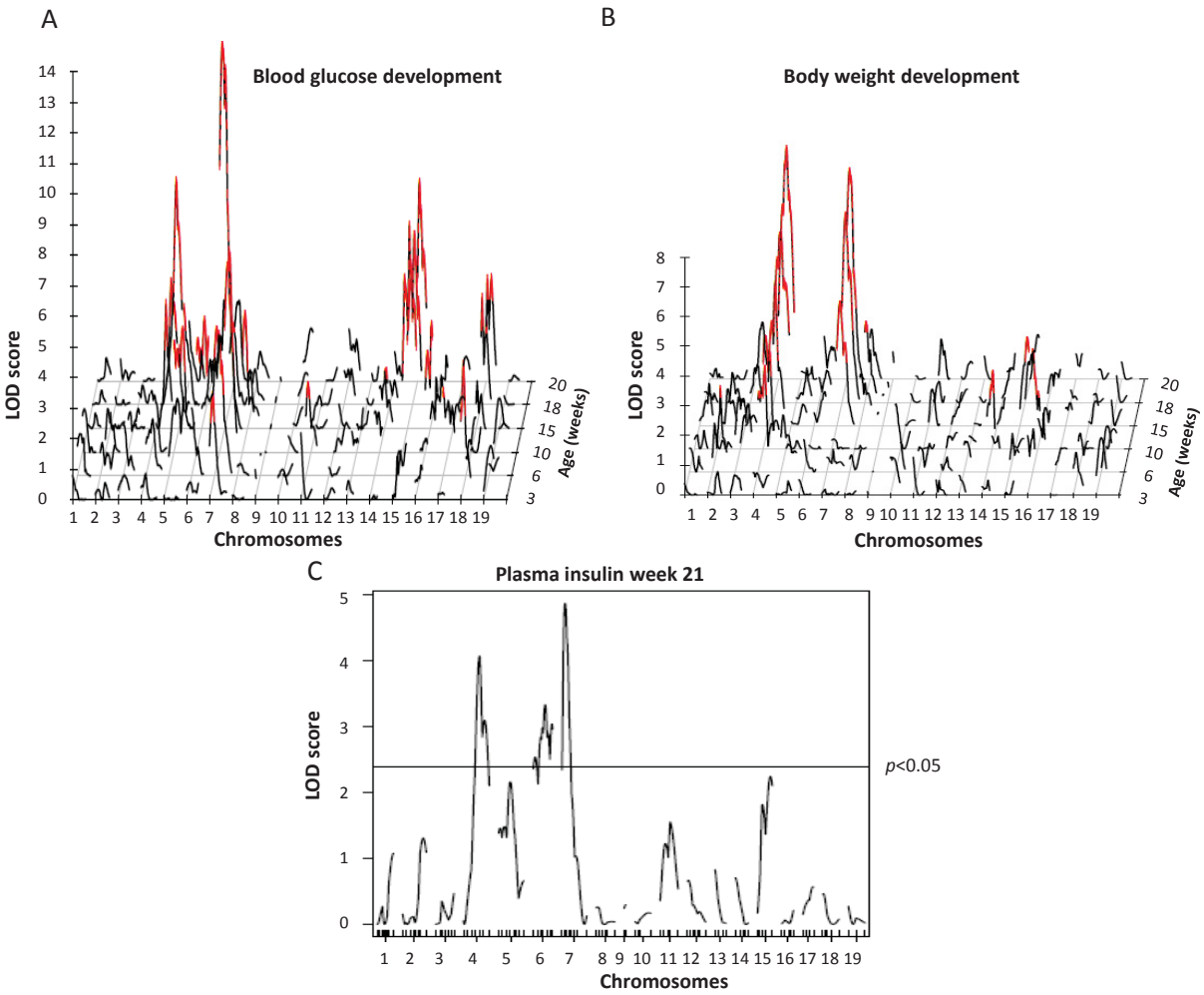

Figure 14: Genome-wide linkage analysis of the male N2(NZOxC3H) population. Genome-wide logarithm of the odds (LOD) scores distribution for the development of blood glucose (A), body weight (B) and for plasma insulin levels at week 21 (C) in male N2(NZOxC3H) mice. Significant linkage is indicated in red (A+B) or with the horizontal line (C), respectively. The analysis was assessed with R/qtl using a 100 permutation test to determine the significance threshold ($p < 0.05$).

3.3.2 Linkage analysis for blood glucose and body weight in the female N2(NZOxC3H) population

Figure 15 visualizes the genome-wide LOD score distributions of the linkage analysis from the female N2(NZOxC3H) population for the traits blood glucose and body weight. Analogue figures for all further traits which were measured in the female N2 population are shown in the supplement (Suppl. Fig. 2).

The linkage analysis for blood glucose levels (Fig. 15A) exposed the strongest association on chromosome 7 (max. LOD 6.8 at 1 cM, week 20 of age). The development of body weight (Fig. 15B) was mainly linked (LOD > 4) to chromosomes 10 (max. LOD 9.3 at 7.2 cM, week 6 of age), 4 (max. LOD 6.9 at 15 cM, week 19 of age), 14 (max. LOD 5.2 at 23 cM, week 6 of age) and 13 (max. LOD 4.2 at 29 cM, week 6 of age). Plasma insulin levels were not measured in female N2(NZOxC3H) mice.

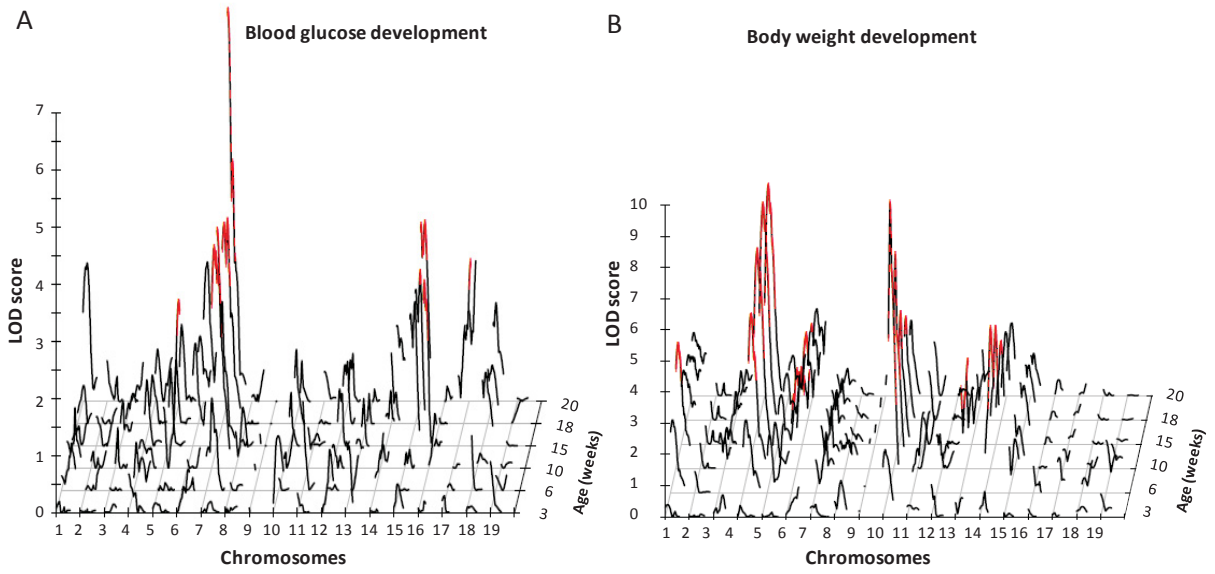

Figure 15: Genome-wide linkage analysis of the female N2(NZOxC3H) population. Genome-wide logarithm of the odds (LOD) scores distribution for the development of blood glucose (A) and body weight (B) in female N2(NZOxC3H) mice. Significant linkage is indicated in red. The analysis was assessed with R/qtl using a 100 permutation test to determine the significance threshold ($p < 0.05$).

3.4 Detection of multiple QTLs on chromosome 7

Chromosome 7 revealed linkage with several metabolic traits (Fig. 16). A proximal locus on chromosome 7 (*Cdp7-prox*) exhibited the most significant QTL for blood glucose (max. LOD 13.3 at 12 cM, week 10 of age) and plasma insulin (max. LOD 4.8 at 17 cM, week 21 of age) in the male N2(NZOxC3H) population. *Cdp7-prox* was further associated with the development of body weight (max. LOD 7.4 at 17 cM, week 17 of age) and lean mass (max. LOD 8.6 at 11 cM, week 15 of age). A second QTL for blood glucose levels (*Cdp7-dis*) from the males was detected at a more distal position on chromosome 7 (max. LOD 12.6 at 26 cM, week 10 of age).

A third QTL (*C07-prox*) from the males revealed linkage with free blood carnitine levels at a more proximal position (max. LOD 7.0 at 5 cM, week 10 of age) compared with the peak of *Cdp7-prox*. Furthermore, chromosome 7 exhibited the most significant QTL for blood glucose levels (*fCdp7-prox*) (max. LOD 6.8 at 1 cM, week 20 of age) in the female N2(NZOxC3H) population. Further significant QTLs (LOD > 3) which were found on chromosome 7 are shown in the supplement (Suppl. Fig. 4A).

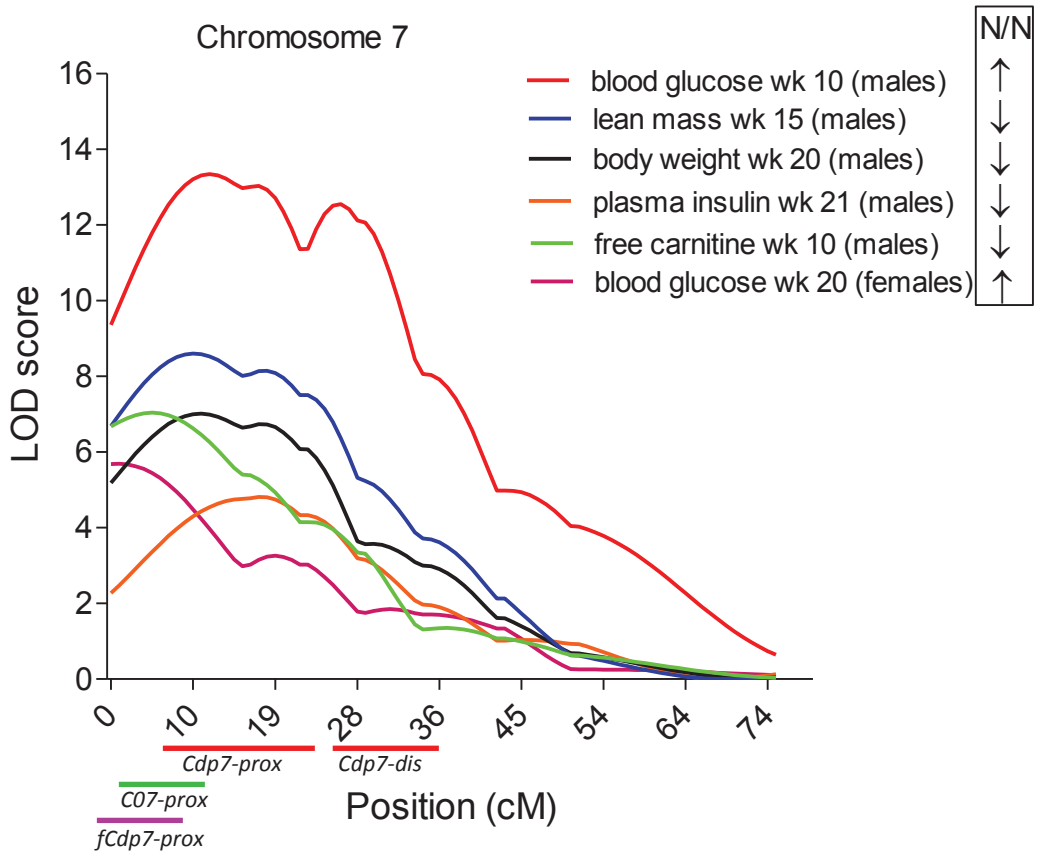

Figure 16: LOD score distribution of all significant QTL (LOD > 4) detected on chromosome 7. A QTL for blood glucose was detected in both male (*Cdp7-prox*) and female (*fCdp7-prox*) N2(NZOxC3H) mice. The locus *Cdp7-prox* further revealed linkage with body weight, lean mass and plasma insulin levels. In the males, a second QTL for blood glucose was detected at a more distal position on chromosome 7 (*Cdp7-dis*). Another QTL for free blood carnitine (*C07-prox*) mapped at a more proximal position. The analysis was assessed with R/qtl using a 100 permutation test to determine the significance threshold. The allelic effects for the different traits are indicated with the arrows. LOD= logarithm of odds, wk= week, N= NZO

3.4.1 Characterization of *Cdp7-prox*: a major T2DM QTL from the males N2(NZOxC3H) population

In the male N2(NZOxC3H) population homozygous NZO-allele carriers exhibited much higher blood glucose levels than heterozygous allele carriers for *Cdp7-prox* (SNP marker: *rs3724525* located at 15.6 cM corresponding to 37.7 Mb), starting already at 5 weeks of age (Fig. 17A). The strongest differences were observed at week 10, when *Cdp7-prox*$^{NZO/NZO}$ males exhibited on average 122 mg/dL higher blood glucose levels compared to *Cdp7-prox*$^{NZO/C3H}$ mice (*Cdp7-prox*$^{NZO/NZO}$ 369 ± 12 mg/dL, *Cdp7-prox*$^{NZO/C3H}$ 247 ± 8 mg/dL). The differences in blood glucose levels were accompanied by strong differences in the T2DM-prevalence (Fig. 17B). Thus, at 10 weeks of age a difference of 40 % in the T2DM-prevalnce was calculated (*Cdp7-prox*$^{NZO/NZO}$ 57 %, *Cdp7-prox*$^{NZO/C3H}$ 17 %). Moreover, differences in the body weight development were observed at later stages of age. Hence, starting at 10 weeks of age *Cdp7-prox*$^{NZO/NZO}$ mice started to gain less body weight than *Cdp7-prox*$^{NZO/C3H}$ mice (week 20 of age: *Cdp7-prox*$^{NZO/NZO}$ 64 ± 0.8 g, *Cdp7-prox*$^{NZO/C3H}$ 71 ± 0.7 g) (Fig. 17C), which was due to

a lower gain of fat- (week 15 of age: *Cdp7-prox*$^{NZO/NZO}$ 22.8 ± 0.5 g, *Cdp7-prox*$^{NZO/C3H}$ 25.0 ± 0.4 g) and lean mass (week 15 of age: *Cdp7-prox*$^{NZO/NZO}$ 31.5 ± 0.2 g, *Cdp7-prox*$^{NZO/C3H}$ 33.3 ± 0.2 g). Furthermore, plasma insulin levels measured at 21 weeks of age were significantly reduced in *Cdp7-prox*$^{NZO/NZO}$ animals (*Cdp7-prox*$^{NZO/NZO}$ 6.5 ± 0.6 µg/L, *Cdp7-prox*$^{NZO/C3H}$ 11.2 ± 1.1 µg/L) (Fig. 17D). In total, the mortality rate reached 27 % in *Cdp7-prox*$^{NZO/NZO}$ mice, compared to 8 % calculated in *Cdp7-prox*$^{NZO/C3H}$ mice (Fig. 17E).

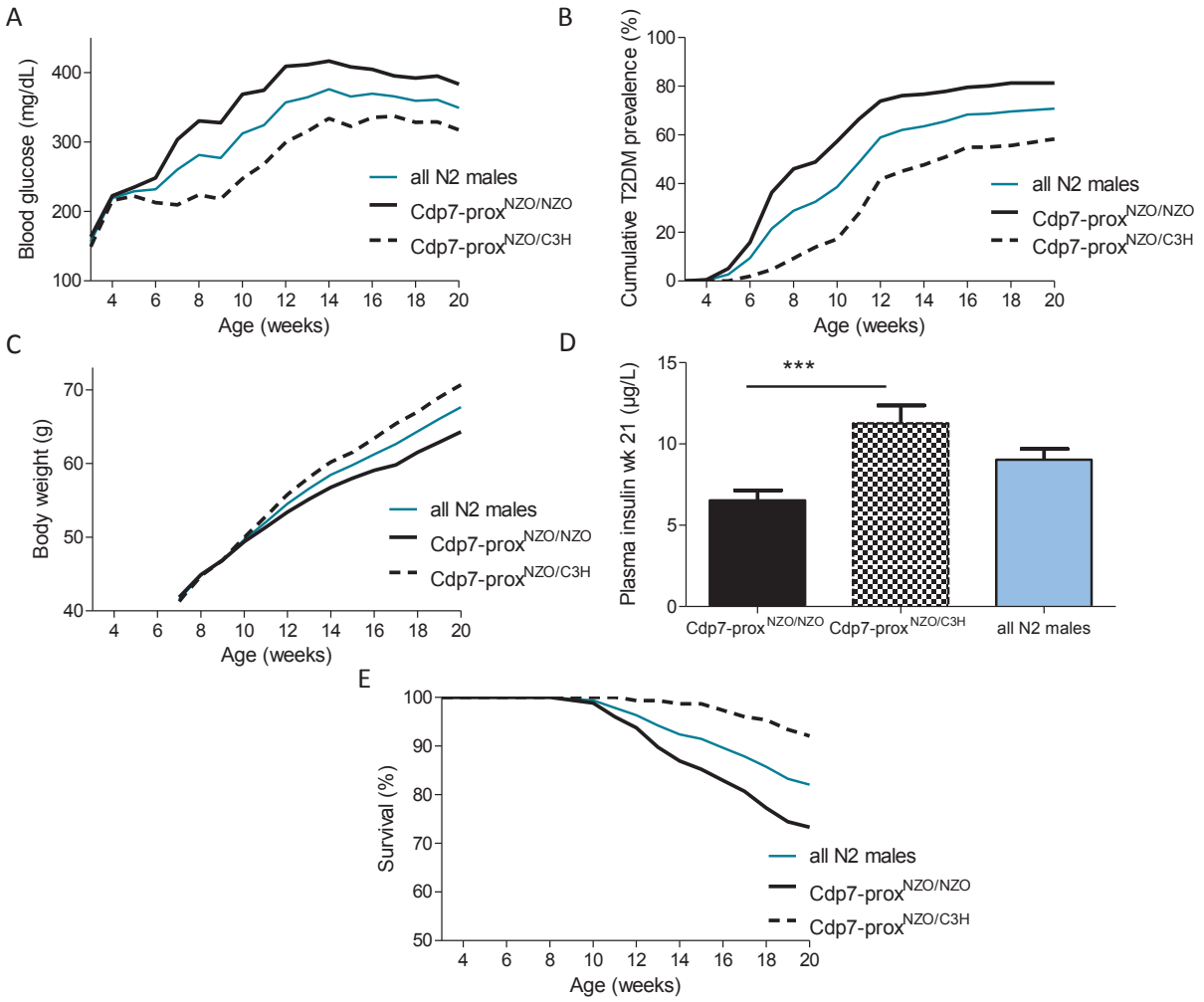

Figure 17: Quantitative effect of *Cdp7-prox* in male N2(NZOxC3H) mice. Development of blood glucose (A), T2DM-prevalence (B), body weight (C), final plasma insulin (D), and survival (E) in *Cdp7-prox*$^{NZO/NZO}$ (continuous line), *Cdp7-prox*$^{NZO/C3H}$ (dotted line), and all N2(NZOxC3H) (blue line) males. Data represent mean values from 150-176 *Cdp7-prox*$^{NZO/NZO}$ and 149-151 *Cdp7-prox*$^{NZO/C3H}$ mice. 1-way-ANOVA followed by Bonferroni's multiple comparisons test, ***p< 0.001

3.4.1.1 Additive effect of *Cdp7-prox* with *Nir4* and *Nir15-prox*

To investigate potential additive effects of *Cdp7-prox* with the other two large-effect blood glucose QTLs on chromosomes 4 (*Nir4*, Suppl. Fig. 4C) and 15 (*Nir15-prox*, Suppl. Fig. 4B), the mean values for blood glucose levels (Fig. 18A), T2DM-prevalence (Fig. 18B), and percentage of survival (Fig. 18C) were calculated for each week for the different allele combinations. An additive effect on all three parameters was observed for the combination of the two QTLs *Cdp7-prox* and *Nir15-prox*. Whereas a maximal difference of 122 mg/dL in glycaemia was observed between the two genotypes for *Cdp7-prox*, the difference was further increased to 172 mg/dL between mice carrying the two risk alleles (*Cdp7-prox*$^{NZO/NZO}$ and *Nir15-prox*$^{NZO/NZO}$) and animals carrying the two protective alleles on chromosomes 7 and 15 (*Cdp7-prox*$^{NZO/C3H}$ and *Nir15-prox*$^{NZO/C3H}$) (week 10 of age: 402 ± 15 mg/dL vs. 230 ± 10 mg/dL). The additive effect on glycaemia was accompanied by an additive effect on the T2DM-prevalence, as the difference of 40 % calculated between the genotypes for *Cdp7-prox* increased to 55 % by the combination of both risk alleles (week 10 of age, 66 % vs. 11 %). Moreover, the survival rate was reduced to 64 % in mice carrying both risk alleles (vs. 95 % in mice carrying the two protective alleles, delta: 32 %) compared to 73% observed in *Cdp7-prox*$^{NZO/NZO}$ mice carrying only one risk allele (vs. 92 % in *Cdp7-prox*$^{NZO/C3H}$ mice, delta: 19 %). Similar effects on blood glucose levels and T2DM-prevalence were found for the combination of *Cdp7-prox* with *Nir4*. Thus, a difference of 173 mg/dL in glycaemia (week 15 of age: 455 ± 17 mg/dL vs. 281 ± 15 mg/dL) and 50 % in the T2DM-prevalence (week 13 of age: 83 % vs. 33 %) was observed between mice carrying both risk alleles (*Cdp7-prox*$^{NZO/NZO}$ and *Nir4*$^{NZO/C3H}$) and animals carrying the two protective alleles (*Cdp7-prox*$^{NZO/C3H}$ and *Nir4*$^{NZO/NZO}$). Unexpectedly, the combination of both risk alleles led to an increase in the survival rate, as 89 % of the mice carrying both risk alleles, but only 73 % of mice carrying only the risk allele for *Cdp7-prox* survived. The combination of all three risk alleles for the QTLs (*Cdp7prox*$^{NZO/NZO}$, *Nir15prox*$^{NZO/NZO}$ and *Nir4*$^{NZO/C3H}$) led to a maximal increase, whereas the protective allele combination led to a maximal decrease in blood glucose levels (week 15 of age: 489 ± 19 mg/dL vs. 238 ± 14 mg/dL, delta: 250 mg/dL) and T2DM-prevalence (week 13 of age: 89 % vs. 21 %, delta: 68 %). At the end of the study almost all (93 %) of the mice carrying all three risk alleles were diabetic, compared to about one third (36 %) of mice with the protective allele combination.

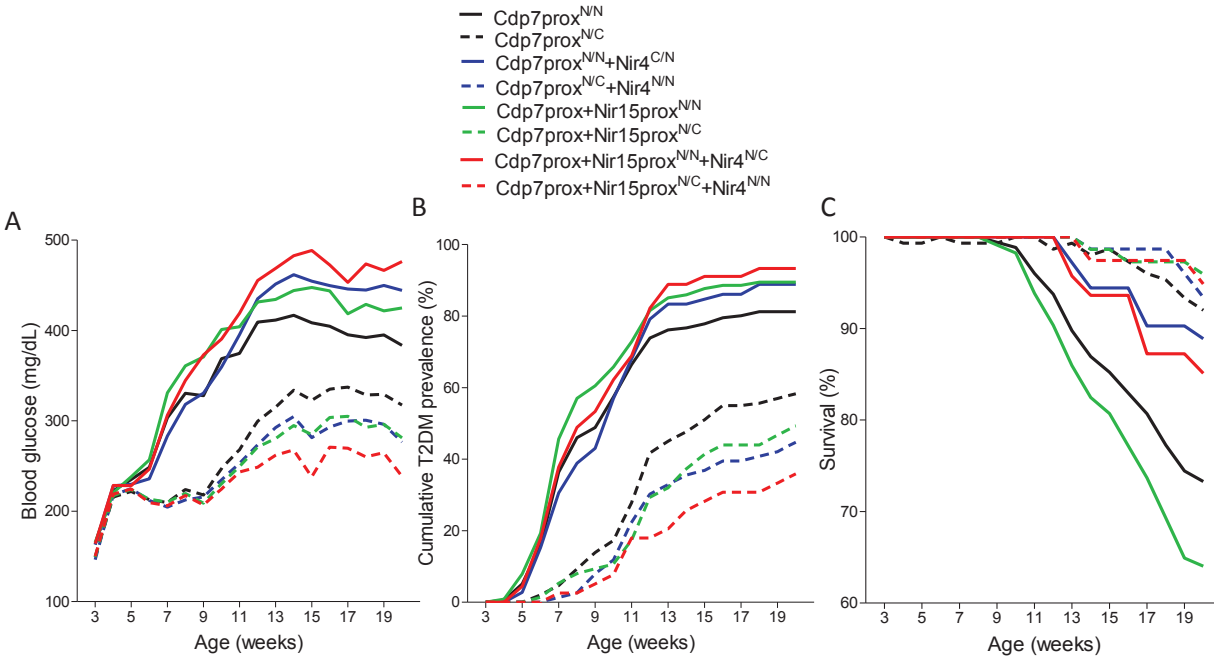

Figure 18: Additive effect of *Cdp7-prox* with two further major blood glucose QTLs from the male N2(NZOxC3H) population. Mean values for blood glucose levels (A), T2DM-prevalence (B) and survival (C) are shown for the different allele combinations for *Cdp7-prox*, *Nir4* and *Nir15-prox*. N=NZO, C=C3H.

3.4.2 Characterization of *fCdp7-prox*: a major T2DM QTL from the female N2(NZOxC3H) population

Homozygous allele carriers for *fCdp7-prox* (*rs3675839* located at 0 cM corresponding to 16.6 Mb) exhibited higher blood glucose levels compared to the heterozygous allele carriers. The differences in glycaemia levels between the two genotypes became already evident at 6 weeks and gradually increased with age (Fig. 19A). At 20 weeks of age, *fCdp7-prox*$^{NZO/NZO}$ females exhibited on average 45 mg/dL higher blood glucose levels compared to *fCdp7-prox*$^{NZO/C3H}$ females (*fCdp7-prox*$^{NZO/NZO}$ 214 ± 7 mg/dL, *fCdp7-prox*$^{NZO/C3H}$ 169 ± 5 mg/dL). At the end of the experiment, 16 % of *fCdp7-prox*$^{NZO/NZO}$ females exceeded the T2D threshold of 300 mg/dL, compared to only 5 % of *fCdp7-prox*$^{NZO/C3H}$ animals (Fig. 19B).

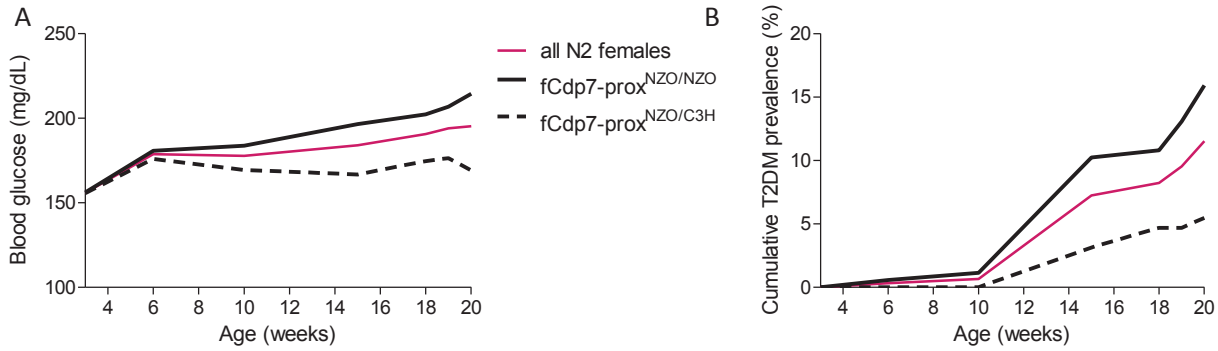

Figure 19: Quantitative effect of *fCdp7-prox* in female N2(NZOxC3H) mice. Development of blood glucose (A) and T2DM-prevalence (B) in *fCdp7-prox*$^{NZO/NZO}$ (continuous line), *fCdp7-prox*$^{NZO/C3H}$ (dotted line), and all N2(NZOxC3H) (pink line) females. Data represent mean values from 175-176 *fCdp7-prox*$^{NZO/NZO}$ and 128 *Cdp7-prox*$^{NZO/C3H}$ mice.

3.5 Introgression of chromosome 7 from C3H into the NZO- and C57BL/6J genome

To validate the linkage of *Cdp7-prox* and *fCdp7-prox* with blood glucose (and plasma insulin), and to allow a deeper characterization of the QTLs, chromosome 7 from C3H was introgressed into the NZO- and C57BL/6J genome using recombinant congenic strains (RCS).

3.5.1 Generation of the RCS NZO.C3H-*Cdp7*con and B6.C3H-*Cdp7*con

To generate RCS carrying chromosome 7 on a genetic NZO or C57BL/6J (B6) background, respectively, a N2 generation was generated according to the same breeding scheme that was already used for the generation of the initial N2(NZOxC3H) population (Fig. 10). For the generation of the RCS, at least three additional backcrosses of mice selected for heterozygous alleles on chromosome 7, with NZO or B6 females, respectively, were performed (Fig. 20A+B). With each backcross, the percentage of alleles from the background / recipient strain (NZO or B6) is predicted to increase by 50 %. Hence, in the N2 population the genetic background of the recipient strain is predicted with 75 %, whereas in the N5 generation the percentage increases theoretically to 97 %. The real percentage of the N2 and N3 generation of the two RCS was calculated by genotyping polymorphic SNPs in a distance of 10-30 Mb on all murine autosomes. By selecting mice that already had a higher recipient background in the N2 (and N3) generation by chance, the number of backcrosses to produce a line with the desired background close to 100 % can be reduced. With the help of this approach, designated “speed congenics”, N2 mice with an 82.5 % NZO- and 77 % B6 background could be selected for the subsequent backcrosses. In the N3 generation, the recipient background was increased to 91.5 % and 86.5 %, respectively (Fig. 20C). In order to produce homozygous C3H alleles on chromosome 7, intercrosses (brother-sister breeding) were conducted in the N5 and N6 generation of NZO.C3H-*Cdp7*con-, and in the N6 generation of B6.C3H-*Cdp7*con mice.

A

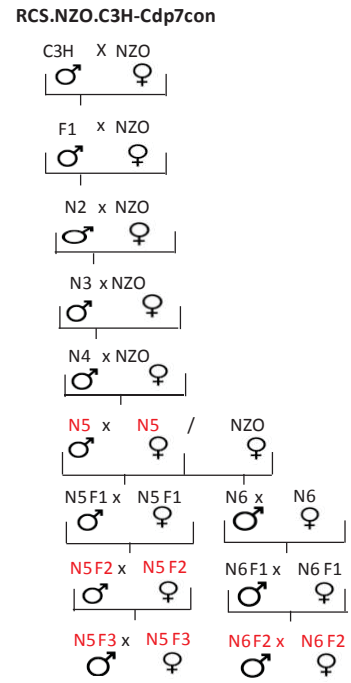

B

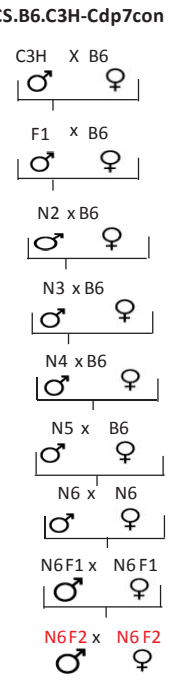

C

	Genetic NZO/ B6 background (%)		
Generation	Predicted	RCS.NZO.C3H-Cdp7con	RCS.B6.C3H-Cdp7con
N2	75	82.5	77
N3	87.5	91.5	86.5
N4	93.8		
N5	96.9		
N6	98.4		

Figure 20: Breeding strategy for the generation of the RCS NZO.C3H-*Cdp7*con and B6.C3H-*Cdp7*con. A: After the generation of the F1 (NZOxC3H) generation, five / six backcrosses with NZO females were conducted to generate heterozygous NZO/C3H allele carriers on Chr.7. Siblings were intercrossed in the N5 and N6 generation to produce homozygous C3H alleles on Chr.7 on a genetic NZO background (N5F1-N5F3 and N6F1+N6F2). Mice from the N5F2+F3- and N6F2 generation (highlighted in red) were phenotyped. B: After six backcrosses of males selected for heterozygous C3H/B6 alleles on Chr.7 with C57BL/6J females, siblings from the N6 generation were intercrossed to generate homozygous C3H alleles on Chr.7 on a genetic C57BL/6J background (N6F1 + N6F2). Mice from the N6F2 generation (highlighted in red) were phenotyped. C: Predicted recipient background (N2-N5) in comparison with the experimentally derived genetic background in the N2 and N3 generation of both RCS. B6= C57BL/6J, con=consomic

3.5.2 Metabolic characterization of the RCS NZO.C3H-*Cdp7*con and B6.C3H-*Cdp7*con

After weaning, NZO.C3H.*Cdp7*con experimental mice received a HFD with 45 kcal % from fat, whereas B6.C3H.*Cdp7*con mice were fed a diet with 60 kcal % from fat. The phenotyping schedule for both RCS was identical (Fig. 21), except for the end time point. Thus, NZO.C3H-*Cdp7*con mice were sacrificed at 17- and B6.C3H-*Cdp7*con at 21 weeks of age. The genotypes of the mice were confirmed using informative SNP markers (Suppl. Tab. 11+12) spread over the sequence of chromosome 7.

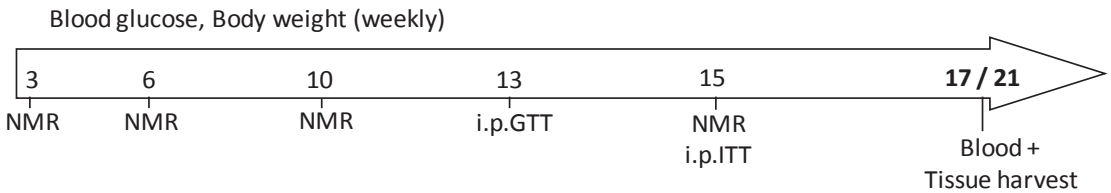

Figure 21: Phenotyping schedule for NZO.C3H-*Cdp7*con and B6.C3H-*Cdp7*con mice. Blood glucose and body weight was measured weekly. The body composition was measured by nuclear magnetic resonance spectroscopy (NMR) at weeks 3, 6, 10 and 15. An intraperitoneal glucose tolerance test (i.p. GTT) was performed at week 13 and an intraperitoneal insulin tolerance tests (i.p. ITT) at week 15. NZO.C3H-*Cdp7*con mice were sacrificed at 17- and B6.C3H-*Cdp7*con at 21 weeks of age for the collection of the blood and tissues.

3.5.2.1 Phenotyping of NZO.C3H.*Cdp7*con males and females

3.5.2.1.1 Blood glucose, body weight and body composition

Both males and females carrying homozygous NZO-alleles (NZO.C3H-*Cdp7*con$^{NZO/NZO}$) exhibited generally higher blood glucose levels, compared to homozygous C3H-allele carriers on chromosome 7 (NZO.C3H-*Cdp7*con$^{C3H/C3H}$). In total, at the end of the experiment six out of 16 NZO.C3H-*Cdp7*con$^{NZO/NZO}$ males exceeded the T2DM-threshold of 300 mg/dL, compared to only two out of 16 NZO.C3H-C*dp7*con$^{C3H/C3H}$ males. Moreover, NZO.C3H-*Cdp7*con$^{NZO/NZO}$ males become earlier diabetic. Thus, at the age of 10 weeks, all six NZO.C3H-*Cdp7*con$^{NZO/NZO}$ males were already diabetic, whereas all NZO.C3H-Cdp7con$^{C3H/C3H}$mice were still normogylcemic (Fig. 22A). The strongest differences in glycaemia were observed at 12 weeks of age, when NZO.C3H-*Cdp7*con$^{NZO/NZO}$ males exhibited 80 mg/dL higher mean blood glucose levels compared to NZO.C3H-*Cdp7*con$^{C3H/C3H}$ males (*Cdp7*con$^{NZO/NZO}$ 299 ± 44 mg/dL, *Cdp7*con$^{C3H/C3H}$ 219 ± 17 mg/dL). However, due to the large variation observed in NZO.C3H-*Cdp7*con$^{NZO/NZO}$ mice, the differences in glycaemia between the two genotypes from the males did not reach statistical significance. By contrast, the differences in blood glucose levels between the two genotypes from the females reached statistical significance starting at 13 weeks of age (Fig. 22B). The strongest differences in glycaemia for the females were observed at week 15, when NZO.C3H-*Cdp7*con$^{NZO/NZO}$ mice exhibited 62 mg/dL higher mean blood glucose levels compared to NZO.C3H-*Cdp7*con$^{C3H/C3H}$ females (*Cdp7*con$^{NZO/NZO}$ 198 ± 15 mg/dL, *Cdp7*con$^{C3H/C3H}$ 136 ± 3 mg/dL, $p< 0.001$). In total, only one NZO.C3H-*Cdp7*con$^{NZO/NZO}$ female exceeded the T2DM-treshold, but none of the NZO.C3H-*Cdp7*con$^{C3H/C3H}$ females. In regard to the body weight development, NZO.C3H-*Cdp7*con$^{C3H/C3H}$ males gained significantly more body weight starting at week 13 of age, which was due to a higher fat mass content (Fig. 22C). Thus, at week 15 NZO.C3H-*Cdp7*con$^{C3H/C3H}$ gained on average 8.7 grams more compared to NZO.C3H-*Cdp7*con$^{NZO/NZO}$ males (*Cdp7*con$^{C3H/C3H}$ 62.4 ± 2.4 g, *Cdp7*con$^{NZO/NZO}$ 53.7 ± 2 g, $p< 0.001$), which was due to a difference of 6.7 grams of fat (*Cdp7*con$^{C3H/C3H}$ 25.4 ± 2, *Cdp7*con$^{NZO/NZO}$ 18.7 ± 1.8, $p=0.002$). In contrast, the development of lean mass did not differ between the two genotypes. In the females, the body weight development was comparable between the genotype (Fig. 22D).

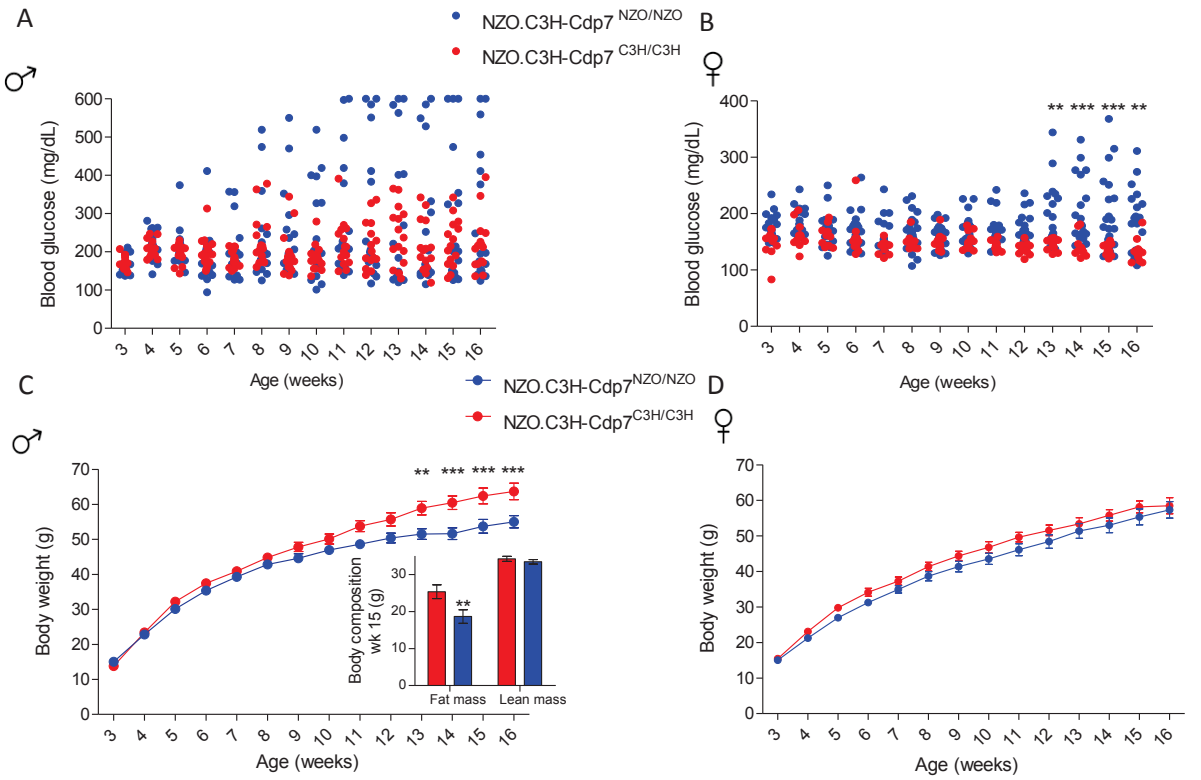

Figure 22: Blood glucose- and body weight development in NZO.C3H-*Cdp7*con males and females. Blood glucose levels (A: male, B: females) and body weight (C: males, D: females) was measured weekly; fat- and lean mass was measured by nuclear magnetic resonance spectroscopy (NMR) at week 15 of age (C). Dots represent single animals (A+B) or mean values ± SEM (C+D) from 11-21 mice. 2-way-ANOVA followed by Bonferroni's multiple comparisons test, ** p< 0.01, ***p<0.001

3.5.2.1.2 Glucose- and insulin tolerance

For the intraperitoneal glucose tolerance test (i.p. GTT), 13-weeks-old animals were fasted for 16 hours before they were injected with glucose (2g/ kg body weight). Whereas the genotypes from the males did not differ in the development of blood glucose- (Fig. 23A) and plasma insulin levels (Fig. 23C), highly significant differences were observed between the genotypes from the females. Thus, NZO.C3H-*Cdp7*con$^{C3H/C3H}$ females exhibited significantly lower blood glucose levels compared to NZO.C3H-*Cdp7*con$^{NZO/NZO}$ females at 30, 60 and 120 minutes after the injection, which was in line with a significant smaller area under the curve (AUC) (*Cdp7*con$^{C3H/C3H}$ 47860 ± 2456, *Cdp7*con$^{NZO/NZO}$ 74363 ± 2938, p<0.001) (Fig. 23B). Decreased blood glucose levels in NZO.C3H-*Cdp7*con$^{C3H/C3H}$ females were accompanied by generally higher insulin levels compared to NZO.C3H-*Cdp7*con$^{NZO/NZO}$ females (Fig. 23D). This difference reached statistical significance at 120 minutes after the injection (*Cdp7*con$^{C3H/C3H}$ 5. 1 ± 0.5 µg/L, *Cdp7*con$^{NZO/NZO}$ 3.3 ±0.3 µg/L, p=0.04). In contrast, after 240 minutes a reverse insulin pattern was measured (*Cdp7*con$^{C3H/C3H}$ 4.9 ± 0.6 µg/L, *Cdp7*con$^{NZO/NZO}$ 6.9 ± 1 µg/L, p=0.015).

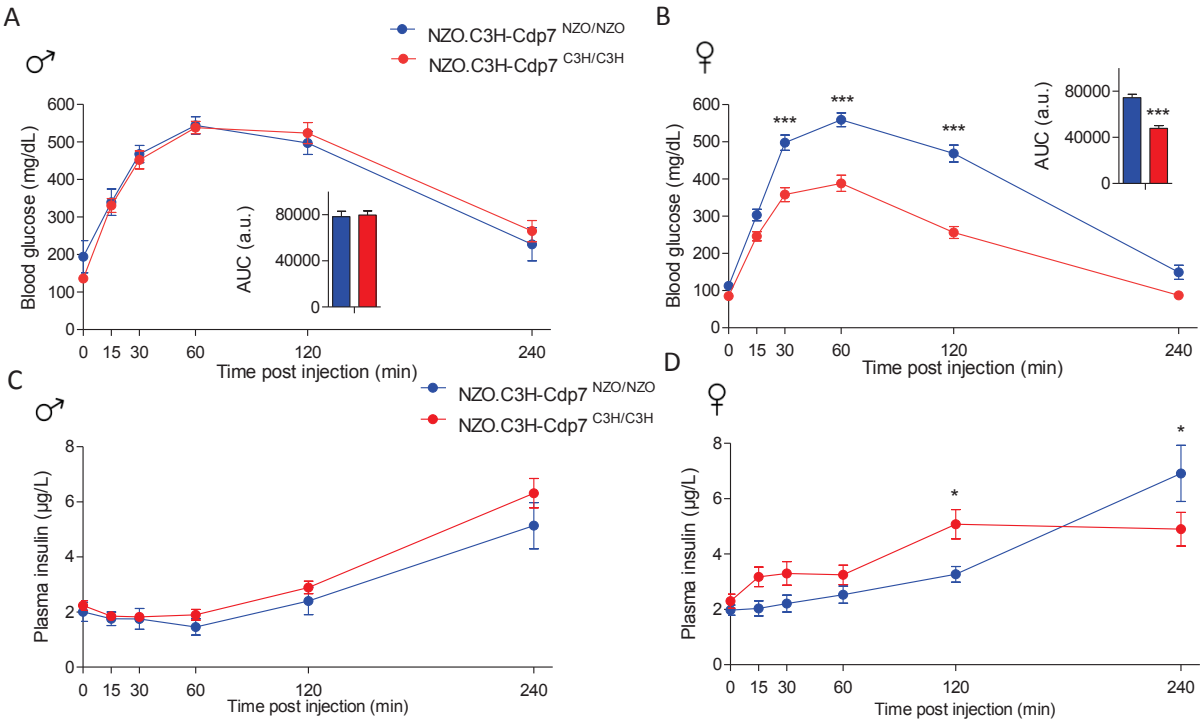

Figure 23: Intraperitoneal glucose tolerance test in NZO.C3H-*Cdp7*con males and females. 13-weeks-old animals were fasted for 16 hours before the injection of glucose (2 g/ kg). Blood glucose- (A: male, B: females) and plasma insulin levels (C: male, D: females) were measured before (0 minutes), as well as at 15, 30, 60, 120, and 240 minutes after the glucose injection. Data represent mean values ± SEM from 11-21 mice. 2-way-ANOVA followed by Bonferroni's multiple comparisons test (blood glucose- and plasma-insulin development) and unpaired t-test, two-tailed (AUC), *p< 0.05, *** p< 0.001. AUC= area under the curve, a.u. = arbitrary units

Moreover, the insulin sensitivity was investigated at 15 weeks of age with the help of an intraperitoneal insulin tolerance test (i.p. ITT). The animals were fasted for 6 hours before the injection of insulin (1U / kg body weight). The injection of insulin could only moderately reduce blood glucose levels in the males with no differences between the genotypes (Fig. 24A). In females, the administration of insulin resulted in a more pronounced drop of blood glucose levels. This drop was stronger in NZO.C3H-*Cdp7*con$^{C3H/C3H}$ mice, as they exhibited significantly lower blood glucose levels 15 and 30 minutes after the injection compared to NZO.C3H-*Cdp7*con$^{NZO/NZO}$ females (Fig. 24B). An improved insulin sensitivity of NZO.C3H-*Cdp7*con$^{C3H/C3H}$ females was further illustrated by a significant smaller AUC (*Cdp7*con$^{C3H/C3H}$ 6984 ± 341, *Cdp7*con$^{NZO/NZO}$ 10543 ± 664, p<0.001).

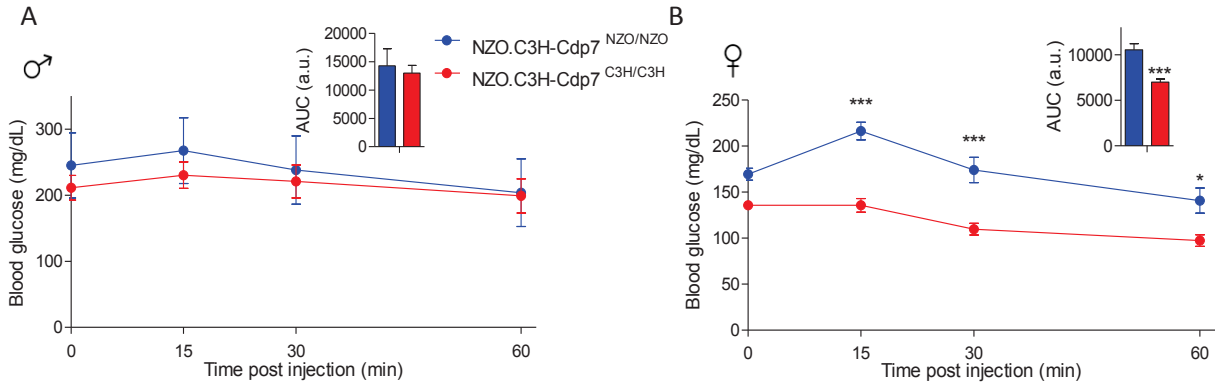

Figure 24: Intraperitoneal insulin tolerance test in NZO.C3H-*Cdp7*con males and females. 15-weeks-old animals were fasted for 6 hours before the injection of insulin (1 U/ kg body weight). Blood glucose levels (A: male, B: females) were measured before (0 minutes), as well as at 15, 30, and 60 minutes after the insulin injection. Data represent mean values ± SEM from 11-21 mice. 2-way-ANOVA followed by Bonferroni's multiple comparisons test (blood glucose development) and unpaired t-test, two-tailed (AUC), *p< 0.05, ***p< 0.001. AUC= area under the curve, a.u. = arbitrary units

3.5.2.1.3 Final plasma insulin- and C-peptide levels

Plasma insulin- and C-peptide levels were measured from 6 hours fasted animals after sacrificing at 17 weeks of age. Compared to NZO.C3H-*Cdp7*con$^{NZO/NZO}$ males, NZO.C3H-*Cdp7*con$^{C3H/C3H}$ males exhibited significantly higher plasma levels of insulin (*Cdp7*con$^{C3H/C3H}$ 18.3 ± 4 µg/L, *Cdp7*con$^{NZO/NZO}$ 3.0 ± 0.5 µg/L, p=0.0012) (Fig. 25A) and C-peptide (*Cdp7*con$^{C3H/C3H}$ 5.5 ± 0.7 µg/L, *Cdp7*con$^{NZO/NZO}$ 2.1 ± 0.2 µg/L, p<0.001) (Fig. 25C). In contrast, the females showed an inverse pattern as NZO.C3H-*Cdp7*con$^{C3H/C3H}$ females exhibited lower plasma levels of insulin (*Cdp7*con$^{C3H/C3H}$ 7.3 ± 1.6 µg/L, *Cdp7*con$^{NZO/NZO}$ 11.7 ± 2 µg/L, p=0.098) (Fig. 25B) and C-peptide (*Cdp7*con$^{C3H/C3H}$ 3.0 ± 0.2 µg/L, *Cdp7*con$^{NZO/NZO}$ 4.7 ± 0.5 µg/L, p=0.012) (Fig. 25D) compared to NZO.C3H-*Cdp7*con$^{NZO/NZO}$ females.

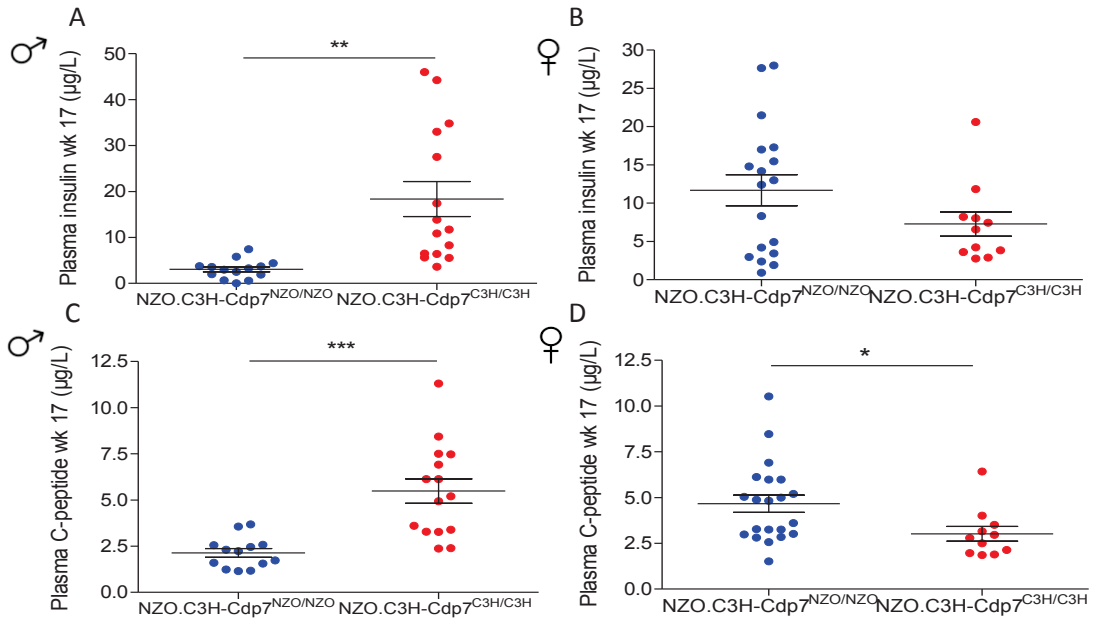

Figure 25: Plasma insulin- and C-peptide levels in NZO.C3H-*Cdp7*con males and females. 17-weeks-old animals were fasted for 6 hours before sacrificing. Plasma insulin (A: males, B: females) and C-peptide-levels (C: males, D: females) were measured by ELISA. Dots represent single animals (n=11-21). Unpaired t-test, two-tailed, *p< 0.05, ** p< 0.01, *** p< 0.001

3.5.2.2 Phenotyping of B6.C3H-*Cdp7*con males

Both genders of B6.C3H-*Cdp7*con were characterized; however, phenotypic differences between the genotypes could only be observed for the males. Phenotyping data for the females are included in the supplement (Suppl. Tab. 7).

3.5.2.2.1 Blood glucose, body weight and body composition

One week after the start of the HFD (60 % fat), B6.C3H-*Cdp7*con$^{C3H/C3H}$ mice exhibited significantly lower blood glucose levels compared to B6.C3H-Cdp7con$^{B6/B6}$ mice (*Cdp7*con$^{C3H/C3H}$ 181 ± 9 mg/dL, *Cdp7*con$^{B6/B6}$ 227 ± 13 mg/dL, p=0.003) (Fig. 26A). The differences in blood glucose levels disappeared afterwards. Moreover, B6.C3H-*Cdp7*con$^{C3H/C3H}$ mice gained less body weight at later stages of age. The strongest differences in body weight were observed at week 20, when B6.C3H-*Cdp7*con$^{C3H/C3H}$ mice exhibited on average 7 grams less compared to B6.C3H-*Cdp7*con$^{B6/B6}$ mice (*Cdp7*con$^{C3H/C3H}$ 39 ± 1.9 g, *Cdp7*con$^{B6/B6}$ 46 ± 2 g, p<0.001). This was mainly due to differences in body fat (week 15 of age: *Cdp7*con$^{C3H/C3H}$ 6.4 ± 1.2 g, *Cdp7*con$^{B6/B6}$ 9.5 ± 1.3 g, p=0.008) (Fig. 26B), whereas the development of lean mass did not differ between the genotypes.

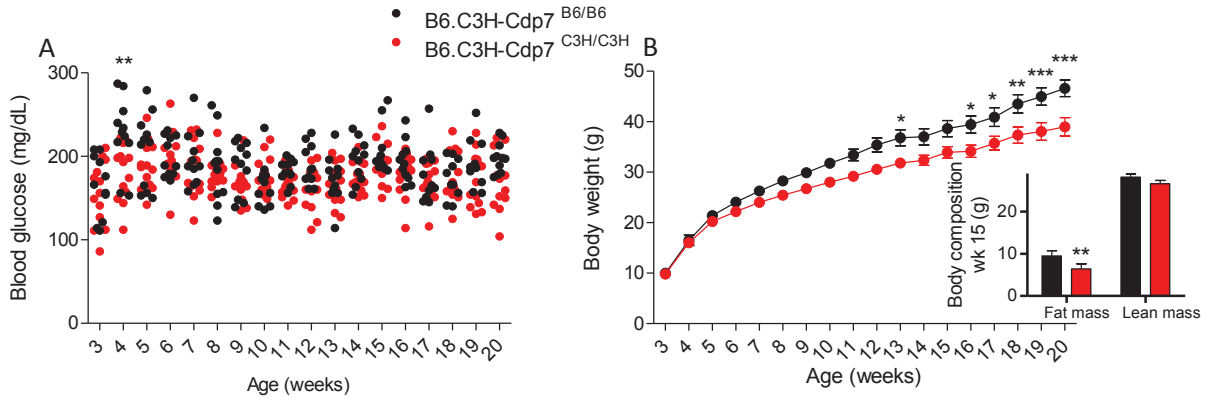

Figure 26: Blood glucose-, body weight- and body composition development in B6.C3H-*Cdp7*con males. Blood glucose (A) and body weight (B) was measured weekly; fat- and lean mass was measured by nuclear magnetic resonance spectroscopy (NMR) at week 15 of age (B). Dots represent single animals (A) or mean values ± SEM (B) from 11-13 mice. 2-way-ANOVA followed by Bonferroni's multiple comparisons test, *p< 0.05, **p<0.01, ***p<0.001

3.5.2.2.2 Glucose- and insulin tolerance

For the intraperitoneal glucose tolerance test (i.p. GTT), 13-weeks-old animals were fasted for six hours before they were injected with glucose. At 30, 60 and 120 minutes after the injection, B6.C3H-*Cdp7*con$^{C3H/C3H}$ mice exhibited significantly lower blood glucose levels compared to B6.C3H-*Cdp7*con$^{NZO/NZO}$ mice (Fig. 27A). This was underlined by a significantly smaller area under the curve (*Cdp7*con$^{C3H/C3H}$ 55166 ± 4594, *Cdp7*con$^{B6/B6}$ 72871 ± 3841, p= 0.073).

Decreased blood glucose levels in B6.C3H-*Cdp7*con$^{C3H/C3H}$ mice were accompanied by a relatively lower secretion of insulin during the i.p. GTT, which reached statistical significance 240 minutes after the injection (*Cdp7*con$^{C3H/C3H}$ 1.4 ± 0.2 µg/L, *Cdp7*con$^{B6/B6}$ 3.1 ± 0.7 µg/L, p<0.001) (Fig. 27B).

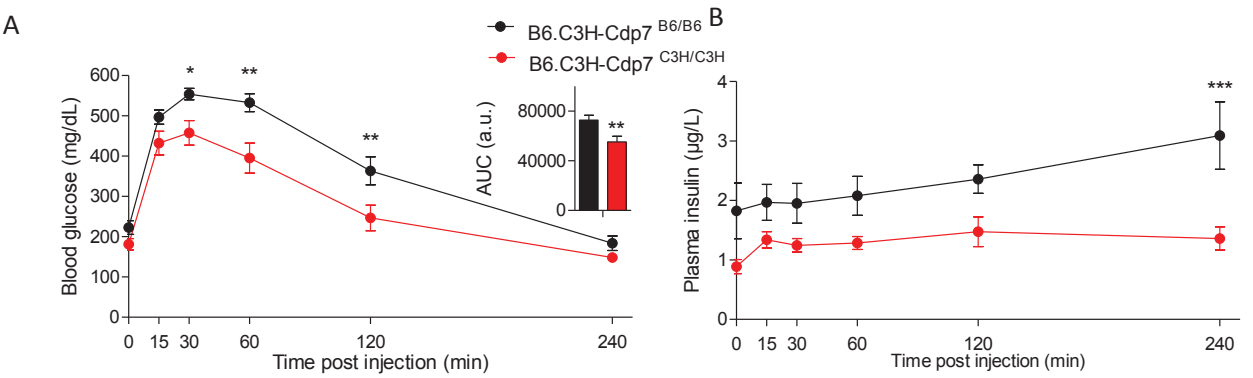

Figure 27: Intraperitoneal glucose tolerance test in B6.C3H-*Cdp7*con males. 13-weeks-old animals were fasted for 16 hours before the injection of glucose (2 g/ kg). Blood glucose- (A) and plasma insulin levels (B) were measured before (0 minutes), as well as at 15, 30, 60, 120, and 240 minutes after the glucose injection. Data represent mean values ± SEM from 11-13 mice. 2-way-ANOVA followed by Bonferroni's multiple comparisons test (blood glucose- and plasma-insulin development) and unpaired t-test, two-tailed (AUC), *p< 0.05, **p< 0.01, ***p< 0.001. AUC= area under the curve, a.u. = arbitrary units

In addition, B6.C3H-*Cdp7*con$^{C3H/C3H}$ mice exhibited lower blood glucose levels compared to B6.C3H-*Cdp7*con$^{B6/B6}$ mice during the intraperitoneal insulin tolerance (i.p. ITT), which was executed in 15-weeks-old not-fasted animals. The improved insulin-sensitivity of B6.C3H-*Cdp7*con$^{C3H/C3H}$ mice was further represented with a significantly smaller area under the curve (*Cdp7*con$^{C3H/C3H}$ 8159 ± 423, *Cdp7*con$^{B6/B6}$ 9943 ± 599) (Fig. 28).

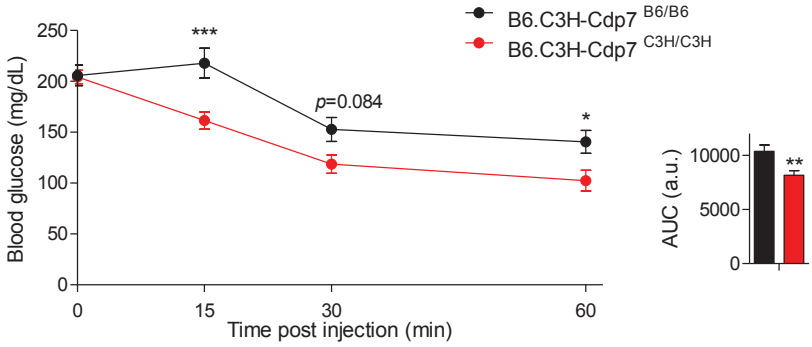

Figure 28: Intraperitoneal insulin tolerance test in B6.C3H-*Cdp7*con males. Blood glucose levels from 15-weeks-old (not fasted) animals were measured before (0 minutes), as well as at 15, 30 and 60 minutes after the injection of insulin (1 U/ kg body weight). Data represent mean values ± SEM from 11-13 mice. 2-way-ANOVA followed by Bonferroni's multiple comparisons test (blood glucose development) and unpaired t-test, two-tailed (AUC), *p< 0.05, ** p< 0.01, *** p< 0.001. AUC= area under the curve, a.u. = arbitrary units

3.5.2.2.3 Final plasma insulin-, C-peptide- and total pancreatic insulin levels

Plasma levels of insulin and C-peptide, as well as total pancreatic insulin concentrations were measured from 6 hours fasted animals after sacrificing at 21 weeks of age. In the plasma from B6.C3H-*Cdp7*con$^{C3H/C3H}$ mice, significantly lower levels of insulin (*Cdp7*con$^{C3H/C3H}$ 1.3 ± 0.3 µg/L, *Cdp7*con$^{B6/B6}$ 4.5 ± 0.8 µg/L, p=0.004) (Fig. 29A) and C-peptide (*Cdp7*con$^{C3H/C3H}$ 1 ± 0.2 µg/L, *Cdp7*con$^{B6/B6}$ 2.7 ± 0.4 µg/L, p<0.001) (Fig. 29B) were measured compared with levels in B6.C3H-*Cdp7*con$^{B6/B6}$ mice. In contrast, total pancreatic insulin levels were not different between the genotypes (Fig. 29C).

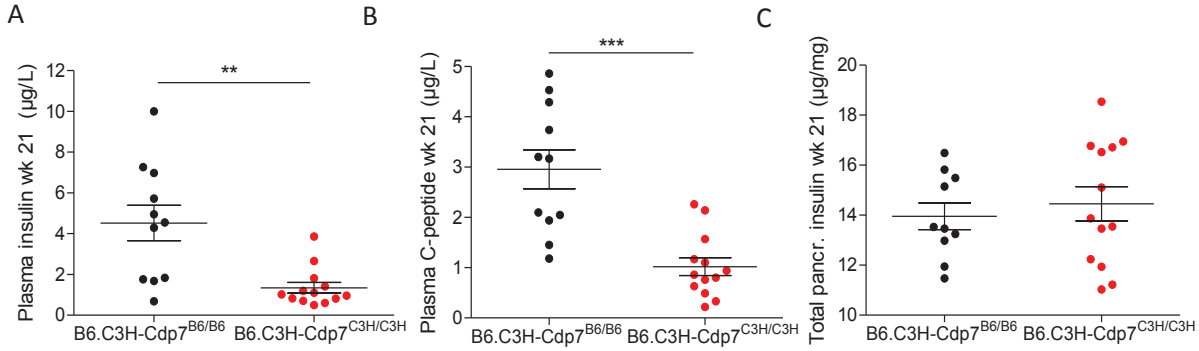

Figure 29: Plasma insulin, plasma C-peptide- and total pancreatic insulin levels in B6.C3H-*Cdp7*con males. 21-weeks-old animals were fasted for 6 hours before sacrificing. Plasma insulin- (A) and C-peptide levels (B) were measured by ELISA. The snap-frozen pancreas was homogenized in acid ethanol. Total pancreatic insulin levels (C) were measured by ELISA and normalized to the total protein content, determined by BCA. Dots represent single animals (n=10-13). Unpaired t-test, two-tailed, **p<0.001, ***p< 0.001

3.6 Strategies for the detection of candidate genes for *Cdp7*-prox

The following chapters focus on strategies for the detection of candidate genes for *Cdp7-prox*, as the most significant QTL for blood glucose and plasma insulin detected in the male N2(NZOxC3H) population. Since the peak position (0 cM) of the strongest blood glucose QTL from the females (*fCdp7-prox*) is located in proximity to *Cdp7-prox* (12 cM), it is possible that both QTL underlie the same gene variant that exerts T2DM-protective effects in both genders. For this reason, the candidate genes which will be presented for *Cdp7-prox* might also be considered as potential candidates for *fCdp7-prox.*

In total, 776 genes are annotated within *Cdp7-prox*, spanning the region from 27- 47 Mb on chromosome 7.

3.6.1 Detection of differential gene expression between the parental strains

One major strategy for the detection of potential candidate genes was the detection of locus-specific differential gene expression between the parental mouse strains C3H and NZO. For this purpose, a DNA microarray analysis was conducted for five tissues collected from 6-weeks-old males: gWAT, BAT, liver, quadriceps and pancreatic islets. Genes mapping within the critical interval and differentially regulated between the two mouse strains are summarized in Figure 30, which also shows the expression ratio C3H / NZO for each gene in the different tissues. In total, 18 genes in the pancreatic islets, 13 genes in gWAT, 10 genes in BAT, 10 genes in liver and 6 genes in the quadriceps muscle were found to be significantly differentially expressed between NZO and C3H; the respective ratios are highlighted in red in the following figure.

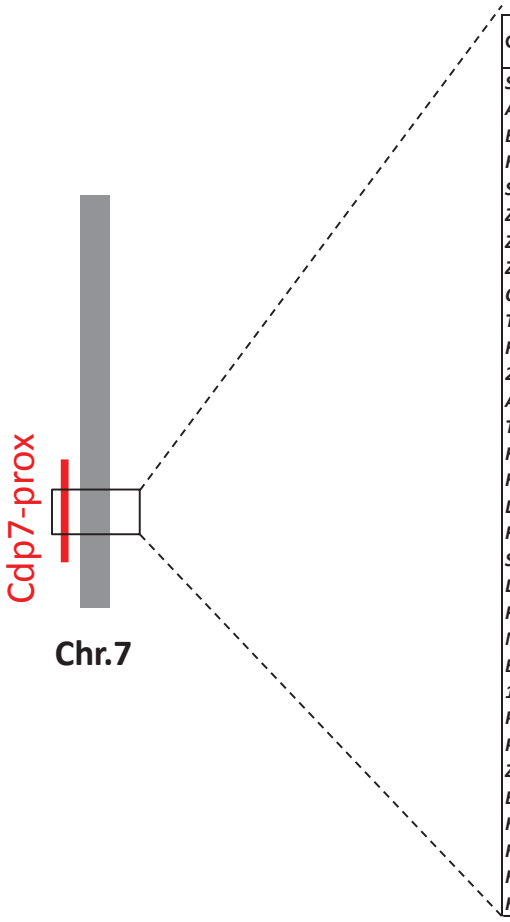

Gene-ID	Mb position	Expression ratio C3H/NZO				
		Liver	Quadr.	gWAT	BAT	Islets
Sync	28.5	1.0	0.9	1.0	0.9	0.2
Actn4	28.9	1.0	1.0	1.1	1.0	1.1
Eif3k	29.0	1.4	1.4	1.1	1.4	1.1
Kcnk6	29.2	1.0	1.0	0.7	0.9	0.7
Spint2	29.3	1.0	0.9	1.9	1.0	1.0
Zfp30	29.8	0.7	0.8	0.9	0.7	0.8
Zfp940	29.8	1.0	1.1	1.1	1.0	1.4
Zfp420	29.7	1.1	1.1	1.2	1.3	0.6
Cox7a1	30.2	1.1	1.1	0.7	1.0	1.0
Tyrobp	30.4	0.9	0.9	0.4	0.9	0.9
Hspb6	30.6	1.2	0.8	1.7	2.1	1.8
2200002J24Rik	30.7	1.1	1.0	1.1	1.0	1.4
Atp4a	30.7	2.1	0.8	1.0	1.1	3.6
Tmem147	30.7	1.3	0.7	1.2	1.1	1.4
Hamp2	30.9	1.7	0.7	1.1	1.0	1.3
Hamp	30.9	2.8	1.3	1.3	0.9	0.8
Lsr	31.0	0.9	1.1	1.5	1.0	1.0
Fxyd3	31.1	1.0	1.0	1.1	1.0	2.0
Scn1b	31.1	1.1	1.0	0.9	1.4	1.1
Lrp3	35.2	1.0	0.7	0.9	0.6	0.9
Rhpn2	35.4	1.4	1.1	1.3	1.5	1.2
Nudt19	35.5	2.2	1.4	1.5	1.4	1.4
B230322F03Rik	35.6	1.0	1.0	1.1	1.2	1.5
1600014C10Rik	38.2	0.8	0.8	0.7	0.9	0.9
Plekhf1	38.2	1.3	1.8	0.9	1.1	0.9
Pop4	38.3	0.5	0.8	0.7	0.7	0.6
Zfp715	43.3	1.4	1.6	1.5	1.9	1.9
Etfb	43.4	1.0	0.9	0.7	0.8	0.9
Klk1b22	44.1	3.3	12.0	4.3	9.4	7.4
Klk1b4	44.2	1.3	1.0	0.9	1.1	0.3
Klk1b5	44.2	1.1	1.0	1.0	1.1	0.2
Klk1	44.2	1.0	1.1	0.9	0.8	0.2

Figure 30: Differential mRNA expression in the peak region of *Cdp7-prox* detected in the microarray analysis. The genes are listed by their chromosomal position from 28.5 to 44.2 Mb according to ENSEMBL (build 74). Relative gene expression is shown with the expression ratio C3H/NZO for the liver, quadriceps, gWAT, BAT and pancreatic islets. Significant ($p < 0.05$) differential gene expression (calculated by one-sided Wilcoxon signed rank test) is marked in red. Quadr= quadriceps, BAT= brown adipose tissue, gWAT= gonadal white adipose tissue, Mb= mega base pairs, Chr.= Chromosome

To validate the differences from the microarray analysis, expression of each gene was further analysed by qPCR. Moreover, gene expression was analysed in tissues from 21-weeks-old C3H and NZO mice (except for the pancreatic islets which were only collected from 6-week old mice) to ensure the stability of the expression difference over time. In addition, genes which are annotated in this region but were not analysed in the microarray were included in the qPCR analysis. The gene *Gpi1* is one of the genes which were not interrogated by the microarray analysis; however, the qPCR revealed differentially expression between C3H and NZO across the tissue panel at juvenile (6 weeks) as well as adult (21 weeks) age (Tab. 19).

Out of 18 pancreatic islet genes that were found to be significantly differentially expressed in the microarray analysis, 14 genes (*Ackn4, Kcnk6, Zfp940, Zfp420, Hspb6, 22000002J24Rik, Atp4a, Fxyd3, Nudt19, B230322F03Rik, Pop4, Zfp15, Klk1b22, Klk1b4*) were validated, whereas four genes (*Tmem147*, *Sync*, *Klk1* and *Klk1b5*) were not differentially expressed in the qPCR.

In liver tissue, seven of ten genes (*Zfp30*, *Atp4a*, *Hamp2*, *Hamp*, *Nudt19*, *Pop4*, *and Klk1b22*) were validated by qPCR. Except for *Pop4*, the same expression differences were observed in livers collected from 21-weeks-old mice. In contrast, the expression differences of the remaining three liver genes (*Eifk3*, *Rhpn2* and *Zfp715*) were not confirmed in the qPCR analysis.

In quadriceps muscle, three out of six genes (*Tmem147*, *Nudt19* and *Klk1b22*) were validated for differential expression at 6- and 21 weeks of age, whereas the expression of the other three genes (*Eifk3*, *Plekhf1* and *Zfp715*) was not confirmed by qPCR.

The expression differences for seven gWAT genes (*Kcnk6*, *Spint2*, *Cox7a1*, *Tryobp*, *Hsp6b*, *Nudt19* and *Klk1b22*) were validated, whereas six genes (*Ackn4, Lsr*, *1600014C10Rik*, *Pop4*, *Zfp715* and *Etfb*) failed to be validated in the qPCR analysis. The stability of the differential gene expression was only confirmed for the two genes *Hspb6* and *Klk1b22*. In contrast, expression of *Kcnk6*, *Spint2*, *Cox7a1* and *Nudt19* was not different between adult (21-weeks-old) C3H and NZO mice. For the gene *Tryobp* a contrary expression pattern could be observed in juvenile and adult mice.

In BAT, four genes were confirmed for differential gene expression at 6- as well as 21 weeks of age, whereas the validation for *Eif3k*, *Scn1b*, *Lrp3*, *Pop4* and *Zfp715* failed in the qPCR analysis.

In total, three genes were shown to be differentially expressed across the tissue panel. *Gpi1* revealed to be upregulated in all NZO tissues, whereas the expression of *Nudt19* and *Klk1b22* was higher in all the C3H tissues. The strongest expression difference was observed for *Klk1b22* which was exclusively expressed in C3H, but not in any of the tissues tested from NZO.

Table 19: Differential gene expression between the parental strains in the peak region of *Cdp7-prox* at 6- and 21 weeks of age. The expression was analysed by qPCR and normalized to the expression of *Actb* (liver, gWAT, BAT and quadriceps) or *Tbp* (pancreatic islets), respectively. The genes are listed according their chromosomal position on chromosome 7 and the relative gene expression is shown with the ratio C3H/NZO. Unpaired t-test, two-tailed,*p<0.05, **p<0.01, ***p<0.001, n=6-8. BAT= brown adipose tissue, gWAT= gonadal white adipose tissue, Mb-Pos= mega base pair position, wk= week

		Expression ratio C3H / NZO ($2^{-\Delta\Delta CT}$)								
		liver		Quadriceps		gWAT		BAT		islets
Gene	Mb-Pos	6 wks	21 wks	6 wks	21 wks	6 wks	21wks	6 wks	21 wks	6 wks
Actn4	28.9									0.8***
Kcnk6	29.2					0.7*	0.8			0.7*
Spint2	29.2					11.1*	1.6			
Zfp30	29.8	0.4***	0.4***					0.4 **	0.4 **	
Zfp940	29.8									17***
Zfp420	29.9									0.3***
Cox7a1	30.2					0.6*	0.2			
Tyrobp	30.4					0.2***	2.0 ***			
Hspb6	30.6					3.7*	2.1*			4.5***
2200002J24 Rik	30.7									4.6***
Atp4a	30.7	3.9 ***	4.3***							2.7***
Tmem147	30.7			0.5**	0.7*					
Hamp2	30.9	2.3*	1.7*							
Hamp	30.9	7.0*	2.5 ***							
Fxyd3	31.1									6.0***
Gpi1	34.2	0.4***	0.3***	0.3***	0.05*	0.3**	0.2**	0.5**	0.5 **	0.2***
Rhpn2	35.4							2.4 **	1.8***	
Nudt19	35.5	2.5***	3.2***	4.2*	1.4***	2.7**	0.9	1.6 **	2.0***	1.2**
B230322F0 3Rik	35.6									1.7***
Pop4	38.3	0.7***	0.9							0.5***
Zfp715	43.3									0.7***
Klk1b22	44.1	10815**	415***	2284***	1459***	349***	949***	591**	2206***	2156**
Klk1b4	44.2									0.1**

3.6.2 Haplotype analysis of the parental strains

The SNP database from the Wellcome Trust Sanger Institute (Keane et al., 2011; Yalcin et al., 2011) was used to identify genes within *Cdp7-prox* carrying polymorphic SNPs between C3H and NZO (Fig. 31A). Furthermore, the frequency of polymorphic SNPs was determined to dissect *Cdp7-prox* into regions that are identical by descent (IBD) and regions that are polymorphic (non-IBDs) between the two strains. For this purpose, windows of 250 kbp and a threshold of 200 SNPs/ window (mean SNP frequency: 50 SNPs/ window) were chosen to calculate a score. Regions exceeding the threshold of 200 SNPs/ window were considered as non-IBDs, whereas regions with a lower SNP frequency were referred to as IBD regions (Fig. 31B). Since the genome from the C3HeB/FeJ strain has not been sequenced and thus is not listed in the database, the sequence from the closely related C3HeB/HeJ strain was used instead.

Out of 559 genes annotated in the database for *Cdp7-prox* (27- 47 Mb), 469 genes were identified carrying polymorphic SNPs, i.e. variant nucleotides between C3H and NZO. By excluding all genes that mapped to non-variant, i.e. IBD regions, the number of candidate genes was narrowed down to 374 genes. The full list of these genes is shown in the supplement (Suppl. Tab. 13). This list includes 18 of 23 genes that were revealed from the gene expression analysis, whereas the other five genes failed to contain polymorphic SNPs (*Kcnk6*, *Cox7a1*, *Klk1b22*, and *Klk1b4*) or resided in an IBD-region (*Spint2*).

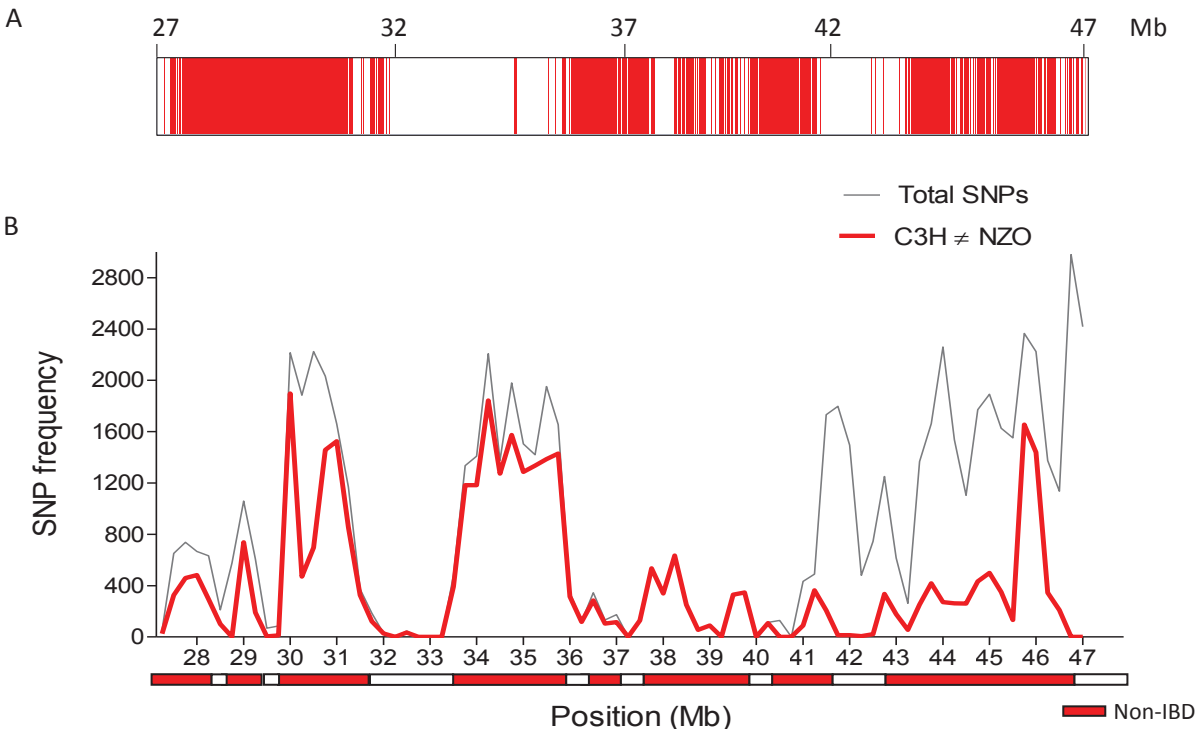

Figure 31: Haplotype analysis of the parental strains in the peak region of *Cdp7-prox*. A: Each single nucleotide polymorphism (SNP) polymorphic between the parental strains C3HeB/HeJ and NZO within the critical region (27- 47 Mb) is presented with a red vertical line. B: Visualization of the number of polymorphic SNPs from A per 250 kb (red line) for the dissection of *Cdp7-prox* into IBD- and non-IBD regions. Genomic regions containing less than 200 polymorphic SNPs per 250 kb are considered as identical between the strains (identical by descent, IBD) and are represented with the white boxes. In contrast, regions containing more than 200 polymorphic SNPs per 250 kb are designated as polymorph (non-IBDs) and are shown with the red boxes. The grey line shows total number of SNPs annotated for C57BL/6J reference genome. Mb= mega base pairs

3.6.3 Detection of expression QTL and correlation analysis in the N2(NZOxC3H) population

3.6.3.1 Expression QTL analysis

Another strategy that was used for the identification of candidate genes was the detection of so called expression quantitative loci (eQTL), in which mRNA transcript levels were used as quantitative traits and mapped to the genome in a linkage analysis. Table 20 shows all genes that were analysed in the N2 population and the results of the subsequent linkage analysis. The genes were selected based on their differential gene expression in the parental strains (3.6.1).

Out of six genes that were analysed in the N2 livers, four genes (*Atp4a*, *Nudt19*, *Pop4* and *Klk1b22*) mapped to their coding region on chromosome 7 (*cis*-eQTL) (Bachelor thesis Miriam Weyers, 2015). In addition, two *trans*-regulating regions (*trans*-eQTL) for the expression of *Pop4* were detected on chromosomes 1 and 19. For the gene *Hamp* a *trans*-eQTL was detected on chromosome 5, whereas the expression of *Hamp2* did not reveal any linkage in the genome. All four genes (*Zfp30*, *Rhpn2*, *Nudt19*, *and Klk1b22*) which were analysed in the BAT of the N2 population revealed *cis*-eQTLs on chromosome 7 located within the metabolic QTLs (Bachelor thesis Janek Masuch, 2016). Also the expression analysis in the gWAT revealed *cis*-eQTLs for all the four analysed genes (*Tryobp*, *Hspb6*, *Gpi1* and *Klk1b22*) and exposed an additional *trans*-eQTL for *Hspb6* on chromosome 11 (Bachelor thesis Angela Pelligra, 2016). In skeletal muscle, the expression analysis of the two genes *Nudt19* and *Klk1b22* both revealed *cis*-eQTLs; whereas *Tmem147* appeared to be regulated by a locus on chromosome 1.

Table 20: Summary of the eQTL analysis of candidate genes for *Cdp7-prox* in the liver, BAT, gWAT, and skeletal muscle of the male N2(NZOxC3H) population. Expression was analysed by qPCR and normalized to the expression of *Actb*. The genes are listed for the different tissues according their chromosomal position on chromosome 7. Genes which were associated with a *cis*-eQTL are marked bolt. The eQTL-analysis was assessed with R/qtl using a 100 permutation test to determine the significance threshold. BAT= brown adipose tissue, gWAT= gonadal white adipose tissue, Mb= mega base pair, pos= position, wk= week

			eQTL analysis			
Tissue	**Gene**	**Mb-Pos**	**Chr.**	**Peak-pos. (cM)**	**max. LOD**	**Peak SNP marker (Mb-pos.)**
Liver	***Atp4a***	30.7	7	11	13.35	37.25
	Hamp2	30.9	/	/	/	/
	Hamp	30.9	5	19	2.4	44.8
	Nudt19	35.5	7	17	8.8	37.25
	Pop4	38.3	7	15.7	2.5	37.25
			1	55	2.2	173
			19	10	2.5	40.3
	Klk1b22	44.2	7	20	39	56.65
BAT	***Zfp30***	29.8	7	0	5.3	16.62
	Rhpn2	35.4	7	17	3	37.25
	Nudt19	35.5	7	12	9	37.25
	Klk1b22	44.2	7	19	33.1	56.65
gWAT	***Troybp***	30.4	7	15.7	4.81	37.25
	Hspb6	30.6	7	6	9.4	16.6
			11	16	3.5	82.7
	Gpi1	34.2	7	14	14.7	37.25
	Klk1b22	44.2	7	21	33.0	56.65
Quadriceps	*Tmem147*	30.7	1	26	3.0	81.37
	Nudt19	35.5	7	15.7	5.6	37.25
	Klk1b22	44.2	7	19	37.5	56.65

Figure 32 shows the LOD score distribution for all the *cis*-eQTLs for each tissue in comparison to the metabolic QTLs for blood glucose, body weight and plasma insulin on chromosome 7.

In all tissues, expression analysis of the gene *Klk1b22* exposed the most significant *cis*-eQTL. Due to the high LOD-score (>33) of the *Klk1b22* eQTL in each tissue, these LOD scores were divided by 5 to allow a better comparison with the QTLs for the metabolic traits. In liver tisue (Fig. 32A), peak positions of all four *cis*-eQTLs (*Atp4a*: 11 cM, *Nudt19*: 17cM, *Pop4*: 15.7 cM and *Klk1b22*: 20 cM) were detected in close proximity to the blood glucose- (12 cM), body weight- and plasma insulin QTL (both 17 cM) peak. Also in skeletal muscle (Fig. 32B), both eQTLs for *Nudt19* (15.7 cM) and *Klk1b22* (19 cM) peaked close to the maximal LOD score positions of the metabolic QTLs. In gWAT, the maximal LOD score of the *Hspb6* eQTL was calculated more proximal (6 cM), whereas the peaks of the other three eQTLs (*Tryobp*: 15.7 cM, *Gpi1*: 14cM, and *Klk1b22*: 21 cM) overlapped with the peak positions of the metabolic QTLs (Fig. 32C). In BAT, the maximal LOD score of the *Zfp30* eQTL was detected at 0 cM and thus did not overlap with the peaks from the other QTLs. In contrast, maximal LOD score for the *Rhpn2* eQTL was detected at 17 cM, which is identical with the maximal LOD score positions of the insulin- and body weight QTLs. Also the peaks of the *Nudt19* (12 cM) - and *Klk1b22* (19 cM) eQTLs were located in close proximity to the peaks of the metabolic QTLs (Fig. 32D).

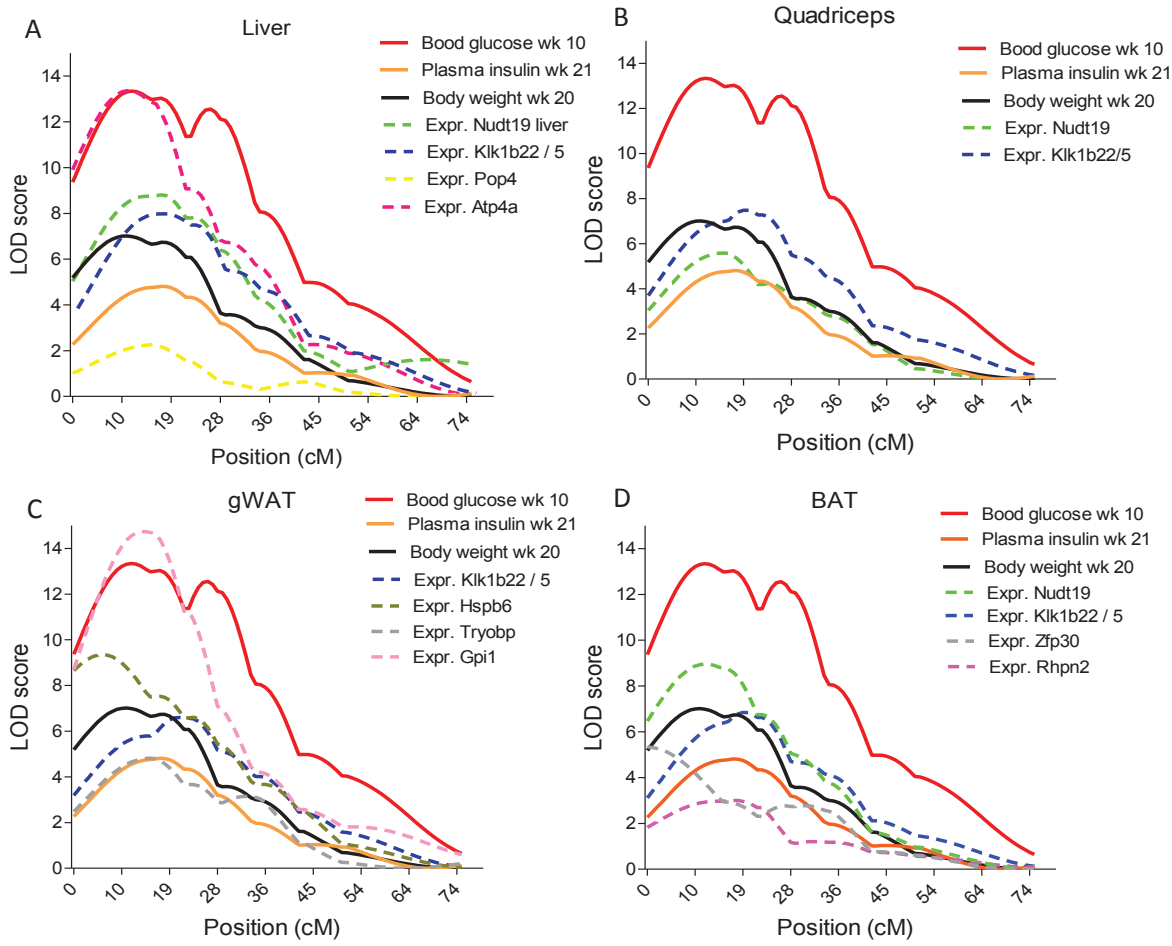

Figure 32: LOD score distribution of all *cis*-eQTLs in comparison with the QTLs for metabolic traits. The eQTLs were detected the liver (A), skeletal muscle (B), gWAT (C) and BAT (D) and compared with the LOD-score patterns of the metabolic QTLs (blood glucose, body weight and plasma insulin) associated with *Cdp7-prox*. The analysis was assessed with R/qtl using a 100 permutation test to determine the significance threshold. The LOD-scores from the *Klk1b22* eQTL were divided by five to allow a better comparison with the other QTLs. LOD= logarithm of the odds, Expr= expression, wk= week, BAT= brown adipose tissue, gWAT= gonadal adipose tissue

3.6.3.2 Correlation analysis

The mRNA transcript levels were further used to investigate potential correlations with *Cdp7-prox*-associated phenotypes (body weight, blood glucose ans plasma insulin) in the N2(NZOxC3H) population. The correlation analysis was conducted in dependence of the genotype for *Cdp7-prox* (*Cdp7-prox*$^{C3H/NZO}$ or *Cdp7-prox*$^{NZO/NZO}$). With exception of the skeletal muscle, significant correlations were identified in each tissue (Tab. 21). All significant correlations are shown as dot plots in the supplement (Suppl. Fig. 5 - 7).

Expression of *Klk1b22* and *Atp4a* in the liver did not correlate with any trait. By contrast, expression of hepatic *Nudt19* significantly negatively correlated with final plasma insulin levels in *Cdp7-prox*$^{NZO/C3H}$ mice (Suppl. Fig. 5A), whereas mRNA levels of hepatic *Pop4* correlated positively with final blood glucose in *Cdp7-prox*$^{NZO/NZO}$ animals (Suppl. Fig. 5B).

In BAT, significant mRNA-phenotype correlations were exclusively found in heterozygous allele carriers for *Cdp7-prox*. Expression of *Zfp30* correlated negatively with body weight (Suppl. Fig. 6A) as well as a positively with blood glucose levels (Suppl. Fig. 6B). Further significant correlations with blood glucose were observed for expression of *Rhpn2* (negative, Suppl. Fig. 6C) and *Klk1b22* (positive, Suppl. Fig. 5D). In addition, expression of *Klk1b22* showed a negative correlation with final plasma insulin levels (Suppl. Fig. 6E).

In gWAT, expression of *Hspb6* correlated negatively with body weight in both genotypes (*Cdp7-prox*$^{NZO/C3H}$: Suppl. Fig. 7A, *Cdp7-prox*$^{NZO/NZO}$: Suppl. Fig. 7B). In the homozygous allele carriers, *Hspb6* mRNA levels correlated negatively with plasma insulin levels (Suppl. Fig. 7C). Another negative correlation with plasma insulin levels was found for the expression of *Klk1b22* in the heterozygous animals (Suppl. Fig. 7D).

Table 21: Summary of the genotype- dependent correlation analysis of mRNA levels from candidate genes with *Cdp7-prox* associated metabolic traits in the male N2(NZOxC3H) population. The genes are listed for the different tissues (liver, BAT, gWAT and quadriceps) according their chromosomal position on chromosome 7. Significant ($p < 0.05$) correlations are marked in bolt. The p-value was calculated by linear regression. Quadr.= quadriceps, BAT= brown adipose tissue, gWAT= gonadal adipose tissue, wk= week

		Expression-phenotype correlation (p-value)					
		Body weight wk 21		**Blood glucose wk 21**		**Insulin wk 21**	
Tissue	Gene	Cdp7 $^{C3H/NZO}$	Cdp7 $^{NZO/NZO}$	Cdp7 $^{C3H/NZO}$	Cdp7 $^{NZO/NZO}$	Cdp7 $^{C3H/NZO}$	Cdp7 $^{NZO/NZO}$
Liver	*Atp4a*	0.5576	0.7934	0.0978	0.9823	0.9905	0.8405
	Nudt19	0.6367	0.4774	0.1071	0.0657	**0.0149**	0.3202
	Pop4	0.9189	0.5833	0.6509	**0.0379**	0.8935	0.5111
	Klk1b22	0.7306	0.5253	0.1961	0.9467	0.7818	0.9293
BAT	*Zfp30*	**0.0106**	0.0916	**0.0208**	0.3282	0.2206	0.2039
	Rhpn2	0.2197	0.2543	**0.0014**	0.7127	0.1478	0.1553
	Nudt19	0.1096	0.5228	0.8158	0.8141	0.2694	0.4094
	Klk1b22	0.6526	0.7905	**0.006**	0.5748	**0.0159**	0.4148
gWAT	*Troybp*	0.7593	0.2726	0.3605	0.1476	0.8633	0.1847
	Hspb6	**0.0144**	**0.0165**	0.936	0.0712	0.7537	**0.0006**
	Gpi1	0.3377	0.3432	0.6682	0.4809	0.1132	0.2532
	Klk1b22	0.2285	0.3104	0.2043	0.9106	**0.0094**	0.3942
Quadr.	*Nudt19*	0.1049	0.7422	0.5391	0.5697	0.7364	0.4339
	Klk1b22	0.3187	0.1969	0.4846	0.876	0.8513	0.1131

3.7 Prioritization of candidate genes and validation of differential expression in RCS.NZO.C3H-*Cdp7*con mice

For the prioritization of candidate genes, the results from the different approaches were combined to search for an overlap. Out of 23 candidate genes that revealed differential expression in the parental mouse strains (3.6.1), five genes could be excluded by the haplotype analysis (3.6.2). In addition, the eQTL analysis in the N2(NZOxC3H) population was further able to exclude the candidacy of three further genes (3.6.3.1). Subsequently, by the combination of the different approaches the number of candidates for *Cdp7-prox* was narrowed down to 15 genes as most likely causative genes.

The mRNA expression of these 15 genes was further analysed in tissues from NZO.C3H.*Cdp7*con males to confirm differential gene expression between genotypes. In addition, due to its outstanding expression difference between the parental mouse strains and between the genotypes from the N2(NZOxC3H) population across the tissue panel, the gene *Klk1b22* was included in the RCS expression analysis. The tissues were selected based on their differential gene expression in the parental strains (Tab. 19). Indeed, differential gene expression between the genotypes could be recovered for most of the genes. Thus, all six genes that were differentially regulated in the liver of the parental strains (*Zfp30, Atp4a, Gpi1, Nudt19, Pop4, and Klk1b22*) further revealed differential expression between the two genotypes from NZO.C3H.*Cdp7*con. In quadriceps muscle, the expression differences for *Gpi1* and *Klk1b22* could be recovered, whereas *Nudt19* was equally expressed between the RCS genotypes. In gWAT, five genes (*Kcnk6*, *Hspb6*, *Gpi1*, *Nudt19*, and *Klk1b22*) were differentially regulated, only the expression of *Tryobp* was comparable between the genotypes. Except for *Rhpn2*, differential expression of the other four BAT genes (*Zfp30*, *Gpi1*, *Nudt19*, and *Klk1b22*) was recovered. From 14 genes that were analysed in the pancreatic islets, 10 genes (*Zfp940*, *Zfp420*, *Hspb6*, *2200002J24Rik*, *Atp4a*, *Fxyd3*, *Gpi1*, *Nudt19*, *Pop4*, and *Klk1b22*) could be confirmed for differential gene expression in the NZO.C3H.*Cdp7*con mice, whereas the expression of the three genes *Zfp715, Ackn4,* and *B230322F03Rik* was not different. In summary, after excluding the genes that were not confirmed for differential gene expression between the genotypes from RCS.NZO.C3H-*Cdp7*con, 12 candidate genes were left for *Cdp7-prox* (Tab. 22). In line with the results from the expression analysis of the paretal strains, the most striking expression differences were found for the gene *Klk1b22* whose expression was detectable exclusevely in NZO.C3H.*Cdp7*con$^{C3H/C3H}$ mice.

Table 22: Differential gene expression of candididates for *Cdp7-prox* in RCS.NZO.C3H-*Cdp7*con mice. Expression was analysed by qPCR and normalized to the expression of *Actb* (liver, gWAT, BAT and quadriceps) or *Tbp* (pancreatic islets), respectively. The islets were collected at 6- and all other tissues at 17 weeks of age. Relative gene expression is shown with the ratio *Cdp7*con$^{C3H/C3H}$/ *Cdp7*con$^{NZO/NZO}$. Unpaired t-test, two-tailed, **p*<0.05, ***p*<0.01, ****p*<0.001, n=5-8. BAT= brown adipose tissue, gWAT= gonadal white adipose tissue, Mb= mega base pairs.

Gene ID	Mb Position	Expression ratio *Cdp7*con$^{C3H/C3H}$ / *Cdp7*con$^{NZO/NZO}$ ($2^{-\Delta\Delta CT}$)				
		Liver	Quadriceps	gWAT	BAT	Islets
Kcnk6	29.2			0.7 *		
Zfp30	29.8	0.3 ***			0.4 ***	
Zfp940	29.8					17.1 ***
Zfp420	29.9					0.3 ***
Hspb6	30.6			4.7 **		4.5 ***
2200002J24Rik	30.7					4.6 ***
Atp4a	30.7	4.3 **				2.7 ***
Fxyd3	31.1					6.0 ***
Gpi1	34.2	0.1 **	0.1 ***	0.2 ***	0.2 ***	0.2 ***
Nudt19	35.5	2.8 ***		1.4 **	1.7 ***	1.2 **
Pop4	38.3	0.5 **				0.5 ***
Klk1b22	44.1	479 **	2071 ***	3781 ***	1151 ***	2155.7 **

3.8 Functional investigation of selected candidate genes

3.8.1 Impact on glucose-stimulated insulin secretion (GSIS) in MIN6 cells

Based on their differential gene expression in the pancreatic islets of the parental strains (Tab. 19) and the two genotypes from RCS.NZO.C3H-*Cdp7*con (Tab. 22), seven genes (*Nudt19*, *Fxyd3*, *Pop4*, *Atp4a*, *Hspb6*, *Zfp420,* and *Klk1b22*) were investigated in regard to a potential impact on glucose-stimulated insulin secretion (GSIS) in MIN6 cells, a murine *in vitro* model for pancreatic β-cells.

3.8.1.1 Investigation of GSIS after knockdown of *Nudt19*, *Fxyd3*, *Pop4*, *Atp4a*, *Hspb6*, and *Zfp420*

The knockdown of the six genes *Nudt19*, *Fxyd3*, *Pop4*, *Atp4a*, *Hspb6*, and *Zfp420* in MIN6 cells was achieved by the electroporation of specific siRNA oligonucleotides (2.2.3.2.2). The knockdown-efficiency was confirmed by analysis of the mRNA expression via qPCR. The lowest knockdown-efficiency with 61 % was achieved for *Zfp420*. For the five other genes, mRNA levels could be reduced by 81 to 96 % (Fig. 33A). In the subsequent assay, no differences in insulin secretion were observed between control- (non-target siRNA-tranfected) and knockdown (target-siRNA- transfected) cells at fasted state (0 mM glucose). In contrast, after glucose stimulation (25 mM glucose) a significantly lower insulin secretion was observed for *Pop4*- (approx. 50% reduction) and *Atp4a*- (approx. 40 % reduction) knockdown cells (Fig. 33B).

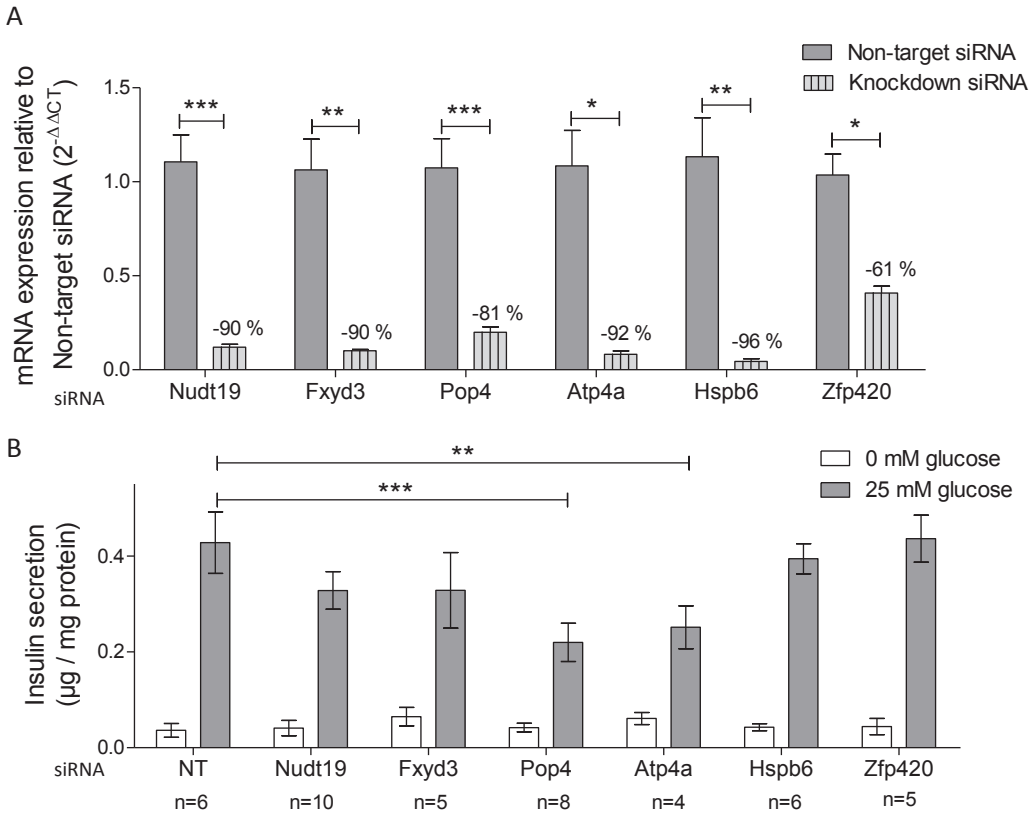

Figure 33: Glucose-stimulated insulin secretion (GSIS) in MIN6 cells after knockdown of six candidate genes from the pancreatic islets. The knockdown of the genes *Nudt19*, *Fxyd3*, *Pop4*, *Atp4a*, *Hspb6,* and *Zfp420* was achieved by electroporation of specific siRNA oligonucleotides. The mRNA expression (analysed by qPCR with *Actb* as housekeeper (A)) and insulin secretion (B) of all knockdown cells were compared to non-target (NT) siRNA- transfected control cells. Data represent mean values ± SEM from 4- 10 independent experiments. Unpaired t-test, two-tailed (A) and 2- way-ANOVA with Bonferroni's multiple comparisons test (B), **p< 0.01. ***p< 0.001

3.8.1.2 Investigation of GSIS after overexpression of *Klk1b22*

Expression of the candidate gene *Klk1b22* in MIN6 cells was achieved by electroporation of an expression plasmid (2.2.3.2.2) for the protein. The success of the transfection was confirmed by the analysis of mRNA expression via qPCR, which revealed a difference of 20 Ct (cycle of threshold) between *Klk1b22* plasmid-transfected cells and controls (*GFP* plasmid-transfected) (Fig. 34A). In the subsequent assay, neither at fasted state (0 mM glucose) nor upon glucose-stimulation (25 mM glucose) differences in insulin secretion between control- and *Klk1b22* overexpressing cells could be observed (Fig. 34B).

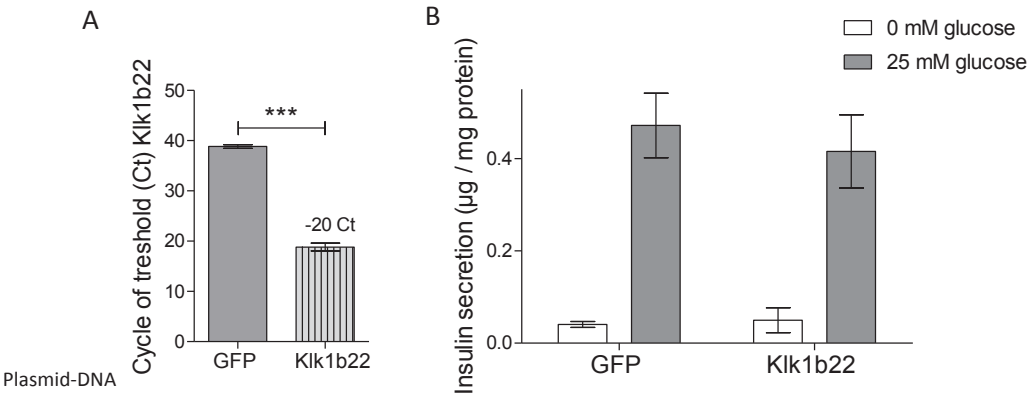

Figure 34: Glucose-stimulated insulin secretion (GSIS) in MIN6 cells after overexpression of *Klk1b22*. The overexpression was achieved by electroporation of a plasmid-DNA. The mRNA expression of *Klk1b22* (analysed by qPCR with *Actb* as housekeeper (A)) and insulin secretion (B) of *Klk1b22* plasmid-DNA transfected cells was compared to *GFP* plasmid-DNA transfected control cells. Data represent mean values ± SEM from 5 independent experiments. Unpaired t-test, two-tailed (A) and 2- way-ANOVA with Bonferroni's multiple comparisons test (B), ***p< 0.001

3.8.2 Investigation of fatty acid β-oxidation (FAO) in Hepa 1-6 cells after knockdown and overexpression of *Nudt19*

Literature research on the candidate gene *Nudt19* revealed a potential connection with fatty acid metabolism. For this reason, the gene was tested for a potential impact on fatty acid β-oxidation (FAO) using cultivated murine liver (Hepa 1-6) cells. By the use of specific siRNA oligonucleotides, mRNA expression of *Nudt19* was reduced by 67 % (Fig. 35A). As a consequence, an approx. 40 % increase of ^{14}C-labelled palmitate β-oxidation was measured in *Nudt19* siRNA-transfected cells at basal state compared to non-target siRNA-transfected control cells (Fig. 35B). Moreover, application of the control compound FFCP, which acts as uncoupler of the mitochondria and therefore serves for the measurement of the maximal respiratory mitochondrial capacity, led to an additional ~20 % increase of the β-oxidation in *Nudt19*- transfected cells compared to controls. The overexpression of *Nudt19* was achieved by the transfection of an expression plasmid for NUDT19. Increased mRNA abundance was confirmed by qPCR which revealed a reduction of 9.6 Ct in *Nudt19* plasmid-DNA-transfected cells, compared to *GFP* plasmid-DNA-transfected control cells (Fig. 35C). Subsequently, the overexpression of *Nudt19* led to a ~30 % decrease of basal ^{14}C-labelled palmitate β-oxidation compared to control cells (Fig. 35D).

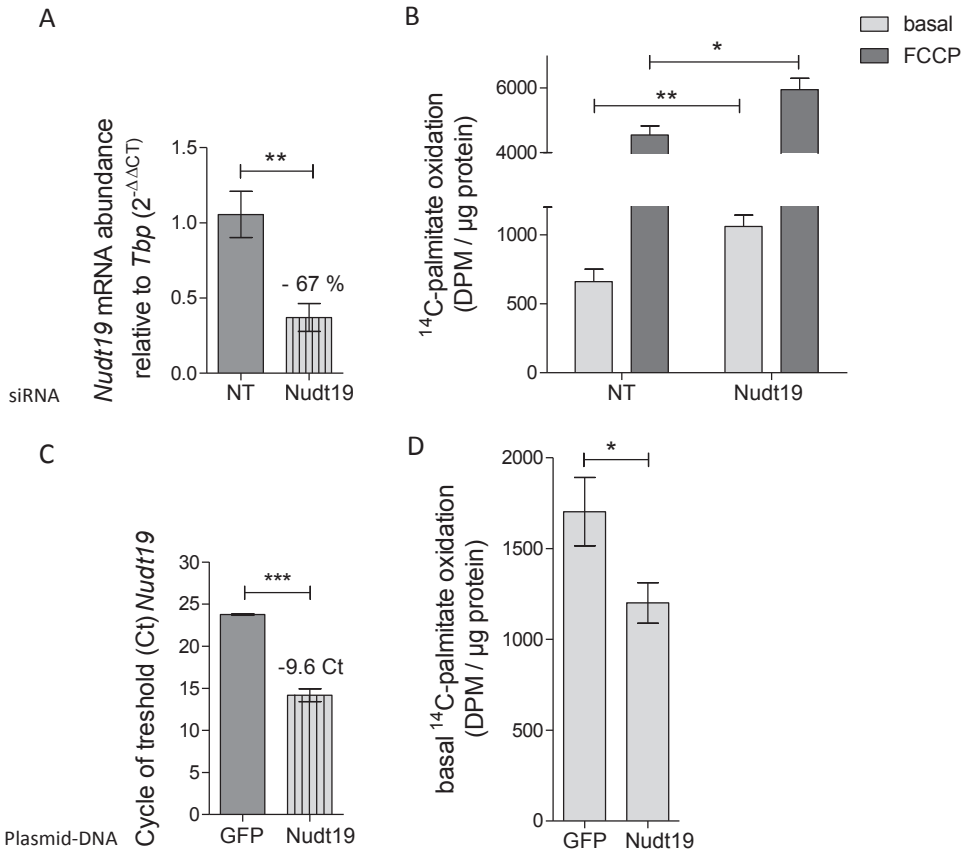

Figure 35: Fatty acid β-oxidation in Hepa 1-6 cells after knockdown and overexpression of *Nudt19*. The knockdown was achieved using Lipofectamine RNAimax and overexpression by the use of Lipofectamin 2000. The mRNA expression of *Nudt19* siRNA-transfected cells (analysed by qPCR with *Tbp* as housekeeper (A)) and ^{14}C-labelled palmitic acid β-oxidation (basal- and FCCP- stimulated (B)) was compared to non-target (NT) siRNA-transfected cells as controls. The mRNA expression of *Nudt19* plasmid-DNA-transfected cells (analysed by qPCR (C)) and basal ^{14}C-labelled palmitic acid β-oxidation (D) was compared to *GFP* plasmid-DNA-transfected cells as controls. Data represent mean values ± SEM from 6-7 independent experiments, Unpaired t-test, two-tailed, *p< 0.05, **p< 0.01, ***p< 0.001. FFCP= Carbonyl cyanide-4-(trifluoromethoxy) phenylhydrazone, NT= Non-target

4 Discussion

In order to further elucidate the genetic architecture of T2DM, the aim of this study consisted in the identification of novel susceptibility genes for T2DM-related traits. For this purpose, a novel crossbreeding approach of obese and T2DM-susceptible NZO with lean C3H mice was conducted. Subsequent linkage scan of the N2(NZOxC3H) population revealed a novel T2DM modifier QTL (*Cdp7-prox*) on proximal chromosome 7. In this study, the locus was further characterized by the generation of RCS and a combined approach of gene expression- and haplotype analysis was used to filter for the most likely candidate genes underlying the QTL.

4.1 Metabolic features of the different mouse generations

4.1.1 NZO and C3H strains are metabolically diverse

The first requirement for the detection of a QTL is the selection of two animal groups that differ in the phenotype of interest (Clee and Attie, 2007). For the identification of novel T2DM-related QTLs, two strains were selected that strongly differ in their susceptibility for the disease. The NZO strain represents an established model for polygenetic T2DM. In response to a HFD, NZO males display all features of the human metabolic syndrome, including early-onset adiposity, insulin resistance, hyperinsulinemia, hyperglycaemia, progressing into severe β-cell loss at later stages of the disease disease (Herberg and Coleman, 1977; Joost and Schurmann, 2014; Ortlepp et al., 2000). By contrast, the lean C3H strain seems to be relatively resistant towards the development of T2DM (Clee and Attie, 2007). The diverse metabolic features of the two mouse strains were further confirmed in this study. As expected, both genders from the NZO strain gained significantly more body weight compared to C3H animals. The differences in body weight were already significant after weaning at 3 weeks of age for the males (Fig. 8A) and at 4 weeks of age for the females (Fig. 8B), clearly demonstrating a genetic origin for the observed differences. In both genders, the increases in body weight were mainly due to increases in fat mass (Fig. 8C+D). In line with the typical course of the disease in humans, obesity mediated a stage of insulin resistance, as male- as well as female NZO mice exhibited clearly higher levels of plasma insulin compared to C3H animals (Fig. 9A+C) to compensate for decreasing efficiency of insulin action. However, severe hyperglycaemia triggered by the gradual loss of pancreatic β-cells, as reflected by significantly lower pancreatic insulin levels compared to C3H (Fig. 9D), was exclusively observed in the NZO males, whereas the females seem to be protected from severe T2DM. This can be explained by the protective influence of the hormone estrogen, which has been shown to protect NZO females from β-cell failure (Lubura et al., 2015; Vogel et al., 2013).

In conclusion, the phenotypic divergence of both strains in basic metabolic traits was confirmed, thereby providing evidence for the suitability of the two strains as breeding partners for the subsequent discovery of obesity- and T2DM- associated QTLs.

4.1.2 N2(NZOxC3H) mice are metabolically heterogeneous and display sex dimorphic phenotypes

The second requirement for the detection of a QTL is the generation of a N2- or F2 population which is heterogeneous for the phenotype(s) of interest (Darvasi, 1998). In contrast to the F1 generation, in which each animal is genetically identical (heterozygous) and therefore typically displays intermediate phenotypes to the parental strains (see Fig. 7+8), each N2- or F2 animal carries a unique combination of parental alleles resulting from genetic recombination events. In this study, a N2 generation was generated by mating F1 (NZOxC3H) males with NZO females. As a consequence, as expected from Mendelian genetics the genome from each backcross mouse consists in theory of 75 % NZO- and 25 % C3H alleles. The increased portion of NZO alleles was supposed to increase the overall prevalence for obesity and T2DM in the population; thereby increasing the probability for the detection of obesity- and T2DM associated QTLs. As expected from their genetic heterogeneity, a wide range of blood glucose levels (Fig. 12A), body weight (Fig. 12B) and body composition (Fig. 12C+D) was observed in both sexes of the N2(NZOxC3H) population. Interestingly, despite the contribution of approx. 25 % alleles from the lean C3H strain, N2 males exhibited equally high blood glucose levels and T2DM-prevalence (NZO 69 %, N2 males 71 %), and gained on average 6 grams more body weight, compared to the parental NZO males. This could be attributed to potentially diabetogenic genes from the C3H genome that might be without an effect in an overall diabetes-protective background; however on a diabetes-susceptible NZO background they might exert diabetogenic effects by the interaction with other genes. Several studies reported different impacts of potentially diabetogenic genes in dependence on the genetic background (Kulkarni et al., 2003; Scherneck et al., 2009; Terauchi et al., 2003), emphasizing the importance of the background strain. The probably most popular example in diabetes research represents the mutation in leptin gene found in *ob/ob* mice, which triggers β-cell failure and severe hyperglycaemia on C57BL/KsJ background. By contrast, on C57BL/6J background, the mutation promotes mild hyperglycaemia; however, these mice are protected from severe β-cell failure (Coleman and Hummel, 1973).

When comparing the males and females from the N2 population, the males exhibited clearly higher blood glucose values compared to the females (Fig. 12A), which was accompanied by a dramatically higher T2DM prevalence and mortality rate. Moreover, the N2 males gained on average more body weight compared to the N2 females, due to a clearly higher gain of lean mass (Fig. 12D), whereas the relative fat mass content was rather higher in the N2 females. These findings are in line with the observed differences in glycaemia and body composition between the two genders from the parental

strains (Fig. 7+8). As already discussed above, despite the development of adiposity and insulin resistance, the N2(NZOxC3H) females seem to be protected from severe T2DM due to hormonal influences (Lubura et al., 2015; Vogel et al., 2013).

4.2 Linkage scan identifies three major QTLs for T2DM-related traits

As expected from the observed metabolic divergence of the parental strains together with the metabolic heterogeneity of the N2 population, the genome-wide linkage analysis revealed numerous QTLs for T2DM- associated traits. In general, the linkage analysis of the N2 males revealed a larger number of significant QTLs (62 in total, Suppl. Tab. 8) compared to the N2 females (28 in total, Suppl. Tab. 9), which can likely be attributed to their clearly higher T2DM-prevalence (males 71 %, females 11 %).

In the males, the strongest QTLs for blood glucose with significance for several life weeks were detected on the chromosomes 4 (*Nir4*), 7 (*Cdp7-prox*) and 15 (*Nir15-prox*) (Fig. 14A). The chromosomes showed different time courses of linkage, indicating that the loci contribute distinctly at different stages in the development of diabetes. *Cdp7-prox* was already significant at 3 weeks of age, clearly indicating that the impact on glycaemia is of genetic origin. Whereas *Cdp7-prox* reaches its maximal statistical significance at 10 weeks of age, *Nir4* did not appear before week 14 and exerts its largest effect at week 20, suggesting that the HFD is the major trigger of the diabetogenic impact. Interestingly, both *Cdp7-prox* and *Nir4* were further associated with body weight development (Fig. 14B) and plasma insulin levels (Fig. 14C), indicating a potential impact on pancreatic islet function. In contrast, *Nir15* revealed significant linkage exclusively with blood glucose levels, rather indicating a central role in the onset of insulin resistance of the peripheral tissues. Chromosome 7 further revealed linkage with blood glucose in the female N2 population, as the only stable significant QTL for glycaemia (*fCdp7-prox*) from the females (Fig. 15). However, the QTL peak was detected at a more proximal position (1 cM) compared to *Cdp7-prox* (12 cM) from the males. The relatively large distance between the two QTLs could be attributed to an imprecise calculation of the linkage analysis, which is limited by the number of SNPs and the size of the population. The other possibility would be that the two QTLs underlie different gene variants with different locations on chromosome 7.

4.3 Characterization of *Cdp7-prox*

4.3.1 *Cdp7-prox* represents a novel diabetes locus

The locus *Cdp7-prox* was the most prominent QTL from the male backcross population, which exhibited the highest LOD score in the linkage analysis for blood glucose- (LOD 13.3) and plasma insulin levels (LOD 4.8) and was further linked with late body weight development (LOD 7.4) (Fig. 14). With the help of the database Diabesitygenes.org (Schmidt et al., 2008), in which T2DM-related QTLs data from 43 genome-wide scans are combined, only one QTL was found that overlapped (by synteny) with the peak position of *Cdp7-prox*, namely the locus *Gisdt1*, which was associated with glucose intolerance in an intercross population of Brown Norway with Spontaneously Diabetic Torii (SDT) rats (Masuyama et al., 2003). However, the causative gene(s) could not have been identified in this study. Further literature research yielded another QTL (*dis1*) associated with defective glucose-mediated insulin secretion, which was recently detected in a crossbreeding between NZO/Wehi and C57BL/6J mice. A sequence variance in the gene *Abcc8* was proposed to underlie the observed deficiencies in insulin secretion of NZO/Wehi mice (Andrikopoulos et al., 2016). However, in context with *Cdp7-prox* the gene *Abcc8* seems to be an implausible candidate, as its mRNA levels in isolated pancreatic islets did neither differ between the parental strains, nor between two genotypes from RCS.NZO.C3H-*Cdp7*con.

4.3.2 The C3H allele for *Cdp7-prox* protects from β-cell failure in the male N2(NZOxC3H) population

Already after weaning, *Cdp7-prox*$^{NZO/NZO}$ mice exhibited significantly higher blood glucose levels, clearly demonstrating an early genetically-driven impact of the QTL. Maximal differences in glycaemia (122 mg/dL) were observed at 10 weeks of age (Fig. 17A), which was accompanied by a 40 % difference in the T2DM prevalence (Fig. 17B). Interestingly, the onset of hyperglycaemia revealed to be independent of the body weight, since the mean body weight values were similar between the genotypes until week 10 (Fig. 17C). The comparable body weight development together with the observation that *Cdp7-prox*$^{NZO/NZO}$ mice exhibited lower levels of plasma insulin at 21 weeks of age (Fig. 17D) suggests that the onset of hyperglycaemia in *Cdp7-prox*$^{NZO/NZO}$ mice resulted from a direct impact of *Cdp7-prox* on pancreatic β-cell function rather than from insulin resistance. With the worsening of the disease, *Cdp7-prox*$^{NZO/NZO}$ animals gained significantly less body weight compared to *Cdp7-prox*$^{NZO/C3H}$ animals (Fig. 17 C), which was due to equal differences in fat- and lean mass. The increasing differences in body weight observed at final stages of age most likely appeared secondarily as a result of a metabolic switch of energy fuels. It is well known that the lack of insulin prevents the uptake of glucose into the tissues. As a consequence, most tissues use alternative energy fuels by the breakdown of fatty acids from fat cells (lipolysis) leading to an increase of acidic

ketone bodies. Acidosis occurs when the levels of ketone bodies exceed the body's buffering capacity (Misra and Oliver, 2015). In addition, the liver generates glucose as energy source through breakdown of protein from muscle tissue, leading to a decline of lean mass (Russell et al., 2009; Wang et al., 2006). In the natural course of the disease, progressive acidosis and loss of proteins lead to death (Palmiere, 2015; Perry et al., 2016). Indeed, the mortality rate was clearly higher in *Cdp7-prox*$^{NZO/NZO}$- compared with *Cdp7-prox*$^{NZO/C3H}$ animals (Fig. 17E), probably as a result of complete depletion of energy fuels. On the other hand, *Cdp7-prox*$^{NZO/C3H}$ animals were largely protected from β-cell loss-mediated hyperglycaemia and subsequent death, demonstrating that the C3H allele, through a yet unknown mechanism, improves pancreatic β-cell health and / or function.

4.3.3 *Cdp7-prox* shows additivity with *Nir4* and *Nir15-prox* in the male N2(NZOxC3H) population

Interestingly, the other two large-effect blood glucose QTLs on chromosomes 4 (*Nir4*, Suppl. Fig. 4C) and 15 (*Nir15-prox*, Suppl. Fig. 4B) showed an additive impact with *Cdp7-prox* on the development of blood glucose levels (Fig. 18A) and T2DM-prevalence (Fig. 18B). The combination of all three risk alleles led to a maximal increase of blood glucose levels and an 89 % T2DM prevalence. This shows that the onset of hyperglycaemia in the male backcross population can almost completely be attributed to limited number of genes that underlie the three loci *Cdp7-prox*, *Nir4* and *Nir15-prox*. This observation seems unexpected when considering that T2DM is assumed to be influenced by dozens of genes scattered all across the genome, each of them contributing to different extents to its pathophysiology (Ali, 2013; Clee and Attie, 2007; Prasad and Groop, 2015). The onset of T2DM due to three loci clearly emphasises the important impacts of the underlying genes. However, since 21 % of the animals carrying the protective allele combination for the three QTL still developed hyperglycaemia, the onset of T2DM in the male backcross population must be triggered by additional factors with smaller effect size.

Surprisingly, despite the observed additive diabetogenic effect on glycaemia, the combination of the risk alleles for *Cdp7-prox* and *Nir4* led to a 16 % increase in survival, compared to mice carrying only the risk allele for *Cdp7-prox* (Fig. 18 C). An explanation for this could be that *Nir4* harbours an additional gene variant that, potentially by the interaction with other genes, protects the C3H allele (risk allele for *Nir4*) carriers from severe β-cell loss. It is also possible that the body weight QTL *Nob4* on chromosome 4 (Suppl. Fig. 4C), which is associated with lower fat mass in the C3H allele carriers, could contribute to the protective influence on survival.

4.4 Phenotypic effect of C3H chromosome 7 on different genetic backgrounds using RCS

In order to validate the linkage of C3H chromosome 7 with improved glycaemia and to further characterize the QTL, chromosome 7 from C3H was introgressed into the NZO- and C57BL/6J background by the generation of recombinant congenic strains (RCS) (Fig. 20). In contrast to the N2(NZOxC3H) population, in which each mouse theoretically carries 75 % NZO alleles randomly distributed across the genome, the two genotypes from the RCS are genetically identical, except for the region of interest. For this reason, phenotypic differences between the genotypes from the RCS can be reliably attributed to region of interest as the only difference in the genome (Demant and Hart, 1986).

4.4.1 C3H chromosome 7 protects from β-cell failure in RCS.NZO.C3H-*Cdp7*con males

In line with the phenotype from male N2 population, the C3H genotype on chromosome 7 was associated with lower blood glucose in RCS.NZO.C3H-*Cdp7*con mice (Fig. 22A). Nonetheless, due to the high variation of blood glucose levels in the NZO.C3H-*Cdp7*con$^{NZO/NZO}$ males, the differences did not reach statistical significance. Moreover, similar to the N2 males, C3H allele carriers exhibited clearly higher plasma insulin- (Fig. 25A) and C-peptide (Fig. 25C) levels at final stage of age. C-peptide (connecting-peptide) is secreted in equimolar amounts with insulin and unlike insulin is not degraded in the liver but in the kidney (Zavaroni et al., 1987). As C-peptide has a half-life of 20-30 minutes and insulin only 3-5 minutes, the peripheral concentration at steady state directly reflects the islet release of insulin (Jones and Hattersley, 2013). Moreover, NZO.C3H-*Cdp7*con$^{C3H/C3H}$ males gained significantly more body weight at later stages of age, mainly due to differences in the body fat content (Fig. 22C). As already discussed for the N2 males, the lower fat mass content in the controls might reflect an increased lipolysis for the use of alternative energy fuels, resulting secondarily from an overall lack of insulin. The lower gain of fat mass in the T2DM-susceptible controls could further derive from potential deficiencies in the process of fat storage. By contrast, NZO.C3H-*Cdp7*con$^{C3H/C3H}$ males might benefit from an increased storage capacity, in particular in the subcutaneous adipose fat tissue (SAT), which is (contrary to the visceral adipose fat tissue) associated with a beneficial impact on metabolism (Fujioka et al., 1987; Hamdy et al., 2006; McLaughlin et al., 2011; Neeland et al., 2012) and is the most important fat tissue in the absorption and storage of circulating lipids (Smith and Kahn, 2016). The increased storage capacity might help the mice to cope with the enduring supply of lipids from the HFD, whereas a lipid overload in the controls might lead to the leakage of lipids into the liver, skeletal muscle, pancreas and other non-SAT (so called ectopic) tissues (Tan and Vidal-Puig, 2008; Zwick et al., 2018). Ectopic fat accumulation is known to mediate lipotoxic effects, which in combination with glycotoxic conditions, is considered as a major driver for the development of T2DM (Smith, 2015; Unger, 2003b). However, potential differences in the SAT content between

the genotypes cannot reliably be confirmed or quantified, since the tissues were not weighted and the NMR was able to distinguish between the different fat depots. The glucose- and insulin tolerance test in the males (Fig. 23A+C, Fig. 24A) could not deliver additional insight on the phenotype. In conclusion, the impact of chromosome 7 on pancreatic β-cell function could be replicated. Nonetheless, it still needs to be further investigated whether this impact has a primary origin in the pancreatic islets or occurs secondarily from a peripheral tissue

4.4.2 C3H chromosome 7 protects from insulin resistance in RCS.NZO.C3H-*Cdp7*con females

Also in the females, the linkage of C3H chromosome 7 with decreased blood glucose levels could be validated (Fig. 22B). In accordance with the phenotype from the N2 females, the body weight did not differ between the genotypes (Fig. 22D). Furthermore, the i.p. GTT revealed an improved glucose tolerance of NZO.C3H-*Cdp7*con$^{C3H/C3H}$ females. The significantly higher rate of glucose clearance observed during the i.p. ITT indicates an improved insulin sensitivity of the peripheral tissues from *Cdp7*con$^{C3H/C3H}$ females, which likely contributes to their improved glucose tolerance. The improved insulin sensitivity is probably also the reason for lower levels of plasma insulin and C-peptide measured at 17 weeks of age (Fig. 25B+D), as the more efficient action of insulin in NZO.C3H-*Cdp7*con$^{C3H/C3H}$ females requires lower secretion of insulin from the β-cells to mediate the glucose uptake into the tissues. On the other hand, the tendency towards higher plasma insulin levels in NZO.C3H-*Cdp7*con$^{C3H/C3H}$ females during the i.p. GTT suggests that the peripheral glucose uptake could further be improved by an increase of insulin secretion to better cope with the excessive glucose administration. Altogether, improved glycaemic control in NZO.C3H-*Cdp7*con$^{C3H/C3H}$ females seems to derive from improved insulin sensitivity in combination with an increased insulin secretion capacity of the pancreatic islets.

4.4.3 C3H chromosome 7 protects from obesity and insulin resistance in RCS.B6.C3H-*Cdp7*con males

The introgression of C3H chromosome 7 into C57BL/6J genetic background resulted in a similar phenotype in the males as observed in NZO.C3H-*Cdp7*con$^{C3H/C3H}$ females. Likewise, B6.C3H-*Cdp7*con$^{C3H/C3H}$ males seem to benefit from an improved insulin tolerance, as indicated with the significantly higher rate of glucose clearance during the i.p. ITT (Fig. 28). This further explains the improved glucose tolerance (Fig. 27A) and lower levels of secreted insulin during the i.p GTT (Fig. 27B), as well as lower levels of circulating plasma insulin (Fig. 29A) and C-peptide (Fig. 29B) at 21 weeks of age. In accordance with this hypothesis, the measurement of total pancreatic insulin levels did not reveal any differences between the genotypes (Fig. 29C), demonstrating that the different levels of plasma insulin- and C-peptide are probably not caused by differences in the β-cell mass. However, different from NZO.C3H-*Cdp7*con$^{C3H/C3H}$ females, the improved insulin sensitivity likely

derives from a protection from HFD-induced obesity, as B6.C3H-*Cdp7*con$^{C3H/C3H}$ males gained significantly less body fat compared to controls (Fig. 26B). Moreover, in contrast to NZO.C3H-*Cdp7*con males and females, the development of blood glucose levels did not differ between the genotypes from B6.C3H-*Cdp7*con, except for one time-point. Thus, at 4 weeks of age, B6.C3H-*Cdp7*con$^{C3H/C3H}$ mice exhibited significantly lower blood glucose levels (Fig. 26A), indicating a genetically-driven ability of B6.C3H-*Cdp7*con$^{C3H/C3H}$ mice to better adapt to the HFD, whereas B6.C3H-*Cdp7con*$^{B6/B6}$ mice might be metabolically more challenged one week after the switch from standard (11 % calories from fat) to the HFD (60 % calories from fat).

In conclusion, the introgression of the C3H chromosome 7 on different genetic backgrounds and between the sexes revealed different phenotypic outcomes. Whereas a protection from insulin resistance could be observed in both B6.C3H-*Cdp7*con males and NZO.C3H-*Cdp7*con females, the phenotype in NZO.C3H-*Cdp7*con males rather seems to result from an impact on the pancreatic β-cell function without prior insulin resistance of the peripheral tissues. These results indicate how the genetic background can essentially influence the phenotypic outcome of genes (Linder, 2001; Linder, 2006). Besides the already mentioned example of the mutation in the leptin gene, which causes β-cell failure and severe hyperglycaemia on C57BL/KsJ-, but only transient T2DM on C57BL/6J background (Coleman and Hummel, 1973), several further examples are known that show how presumably background-unique modifier genes influence the phenotype of a gene. To assess the impact of the genetic background, Kulkarni and colleagues generated mice double heterozygous for knockout of the insulin receptor and insulin receptor substrate-1 on three genetic backgrounds (C57BL/6, 129Sv, and DBA) and found dramatically different phenotypes. Whereas severe hyperglycaemia with 85 % incidence of T2DM was observed on C57BL/6 background, the same genetic defects caused only mild hyperinsulinemia without onset of T2DM on 129Sv background. On DBA background, an intermediate phenotype could be observed, with relatively late-onset of hyperglycaemia in 67 % of the mice (Kulkarni et al., 2003). A more recent example represents the diabetogenic impact of the gene *Zfp69*, whose identification was initiated by QTL analysis in an outcross population generated from the breeding of obese NZO with lean Swiss Jim Lambert (SJL) mice (Plum et al., 2000; Scherneck et al., 2009). In the SJL strain, the diabetogenic features of *Zfp69* were completely hidden, probably due to the majority impact of diabetes-suppressor genes. However, after introgression of the QTL into the diabetes-prone NZO background, the mice suffered from β-cell degradation and severe hyperglycaemia (Scherneck et al., 2009). Overexpression of *Zfp69* on C57BL/6J genetic background mediated hyperlipidaemia, liver fat accumulation and mild insulin resistance without onset of hyperglycaemia, supporting the hypothesis that the diabetogenic effect of *Zfp69* requires synergy with at least one further gene from the NZO genome (Chung et al., 2015).

Besides the possibility that genetic background effects cause different phenotypic outcomes of the same gene variant, it is further possible that the observed phenotypes in the RCS underlie different gene variants with different locations on chromosome 7. Since the linkage analysis is limited in the precise estimation of genetic effects, almost the full murine chromosome 7 (17-111 Mb) was introgressed, thereby ensuring that the critical fragment of (*f*)*Cdp7-prox* was retained. As a disadvantage, the probability is increased that additional genes from C3H contribute to the phenotype. For this reason, the observed differences cannot reliably be attributed to (*f*)*Cdp7-prox* alone. Especially in NZO.C3H-*Cdp7*con males, it is even likely that further impact might derive from the two additional QTLs detected on chromosome 7, namely *Cdp7-dis* (associated with blood glucose) and *C07-prox* (associated with free carnitine) (Fig. 16), since these QTLs obviously underlie different gene variants between C3H and NZO. In order to validate that (*f*)*Cdp7-prox* is the main contributor to the observed differences, RCS carrying only the confidence interval for the QTLs need to be generated as a next step. Once the phenotype can be replicated in these mice, it would be useful to break the candidate region into even smaller fragments of little base pairs thereby substantially reducing the number of candidate genes (Brockmann and Neuschl, 2012; Darvasi, 1997).

4.5 Detection of candidate genes for *Cdp7-prox*

The following chapters focus on the detection of candidate genes for *the Cdp7-prox* locus from the males. However, since it seems possible that the *fCdp7-prox* locus from the females underlies the same gene variant, the candidate genes that will be discussed in the next chapters should be considered for both QTLs. In total, 776 genes are annotated in the critical region of *Cdp7-prox*, which spans the region from 27- 47 Mb on chromosome 7. To reduce the number of candidate genes it is recommended to combine different strategies (Flint et al., 2005; Solberg Woods, 2014). In this study, a combined approach of gene expression- and haplotype analysis of the critical region was used to filter for the most likely candidates for *Cdp7-prox*.

4.5.1 Combined gene expression- and haplotype analysis of the parental strains identifies 18 candidate genes

Based on the assumption that the causative gene(s) for *Cdp7-prox* is / are differentially expressed in the male parental strains C3H and NZO, a DNA microarray was conducted. Microarrays, which allow the simultaneous measurement of several thousand transcripts, represent the most used technique to measure mRNA levels (Draghici et al., 2006). The tissues (liver, pancreatic islets, quadriceps muscle, gWAT and BAT) for the genome-wide expression analysis were collected at juvenile age (week 6) to decrease the chance of detecting secondarily induced expression changes in NZO,

resulting from manifest T2DM. Since microarrays are to some extent prone to generating artifacts (Draghici et al., 2006) all genes which were found to be differentially expressed in the array (Fig.20) were further investigated by qPCR to validate the expression differences. Since expression of genes can be restricted to a specific development stage (Gross et al., 2002), the expression was further investigated in tissues collected at 21 weeks of age to ensure the stability of the expression differences over time. However, due to the gradual loss of the islets with the progression of T2DM in the NZO males, the pancreatic islets were only collected and analysed from 6-weeks-old males. In total, 23 genes were confirmed to be differentially regulated between the two strains C3H and NZO (Tab. 19). The most expression changes within *Cdp7-prox* were found in the pancreatic islets, which might already point towards genetically-driven structural- and physiological differences between the strains in this tissue, potentially with important contribution from *Cdp7-prox*. The most striking expression difference was observed for the gene *Klk1b22*, whose mRNA abundance was relatively high in all C3H-, but completely absent in all NZO tissues.

In addition, to further reduce the number of candidate genes a haplotype analysis of the parental strains was integrated. This approach makes use of the observation that genetic variation within species is not randomly distributed in the genome but appears as clusters which are dependently inherited, so called haplotype blocks (Gabriel et al., 2002). The haplotype analysis between C3H and NZO by the use of SNPs provided from the Wellcome Trust Sanger Institute (Keane et al., 2011; Yalcin et al., 2011) could successfully dissect *Cdp7-prox* into regions that are identical by descent (IBD), and regions that are polymorphic (non-IBDs) between the two strains (Fig.31). Based on the hypothesis that IBDs are highly unlikely to contain the causal genetic polymorphism underlying a QTL (Browning and Browning, 2011a; Wiltshire et al., 2003), only genes with polymorphic SNPs that mapped to non-IBD regions were selected as candidate genes for *Cdp7-prox* (Fig. 31B, Suppl. Tab. 13). Subsequently, out of 23 genes revealed from the gene expression analysis, 18 genes further fulfilled the criteria of the haplotype analysis, whereas the other five genes failed to contain polymorphic SNPs (*Kcnk6*, *Cox7a1*, *Klk1b22*, and *Klk1b4*) or resided in an IBD-region (*Spint2*). Consequently, the combined gene expression- and haplotype analysis reduced the number of candidates for *Cdp7-prox* from 776 annotated genes to 18 most likely candidates.

However, it has to be mentioned that both of the applied approaches are not sufficient for the reliable exclusion of candidate genes. Although the detection of differential gene expression could already help with the identification of the causative gene for many QTLs (Aitman et al., 1999; Andrikopoulos et al., 2016; Chadt et al., 2008; Clee et al., 2006; Dokmanovic-Chouinard et al., 2008; Scherneck et al., 2009; Vogel et al., 2012), there is no guarantee that a functional alteration of a disease gene is reflected by changes in its mRNA expression. Due to posttranscriptional regulatory

mechanisms it is possible that differences in the protein abundance are not detectable on mRNA level and vice versa (Maier et al., 2009). Moreover, even if the protein abundance is not affected, an altered protein structure can have severe functional consequences. Also the haplotype analysis was already successful in many previous QTL studies (Liu et al., 2007; Manenti et al., 2004; Park et al., 2003; Vogel et al., 2018). However, it cannot be excluded that the here applied analysis may have led to the wrong exclusion of genes, especially when considering that the sequence from the C3HeB/HeJ, but not from C3HeB/FeJ, was used. Even though the two C3H substrains are closely related, it is possible that the C3HeB/FeJ genome harbors unique sequence variants within the critical region which may play an important role in the phenotype underlying *Cdp7-prox*. Indeed, besides the already mentioned mutation in the toll-like receptor 4 gene (*Tlr4*^{lps}) at the lipopolysaccharide response locus that confers an endotoxin resistance in C3H/HeJ, but not the C3H/FeJ mice (Poltorak et al., 1998), at least one further substrain-specific mutation with important phenotypic impact is known (Beyer et al., 2009). Furthermore, the statistical power of the haplotype analysis for *Cdp7-prox* is limited by incomplete SNP information for the full sequence. Thus, in the region from 32.5 to 33.27 Mb no SNPs are annotated for the C57BL/6J reference sequence (Fig. 31B). For this reason, this interval cannot be reliably distinguished into an IBD or non-IBD region and therefore the genes cannot be certainly excluded as potential candidates. Moreover, even if it is obvious that a region is an IBD region, there is no guarantee that this interval does not contain the causal genetic polymorphism underlying a QTL. It is also possible that enhancers in non-IBD regions may regulate expression of genes that are in IBDs (Verdugo et al., 2010). One example where the use of the IBD criterion would have led to the wrong exclusion of the causal gene represents the discovery of the gene *Prcp* (Diament and Warden, 2004; Wallingford et al., 2009). This gene was shown to play an important role in the melanocortin signalling and weight maintenance, even though it mapped to an IBD region between the parental strains BALB/cByJ and C57BL/6ByJ of the used RCS line, which exhibited the phenotype. Altogether, also for *Cdp7-prox* it cannot be excluded that the here applied criteria may have falsely excluded the actual causative gene(s).

4.5.2 Gene expression analysis in N2(NZOxC3H) males excludes the candidacy of three genes

Based on their differential gene expression in the parental strains, mRNA levels from candidate genes in the liver, gWAT, BAT and skeletal muscle were further measured in the respective tissues from each N2(NZOxC3H) male for the identification of eQTLs. The eQTL analysis represents an useful tool to confirm or exclude the candidacy of genes for a QTL. In general, each gene whose mRNA expression is not associated with a *cis*-eQTL represents an unlikely candidate for a QTL (Bao et al., 2007; Drake et al., 2005; Hubner et al., 2005; Schadt et al., 2003). In contrast, genes associated with a *cis*-eQTL harbour a genetic sequence variation between two genotypes, presumably within the gene

itself, which resides within the physiological QTL. Therefore, a causal relationship between the expression- and physiological QTL is possible. In context with *Cdp7-prox*, the eQTL analysis was able to exclude the candidacy of three genes (*Hamp* and *Hamp2* in liver, T*mem147* in skeletal muscle) as their expressions were not associated with *cis*-eQTLs (Tab. 20). By contrast, all further genes that were analysed in the N2 tissues mapped to chromosome 7, thereby confirming their candidacy for the *Cdp7-pox* locus.

The mRNA levels were further correlated with the *Cdp7-prox*- associated traits blood glucose, body weight and plasma insulin from the N2 mice (Tab. 21). In line with the principle of the Mendelian Randomization, it is expected that the transcript level of the causative gene significantly correlates with the physiological traits (Drake et al., 2005). In summary, this correlation analysis revealed three genes, whose mRNA levels showed significant correlations that matched the phenotypes of respective genotypes. The positive correlation of hepatic *Pop4* mRNA- with blood glucose levels (Suppl. Fig. 5B) indicates that *Pop4* exerts diabetogenic effects in *Cdp7-prox*$^{NZO/NZO}$ livers. Likewise, the positive correlation of *Zfp30* transcript levels in BAT with blood glucose levels (Suppl. Fig. 6B) as well as the negative correlation with final body weight (Suppl. Fig. 6A) suggests a T2DM-promoting role. By contrast, the negative correlation of *Rhpn2* expression in the BAT with blood glucose levels (Suppl. Fig. 6C) argues for a T2DM-protective function of the gene in *Cdp7-prox*$^{C3H/C3H}$mice.

However, the gene expression analysis of candidate genes in the N2(NZOxC3H) population suffers from a serious limitation, as the pancreatic islets were not collected from these mice. Although the eQTL analysis was successful in the exclusion of three genes (two for liver and one for skeletal muscle), the candidacy of all genes from the pancreatic islets could not be evaluated, neither with the eQTL-, nor with the correlation analysis. When considering that *Cdp7-prox* likely acts in the pancreatic islets, the expression analysis in the N2(NZOxC3H) population could only partly help with the identification of candidate genes.

4.5.3 Gene expression analysis in RCS.NZO.C3H-*Cdp7*con males confirms the candidacy of 11 genes

After combining the results from gene expression- and haplotype analysis of the parental strains, together with the results from the eQTL analysis of the N2(NZOxC3H) population, 15 genes were left as the most likely candidates for *Cdp7-prox*. The expression of these genes was further tested in the tissues from RCS.NZOxC3H-*Cdp7con* mice, to confirm their candidacy. In contrast to the parental strains, the two genomes from the RCS only differ in a single chromosome, ensuring that expression differences are unlikely further triggered by the interaction with other genes in the genome. Moreover, the RCS exhibit a specific phenotype, making causality between expression- and phenotypic differences between the genotypes more likely (Demant and Hart, 1986). In addition to

Klk1b22, which was included in the RCS expression analysis due to its C3H-unique expression, 11 out of 15 genes were confirmed for differential expression in the RCS (Tab. 22). Based on the different criteria that were used in this study, these genes represent the most likely candidate genes for *Cdp7-prox*. However, neither the gene expression, nor the haplotype analysis is able to provide information on the function of the genes. Therefore, appropriate cell models for the knockdown or overexpression of the candidate genes in combination with functional *in vitro* assays are useful to prove a functional impact (Abiola et al., 2003). To further investigate causality with *Cdp7-prox*, seven candidate genes have been tested in regard to a potential impact on GSIS in cultivated MIN6 cells (Fig. 33+34). Indeed, two genes (*Pop4* and *Atp4a*) were able to alter the rate of GSIS, as their knockdown was associated with a decreased insulin secretion (Fig.34). In addition, due to its described role in the cleavage of cellular CoA levels the gene *Nudt19* was further investigated in regard to a potential role in FAO by the use of cultivated Hepa 1-6 cells. For the first time, a functional impact from *Nudt19* on hepatic FAO could be demonstrated in this study (Fig. 35). The potential roles of the candidate genes *Pop4*, *Atp4a*, *Klk1b22,* and *Nudt19* in the phenotype underlying *Cdp7-prox* are further discussed in the following chapters.

4.5.3.1 *Processing of precursor 4* (*Pop4*)

The gene *Pop4* (*processing of precursor 4*) was higher expressed in pancreatic islets and liver in the NZO genotype of the parental strains (Tab. 19) and NZO.C3H-*Cdp7*con mice (Tab. 22). Moreover, in the N2(NZOxC3H) population a weak but significant correlation of hepatic mRNA- with blood glucose levels was observed (Suppl. Fig. 5B). The knockdown of *Pop4* in MIN6 cells resulted in a decreased GSIS (Fig. 33), indicating that the gene functions as stimulator of insulin secretion. At first sight, this is in contrast to the observation that plasma insulin levels were decreased in the NZO genotype. On the other hand, the mRNA levels were measured at 6 weeks-, whereas plasma insulin levels were measured at final stages of age in the N2 (week 21) and RCS mice (week 17), therefore the correlation might be of limited value. Further plasma insulin levels were measured after 16 hours of fasting in 8-weeks-old N2 animals. At this time point, a reverse insulin pattern was observed, as NZO.C3H-Cdp7-prox$^{NZO/NZO}$ mice tended (however not significantly) to exhibit higher levels of insulin, possibly influenced by the stimulating impact on insulin secretion of *Pop4*. One could assume that this persisting stimulation might later contribute to the overstimulation and subsequent failure of the pancreatic islets, which would explain the reduction of plasma insulin at final stages of age.

Literature research on *Pop4* (also known as *Rpp29*) yielded that the gene encodes one of the protein subunits of the ribonuclease P complex, a protein which was originally discovered as the endoribonuclease that processes the 5' leader of precursor transfer RNA (tRNA) (Guerrier-Takada et al., 1983). The processing of tRNA, which serves as the physical link between the mRNA and the

amino acid sequence of proteins, is essential for the stabilization of the RNA structure during its maturation. Whereas critical defects in this processing machinery are lethal, less severe point mutations are associated with complex clinical phenotypes, including neuropathologies and sterility (Abbott et al., 2014; Kirchner and Ignatova, 2015). In the last years it has become increasingly clearer, that the different subunits from the ribonase P complex engage further important roles. *Pop4* has recently been shown to be involved in DNA damage response machinery (Abu-Zhayia et al., 2017) and to participate in the regulation of the chromatin structure and function (Newhart et al., 2016), which is known to play a fundamental role in the epigenetic modification of the genome. Altogether, the gene seems to be a global player in the posttranslational regulation of gene expression, therefore it is even likely that potential sequence alterations may have phenotypic consequences that could also be related with glucose metabolism.

4.5.3.2 Gastric *Hydrogen-potassium exchanging ATPase alpha* (*Atp4a*)

Expression of *Atp4a* (*ATPase, H^+/K^+ exchanging, gastric, alpha polypeptide*) was higher in pancreatic islets and liver in the C3H genotype of the parental strains (Tab. 19) and NZO.C3H-*Cdp7*con mice (Tab. 22). Similar to *Pop4*, *Atp4a* seems to act as stimulator of GSIS as observed in MIN6 cells (Fig. 33). In line with this function, the C3H allele for *Cdp7-prox* is associated with higher plasma insulin levels.

The gene encodes the alpha subunit of the heterodimeric gastric proton pump H^+/K^+-ATPase and functions in the catalyzation of the proton exchange to maintain an acidic environment within the stomach (Spicer et al., 2000). Recently, the gastric H^+/K^+-ATPase has also been shown to be expressed in the human pancreas where it contributes to the pancreatic acid secretion (Wang et al., 2015). However, nothing is described about a potential role of the H^+/K^+-ATPases in the secretion of insulin from the pancreatic islets. It is well established that GSIS in pancreatic islets involves the closure of K_{ATP} channels to allow the depolarization of the cell membrane, followed by calcium influx through voltage-dependent Ca^{2+} channels which subsequently triggers the exocytosis of insulin vesicles. The here observed impact of the H^+/K^+-ATPase on GSIS in MIN6 cells suggests that this proton pump further participates in this process, possibly by contributing to the regulation of the intracellular ion concentration. Consistent with this hypothesis, the autoimmune disease atrophic body gastritis (ABG), which is characterized by the persistent presence ATP4A autoantibodies, has been associated with T1DM in humans (Chobot et al., 2014).

4.5.3.3 *Kallikrein 1-related peptidase b22* (*Klk1b22*)

The gene *Klk1b22* (*kallikrein 1-related peptidase b22*) was the only candidate gene whose expression was detectable exclusevely in one genotype (C3H), whereas the NZO mouse strain represents a natural knockout for this gene. The only finding which might argue against *Klk1b22* as causative gene for *Cdp7-prox* is be the fact that the SNP analysis could not discover any polymorphic SNPs within the gene sequence, a criterion that was actually used to exclude potential candidate genes (see 3.6.2). However, since the SNP analysis is not sufficient to discover single sequence mutations, and when considering that the sequence from the C3HeB/HeJ substrain was used in the analysis, the absence of polymorphic SNPs in the sequence can only marginally weaken its candidacy for *Cdp7-prox* as a C3H-specific T2DM-supressor gene.

Klk1b22 is a member of the kallikrein gene cluster that has been expanded by tandem gene duplication and codes for several serine proteases. The different kallikrein genes are essential to many biological processes, including inflammation and the organization of the extracellular matrix (Lawrence et al., 2010), but they have also been proposed to improve insulin sensitivity (Damas et al., 2004). The kallikrein locus is also conserved in humans; however, *Klk1b22* is not part of this locus but *KLK1* is described as its human orthologue. Interestingly, the administration of recombinant human KLK1 protein has been reported to decelerate the onset of T1DM in non-obese diabetic (NOD) mice by suppressing the autoimmune reaction against the pancreatic β-cells (Maneva-Radicheva et al., 2014). In line with the phenotype observed in RCS.NZO.C3H-*Cdp7-prox*$^{C3H/C3H}$ mice, the application of the recombinant protein led to a dose-dependent increase of C-peptide levels. It might be possible that the murine KLK1b22 uses a similar mechanism to protect the C3H strain from β-cell failure.

4.5.3.4 *Nudix (nucleoside diphosphate linked moiety X)-type motif 19* (*Nudt19*)

Expression of *Nudt19* (*nudix (nucleoside diphosphate linked moiety X)-type motif 19*) was higher in parental C3H- and RCS.NZO.C3H-*Cdp7con*$^{C3H/C3H}$ mice in four different tissues (Tab. 19+22). In addition, the gene was shown to function as inhibitor of fatty acid β-oxidation (FAO) in Hepa 1-6 cells (Fig. 35). This observation fits to the presumed function of *Nudt19*, namely the degradation of intracellular Coenzyme A (CoA) (Gasmi and McLennan, 2001; Ofman et al., 2006; Shumar et al., 2018), which represents the major acyl carrier in mammals and an important cofactor in numerous metabolic reactions (Leonardi et al., 2005). In context with *Cdp7-prox*, which rather seems to acts on pancreatic β-cell function, it is possible that a deregulated hepatic CoA-metabolism secondarily contributes to the failure of the β-cells. However, it may also be possible that *Nudt19* exerts similar effects on FAO in the pancreatic islets, thereby directly influencing β-cell health and / or function.

Indeed, even though the underlying mechanisms are still not well understood, fatty acid metabolism in the pancreatic β-cells seems to play a significant role in the regulation of insulin secretion and in the protection against lipotoxicity-induced β-cell death (Hellemans et al., 2007; Yaney and Corkey, 2003).

4.6 Conclusions and future perspectives

With the help of a mouse genetic approach a novel T2DM modifier QTL was detected on proximal murine chromosome 7 (*Cdp7-prox*). Based on the phenotype observed in the backcross- and in RCS.NZO.C3H-*Cdp7con* mice, the most likely tissue affected by the *Cdp7-prox* locus seem to be the pancreatic islets. To provide evidence that the QTL directly targets pancreatic islet function, the islet function of RCS.NZO.C3H-*Cdp7con* mice should be assessed with more sensitive methods in the future. A useful experiment to test whether the insulin secretion is affected is the GSIS of isolated pancreatic islets. Moreover, a histological analysis of the pancreatic tissue, e.g. by the use of a hematoxylin and eosin (H & E) staining in pancreatic slices, could provide valuable information on a potential impact on the β-cell mass. In fact, these experiments are currently underway in the working group (Master Thesis Sarah Görigk, in preparation).

Once the target tissue for *Cdp7-prox* is certain, the candidate genes should be further investigated in regard to causality with *Cdp7-prox*. A possibility to directly access the impact of the genes *in vivo* would be the injection of adeno-associated viruses (AAVs) for the respective genes in the target tissue, followed by the metabolic phenotyping of the animals. Besides their functional investigation, a sequence analysis could further help to detect potential strain-specific mutations, which might not be visible in the Sanger database.

Finally, this work bears a huge potential for the detection of many further T2DM-related disease genes. The linkage analysis of the N2(NZOxC3H) population revealed a huge number of novel metabolic QTLs that can be analysed in a similar way in the future to further elucidate the genetic architecture of T2DM.

5 Literature

Abbott, J.A., C.S. Francklyn, and S.M. Robey-Bond. 2014. Transfer RNA and human disease. *Frontiers in genetics*. 5:158.

Abiola, O., J.M. Angel, P. Avner, A.A. Bachmanov, J.K. Belknap, B. Bennett, E.P. Blankenhorn, D.A. Blizard, V. Bolivar, G.A. Brockmann, K.J. Buck, J.F. Bureau, W.L. Casley, E.J. Chesler, J.M. Cheverud, G.A. Churchill, M. Cook, J.C. Crabbe, W.E. Crusio, A. Darvasi, G. de Haan, P. Dermant, R.W. Doerge, R.W. Elliot, C.R. Farber, L. Flaherty, J. Flint, H. Gershenfeld, J.P. Gibson, J. Gu, W. Gu, H. Himmelbauer, R. Hitzemann, H.C. Hsu, K. Hunter, F.F. Iraqi, R.C. Jansen, T.E. Johnson, B.C. Jones, G. Kempermann, F. Lammert, L. Lu, K.F. Manly, D.B. Matthews, J.F. Medrano, M. Mehrabian, G. Mittlemann, B.A. Mock, J.S. Mogil, X. Montagutelli, G. Morahan, J.D. Mountz, H. Nagase, R.S. Nowakowski, B.F. O'Hara, A.V. Osadchuk, B. Paigen, A.A. Palmer, J.L. Peirce, D. Pomp, M. Rosemann, G.D. Rosen, L.C. Schalkwyk, Z. Seltzer, S. Settle, K. Shimomura, S. Shou, J.M. Sikela, L.D. Siracusa, J.L. Spearow, C. Teuscher, D.W. Threadgill, L.A. Toth, A.A. Toye, C. Vadasz, G. Van Zant, E. Wakeland, R.W. Williams, H.G. Zhang, F. Zou, and C. Complex Trait. 2003. The nature and identification of quantitative trait loci: a community's view. *Nature reviews. Genetics*. 4:911-916.

Abu-Qamar, M., and A. Wilson. 2007. Evidence-based decision-making: the case for diabetes care. *Int J Evid Based Healthc*. 5:254-260.

Abu-Zhayia, E.R., H. Khoury-Haddad, N. Guttmann-Raviv, R. Serruya, N. Jarrous, and N. Ayoub. 2017. A role of human RNase P subunits, Rpp29 and Rpp21, in homology directed-repair of double-strand breaks. *Scientific reports*. 7:1002.

Adamski, J. 2016. Key elements of metabolomics in the study of biomarkers of diabetes. *Diabetologia*. 59:2497-2502.

Ahren, B., and G. Pacini. 2002. Insufficient islet compensation to insulin resistance vs. reduced glucose effectiveness in glucose-intolerant mice. *Am J Physiol Endocrinol Metab*. 283:E738-744.

Aitman, T.J., A.M. Glazier, C.A. Wallace, L.D. Cooper, P.J. Norsworthy, F.N. Wahid, K.M. Al-Majali, P.M. Trembling, C.J. Mann, C.C. Shoulders, D. Graf, E. St Lezin, T.W. Kurtz, V. Kren, M. Pravenec, A. Ibrahimi, N.A. Abumrad, L.W. Stanton, and J. Scott. 1999. Identification of Cd36 (Fat) as an insulin-resistance gene causing defective fatty acid and glucose metabolism in hypertensive rats. *Nature genetics*. 21:76-83.

Akinmokun, A., P.L. Selby, K. Ramaiya, and K.G. Alberti. 1992. The short insulin tolerance test for determination of insulin sensitivity: a comparison with the euglycaemic clamp. *Diabetic medicine : a journal of the British Diabetic Association*. 9:432-437.

Ali, O. 2013. Genetics of type 2 diabetes. *World J Diabetes*. 4:114-123.

Altshuler, D., J.N. Hirschhorn, M. Klannemark, C.M. Lindgren, M.C. Vohl, J. Nemesh, C.R. Lane, S.F. Schaffner, S. Bolk, C. Brewer, T. Tuomi, D. Gaudet, T.J. Hudson, M. Daly, L. Groop, and E.S. Lander. 2000. The common PPARgamma Pro12Ala polymorphism is associated with decreased risk of type 2 diabetes. *Nature genetics*. 26:76-80.

American Diabetes Association. 2018. 2. Classification and Diagnosis of Diabetes: Standards of Medical Care in Diabetes-2018. *Diabetes care*. 41:S13-S27.

Andrikopoulos, S., B.C. Fam, A. Holdsworth, S. Visinoni, Z. Ruan, M. Stathopoulos, A.W. Thorburn, C.N. Joannides, M. Cancilla, L. Balmer, J. Proietto, and G. Morahan. 2016. Identification of ABCC8 as a contributory gene to impaired early-phase insulin secretion in NZO mice. *The Journal of endocrinology*. 228:61-73.

Bao, L., J.L. Peirce, M. Zhou, H. Li, D. Goldowitz, R.W. Williams, L. Lu, and Y. Cui. 2007. An integrative genomics strategy for systematic characterization of genetic loci modulating phenotypes. *Human molecular genetics*. 16:1381-1390.

Beagley, J., L. Guariguata, C. Weil, and A.A. Motala. 2014. Global estimates of undiagnosed diabetes in adults. *Diabetes research and clinical practice*. 103:150-160.

Bhatnagar, S., A.T. Oler, M.E. Rabaglia, D.S. Stapleton, K.L. Schueler, N.A. Truchan, S.L. Worzella, J.P. Stoehr, S.M. Clee, B.S. Yandell, M.P. Keller, D.C. Thurmond, and A.D. Attie. 2011. Positional cloning of a type 2 diabetes quantitative trait locus; tomosyn-2, a negative regulator of insulin secretion. *PLoS genetics*. 7:e1002323.

Bielschowsky, M., and F. Bielschowsky. 1953. A new strain of mice with hereditary obesity. 29-31 pp.

Bielschowsky, M., and C.M. Goodall. 1970. Origin of inbred NZ mouse strains. *Cancer Res*. 30:834-836.

Bock, T., B. Pakkenberg, and K. Buschard. 2005. Genetic background determines the size and structure of the endocrine pancreas. *Diabetes*. 54:133-137.

Bonifacio, E. 2015. Predicting type 1 diabetes using biomarkers. *Diabetes care*. 38:989-996.

Bonnefond, A., and P. Froguel. 2015. Rare and common genetic events in type 2 diabetes: what should biologists know? *Cell Metab*. 21:357-368.

Brockmann, G.A., and C. Neuschl. 2012. Positional cloning of diabetes genes. *Methods in molecular biology*. 933:275-289.

Brown, R., and P. Gorden. 2015. Leptin Therapy in Patients with Lipodystrophy and Syndromic Insulin Resistance. *In* Leptin: Regulation and Clinical Applications. e. Dagogo-Jack S, editor. Springer International Publishing, Switzerland.

Browning, B.L., and S.R. Browning. 2011a. A fast, powerful method for detecting identity by descent. *American journal of human genetics*. 88:173-182.

Browning, S.R., and B.L. Browning. 2011b. Haplotype phasing: existing methods and new developments. *Nature reviews. Genetics*. 12:703-714.

Bultman, S.J., E.J. Michaud, and R.P. Woychik. 1992. Molecular characterization of the mouse agouti locus. *Cell*. 71:1195-1204.

Burkhardt, R., H. Kirsten, F. Beutner, L.M. Holdt, A. Gross, A. Teren, A. Tonjes, S. Becker, K. Krohn, P. Kovacs, M. Stumvoll, D. Teupser, J. Thiery, U. Ceglarek, and M. Scholz. 2015. Integration of Genome-Wide SNP Data and Gene-Expression Profiles Reveals Six Novel Loci and Regulatory Mechanisms for Amino Acids and Acylcarnitines in Whole Blood. *PLoS genetics*. 11:e1005510.

Cardinal, J.W., D.J. Allan, and D.P. Cameron. 1998. Differential metabolite accumulation may be the cause of strain differences in sensitivity to streptozotocin-induced beta cell death in inbred mice. *Endocrinology*. 139:2885-2891.

Chadt, A., K. Leicht, A. Deshmukh, L.Q. Jiang, S. Scherneck, U. Bernhardt, T. Dreja, H. Vogel, K. Schmolz, R. Kluge, J.R. Zierath, C. Hultschig, R.C. Hoeben, A. Schurmann, H.G. Joost, and H. Al-Hasani. 2008. Tbc1d1 mutation in lean mouse strain confers leanness and protects from diet-induced obesity. *Nature genetics*. 40:1354-1359.

Chadt, A., S. Scherneck, H.G. Joost, and H. Al-Hasani. 2014. Molecular links between Obesity and Diabetes: "Diabesity". *In* Endotext. L.J. De Groot, G. Chrousos, K. Dungan, K.R. Feingold, A. Grossman, J.M. Hershman, C. Koch, M. Korbonits, R. McLachlan, M. New, J. Purnell, R. Rebar, F. Singer, and A. Vinik, editors, South Dartmouth (MA).

Champy, M.F., M. Selloum, V. Zeitler, C. Caradec, B. Jung, S. Rousseau, L. Pouilly, T. Sorg, and J. Auwerx. 2008. Genetic background determines metabolic phenotypes in the mouse. *Mamm Genome*. 19:318-331.

Chankiewitz, E., D. Peschke, L. Herberg, I. Bazwinsky, E. Muhlbauer, H.J. Bromme, and E. Peschke. 2006. Did the gradual loss of GLUT2 cause a shift to diabetic disorders in the New Zealand obese mouse (NZO/Hl)? *Exp Clin Endocrinol Diabetes*. 114:262-269.

Chen, Y., J. Zhu, P.Y. Lum, X. Yang, S. Pinto, D.J. MacNeil, C. Zhang, J. Lamb, S. Edwards, S.K. Sieberts, A. Leonardson, L.W. Castellini, S. Wang, M.F. Champy, B. Zhang, V. Emilsson, S. Doss, A. Ghazalpour, S. Horvath, T.A. Drake, A.J. Lusis, and E.E. Schadt. 2008. Variations in DNA elucidate molecular networks that cause disease. *Nature*. 452:429-435.

Chobot, A., J. Wenzlau, K. Bak-Drabik, J. Kwiecien, J. Polanska, and M. Rewers. 2014. ATP4A autoimmunity and Helicobacter pylori infection in children with type 1 diabetes. *Clinical and experimental immunology*. 177:598-602.

Chua, S.C., Jr., W.K. Chung, X.S. Wu-Peng, Y. Zhang, S.M. Liu, L. Tartaglia, and R.L. Leibel. 1996. Phenotypes of mouse diabetes and rat fatty due to mutations in the OB (leptin) receptor. *Science*. 271:994-996.

Chung, B., M. Stadion, N. Schulz, D. Jain, S. Scherneck, H.G. Joost, and A. Schurmann. 2015. The diabetes gene Zfp69 modulates hepatic insulin sensitivity in mice. *Diabetologia*. 58:2403-2413.

Clee, S.M., and A.D. Attie. 2007. The genetic landscape of type 2 diabetes in mice. *Endocrine reviews*. 28:48-83.

Clee, S.M., B.S. Yandell, K.M. Schueler, M.E. Rabaglia, O.C. Richards, S.M. Raines, E.A. Kabara, D.M. Klass, E.T. Mui, D.S. Stapleton, M.P. Gray-Keller, M.B. Young, J.P. Stoehr, H. Lan, I. Boronenkov, P.W. Raess, M.T. Flowers, and A.D. Attie. 2006. Positional cloning of Sorcs1, a type 2 diabetes quantitative trait locus. *Nature genetics*. 38:688-693.

Coleman, D.L. 1978. Obese and diabetes: two mutant genes causing diabetes-obesity syndromes in mice. *Diabetologia*. 14:141-148.

Coleman, D.L., and E.M. Eicher. 1990. Fat (fat) and tubby (tub): two autosomal recessive mutations causing obesity syndromes in the mouse. *J Hered*. 81:424-427.

Coleman, D.L., and K.P. Hummel. 1973. The influence of genetic background on the expression of the obese (Ob) gene in the mouse. *Diabetologia*. 9:287-293.

Collins, S., T.L. Martin, R.S. Surwit, and J. Robidoux. 2004. Genetic vulnerability to diet-induced obesity in the C57BL/6J mouse: physiological and molecular characteristics. *Physiol Behav*. 81:243-248.

Damas, J., N. Garbacki, and P.J. Lefebvre. 2004. The kallikrein-kinin system, angiotensin converting enzyme inhibitors and insulin sensitivity. *Diabetes/metabolism research and reviews*. 20:288-297.

Darlington, G.J., H.P. Bernhard, R.A. Miller, and F.H. Ruddle. 1980. Expression of liver phenotypes in cultured mouse hepatoma cells. *Journal of the National Cancer Institute*. 64:809-819.

Darvasi, A. 1997. Interval-specific congenic strains (ISCS): an experimental design for mapping a QTL into a 1-centimorgan interval. *Mammalian genome : official journal of the International Mammalian Genome Society*. 8:163-167.

Darvasi, A. 1998. Experimental strategies for the genetic dissection of complex traits in animal models. *Nature genetics*. 18:19-24.

Dash, S., H. Sano, J.J. Rochford, R.K. Semple, G. Yeo, C.S. Hyden, M.A. Soos, J. Clark, A. Rodin, C. Langenberg, C. Druet, K.A. Fawcett, Y.C. Tung, N.J. Wareham, I. Barroso, G.E. Lienhard, S. O'Rahilly, and D.B. Savage. 2009. A truncation mutation in TBC1D4 in a family with acanthosis nigricans and postprandial hyperinsulinemia. *Proceedings of the National Academy of Sciences of the United States of America*. 106:9350-9355.

DeFronzo, R.A., J.D. Tobin, and R. Andres. 1979. Glucose clamp technique: a method for quantifying insulin secretion and resistance. *Am J Physiol*. 237:E214-223.

Demant, P., and A.A. Hart. 1986. Recombinant congenic strains--a new tool for analyzing genetic traits determined by more than one gene. *Immunogenetics*. 24:416-422.

Diament, A.L., and C.H. Warden. 2004. Multiple linked mouse chromosome 7 loci influence body fat mass. *International journal of obesity and related metabolic disorders : journal of the International Association for the Study of Obesity*. 28:199-210.

Dokas, J., A. Chadt, T. Nolden, H. Himmelbauer, J.R. Zierath, H.G. Joost, and H. Al-Hasani. 2013. Conventional knockout of Tbc1d1 in mice impairs insulin- and AICAR-stimulated glucose uptake in skeletal muscle. *Endocrinology*. 154:3502-3514.

Dokmanovic-Chouinard, M., W.K. Chung, J.C. Chevre, E. Watson, J. Yonan, B. Wiegand, Y. Bromberg, N. Wakae, C.V. Wright, J. Overton, S. Ghosh, G.M. Sathe, C.E. Ammala, K.K. Brown, R. Ito, C.

LeDuc, K. Solomon, S.G. Fischer, and R.L. Leibel. 2008. Positional cloning of "Lisch-Like", a candidate modifier of susceptibility to type 2 diabetes in mice. *PLoS genetics*. 4:e1000137.

Dorajoo, R., J. Liu, and B.O. Boehm. 2015. Genetics of Type 2 Diabetes and Clinical Utility. *Genes (Basel)*. 6:372-384.

Doss, S., E.E. Schadt, T.A. Drake, and A.J. Lusis. 2005. Cis-acting expression quantitative trait loci in mice. *Genome research*. 15:681-691.

Draghici, S., P. Khatri, A.C. Eklund, and Z. Szallasi. 2006. Reliability and reproducibility issues in DNA microarray measurements. *Trends in genetics : TIG*. 22:101-109.

Drake, T.A., E.E. Schadt, R.C. Davis, and A.J. Lusis. 2005. Integrating genetic and gene expression data to study the metabolic syndrome and diabetes in mice. *American journal of therapeutics*. 12:503-511.

Dreja, T., Z. Jovanovic, A. Rasche, R. Kluge, R. Herwig, Y.C. Tung, H.G. Joost, G.S. Yeo, and H. Al-Hasani. 2010. Diet-induced gene expression of isolated pancreatic islets from a polygenic mouse model of the metabolic syndrome. *Diabetologia*. 53:309-320.

Dupuis, J., C. Langenberg, I. Prokopenko, R. Saxena, N. Soranzo, A.U. Jackson, E. Wheeler, N.L. Glazer, N. Bouatia-Naji, A.L. Gloyn, C.M. Lindgren, R. Magi, A.P. Morris, J. Randall, T. Johnson, P. Elliott, D. Rybin, G. Thorleifsson, V. Steinthorsdottir, P. Henneman, H. Grallert, A. Dehghan, J.J. Hottenga, C.S. Franklin, P. Navarro, K. Song, A. Goel, J.R. Perry, J.M. Egan, T. Lajunen, N. Grarup, T. Sparso, A. Doney, B.F. Voight, H.M. Stringham, M. Li, S. Kanoni, P. Shrader, C. Cavalcanti-Proenca, M. Kumari, L. Qi, N.J. Timpson, C. Gieger, C. Zabena, G. Rocheleau, E. Ingelsson, P. An, J. O'Connell, J. Luan, A. Elliott, S.A. McCarroll, F. Payne, R.M. Roccasecca, F. Pattou, P. Sethupathy, K. Ardlie, Y. Ariyurek, B. Balkau, P. Barter, J.P. Beilby, Y. Ben-Shlomo, R. Benediktsson, A.J. Bennett, S. Bergmann, M. Bochud, E. Boerwinkle, A. Bonnefond, L.L. Bonnycastle, K. Borch-Johnsen, Y. Bottcher, E. Brunner, S.J. Bumpstead, G. Charpentier, Y.D. Chen, P. Chines, R. Clarke, L.J. Coin, M.N. Cooper, M. Cornelis, G. Crawford, L. Crisponi, I.N. Day, E.J. de Geus, J. Delplanque, C. Dina, M.R. Erdos, A.C. Fedson, A. Fischer-Rosinsky, N.G. Forouhi, C.S. Fox, R. Frants, M.G. Franzosi, P. Galan, M.O. Goodarzi, J. Graessler, C.J. Groves, S. Grundy, R. Gwilliam, U. Gyllensten, S. Hadjadj, et al. 2010. New genetic loci implicated in fasting glucose homeostasis and their impact on type 2 diabetes risk. *Nature genetics*. 42:105-116.

European Commission. 2013. Seventh Report on the Statistics on the Number of Animals used for Experimental and other Scientific Purposes in theMember States of the European Union.

Fawwad, A., I.A. Siddiqui, A. Basit, N.F. Zeeshan, S.M. Shahid, S.N. Nawab, and S. Siddiqui. 2016. Common variant within the FTO gene, rs9939609, obesity and type 2 diabetes in population of Karachi, Pakistan. *Diabetes Metab Syndr*. 10:43-47.

Flint, J., W. Valdar, S. Shifman, and R. Mott. 2005. Strategies for mapping and cloning quantitative trait genes in rodents. *Nature reviews. Genetics*. 6:271-286.

Floegel, A., N. Stefan, Z. Yu, K. Muhlenbruch, D. Drogan, H.G. Joost, A. Fritsche, H.U. Haring, M. Hrabe de Angelis, A. Peters, M. Roden, C. Prehn, R. Wang-Sattler, T. Illig, M.B. Schulze, J. Adamski, H. Boeing, and T. Pischon. 2013. Identification of serum metabolites associated with risk of type 2 diabetes using a targeted metabolomic approach. *Diabetes*. 62:639-648.

Florez, J.C., J. Hirschhorn, and D. Altshuler. 2003. The inherited basis of diabetes mellitus: implications for the genetic analysis of complex traits. *Annu Rev Genomics Hum Genet*. 4:257-291.

Frayling, T.M., N.J. Timpson, M.N. Weedon, E. Zeggini, R.M. Freathy, C.M. Lindgren, J.R. Perry, K.S. Elliott, H. Lango, N.W. Rayner, B. Shields, L.W. Harries, J.C. Barrett, S. Ellard, C.J. Groves, B. Knight, A.M. Patch, A.R. Ness, S. Ebrahim, D.A. Lawlor, S.M. Ring, Y. Ben-Shlomo, M.R. Jarvelin, U. Sovio, A.J. Bennett, D. Melzer, L. Ferrucci, R.J. Loos, I. Barroso, N.J. Wareham, F. Karpe, K.R. Owen, L.R. Cardon, M. Walker, G.A. Hitman, C.N. Palmer, A.S. Doney, A.D. Morris, G.D. Smith, A.T. Hattersley, and M.I. McCarthy. 2007. A common variant in the FTO gene is associated with body mass index and predisposes to childhood and adult obesity. *Science*. 316:889-894.

Frazer, K.A., C.M. Wade, D.A. Hinds, N. Patil, D.R. Cox, and M.J. Daly. 2004. Segmental phylogenetic relationships of inbred mouse strains revealed by fine-scale analysis of sequence variation across 4.6 mb of mouse genome. *Genome research*. 14:1493-1500.

Froguel, P., M. Vaxillaire, F. Sun, G. Velho, H. Zouali, M.O. Butel, S. Lesage, N. Vionnet, K. Clement, F. Fougerousse, and et al. 1992. Close linkage of glucokinase locus on chromosome 7p to early-onset non-insulin-dependent diabetes mellitus. *Nature*. 356:162-164.

Fujioka, S., Y. Matsuzawa, K. Tokunaga, and S. Tarui. 1987. Contribution of intra-abdominal fat accumulation to the impairment of glucose and lipid metabolism in human obesity. *Metabolism: clinical and experimental*. 36:54-59.

Gabriel, S.B., S.F. Schaffner, H. Nguyen, J.M. Moore, J. Roy, B. Blumenstiel, J. Higgins, M. DeFelice, A. Lochner, M. Faggart, S.N. Liu-Cordero, C. Rotimi, A. Adeyemo, R. Cooper, R. Ward, E.S. Lander, M.J. Daly, and D. Altshuler. 2002. The structure of haplotype blocks in the human genome. *Science*. 296:2225-2229.

Gasmi, L., and A.G. McLennan. 2001. The mouse Nudt7 gene encodes a peroxisomal nudix hydrolase specific for coenzyme A and its derivatives. *The Biochemical journal*. 357:33-38.

Gaulton, K.J., T. Ferreira, Y. Lee, A. Raimondo, R. Magi, M.E. Reschen, A. Mahajan, A. Locke, N.W. Rayner, N. Robertson, R.A. Scott, I. Prokopenko, L.J. Scott, T. Green, T. Sparso, D. Thuillier, L. Yengo, H. Grallert, S. Wahl, M. Franberg, R.J. Strawbridge, H. Kestler, H. Chheda, L. Eisele, S. Gustafsson, V. Steinthorsdottir, G. Thorleifsson, L. Qi, L.C. Karssen, E.M. van Leeuwen, S.M. Willems, M. Li, H. Chen, C. Fuchsberger, P. Kwan, C. Ma, M. Linderman, Y. Lu, S.K. Thomsen, J.K. Rundle, N.L. Beer, M. van de Bunt, A. Chalisey, H.M. Kang, B.F. Voight, G.R. Abecasis, P. Almgren, D. Baldassarre, B. Balkau, R. Benediktsson, M. Bluher, H. Boeing, L.L. Bonnycastle, E.P. Bottinger, N.P. Burtt, J. Carey, G. Charpentier, P.S. Chines, M.C. Cornelis, D.J. Couper, A.T. Crenshaw, R.M. van Dam, A.S. Doney, M. Dorkhan, S. Edkins, J.G. Eriksson, T. Esko, E. Eury, J. Fadista, J. Flannick, P. Fontanillas, C. Fox, P.W. Franks, K. Gertow, C. Gieger, B. Gigante, O. Gottesman, G.B. Grant, N. Grarup, C.J. Groves, M. Hassinen, C.T. Have, C. Herder, O.L. Holmen, A.B. Hreidarsson, S.E. Humphries, D.J. Hunter, A.U. Jackson, A. Jonsson, M.E. Jorgensen, T. Jorgensen, W.H. Kao, N.D. Kerrison, L. Kinnunen, N. Klopp, A. Kong, P. Kovacs, P. Kraft, J. Kravic, C. Langford, et al. 2015. Genetic fine mapping and genomic annotation defines causal mechanisms at type 2 diabetes susceptibility loci. *Nature genetics*. 47:1415-1425.

Giesen, K., L. Plum, R. Kluge, J. Ortlepp, and H.G. Joost. 2003. Diet-dependent obesity and hypercholesterolemia in the New Zealand obese mouse: identification of a quantitative trait locus for elevated serum cholesterol on the distal mouse chromosome 5. *Biochemical and biophysical research communications*. 304:812-817.

Gloyn, A.L., M.N. Weedon, K.R. Owen, M.J. Turner, B.A. Knight, G. Hitman, M. Walker, J.C. Levy, M. Sampson, S. Halford, M.I. McCarthy, A.T. Hattersley, and T.M. Frayling. 2003. Large-scale association studies of variants in genes encoding the pancreatic beta-cell KATP channel subunits Kir6.2 (KCNJ11) and SUR1 (ABCC8) confirm that the KCNJ11 E23K variant is associated with type 2 diabetes. *Diabetes*. 52:568-572.

Gonzalez-Franquesa, A., A.M. Burkart, E. Isganaitis, and M.E. Patti. 2016. What Have Metabolomics Approaches Taught Us About Type 2 Diabetes? *Curr Diab Rep*. 16:74.

Goodarzi, M.O. 2017. Genetics of obesity: what genetic association studies have taught us about the biology of obesity and its complications. *Lancet Diabetes Endocrinol*.

Grant, R.W., and V.D. Dixit. 2015. Adipose tissue as an immunological organ. *Obesity*. 23:512-518.

Grant, S.F., G. Thorleifsson, I. Reynisdottir, R. Benediktsson, A. Manolescu, J. Sainz, A. Helgason, H. Stefansson, V. Emilsson, A. Helgadottir, U. Styrkarsdottir, K.P. Magnusson, G.B. Walters, E. Palsdottir, T. Jonsdottir, T. Gudmundsdottir, A. Gylfason, J. Saemundsdottir, R.L. Wilensky, M.P. Reilly, D.J. Rader, Y. Bagger, C. Christiansen, V. Gudnason, G. Sigurdsson, U. Thorsteinsdottir, J.R. Gulcher, A. Kong, and K. Stefansson. 2006. Variant of transcription factor 7-like 2 (TCF7L2) gene confers risk of type 2 diabetes. *Nature genetics*. 38:320-323.

Griffiths, A., J. Miller, and D. Suzuki. 2000. An Introduction to Genetic Analysis. 7th edition. W. H. Freeman and Company, New York.

Groot, P.C., C.J. Moen, W. Dietrich, J.P. Stoye, E.S. Lander, and P. Demant. 1992. The recombinant congenic strains for analysis of multigenic traits: genetic composition. *FASEB journal : official publication of the Federation of American Societies for Experimental Biology*. 6:2826-2835.

Gross, C., X. Zhuang, K. Stark, S. Ramboz, R. Oosting, L. Kirby, L. Santarelli, S. Beck, and R. Hen. 2002. Serotonin1A receptor acts during development to establish normal anxiety-like behaviour in the adult. *Nature*. 416:396-400.

Grupe, A., S. Germer, J. Usuka, D. Aud, J.K. Belknap, R.F. Klein, M.K. Ahluwalia, R. Higuchi, and G. Peltz. 2001. In silico mapping of complex disease-related traits in mice. *Science*. 292:1915-1918.

Guasch-Ferre, M., A. Hruby, E. Toledo, C.B. Clish, M.A. Martinez-Gonzalez, J. Salas-Salvado, and F.B. Hu. 2016. Metabolomics in Prediabetes and Diabetes: A Systematic Review and Meta-analysis. *Diabetes care*. 39:833-846.

Guerrier-Takada, C., K. Gardiner, T. Marsh, N. Pace, and S. Altman. 1983. The RNA moiety of ribonuclease P is the catalytic subunit of the enzyme. *Cell*. 35:849-857.

Hamdy, O., S. Porramatikul, and E. Al-Ozairi. 2006. Metabolic obesity: the paradox between visceral and subcutaneous fat. *Curr Diabetes Rev*. 2:367-373.

Hardy, O.T., M.P. Czech, and S. Corvera. 2012. What causes the insulin resistance underlying obesity? *Curr Opin Endocrinol Diabetes Obes*. 19:81-87.

Haskell, B.D., K. Flurkey, T.M. Duffy, E.E. Sargent, and E.H. Leiter. 2002. The diabetes-prone NZO/HlLt strain. I. Immunophenotypic comparison to the related NZB/BlNJ and NZW/LacJ strains. *Lab Invest*. 82:833-842.

Hellemans, K., K. Kerckhofs, J.C. Hannaert, G. Martens, P. Van Veldhoven, and D. Pipeleers. 2007. Peroxisome proliferator-activated receptor alpha-retinoid X receptor agonists induce beta-cell protection against palmitate toxicity. *The FEBS journal*. 274:6094-6105.

Herberg, L., and D.L. Coleman. 1977. Laboratory animals exhibiting obesity and diabetes syndromes. *Metabolism: clinical and experimental*. 26:59-99.

Herder, C., J. Baumert, A. Zierer, M. Roden, C. Meisinger, M. Karakas, L. Chambless, W. Rathmann, A. Peters, W. Koenig, and B. Thorand. 2011. Immunological and cardiometabolic risk factors in the prediction of type 2 diabetes and coronary events: MONICA/KORA Augsburg case-cohort study. *PloS one*. 6:e19852.

Heston, W.E., and G. Vlahakis. 1971. Mammary tumors, plaques, and hyperplastic alveolar nodules in various combinations of mouse inbred strains and the different lines of the mammary tumor virus. *Int J Cancer*. 7:141-148.

Hinney, A., T.T. Nguyen, A. Scherag, S. Friedel, G. Bronner, T.D. Muller, H. Grallert, T. Illig, H.E. Wichmann, W. Rief, H. Schafer, and J. Hebebrand. 2007. Genome wide association (GWA) study for early onset extreme obesity supports the role of fat mass and obesity associated gene (FTO) variants. *PloS one*. 2:e1361.

Hossain, P., B. Kawar, and M. El Nahas. 2007. Obesity and diabetes in the developing world--a growing challenge. *N Engl J Med*. 356:213-215.

Hotamisligil, G.S. 2008. Inflammation and endoplasmic reticulum stress in obesity and diabetes. *Int J Obes (Lond)*. 32 Suppl 7:S52-54.

Hubner, N., C.A. Wallace, H. Zimdahl, E. Petretto, H. Schulz, F. Maciver, M. Mueller, O. Hummel, J. Monti, V. Zidek, A. Musilova, V. Kren, H. Causton, L. Game, G. Born, S. Schmidt, A. Muller, S.A. Cook, T.W. Kurtz, J. Whittaker, M. Pravenec, and T.J. Aitman. 2005. Integrated transcriptional profiling and linkage analysis for identification of genes underlying disease. *Nature genetics*. 37:243-253.

Igel, M., W. Becker, L. Herberg, and H.G. Joost. 1997. Hyperleptinemia, leptin resistance, and polymorphic leptin receptor in the New Zealand obese mouse. *Endocrinology*. 138:4234-4239.

Indiveri, C., V. Iacobazzi, A. Tonazzi, N. Giangregorio, V. Infantino, P. Convertini, L. Console, and F. Palmieri. 2011. The mitochondrial carnitine/acylcarnitine carrier: function, structure and physiopathology. *Mol Aspects Med*. 32:223-233.

Ingalls, A.M., M.M. Dickie, and G.D. Snell. 1950. Obese, a new mutation in the house mouse. *J Hered*. 41:317-318.

International Diabetes Federation. 2015. IDF DIABETES ATLAS Seventh Edition.

International Diabetes Federation. 2017. IDF DIABETES ATLAS Eighth edition

International HapMap, C. 2003. The International HapMap Project. *Nature*. 426:789-796.

Jones, A.G., and A.T. Hattersley. 2013. The clinical utility of C-peptide measurement in the care of patients with diabetes. *Diabetic medicine : a journal of the British Diabetic Association*. 30:803-817.

Joost, H.G. 2010. The genetic basis of obesity and type 2 diabetes: lessons from the new zealand obese mouse, a polygenic model of the metabolic syndrome. *Results Probl Cell Differ*. 52:1-11.

Joost, H.G., and A. Schurmann. 2014. The genetic basis of obesity-associated type 2 diabetes (diabesity) in polygenic mouse models. *Mamm Genome*. 25:401-412.

Junger, E., L. Herberg, K. Jeruschke, and E.H. Leiter. 2002. The diabetes-prone NZO/Hl strain. II. Pancreatic immunopathology. *Lab Invest*. 82:843-853.

Jurgens, H.S., S. Neschen, S. Ortmann, S. Scherneck, K. Schmolz, G. Schuler, S. Schmidt, M. Bluher, S. Klaus, D. Perez-Tilve, M.H. Tschop, A. Schurmann, and H.G. Joost. 2007. Development of diabetes in obese, insulin-resistant mice: essential role of dietary carbohydrate in beta cell destruction. *Diabetologia*. 50:1481-1489.

Jurgens, H.S., A. Schurmann, R. Kluge, S. Ortmann, S. Klaus, H.G. Joost, and M.H. Tschop. 2006. Hyperphagia, lower body temperature, and reduced running wheel activity precede development of morbid obesity in New Zealand obese mice. *Physiological genomics*. 25:234-241.

Kahn, S.E., R.L. Hull, and K.M. Utzschneider. 2006. Mechanisms linking obesity to insulin resistance and type 2 diabetes. *Nature*. 444:840-846.

Kahn, S.E., R.L. Prigeon, D.K. McCulloch, E.J. Boyko, R.N. Bergman, M.W. Schwartz, J.L. Neifing, W.K. Ward, J.C. Beard, J.P. Palmer, and et al. 1993. Quantification of the relationship between insulin sensitivity and beta-cell function in human subjects. Evidence for a hyperbolic function. *Diabetes*. 42:1663-1672.

Kaku, K., F.T. Fiedorek, Jr., M. Province, and M.A. Permutt. 1988. Genetic analysis of glucose tolerance in inbred mouse strains. Evidence for polygenic control. *Diabetes*. 37:707-713.

Kaku, K., J. McGill, M. Province, and M.A. Permutt. 1989. A single major gene controls most of the difference in susceptibility to streptozotocin-induced diabetes between C57BL/6J and C3H/HeJ mice. *Diabetologia*. 32:716-723.

Kaprio, J., J. Tuomilehto, M. Koskenvuo, K. Romanov, A. Reunanen, J. Eriksson, J. Stengard, and Y.A. Kesaniemi. 1992. Concordance for type 1 (insulin-dependent) and type 2 (non-insulin-dependent) diabetes mellitus in a population-based cohort of twins in Finland. *Diabetologia*. 35:1060-1067.

Kayo, T., H. Fujita, J. Nozaki, X. E, and A. Koizumi. 2000. Identification of two chromosomal loci determining glucose intolerance in a C57BL/6 mouse strain. *Comp Med*. 50:296-302.

Keane, T.M., L. Goodstadt, P. Danecek, M.A. White, K. Wong, B. Yalcin, A. Heger, A. Agam, G. Slater, M. Goodson, N.A. Furlotte, E. Eskin, C. Nellaker, H. Whitley, J. Cleak, D. Janowitz, P. Hernandez-Pliego, A. Edwards, T.G. Belgard, P.L. Oliver, R.E. McIntyre, A. Bhomra, J. Nicod, X. Gan, W. Yuan, L. van der Weyden, C.A. Steward, S. Bala, J. Stalker, R. Mott, R. Durbin, I.J. Jackson, A. Czechanski, J.A. Guerra-Assuncao, L.R. Donahue, L.G. Reinholdt, B.A. Payseur, C.P. Ponting, E. Birney, J. Flint, and D.J. Adams. 2011. Mouse genomic variation and its effect on phenotypes and gene regulation. *Nature*. 477:289-294.

Keaton, J.M., J.N. Cooke Bailey, N.D. Palmer, B.I. Freedman, C.D. Langefeld, M.C. Ng, and D.W. Bowden. 2014. A comparison of type 2 diabetes risk allele load between African Americans and European Americans. *Hum Genet*. 133:1487-1495.

Kebede, M.A., and A.D. Attie. 2014. Insights into obesity and diabetes at the intersection of mouse and human genetics. *Trends in endocrinology and metabolism: TEM*. 25:493-501.

Kesaniemi, Y.A., M. Lilja, K. Kervinen, and A. Rantala. 1992. Multiple metabolic syndrome: aspects of genetic epidemiology and molecular genetics. *Ann Med*. 24:461-464.

Kirchner, S., and Z. Ignatova. 2015. Emerging roles of tRNA in adaptive translation, signalling dynamics and disease. *Nature reviews. Genetics*. 16:98-112.

Kleinert, M., C. Clemmensen, S.M. Hofmann, M.C. Moore, S. Renner, S.C. Woods, P. Huypens, J. Beckers, M.H. de Angelis, A. Schurmann, M. Bakhti, M. Klingenspor, M. Heiman, A.D. Cherrington, M. Ristow, H. Lickert, E. Wolf, P.J. Havel, T.D. Muller, and M.H. Tschop. 2018. Animal models of obesity and diabetes mellitus. *Nat Rev Endocrinol*. 14:140-162.

Kloting, N., D. Schleinitz, K. Ruschke, J. Berndt, M. Fasshauer, A. Tonjes, M.R. Schon, P. Kovacs, M. Stumvoll, and M. Bluher. 2008. Inverse relationship between obesity and FTO gene expression in visceral adipose tissue in humans. *Diabetologia*. 51:641-647.

Kluge, R., K. Giesen, G. Bahrenberg, L. Plum, J.R. Ortlepp, and H.G. Joost. 2000. Quantitative trait loci for obesity and insulin resistance (Nob1, Nob2) and their interaction with the leptin receptor allele (LeprA720T/T1044I) in New Zealand obese mice. *Diabetologia*. 43:1565-1572.

Kluge, R., S. Scherneck, A. Schurmann, and H.G. Joost. 2012. Pathophysiology and genetics of obesity and diabetes in the New Zealand obese mouse: a model of the human metabolic syndrome. *Methods in molecular biology*. 933:59-73.

Kluth, O., D. Matzke, A. Kamitz, M. Jahnert, H. Vogel, S. Scherneck, M. Schulze, H. Staiger, F. Machicao, H.U. Haring, H.G. Joost, and A. Schurmann. 2015. Identification of Four Mouse Diabetes Candidate Genes Altering beta-Cell Proliferation. *PLoS genetics*. 11:e1005506.

Kluth, O., F. Mirhashemi, S. Scherneck, D. Kaiser, R. Kluge, S. Neschen, H.G. Joost, and A. Schurmann. 2011. Dissociation of lipotoxicity and glucotoxicity in a mouse model of obesity associated diabetes: role of forkhead box O1 (FOXO1) in glucose-induced beta cell failure. *Diabetologia*. 54:605-616.

Köbberling, J., and H. Tillil. 1982. The genetics of diabetes mellitus. *London: Academic Press*:201-209.

Koves, T.R., J.R. Ussher, R.C. Noland, D. Slentz, M. Mosedale, O. Ilkayeva, J. Bain, R. Stevens, J.R. Dyck, C.B. Newgard, G.D. Lopaschuk, and D.M. Muoio. 2008. Mitochondrial overload and incomplete fatty acid oxidation contribute to skeletal muscle insulin resistance. *Cell Metab*. 7:45-56.

Krotkiewski, M., P. Bjorntorp, L. Sjostrom, and U. Smith. 1983. Impact of obesity on metabolism in men and women. Importance of regional adipose tissue distribution. *The Journal of clinical investigation*. 72:1150-1162.

Kulkarni, R.N., K. Almind, H.J. Goren, J.N. Winnay, K. Ueki, T. Okada, and C.R. Kahn. 2003. Impact of genetic background on development of hyperinsulinemia and diabetes in insulin receptor/insulin receptor substrate-1 double heterozygous mice. *Diabetes*. 52:1528-1534.

Lander, E., and L. Kruglyak. 1995. Genetic dissection of complex traits: guidelines for interpreting and reporting linkage results. *Nature genetics*. 11:241-247.

Lander, E.S., and D. Botstein. 1989. Mapping mendelian factors underlying quantitative traits using RFLP linkage maps. *Genetics*. 121:185-199.

Lange, C., K. Jeruschke, L. Herberg, E.H. Leiter, and E. Junger. 2006. The diabetes-prone NZO/Hl strain. Proliferation capacity of beta cells in hyperinsulinemia and hyperglycemia. *Arch Physiol Biochem*. 112:49-58.

Lawrence, M.G., J. Lai, and J.A. Clements. 2010. Kallikreins on steroids: structure, function, and hormonal regulation of prostate-specific antigen and the extended kallikrein locus. *Endocrine reviews*. 31:407-446.

Lehotay, D.C., P. Hall, J. Lepage, J.C. Eichhorst, M.L. Etter, and C.R. Greenberg. 2011. LC-MS/MS progress in newborn screening. *Clin Biochem*. 44:21-31.

Leiter, E.H., P.C. Reifsnyder, K. Flurkey, H.J. Partke, E. Junger, and L. Herberg. 1998. NIDDM genes in mice: deleterious synergism by both parental genomes contributes to diabetogenic thresholds. *Diabetes*. 47:1287-1295.

Leonardi, R., Y.M. Zhang, C.O. Rock, and S. Jackowski. 2005. Coenzyme A: back in action. *Progress in lipid research*. 44:125-153.

Linder, C.C. 2001. The influence of genetic background on spontaneous and genetically engineered mouse models of complex diseases. *Lab animal*. 30:34-39.

Linder, C.C. 2006. Genetic variables that influence phenotype. *ILAR journal*. 47:132-140.

Liu, P., H. Vikis, Y. Lu, D. Wang, and M. You. 2007. Large-scale in silico mapping of complex quantitative traits in inbred mice. *PloS one*. 2:e651.

Livak, K.J., and T.D. Schmittgen. 2001. Analysis of relative gene expression data using real-time quantitative PCR and the 2(-Delta Delta C(T)) Method. *Methods*. 25:402-408.

Lubura, M., D. Hesse, M. Kraemer, N. Hallahan, M. Schupp, C. von Loffelholz, J. Kriebel, N. Rudovich, A. Pfeiffer, C. John, L. Scheja, J. Heeren, C. Koliaki, M. Roden, and A. Schurmann. 2015. Diabetes prevalence in NZO females depends on estrogen action on liver fat content. *Am J Physiol Endocrinol Metab*. 309:E968-980.

Lynch, M., and B. Walsh. 1992. Genetics and Analysis of Quantitative Traits,. Sinauer.

Lyon, M.F., S. Rastan, and B. D.M. 1996. Genetic variants and strains of the laboratory mouse, 3rd ed. Oxford University Press, Oxford, England.

Mai, M., A. Tonjes, P. Kovacs, M. Stumvoll, G.M. Fiedler, and A.B. Leichtle. 2013. Serum levels of acylcarnitines are altered in prediabetic conditions. *PloS one*. 8:e82459.

Maier, T., M. Guell, and L. Serrano. 2009. Correlation of mRNA and protein in complex biological samples. *FEBS letters*. 583:3966-3973.

Manenti, G., F. Galbiati, R. Gianni-Barrera, A. Pettinicchio, A. Acevedo, and T.A. Dragani. 2004. Haplotype sharing suggests that a genomic segment containing six genes accounts for the pulmonary adenoma susceptibility 1 (Pas1) locus activity in mice. *Oncogene*. 23:4495-4504.

Maneva-Radicheva, L., C. Amatya, C. Parker, J. Ellefson, I. Radichev, A. Raghavan, M.L. Charles, M.S. Williams, M.S. Robbins, and A.Y. Savinov. 2014. Autoimmune diabetes is suppressed by treatment with recombinant human tissue Kallikrein-1. *PloS one*. 9:e107213.

Markel, P., P. Shu, C. Ebeling, G.A. Carlson, D.L. Nagle, J.S. Smutko, and K.J. Moore. 1997. Theoretical and empirical issues for marker-assisted breeding of congenic mouse strains. *Nature genetics*. 17:280-284.

Masuyama, T., M. Fuse, N. Yokoi, M. Shinohara, H. Tsujii, M. Kanazawa, Y. Kanazawa, K. Komeda, and K. Taniguchi. 2003. Genetic analysis for diabetes in a new rat model of nonobese type 2 diabetes, Spontaneously Diabetic Torii rat. *Biochemical and biophysical research communications*. 304:196-206.

McCarthy, M.I. 2010. Genomics, type 2 diabetes, and obesity. *N Engl J Med*. 363:2339-2350.

McLaughlin, T., C. Lamendola, A. Liu, and F. Abbasi. 2011. Preferential fat deposition in subcutaneous versus visceral depots is associated with insulin sensitivity. *The Journal of clinical endocrinology and metabolism*. 96:E1756-1760.

Menni, C., E. Fauman, I. Erte, J.R. Perry, G. Kastenmuller, S.Y. Shin, A.K. Petersen, C. Hyde, M. Psatha, K.J. Ward, W. Yuan, M. Milburn, C.N. Palmer, T.M. Frayling, J. Trimmer, J.T. Bell, C. Gieger, R.P. Mohney, M.J. Brosnan, K. Suhre, N. Soranzo, and T.D. Spector. 2013. Biomarkers for type 2 diabetes and impaired fasting glucose using a nontargeted metabolomics approach. *Diabetes*. 62:4270-4276.

Mihalik, S.J., B.H. Goodpaster, D.E. Kelley, D.H. Chace, J. Vockley, F.G. Toledo, and J.P. DeLany. 2010. Increased levels of plasma acylcarnitines in obesity and type 2 diabetes and identification of a marker of glucolipotoxicity. *Obesity*. 18:1695-1700.

Misra, S., and N.S. Oliver. 2015. Diabetic ketoacidosis in adults. *Bmj*. 351:h5660.

Miyazaki, J., K. Araki, E. Yamato, H. Ikegami, T. Asano, Y. Shibasaki, Y. Oka, and K. Yamamura. 1990. Establishment of a pancreatic beta cell line that retains glucose-inducible insulin secretion: special reference to expression of glucose transporter isoforms. *Endocrinology*. 127:126-132.

Moitra, J., M.M. Mason, M. Olive, D. Krylov, O. Gavrilova, B. Marcus-Samuels, L. Feigenbaum, E. Lee, T. Aoyama, M. Eckhaus, M.L. Reitman, and C. Vinson. 1998. Life without white fat: a transgenic mouse. *Genes & development*. 12:3168-3181.

Monda, K.L., G.K. Chen, K.C. Taylor, C. Palmer, T.L. Edwards, L.A. Lange, M.C. Ng, A.A. Adeyemo, M.A. Allison, L.F. Bielak, G. Chen, M. Graff, M.R. Irvin, S.K. Rhie, G. Li, Y. Liu, Y. Liu, Y. Lu, M.A. Nalls, Y.V. Sun, M.K. Wojczynski, L.R. Yanek, M.C. Aldrich, A. Ademola, C.I. Amos, E.V. Bandera, C.H. Bock, A. Britton, U. Broeckel, Q. Cai, N.E. Caporaso, C.S. Carlson, J. Carpten, G. Casey, W.M. Chen, F. Chen, Y.D. Chen, C.W. Chiang, G.A. Coetzee, E. Demerath, S.L. Deming-Halverson, R.W. Driver, P. Dubbert, M.F. Feitosa, Y. Feng, B.I. Freedman, E.M. Gillanders, O. Gottesman, X. Guo, T. Haritunians, T. Harris, C.C. Harris, A.J. Hennis, D.G. Hernandez, L.H. McNeill, T.D. Howard, B.V. Howard, V.J. Howard, K.C. Johnson, S.J. Kang, B.J. Keating, S. Kolb, L.H. Kuller, A. Kutlar, C.D. Langefeld, G. Lettre, K. Lohman, V. Lotay, H. Lyon, J.E. Manson, W. Maixner, Y.A. Meng, K.R. Monroe, I. Morhason-Bello, A.B. Murphy, J.C. Mychaleckyj, R. Nadukuru, K.L. Nathanson, U. Nayak, A. N'Diaye, B. Nemesure, S.Y. Wu, M.C. Leske, C. Neslund-Dudas, M. Neuhouser, S. Nyante, H. Ochs-Balcom, A. Ogunniyi, T.O. Ogundiran, O. Ojengbede, O.I. Olopade, J.R. Palmer, E.A. Ruiz-Narvaez, N.D. Palmer, M.F. Press, E. Rampersaud, L.J. Rasmussen-Torvik, J.L. Rodriguez-Gil, B. Salako, E.E. Schadt, et al. 2013. A meta-analysis identifies new loci associated with body mass index in individuals of African ancestry. *Nature genetics*. 45:690-696.

Moritani, M., K. Togawa, H. Yaguchi, Y. Fujita, Y. Yamaguchi, H. Inoue, N. Kamatani, and M. Itakura. 2006. Identification of diabetes susceptibility loci in db mice by combined quantitative trait loci analysis and haplotype mapping. *Genomics*. 88:719-730.

Morris, A.P., B.F. Voight, T.M. Teslovich, T. Ferreira, A.V. Segre, V. Steinthorsdottir, R.J. Strawbridge, H. Khan, H. Grallert, A. Mahajan, I. Prokopenko, H.M. Kang, C. Dina, T. Esko, R.M. Fraser, S. Kanoni, A. Kumar, V. Lagou, C. Langenberg, J. Luan, C.M. Lindgren, M. Muller-Nurasyid, S. Pechlivanis, N.W. Rayner, L.J. Scott, S. Wiltshire, L. Yengo, L. Kinnunen, E.J. Rossin, S. Raychaudhuri, A.D. Johnson, A.S. Dimas, R.J. Loos, S. Vedantam, H. Chen, J.C. Florez, C. Fox, C.T. Liu, D. Rybin, D.J. Couper, W.H. Kao, M. Li, M.C. Cornelis, P. Kraft, Q. Sun, R.M. van Dam, H.M. Stringham, P.S. Chines, K. Fischer, P. Fontanillas, O.L. Holmen, S.E. Hunt, A.U. Jackson, A. Kong, R. Lawrence, J. Meyer, J.R. Perry, C.G. Platou, S. Potter, E. Rehnberg, N. Robertson, S. Sivapalaratnam, A. Stancakova, K. Stirrups, G. Thorleifsson, E. Tikkanen, A.R. Wood, P. Almgren, M. Atalay, R. Benediktsson, L.L. Bonnycastle, N. Burtt, J. Carey, G. Charpentier, A.T. Crenshaw, A.S. Doney, M. Dorkhan, S. Edkins, V. Emilsson, E. Eury, T. Forsen, K. Gertow, B. Gigante, G.B. Grant, C.J. Groves, C. Guiducci, C. Herder, A.B. Hreidarsson, J. Hui, A. James, A. Jonsson, W. Rathmann, N. Klopp, J. Kravic, K. Krjutskov, C. Langford, K. Leander, E. Lindholm, S. Lobbens, S. Mannisto, et al. 2012. Large-scale association analysis provides insights into the genetic architecture and pathophysiology of type 2 diabetes. *Nature genetics*. 44:981-990.

Naggert, J.K., L.D. Fricker, O. Varlamov, P.M. Nishina, Y. Rouille, D.F. Steiner, R.J. Carroll, B.J. Paigen, and E.H. Leiter. 1995. Hyperproinsulinaemia in obese fat/fat mice associated with a carboxypeptidase E mutation which reduces enzyme activity. *Nature genetics*. 10:135-142.

Neeland, I.J., A.T. Turer, C.R. Ayers, T.M. Powell-Wiley, G.L. Vega, R. Farzaneh-Far, S.M. Grundy, A. Khera, D.K. McGuire, and J.A. de Lemos. 2012. Dysfunctional adiposity and the risk of prediabetes and type 2 diabetes in obese adults. *JAMA*. 308:1150-1159.

Nettleton, J.A., M.F. Hivert, R.N. Lemaitre, N.M. McKeown, D. Mozaffarian, T. Tanaka, M.K. Wojczynski, A. Hruby, L. Djousse, J.S. Ngwa, J.L. Follis, M. Dimitriou, A. Ganna, D.K. Houston, S. Kanoni, V. Mikkila, A. Manichaikul, I. Ntalla, F. Renstrom, E. Sonestedt, F.J. van Rooij, S. Bandinelli, L. de Koning, U. Ericson, N. Hassanali, J.C. Kiefte-de Jong, K.K. Lohman, O. Raitakari, C. Papoutsakis, P. Sjogren, K. Stirrups, E. Ax, P. Deloukas, C.J. Groves, P.F. Jacques, I. Johansson, Y. Liu, M.I. McCarthy, K. North, J. Viikari, M.C. Zillikens, J. Dupuis, A. Hofman, G. Kolovou, K. Mukamal, I. Prokopenko, O. Rolandsson, I. Seppala, L.A. Cupples, F.B. Hu, M. Kahonen, A.G. Uitterlinden, I.B. Borecki, L. Ferrucci, D.R. Jacobs, Jr., S.B. Kritchevsky, M.

Orho-Melander, J.S. Pankow, T. Lehtimaki, J.C. Witteman, E. Ingelsson, D.S. Siscovick, G. Dedoussis, J.B. Meigs, and P.W. Franks. 2013. Meta-analysis investigating associations between healthy diet and fasting glucose and insulin levels and modification by loci associated with glucose homeostasis in data from 15 cohorts. *Am J Epidemiol*. 177:103-115.

Newhart, A., S.L. Powers, P.K. Shastrula, I. Sierra, L.M. Joo, J.E. Hayden, A.R. Cohen, and S.M. Janicki. 2016. RNase P protein subunit Rpp29 represses histone H3.3 nucleosome deposition. *Molecular biology of the cell*. 27:1154-1169.

Newman, B., J.V. Selby, M.C. King, C. Slemenda, R. Fabsitz, and G.D. Friedman. 1987. Concordance for type 2 (non-insulin-dependent) diabetes mellitus in male twins. *Diabetologia*. 30:763-768.

Nicholson, J.K., and I.D. Wilson. 2003. Opinion: understanding 'global' systems biology: metabonomics and the continuum of metabolism. *Nat Rev Drug Discov*. 2:668-676.

Noben-Trauth, K., J.K. Naggert, M.A. North, and P.M. Nishina. 1996. A candidate gene for the mouse mutation tubby. *Nature*. 380:534-538.

Ofman, R., D. Speijer, R. Leen, and R.J. Wanders. 2006. Proteomic analysis of mouse kidney peroxisomes: identification of RP2p as a peroxisomal nudix hydrolase with acyl-CoA diphosphatase activity. *The Biochemical journal*. 393:537-543.

Ortlepp, J.R., R. Kluge, K. Giesen, L. Plum, P. Radke, P. Hanrath, and H.G. Joost. 2000. A metabolic syndrome of hypertension, hyperinsulinaemia and hypercholesterolaemia in the New Zealand obese mouse. *Eur J Clin Invest*. 30:195-202.

Ouchi, N., J.L. Parker, J.J. Lugus, and K. Walsh. 2011. Adipokines in inflammation and metabolic disease. *Nat Rev Immunol*. 11:85-97.

Outzen, H.C., D. Corrow, and L.D. Shultz. 1985. Attenuation of exogenous murine mammary tumor virus virulence in the C3H/HeJ mouse substrain bearing the Lps mutation. *J Natl Cancer Inst*. 75:917-923.

Paigen, K. 2003. One hundred years of mouse genetics: an intellectual history. II. The molecular revolution (1981-2002). *Genetics*. 163:1227-1235.

Palmer, N.D., R.D. Stevens, P.A. Antinozzi, A. Anderson, R.N. Bergman, L.E. Wagenknecht, C.B. Newgard, and D.W. Bowden. 2015. Metabolomic profile associated with insulin resistance and conversion to diabetes in the Insulin Resistance Atherosclerosis Study. *The Journal of clinical endocrinology and metabolism*. 100:E463-468.

Palmiere, C. 2015. Postmortem diagnosis of diabetes mellitus and its complications. *Croatian medical journal*. 56:181-193.

Park, Y.G., R. Clifford, K.H. Buetow, and K.W. Hunter. 2003. Multiple cross and inbred strain haplotype mapping of complex-trait candidate genes. *Genome research*. 13:118-121.

Parker, C.C., S. Gopalakrishnan, P. Carbonetto, N.M. Gonzales, E. Leung, Y.J. Park, E. Aryee, J. Davis, D.A. Blizard, C.L. Ackert-Bicknell, A. Lionikas, J.K. Pritchard, and A.A. Palmer. 2016. Genome-wide association study of behavioral, physiological and gene expression traits in outbred CFW mice. *Nature genetics*. 48:919-926.

Pereira, S.S., and J.I. Alvarez-Leite. 2014. Low-Grade Inflammation, Obesity, and Diabetes. *Curr Obes Rep*. 3:422-431.

Perry, B.D., M.K. Caldow, T.C. Brennan-Speranza, M. Sbaraglia, G. Jerums, A. Garnham, C. Wong, P. Levinger, M. Asrar Ul Haq, D.L. Hare, S.R. Price, and I. Levinger. 2016. Muscle atrophy in patients with Type 2 Diabetes Mellitus: roles of inflammatory pathways, physical activity and exercise. *Exercise immunology review*. 22:94-109.

Peters, A.L., M.B. Davidson, D.L. Schriger, and V. Hasselblad. 1996. A clinical approach for the diagnosis of diabetes mellitus: an analysis using glycosylated hemoglobin levels. Meta-analysis Research Group on the Diagnosis of Diabetes Using Glycated Hemoglobin Levels. *JAMA*. 276:1246-1252.

Peters, L.L., R.F. Robledo, C.J. Bult, G.A. Churchill, B.J. Paigen, and K.L. Svenson. 2007. The mouse as a model for human biology: a resource guide for complex trait analysis. *Nature reviews. Genetics*. 8:58-69.

Petretto, E., J. Mangion, N.J. Dickens, S.A. Cook, M.K. Kumaran, H. Lu, J. Fischer, H. Maatz, V. Kren, M. Pravenec, N. Hubner, and T.J. Aitman. 2006. Heritability and tissue specificity of expression quantitative trait loci. *PLoS genetics*. 2:e172.

Pettersson, U.S., T.B. Walden, P.O. Carlsson, L. Jansson, and M. Phillipson. 2012. Female mice are protected against high-fat diet induced metabolic syndrome and increase the regulatory T cell population in adipose tissue. *PloS one*. 7:e46057.

Plum, L., R. Kluge, K. Giesen, J. Altmuller, J.R. Ortlepp, and H.G. Joost. 2000. Type 2 diabetes-like hyperglycemia in a backcross model of NZO and SJL mice: characterization of a susceptibility locus on chromosome 4 and its relation with obesity. *Diabetes*. 49:1590-1596.

Plumpton, F.S., and G.M. Besser. 1969. The adrenocortical response to surgery and insulin-induced hypoglycaemia in corticosteroid-treated and normal subjects. *The British journal of surgery*. 56:216-219.

Polonsky, K.S., B.D. Given, and E. Van Cauter. 1988. Twenty-four-hour profiles and pulsatile patterns of insulin secretion in normal and obese subjects. *The Journal of clinical investigation*. 81:442-448.

Poltorak, A., X. He, I. Smirnova, M.Y. Liu, C. Van Huffel, X. Du, D. Birdwell, E. Alejos, M. Silva, C. Galanos, M. Freudenberg, P. Ricciardi-Castagnoli, B. Layton, and B. Beutler. 1998. Defective LPS signaling in C3H/HeJ and C57BL/10ScCr mice: mutations in Tlr4 gene. *Science*. 282:2085-2088.

Poulsen, P., K.O. Kyvik, A. Vaag, and H. Beck-Nielsen. 1999. Heritability of type II (non-insulin-dependent) diabetes mellitus and abnormal glucose tolerance--a population-based twin study. *Diabetologia*. 42:139-145.

Poulsen, P., K. Levin, I. Petersen, K. Christensen, H. Beck-Nielsen, and A. Vaag. 2005. Heritability of insulin secretion, peripheral and hepatic insulin action, and intracellular glucose partitioning in young and old Danish twins. *Diabetes*. 54:275-283.

Prasad, R.B., and L. Groop. 2015. Genetics of type 2 diabetes-pitfalls and possibilities. *Genes (Basel)*. 6:87-123.

Ramos-Roman, M.A., L. Sweetman, M.J. Valdez, and E.J. Parks. 2012. Postprandial changes in plasma acylcarnitine concentrations as markers of fatty acid flux in overweight and obesity. *Metabolism: clinical and experimental*. 61:202-212.

Rebuffe-Scrive, M., R. Surwit, M. Feinglos, C. Kuhn, and J. Rodin. 1993. Regional fat distribution and metabolism in a new mouse model (C57BL/6J) of non-insulin-dependent diabetes mellitus. *Metabolism: clinical and experimental*. 42:1405-1409.

Reifsnyder, P.C., G. Churchill, and E.H. Leiter. 2000. Maternal environment and genotype interact to establish diabesity in mice. *Genome research*. 10:1568-1578.

Reifsnyder, P.C., and E.H. Leiter. 2002. Deconstructing and reconstructing obesity-induced diabetes (diabesity) in mice. *Diabetes*. 51:825-832.

Roberts, L.D., A. Koulman, and J.L. Griffin. 2014. Towards metabolic biomarkers of insulin resistance and type 2 diabetes: progress from the metabolome. *Lancet Diabetes Endocrinol*. 2:65-75.

Rockman, M.V., and L. Kruglyak. 2006. Genetics of global gene expression. *Nature reviews. Genetics*. 7:862-872.

Rosen, E.D., and B.M. Spiegelman. 2014. What we talk about when we talk about fat. *Cell*. 156:20-44.

Rossini, A.A., M.C. Appel, R.M. Williams, and A.A. Like. 1977. Genetic influence of the streptozotocin-induced insulitis and hyperglycemia. *Diabetes*. 26:916-920.

Russell, S.T., S. Rajani, R.S. Dhadda, and M.J. Tisdale. 2009. Mechanism of induction of muscle protein loss by hyperglycaemia. *Experimental cell research*. 315:16-25.

Schadt, E.E., J. Lamb, X. Yang, J. Zhu, S. Edwards, D. Guhathakurta, S.K. Sieberts, S. Monks, M. Reitman, C. Zhang, P.Y. Lum, A. Leonardson, R. Thieringer, J.M. Metzger, L. Yang, J. Castle, H. Zhu, S.F. Kash, T.A. Drake, A. Sachs, and A.J. Lusis. 2005. An integrative genomics approach to infer causal associations between gene expression and disease. *Nature genetics*. 37:710-717.

Schadt, E.E., S.A. Monks, T.A. Drake, A.J. Lusis, N. Che, V. Colinayo, T.G. Ruff, S.B. Milligan, J.R. Lamb, G. Cavet, P.S. Linsley, M. Mao, R.B. Stoughton, and S.H. Friend. 2003. Genetics of gene expression surveyed in maize, mouse and man. *Nature*. 422:297-302.

Schaffler, A., and J. Scholmerich. 2010. Innate immunity and adipose tissue biology. *Trends Immunol*. 31:228-235.

Scherneck, S., M. Nestler, H. Vogel, M. Bluher, M.D. Block, M. Berriel Diaz, S. Herzig, N. Schulz, M. Teichert, S. Tischer, H. Al-Hasani, R. Kluge, A. Schurmann, and H.G. Joost. 2009. Positional cloning of zinc finger domain transcription factor Zfp69, a candidate gene for obesity-associated diabetes contributed by mouse locus Nidd/SJL. *PLoS genetics*. 5:e1000541.

Schmidt, C., N.P. Gonzaludo, S. Strunk, S. Dahm, J. Schuchhardt, F. Kleinjung, S. Wuschke, H.G. Joost, and H. Al-Hasani. 2008. A meta-analysis of QTL for diabetes-related traits in rodents. *Physiological genomics*. 34:42-53.

Schooneman, M.G., F.M. Vaz, S.M. Houten, and M.R. Soeters. 2013. Acylcarnitines: reflecting or inflicting insulin resistance? *Diabetes*. 62:1-8.

Schousboe, K., P.M. Visscher, J.E. Henriksen, J.L. Hopper, T.I. Sorensen, and K.O. Kyvik. 2003. Twin study of genetic and environmental influences on glucose tolerance and indices of insulin sensitivity and secretion. *Diabetologia*. 46:1276-1283.

Schwenk, R.W., H. Vogel, and A. Schurmann. 2013. Genetic and epigenetic control of metabolic health. *Mol Metab*. 2:337-347.

Scuteri, A., S. Sanna, W.M. Chen, M. Uda, G. Albai, J. Strait, S. Najjar, R. Nagaraja, M. Orru, G. Usala, M. Dei, S. Lai, A. Maschio, F. Busonero, A. Mulas, G.B. Ehret, A.A. Fink, A.B. Weder, R.S. Cooper, P. Galan, A. Chakravarti, D. Schlessinger, A. Cao, E. Lakatta, and G.R. Abecasis. 2007. Genome-wide association scan shows genetic variants in the FTO gene are associated with obesity-related traits. *PLoS genetics*. 3:e115.

Shumar, S.A., E.W. Kerr, W.J. Geldenhuys, G.E. Montgomery, P. Fagone, P. Thirawatananond, H. Saavedra, S.B. Gabelli, and R. Leonardi. 2018. Nudt19 is a renal CoA diphosphohydrolase with biochemical and regulatory properties that are distinct from the hepatic Nudt7 isoform. *The Journal of biological chemistry*.

Sladek, R., G. Rocheleau, J. Rung, C. Dina, L. Shen, D. Serre, P. Boutin, D. Vincent, A. Belisle, S. Hadjadj, B. Balkau, B. Heude, G. Charpentier, T.J. Hudson, A. Montpetit, A.V. Pshezhetsky, M. Prentki, B.I. Posner, D.J. Balding, D. Meyre, C. Polychronakos, and P. Froguel. 2007. A genome-wide association study identifies novel risk loci for type 2 diabetes. *Nature*. 445:881-885.

Smemo, S., J.J. Tena, K.H. Kim, E.R. Gamazon, N.J. Sakabe, C. Gomez-Marin, I. Aneas, F.L. Credidio, D.R. Sobreira, N.F. Wasserman, J.H. Lee, V. Puviindran, D. Tam, M. Shen, J.E. Son, N.A. Vakili, H.K. Sung, S. Naranjo, R.D. Acemel, M. Manzanares, A. Nagy, N.J. Cox, C.C. Hui, J.L. Gomez-Skarmeta, and M.A. Nobrega. 2014. Obesity-associated variants within FTO form long-range functional connections with IRX3. *Nature*. 507:371-375.

Smith, U. 2015. Abdominal obesity: a marker of ectopic fat accumulation. *The Journal of clinical investigation*. 125:1790-1792.

Smith, U., and B.B. Kahn. 2016. Adipose tissue regulates insulin sensitivity: role of adipogenesis, de novo lipogenesis and novel lipids. *Journal of internal medicine*. 280:465-475.

Solberg Woods, L.C. 2014. QTL mapping in outbred populations: successes and challenges. *Physiological genomics*. 46:81-90.

Spicer, Z., M.L. Miller, A. Andringa, T.M. Riddle, J.J. Duffy, T. Doetschman, and G.E. Shull. 2000. Stomachs of mice lacking the gastric H,K-ATPase alpha -subunit have achlorhydria, abnormal parietal cells, and ciliated metaplasia. *The Journal of biological chemistry*. 275:21555-21565.

Stefan, N., A. Fritsche, C. Weikert, H. Boeing, H.G. Joost, H.U. Haring, and M.B. Schulze. 2008. Plasma fetuin-A levels and the risk of type 2 diabetes. *Diabetes*. 57:2762-2767.

Stinkens, R., G.H. Goossens, J.W. Jocken, and E.E. Blaak. 2015. Targeting fatty acid metabolism to improve glucose metabolism. *Obes Rev*. 16:715-757.

Surwit, R.S., M.N. Feinglos, J. Rodin, A. Sutherland, A.E. Petro, E.C. Opara, C.M. Kuhn, and M. Rebuffe-Scrive. 1995. Differential effects of fat and sucrose on the development of obesity and diabetes in C57BL/6J and A/J mice. *Metabolism: clinical and experimental*. 44:645-651.

Surwit, R.S., C.M. Kuhn, C. Cochrane, J.A. McCubbin, and M.N. Feinglos. 1988. Diet-induced type II diabetes in C57BL/6J mice. *Diabetes*. 37:1163-1167.

Suzuki, Y., C. Lanner, J.H. Kim, P.G. Vilardo, H. Zhang, J. Yang, L.D. Cooper, M. Steele, A. Kennedy, C.B. Bock, A. Scrimgeour, J.C. Lawrence, Jr., and A.A. DePaoli-Roach. 2001. Insulin control of glycogen metabolism in knockout mice lacking the muscle-specific protein phosphatase PP1G/RGL. *Molecular and cellular biology*. 21:2683-2694.

Swellam, M., M. Sayed, and A. Abdel-Fatah Ali. 2009. Clinical implications of adiponectin and inflammatory biomarkers in type 2 diabetes mellitus. *Dis Markers*. 27:269-278.

Tan, C.Y., and A. Vidal-Puig. 2008. Adipose tissue expandability: the metabolic problems of obesity may arise from the inability to become more obese. *Biochem Soc Trans*. 36:935-940.

Tanti, J.F., and J. Jager. 2009. Cellular mechanisms of insulin resistance: role of stress-regulated serine kinases and insulin receptor substrates (IRS) serine phosphorylation. *Curr Opin Pharmacol*. 9:753-762.

Taylor, B.A., C. Wnek, D. Schroeder, and S.J. Phillips. 2001. Multiple obesity QTLs identified in an intercross between the NZO (New Zealand obese) and the SM (small) mouse strains. *Mamm Genome*. 12:95-103.

Terauchi, Y., J. Matsui, R. Suzuki, N. Kubota, K. Komeda, S. Aizawa, K. Eto, S. Kimura, R. Nagai, K. Tobe, G.E. Lienhard, and T. Kadowaki. 2003. Impact of genetic background and ablation of insulin receptor substrate (IRS)-3 on IRS-2 knock-out mice. *The Journal of biological chemistry*. 278:14284-14290.

The Jackson Laboratory. 2018a. Mouse Genome Informatics Web Site. *In* URL: http://www.informatics.jax.org.

The Jackson Laboratory. 2018b. PHENOTYPE INFORMATION FOR DIET-INDUCED OBESE C57BL/6J (380050). *In* https://www.jax.org/jax-mice-and-services/strain-data-sheet-pages/phenotype-information-380050.

Thomas, D., and C. Apovian. 2017. Macrophage functions in lean and obese adipose tissue. *Metabolism: clinical and experimental*. 72:120-143.

Torn, C. 2003. C-peptide and autoimmune markers in diabetes. *Clin Lab*. 49:1-10.

Toye, A.A., J.D. Lippiat, P. Proks, K. Shimomura, L. Bentley, A. Hugill, V. Mijat, M. Goldsworthy, L. Moir, A. Haynes, J. Quarterman, H.C. Freeman, F.M. Ashcroft, and R.D. Cox. 2005. A genetic and physiological study of impaired glucose homeostasis control in C57BL/6J mice. *Diabetologia*. 48:675-686.

Trayhurn, P., and I.S. Wood. 2005. Signalling role of adipose tissue: adipokines and inflammation in obesity. *Biochem Soc Trans*. 33:1078-1081.

Tsaih, S.W., K. Holl, S. Jia, M. Kaldunski, M. Tschannen, H. He, J.W. Andrae, S.H. Li, A. Stoddard, A. Wiederhold, J. Parrington, M. Ruas da Silva, A. Galione, J. Meigs, G. Meta-Analyses of, I. Insulin-Related Traits Consortium, R.G. Hoffmann, P. Simpson, H. Jacob, M. Hessner, and L.C. Solberg Woods. 2014. Identification of a novel gene for diabetic traits in rats, mice, and humans. *Genetics*. 198:17-29.

Tu, Z., M.P. Keller, C. Zhang, M.E. Rabaglia, D.M. Greenawalt, X. Yang, I.M. Wang, H. Dai, M.D. Bruss, P.Y. Lum, Y.P. Zhou, D.M. Kemp, C. Kendziorski, B.S. Yandell, A.D. Attie, E.E. Schadt, and J. Zhu. 2012. Integrative analysis of a cross-loci regulation network identifies App as a gene regulating insulin secretion from pancreatic islets. *PLoS genetics*. 8:e1003107.

Tuomilehto, J., P. Jousilahti, D. Rastenyte, V. Moltchanov, A. Tanskanen, P. Pietinen, and A. Nissinen. 2001. Urinary sodium excretion and cardiovascular mortality in Finland: a prospective study. *Lancet*. 357:848-851.

Unger, R.H. 2003a. Lipid overload and overflow: metabolic trauma and the metabolic syndrome. *Trends in endocrinology and metabolism: TEM*. 14:398-403.

Unger, R.H. 2003b. Minireview: weapons of lean body mass destruction: the role of ectopic lipids in the metabolic syndrome. *Endocrinology*. 144:5159-5165.

Van Baak, T.E., C. Coarfa, P.A. Dugue, G. Fiorito, E. Laritsky, M.S. Baker, N.J. Kessler, J. Dong, J.D. Duryea, M.J. Silver, A. Saffari, A.M. Prentice, S.E. Moore, A. Ghantous, M.N. Routledge, Y.Y. Gong, Z. Herceg, P. Vineis, G. Severi, J.L. Hopper, M.C. Southey, G.G. Giles, R.L. Milne, and R.A. Waterland. 2018. Epigenetic supersimilarity of monozygotic twin pairs. *Genome Biol*. 19:2.

Venter, J.C., M.D. Adams, E.W. Myers, P.W. Li, R.J. Mural, G.G. Sutton, H.O. Smith, M. Yandell, C.A. Evans, R.A. Holt, J.D. Gocayne, P. Amanatides, R.M. Ballew, D.H. Huson, J.R. Wortman, Q. Zhang, C.D. Kodira, X.H. Zheng, L. Chen, M. Skupski, G. Subramanian, P.D. Thomas, J. Zhang, G.L. Gabor Miklos, C. Nelson, S. Broder, A.G. Clark, J. Nadeau, V.A. McKusick, N. Zinder, A.J. Levine, R.J. Roberts, M. Simon, C. Slayman, M. Hunkapiller, R. Bolanos, A. Delcher, I. Dew, D. Fasulo, M. Flanigan, L. Florea, A. Halpern, S. Hannenhalli, S. Kravitz, S. Levy, C. Mobarry, K. Reinert, K. Remington, J. Abu-Threideh, E. Beasley, K. Biddick, V. Bonazzi, R. Brandon, M. Cargill, I. Chandramouliswaran, R. Charlab, K. Chaturvedi, Z. Deng, V. Di Francesco, P. Dunn, K. Eilbeck, C. Evangelista, A.E. Gabrielian, W. Gan, W. Ge, F. Gong, Z. Gu, P. Guan, T.J. Heiman, M.E. Higgins, R.R. Ji, Z. Ke, K.A. Ketchum, Z. Lai, Y. Lei, Z. Li, J. Li, Y. Liang, X. Lin, F. Lu, G.V. Merkulov, N. Milshina, H.M. Moore, A.K. Naik, V.A. Narayan, B. Neelam, D. Nusskern, D.B. Rusch, S. Salzberg, W. Shao, B. Shue, J. Sun, Z. Wang, A. Wang, X. Wang, J. Wang, M. Wei, R. Wides, C. Xiao, C. Yan, et al. 2001. The sequence of the human genome. *Science*. 291:1304-1351.

Verdugo, R.A., C.R. Farber, C.H. Warden, and J.F. Medrano. 2010. Serious limitations of the QTL/microarray approach for QTL gene discovery. *BMC biology*. 8:96.

Veroni, M.C., J. Proietto, and R.G. Larkins. 1991. Evolution of insulin resistance in New Zealand obese mice. *Diabetes*. 40:1480-1487.

Visscher, P.M., M.A. Brown, M.I. McCarthy, and J. Yang. 2012. Five years of GWAS discovery. *American journal of human genetics*. 90:7-24.

Vogel, H., M. Jahnert, M. Stadion, D. Matzke, S. Scherneck, and A. Schurmann. 2017. A vast genomic deletion in the C56BL/6 genome affects different genes within the Ifi200 cluster on chromosome 1 and mediates obesity and insulin resistance. *BMC genomics*. 18:172.

Vogel, H., A. Kamitz, N. Hallahan, S. Lebek, T. Schallschmidt, W. Jonas, M. Jahnert, P. Gottmann, L. Zellner, T. Kanzleiter, M. Damen, D. Altenhofen, R. Burkhardt, S. Renner, M. Dahlhoff, E. Wolf, T.D. Muller, M. Bluher, H.G. Joost, A. Chadt, H. Al-Hasani, and A. Schurmann. 2018. A collective diabetes cross in combination with a computational framework to dissect the genetics of human obesity and Type 2 diabetes. *Human molecular genetics*. 27:3099-3112

Vogel, H., F. Mirhashemi, B. Liehl, F. Taugner, O. Kluth, R. Kluge, H.G. Joost, and A. Schurmann. 2013. Estrogen deficiency aggravates insulin resistance and induces beta-cell loss and diabetes in female New Zealand obese mice. *Hormone and metabolic research = Hormon- und Stoffwechselforschung = Hormones et metabolisme*. 45:430-435.

Vogel, H., M. Nestler, F. Ruschendorf, M.D. Block, S. Tischer, R. Kluge, A. Schurmann, H.G. Joost, and S. Scherneck. 2009. Characterization of Nob3, a major quantitative trait locus for obesity and hyperglycemia on mouse chromosome 1. *Physiological genomics*. 38:226-232.

Vogel, H., S. Scherneck, T. Kanzleiter, V. Benz, R. Kluge, M. Stadion, S. Kryvych, M. Bluher, N. Kloting, H.G. Joost, and A. Schurmann. 2012. Loss of function of Ifi202b by a microdeletion on chromosome 1 of C57BL/6J mice suppresses 11beta-hydroxysteroid dehydrogenase type 1 expression and development of obesity. *Human molecular genetics*. 21:3845-3857.

Wade, C.M., E.J. Kulbokas, 3rd, A.W. Kirby, M.C. Zody, J.C. Mullikin, E.S. Lander, K. Lindblad-Toh, and M.J. Daly. 2002. The mosaic structure of variation in the laboratory mouse genome. *Nature*. 420:574-578.

Wallingford, N., B. Perroud, Q. Gao, A. Coppola, E. Gyengesi, Z.W. Liu, X.B. Gao, A. Diament, K.A. Haus, Z. Shariat-Madar, F. Mahdi, S.L. Wardlaw, A.H. Schmaier, C.H. Warden, and S. Diano.

2009. Prolylcarboxypeptidase regulates food intake by inactivating alpha-MSH in rodents. *The Journal of clinical investigation*. 119:2291-2303.

Wang, C.Y., D.S. Stapleton, K.L. Schueler, M.E. Rabaglia, A.T. Oler, M.P. Keller, C.M. Kendziorski, K.W. Broman, B.S. Yandell, E.E. Schadt, and A.D. Attie. 2012. Tsc2, a positional candidate gene underlying a quantitative trait locus for hepatic steatosis. *Journal of lipid research*. 53:1493-1501.

Wang, J., D. Barbuskaite, M. Tozzi, A. Giannuzzo, C.E. Sorensen, and I. Novak. 2015. Proton Pump Inhibitors Inhibit Pancreatic Secretion: Role of Gastric and Non-Gastric H+/K+-ATPases. *PloS one*. 10:e0126432.

Wang, X., Z. Hu, J. Hu, J. Du, and W.E. Mitch. 2006. Insulin resistance accelerates muscle protein degradation: Activation of the ubiquitin-proteasome pathway by defects in muscle cell signaling. *Endocrinology*. 147:4160-4168.

Wang, X., R. Korstanje, D. Higgins, and B. Paigen. 2004. Haplotype analysis in multiple crosses to identify a QTL gene. *Genome research*. 14:1767-1772.

Willemsen, G., K.J. Ward, C.G. Bell, K. Christensen, J. Bowden, C. Dalgard, J.R. Harris, J. Kaprio, R. Lyle, P.K. Magnusson, K.A. Mather, J.R. Ordonana, F. Perez-Riquelme, N.L. Pedersen, K.H. Pietilainen, P.S. Sachdev, D.I. Boomsma, and T. Spector. 2015. The Concordance and Heritability of Type 2 Diabetes in 34,166 Twin Pairs From International Twin Registers: The Discordant Twin (DISCOTWIN) Consortium. *Twin Res Hum Genet*. 18:762-771.

Wiltshire, T., M.T. Pletcher, S. Batalov, S.W. Barnes, L.M. Tarantino, M.P. Cooke, H. Wu, K. Smylie, A. Santrosyan, N.G. Copeland, N.A. Jenkins, F. Kalush, R.J. Mural, R.J. Glynne, S.A. Kay, M.D. Adams, and C.F. Fletcher. 2003. Genome-wide single-nucleotide polymorphism analysis defines haplotype patterns in mouse. *Proceedings of the National Academy of Sciences of the United States of America*. 100:3380-3385.

Wong, T.K., and E. Neumann. 1982. Electric field mediated gene transfer. *Biochemical and biophysical research communications*. 107:584-587.

World Health Organization. 2016. GLOBAL REPORT ON DIABETES.

Yalcin, B., K. Wong, A. Agam, M. Goodson, T.M. Keane, X. Gan, C. Nellaker, L. Goodstadt, J. Nicod, A. Bhomra, P. Hernandez-Pliego, H. Whitley, J. Cleak, R. Dutton, D. Janowitz, R. Mott, D.J. Adams, and J. Flint. 2011. Sequence-based characterization of structural variation in the mouse genome. *Nature*. 477:326-329.

Yaney, G.C., and B.E. Corkey. 2003. Fatty acid metabolism and insulin secretion in pancreatic beta cells. *Diabetologia*. 46:1297-1312.

Yang, X., J.L. Deignan, H. Qi, J. Zhu, S. Qian, J. Zhong, G. Torosyan, S. Majid, B. Falkard, R.R. Kleinhanz, J. Karlsson, L.W. Castellani, S. Mumick, K. Wang, T. Xie, M. Coon, C. Zhang, D. Estrada-Smith, C.R. Farber, S.S. Wang, A. van Nas, A. Ghazalpour, B. Zhang, D.J. Macneil, J.R. Lamb, K.M. Dipple, M.L. Reitman, M. Mehrabian, P.Y. Lum, E.E. Schadt, A.J. Lusis, and T.A. Drake. 2009. Validation of candidate causal genes for obesity that affect shared metabolic pathways and networks. *Nature genetics*. 41:415-423.

You, W.P., and M. Henneberg. 2016. Type 1 diabetes prevalence increasing globally and regionally: the role of natural selection and life expectancy at birth. *BMJ Open Diabetes Res Care*. 4:e000161.

Zavaroni, I., G. Deferrari, R. Lugari, E. Bonora, G. Garibotto, E. Dall'Aglio, C. Robaudo, and A. Gnudi. 1987. Renal metabolism of C-peptide in man. *The Journal of clinical endocrinology and metabolism*. 65:494-498.

Zheng, Y., S.H. Ley, and F.B. Hu. 2018. Global aetiology and epidemiology of type 2 diabetes mellitus and its complications. *Nat Rev Endocrinol*. 14:88-98.

Zwick, R.K., C.F. Guerrero-Juarez, V. Horsley, and M.V. Plikus. 2018. Anatomical, Physiological, and Functional Diversity of Adipose Tissue. *Cell Metab*. 27:68-83.

6 Supplements

6.1 Publications and contribution statement

The work of this dissertation is published in the following manuscripts:

Tanja Schallschmidt, Sandra Lebek, Delsi Altenhofen, Mareike Damen, Yvonne Schulte, Birgit Knebel, Ralf Herwig, Axel Rasche, Torben Stermann, Anne Kamitz, Nicole Hallahan, Markus Jähnert, Heike Vogel, Annette Schürmann, Alexandra Chadt and Hadi Al-Hasani (2018): "Two novel candidate genes for insulin secretion identified by comparative genomics of multiple backcross mouse populations". *GENETICS* (Accepted October 16, 2018)

The manuscript was in most parts written by myself together with Sandra Lebek and completed with parts from Dr. Alexandra Chadt and Prof. Hadi Al-Hasani. Figures 1 and 2 as well as Table 1 from the manuscript were generated by me and Sandra Lebek, whereas Figure 3 was generated by Sandra Lebek. Dr. Birgit Knebel conducted the microarray analysis, whose results are shown in Figure 6B. All other Figures were prepared by myself and are based on experimental data colleted by myself.

Heike Vogel, Anne Kamitz, Nicole Hallahan, Sandra Lebek, **Tanja Schallschmidt**, Wenke Jonas, Markus Jähnert, Pascal Gottmann, Lisa Zellner, Timo Kanzleiter, Mareike Damen, Delsi Altenhofen, Ralph Burkhardt, Simone Renner, Maik Dahlhoff, Eckhard Wolf, Timo D. Müller, Matthias Blüher, Hans-Georg Joost, Alexandra Chadt, Hadi Al-Hasani and Annette Schürmann (2018): "A collective diabetes cross in combination with a computational framework to dissect the genetics of human obesity and type 2 diabetes". *Human Molecular Genetics* 27: 3099-3112.

My dissertation is part of the "collective diabetes cross", which has been established in the German Center for Diabetes Research (DZD) to identify novel diabetes susceptibility genes. The results from the four different crossbreedings are combined in the paper from Vogel *et al*. I contributed to Figures 1-3, which include QTL data from the NZOxC3H crossbreeding. In addition, I contributed to Figure 4 which shows whole-genome transcriptome data from the different parental mouse strains.

6.2 List of Figures

6.3 List of Tables

6.4 Additional Tables

6.4.1 Phenotyping data

Supplementary Table 1: Phenotyping data from the parental-, F1-, and N2(NZOxC3H) males on 45 % HFD. wk= week, Ins= insulin, TG= triglycerides. Unit for body weight, fat- and lean mass = g, unit for blood glucose: mg/dL. n=258 -329

Trait	C3H males		NZO males		F1 males		N2 males	
	Mean	SEM	Mean	SEM	Mean	SEM	Mean	SEM
Body weight wk 3	8.7	0.3	15.1	0.5	15.8	0.5	12.9	0.2
Body weight wk 4	15.9	0.4	25.4	0.6	24.7	0.7	22.8	0.2
Body weight wk 5	21.8	0.3	34.3	0.5	30.9	0.7	31.7	0.2
Body weight wk 6	25.3	0.5	39.8	0.4	35.3	0.8	37.3	0.2
Body weight wk 7	27.4	0.6	43.1	0.4	38.9	0.9	41.6	0.2
Body weight wk 8	29.8	0.7	45.9	0.5	42.4	1.0	44.8	0.2
Body weight wk 9	31.1	0.7	47.4	0.6	43.9	1.0	46.9	0.2
Body weight wk 10	33.4	0.8	50.2	0.7	45.5	1.0	49.7	0.3
Body weight wk 11	34.5	0.7	52.3	0.5	47.1	0.9	52.0	0.3
Body weight wk 12	36.8	0.7	54.6	0.9	50.6	1.1	54.5	0.3
Body weight wk 13	38.3	0.8	56.3	0.8	52.4	1.1	56.6	0.3
Body weight wk 14	39.5	0.7	56.5	1.1	54.6	1.1	58.5	0.4
Body weight wk 15	40.2	0.6	57.9	1.2	55.0	1.0	59.8	0.4
Body weight wk 16	41.3	0.5	58.6	1.3	56.7	1.0	61.3	0.4
Body weight wk 17	42.2	0.5	59.6	1.5	59.5	1.2	62.6	0.5
Body weight wk 18	42.7	0.4	59.6	1.8	60.9	1.1	64.3	0.5
Body weight wk 19	43.6	0.4	60.2	2.0	62.5	1.2	66.1	0.5
Body weight wk 20	44.1	0.4	62.1	2.3	63.2	1.0	67.6	0.6
Blood glucose wk 3	97.0	3.8	139.4	4.2	152.6	4.3	156.8	1.8
Blood glucose wk 4	190.6	4.7	260.8	6.2	226.3	7.0	219.4	1.8
Blood glucose wk 5	177.0	4.3	250.4	10.0	206.1	8.3	228.9	2.5
Blood glucose wk 6	168.7	4.3	309.9	14.9	198.7	7.4	231.7	3.8
Blood glucose wk 7	149.4	6.9	310.5	20.2	196.4	10.0	259.9	6.4
Blood glucose wk 8	160.2	8.2	312.1	21.8	192.8	9.8	281.0	7.3
Blood glucose wk 9	152.9	5.2	335.4	25.3	192.0	12.4	276.8	7.7
Blood glucose wk 10	165.6	5.3	329.6	27.7	215.8	23.4	311.8	7.9
Blood glucose wk 11	165.6	6.2	330.7	24.6	217.7	19.2	324.1	8.3
Blood glucose wk 12	156.7	6.9	339.2	26.0	245.2	23.9	357.1	8.4
Blood glucose wk 13	149.7	5.1	343.1	31.0	264.5	29.7	364.7	8.5
Blood glucose wk 14	159.7	7.5	367.3	31.7	282.9	28.7	376.0	8.4
Blood glucose wk 15	160.4	7.5	361.3	32.2	259.3	29.9	366.1	8.9
Blood glucose wk 16	161.8	7.2	358.1	31.9	311.3	26.5	369.8	8.7
Blood glucose wk 17	156.2	6.3	355.3	34.2	346.9	29.6	365.8	8.8
Blood glucose wk 18	165.5	8.5	343.0	34.3	322.4	23.7	359.7	9.0
Blood glucose wk 19	159.1	7.6	355.3	36.0	350.7	27.5	360.7	9.0
Blood glucose wk 20	157.0	6.9	342.4	33.9	377.9	23.5	349.1	9.4
Fasting Blood glucose wk 21	180.0	6.0	292.8	34.6	277.5	34.4	330.5	10.1
Fat mass wk3	0.7	0.1	2.6	0.1	2.6	0.1	2.0	0.0
Fat mass wk 6	3.0	0.2	11.3	0.2	8.6	0.5	9.6	0.1
Fat mass wk 10	7.4	0.6	16.8	0.6	13.9	0.6	16.8	0.2
Fat mass wk 15	10.7	0.3	22.5	1.2	19.7	0.7	23.9	0.3
Lean mass wk 3	8.5	0.3	12.4	0.4	13.7	0.4	10.9	0.1
Lean mass wk 6	20.7	0.2	27.2	0.2	25.0	0.3	26.3	0.1
Lean mass wk 10	25.0	0.3	31.5	0.3	29.1	0.4	30.9	0.1
Lean mass wk 15	27.6	0.5	33.1	0.3	33.3	0.3	32.4	0.1
Fasting plasma Ins wk 21 (µg/l)	4.9	0.7	6.2	1.1			9.0	0.7
Total pancr. Ins wk21 (µg/mg)	32.8	3.2	11.3	2.1			9818.4	879.0
Leber TG wk 21 (µg/mg)	38.3	3.4	53.3	4.5			40.5	0.9
Leber Glycogen wk 21 (µg/mg)	8.0	1.4	5.0	1.4			15.0	0.6
Fasting plasma Ins wk8 (µg/l)	0.2	0.0	1.0	0.1			0.2	0.1
Plasma TG wk 21 (mg/dl)	73.7	7.4	238.4	81.3			105.9	4.0
Plasma Cholesterol wk21 (mg/dl)							11.9	0.2

Supplementary Table 2: Phenotyping data from the parental- and N2(NZOxC3H) females on 45 % HFD. wk= week, Ins= insulin. Unit for body weight, fat- and lean mass = g, unit for blood glucose: mg/dL. n= 304- 310

Trait	C3H females		NZO females		N2 females	
	Mean	SEM	Mean	SEM	Mean	SEM
Body weight wk 3	13.7	0.5	13.4	0.5	12.6	0.2
Body weight wk 6	21.7	0.6	32.3	0.8	31.0	0.2
Body weight wk 10	31.3	1.4	47.8	1.0	43.9	0.4
Body weight wk 15	38.1	1.6	59.1	1.6	54.0	0.5
Body weight wk 18	40.2	1.6	64.9	1.9	58.4	0.6
Body weight wk 19	41.5	1.4	65.9	1.9	59.6	0.6
Body weight wk 20	42.5	1.5	66.4	2.0	60.9	0.6
Body weight wk 21	43.4	1.4	67.7	2.1		
Blood glucose wk 3	138.4	2.7	136.8	5.7	155.6	1.8
Blood glucose wk 6	140.6	6.2	171.3	8.0	178.5	1.5
Blood glucose wk 10	129.2	4.3	163.1	10.6	177.5	2.1
Blood glucose wk 15	124.8	4.7	213.8	17.2	183.5	3.8
Blood glucose wk 18	133.3	3.7	231.2	23.1	190.3	4.1
Blood glucose wk 19	121.9	2.5	223.4	20.6	193.6	4.3
Blood glucose wk 20	119.2	3.1	205.2	21.7	194.4	4.5
Blood glucose wk 21	120.8	3.7	190.7	22.9		
Fasting Blood glucose wk 21/ 22	136.8	4.7	181.1	20.9	191.8	4.6
Fat mass wk3	1.2	0.1	2.7	0.2	2.1	0.1
Fat mass wk 6	3.5	0.4	11.7	0.5	10.0	0.1
Fat mass wk 10	10.0	1.0	22.9	0.8	19.4	0.3
Fat mass wk 15	14.2	0.9	32.2	1.2	26.9	0.4
Lean mass wk 3	11.8	0.4	10.3	0.4	10.4	0.1
Lean mass wk 6	17.5	0.3	19.7	0.3	19.8	0.1
Lean mass wk 10	20.3	0.4	22.5	0.4	22.8	0.1
Lean mass wk 15	22.5	0.6	25.8	0.4	24.9	0.1
Fasting plasma Ins wk 22 (µg / L)	4.7	0.8	9.9	1.5		
Total pancr. Ins wk22 (µg/mg)	26.5	1.9	40.1	6.6		

Supplementary Table 3: Metabolome data from the N2(NZOxC3H) males and females on 45 % HFD. The blood samples were collected at 10 weeks of age. Unit= µmol/L, n= 319 males and 304 females

	N2 males		N2 females	
Metabolite	**Mean**	**SEM**	**Mean**	**SEM**
Gln	0.905	0.016	0.848	0.024
Lys	236.786	4.928	237.752	3.486
OH-Prol	646.430	16.489	516.134	9.942
PiPA	82.387	2.503	73.158	1.646
Aba	1.857	0.143	1.423	0.050
Ala	250.210	4.121	223.156	3.635
Arg	64.328	0.828	51.331	0.523
Asn	2.126	0.071	1.364	0.040
Asp	295.652	6.198	135.116	3.435
Carnosin	0.153	0.016	0.142	0.014
Cit	45.323	0.453	45.120	0.508
Glu	260.506	2.996	189.902	1.897
Gly	179.034	4.408	141.780	1.874
His	230.650	4.143	164.612	3.167
Leu/Ile	284.066	5.840	193.907	2.511
MeHis	26.130	1.124	7.922	0.273
Met	60.988	1.187	59.358	1.294
Orn	154.341	15.606	46.453	2.621
Phe	87.154	1.165	72.879	0.905
Pro	177.653	3.662	133.151	2.947
Sarc	109.432	1.678	141.867	3.121
Ser	371.312	6.508	440.422	12.801
Tau	1.545	0.034	1.714	0.047

	N2 males		N2 females	
Metabolite	**Mean**	**SEM**	**Mean**	**SEM**
Thr	57.114	0.786	54.822	0.962
Trp	98.357	1.747	57.136	1.305
Tyr	130.694	2.135	100.780	1.586
Val	254.620	6.763	180.576	3.209
C0	26.481	0.416	23.785	0.342
C2 (263)	20.526	0.264	16.665	0.217
C3	0.790	0.024	0.706	0.023
C3DC	0.111	0.009	0.077	0.007
C4	0.425	0.014	0.407	0.014
C4-OH	0.282	0.012	0.222	0.010
C5	0.250	0.010	0.194	0.008
C5 OH+HMG	0.214	0.008	0.189	0.008
C5:1	0.008	0.002	0.012	0.002
C6	0.080	0.005	0.061	0.005
C6DC	0.015	0.002	0.010	0.002
C8	0.203	0.008	0.199	0.009
C8:1	0.008	0.002	0.008	0.002
C10	0.143	0.007	0.130	0.008
C10:1	0.059	0.005	0.050	0.005
C12	0.223	0.008	0.185	0.008
C14	0.484	0.016	0.381	0.012
C14:1	0.199	0.008	0.149	0.007
C14OH	0.064	0.005	0.048	0.004
C16	1.890	0.032	1.680	0.027
C16:1	0.251	0.009	0.191	0.009
C16:1OH	0.071	0.005	0.053	0.004
C16OH	0.176	0.009	0.120	0.007
Glut	0.082	0.006	0.064	0.006
MeGlut	0.015	0.002	0.011	0.002
MMA	0.310	0.011	0.298	0.011
C18	0.701	0.014	0.650	0.014
C18:1	0.767	0.017	0.692	0.013
C18:1OH	0.075	0.005	0.064	0.005
C18:2	0.237	0.008	0.158	0.006
C18:2OH	0.018	0.002	0.011	0.002
C18OH	0.051	0.004	0.044	0.004
C20:1	0.014	0.002	0.007	0.002
C20:2	0.013	0.002	0.013	0.002
C20:3	0.006	0.001	0.003	0.001

Supplementary Table 4: Phenotyping data for *Cdp7-prox*-associated traits from *Cdp7-prox*$^{NZO/NZO}$ and *Cdp7-prox*$^{NZO/C3H}$ N2(NZOxC3H) males on 45 % HFD. wk= week, Ins= insulin, FFA= final free fatty acids. Unit for body weight, fat- and lean mass = g, unit for blood glucose: mg/dL. n= 150-176 Cdp7-prox$^{NZO/NZO}$ and 149-151 Cdp7-prox$^{NZO/C3H}$

Trait	N2 males			
	Cdp7-prox $^{NZO/NZO}$		*Cdp7-prox* $^{NZO/C3H}$	
	Mean	SEM	Mean	SEM
Body weight wk 3	13.0	0.2	12.7	0.2
Body weight wk 4	23.1	0.4	22.4	0.3
Body weight wk 5	31.8	0.3	31.5	0.3
Body weight wk 6	37.5	0.3	37.0	0.3
Body weight wk 7	41.9	0.3	41.3	0.3
Body weight wk 8	44.9	0.3	44.7	0.4
Body weight wk 9	46.9	0.3	46.9	0.4
Body weight wk 10	49.4	0.3	50.0	0.4
Body weight wk 11	51.4	0.4	52.8	0.4
Body weight wk 12	53.4	0.4	55.8	0.5
Body weight wk 13	55.2	0.5	58.1	0.5
Body weight wk 14	56.8	0.5	60.2	0.5
Body weight wk 15	58.0	0.6	61.5	0.6
Body weight wk 16	59.1	0.6	63.4	0.6
Body weight wk 17	59.8	0.7	65.4	0.6
Body weight wk 18	61.5	0.7	67.0	0.7
Body weight wk 19	62.9	0.8	69.0	0.7
Body weight wk 20	64.3	0.9	70.7	0.7
Blood glucose wk 3	163.6	2.5	149.1	2.5
Blood glucose wk 4	222.6	2.6	215.6	2.4
Blood glucose wk 5	235.1	3.9	222.0	2.7
Blood glucose wk 6	248.5	6.1	212.6	3.8
Blood glucose wk 7	303.5	10.2	209.6	4.9
Blood glucose wk 8	330.6	11.1	224.0	6.7
Blood glucose wk 9	327.9	12.1	217.9	6.3
Blood glucose wk 10	368.8	11.8	247.2	7.5
Blood glucose wk 11	374.8	12.2	268.0	9.2
Blood glucose wk 12	409.3	11.9	299.5	10.2
Blood glucose wk 13	411.5	12.0	314.9	10.8
Blood glucose wk 14	416.9	11.9	333.9	11.0
Blood glucose wk 15	408.5	12.2	322.6	12.0
Blood glucose wk 16	404.7	12.4	335.1	11.6
Blood glucose wk 17	395.3	12.8	337.2	11.9
Blood glucose wk 18	392.3	13.3	328.6	11.8
Blood glucose wk 19	395.1	13.2	329.2	12.0
Blood glucose wk 20	383.6	14.0	317.5	12.1
FFBG wk 21	136.5	4.7	116.3	2.0
Fat mass wk3	2.0	0.1	1.9	0.1
Fat mass wk 6	9.8	0.2	9.3	0.2
Fat mass wk 10	16.7	0.3	16.8	0.3
Fat mass wk 15	22.8	0.5	25.0	0.4
Lean mass wk 3	10.9	0.2	10.8	0.2
Lean mass wk 6	26.3	0.2	26.3	0.2
Lean mass wk 10	30.5	0.2	31.3	0.2
Lean mass wk 15	31.5	0.2	33.2	0.2
Fasting plasma Ins wk 21 (µg /L)	6.5	0.6	11.3	1.1
Fasting FFA wk 8	1.6	0.0	1.8	0.0
Propionylcarnitine wk 10 (µmol/L)	0.7	0.0	0.9	0.0

Supplementary Table 5: Phenotyping data for *fCdp7-prox*-associated traits from *Cdp7-prox*$^{NZO/NZO}$ and *Cdp7-prox*$^{NZO/C3H}$ N2(NZOxC3H) females on 45 % HFD. wk= week, unit for blood glucose: mg/dL, n= 175-176 *fCdp7-prox*$^{NZO/NZO}$ and 128 *Cdp7-prox*$^{NZO/C3H}$ mice

	N2 females			
	fCdp7-prox $^{NZO/NZO}$		*fCdp7-prox* $^{NZO/C3H}$	
Trait	**Mean**	**SEM**	**Mean**	**SEM**
Blood glucose wk 3	156.2	2.5	155.8	2.5
Blood glucose wk 6	180.8	2.2	175.9	2.2
Blood glucose wk 10	183.8	3.1	169.4	2.8
Blood glucose wk 15	196.6	5.8	166.7	4.2
Blood glucose wk 18	202.4	5.9	174.6	5.4
Blood glucose wk 19	206.8	6.4	176.4	5.3
Blood glucose wk 20	214.4	6.6	169.1	5.1
Fasting Blood glucose wk 21	205.0	6.6	175.3	5.9

Supplementary Table 6: Phenotyping data from RCS.NZO.C3H-*Cdp7*con mice on 45 % HFD. The significance for body weight, blood glucose and body composition were determined by 2-way-ANOVA followed by Bonferroni's multiple comparisons test; an unpaired t-test (two-tailed) was applied for the other traits, *p< 0.05, **p<0.01, ***p<0.001. ns= not significant, wk= week, Ins= insulin, AUC= Area under the curve. Unit for body weight, fat- and lean mass = g, unit for blood glucose: mg/dL. n= 15-16 males and 11-21 females

	RCS.NZO.C3H-Cdp7con males					RCS.NZO.C3H-Cdp7con females				
	Cdp7 $^{NZO/NZO}$		*Cdp7* $^{C3H/C3H}$			*Cdp7* $^{NZO/NZO}$		*Cdp7* $^{C3H/C3H}$		
Trait	**Mean**	**SEM**	**Mean**	**SEM**	**significance**	**Mean**	**SEM**	**Mean**	**SEM**	**significance**
Body weight wk 3	15.1	0.7	13.8	0.5	*ns*	15.1	0.5	15.5	0.9	*ns*
Body weight wk 4	22.8	0.6	23.4	0.6	*ns*	21.3	0.5	23.1	0.8	*ns*
Body weight wk 5	30.1	0.8	32.2	0.6	*ns*	27.0	0.7	29.8	0.8	*ns*
Body weight wk 6	35.4	1.0	37.5	0.8	*ns*	31.3	0.9	34.1	1.1	*ns*
Body weight wk 7	39.3	1.1	40.9	1.1	*ns*	35.0	1.0	37.3	1.1	*ns*
Body weight wk 8	42.8	1.2	44.8	1.3	*ns*	38.7	1.3	41.4	1.2	*ns*
Body weight wk 9	44.6	1.3	47.8	2.5	*ns*	41.4	1.5	44.4	1.3	*ns*
Body weight wk 10	46.9	1.2	50.1	1.5	*ns*	43.5	1.6	46.8	1.6	*ns*
Body weight wk 11	48.6	1.2	53.8	1.7	*ns*	46.1	1.7	49.6	1.3	*ns*
Body weight wk 12	50.4	1.4	55.7	2.0	*ns*	48.4	1.9	51.5	1.5	*ns*
Body weight wk 13	51.5	1.5	58.9	2.1	**	51.4	2.1	52.5	2.3	*ns*
Body weight wk 14	51.6	1.7	60.5	2.1	***	53.0	2.1	55.8	1.6	*ns*
Body weight wk 15	53.7	2.0	62.4	2.4	***	55.3	2.2	58.2	1.7	*ns*
Body weight wk 16	55.0	1.8	63.7	2.5	***	57.0	2.4	58.5	2.3	*ns*
Blood glucose wk 3	166.9	5.4	170.1	4.3	*ns*	174.8	4.8	147.2	7.5	*ns*
Blood glucose wk 4	221.4	9.5	207.2	5.8	*ns*	184.3	4.9	162.2	7.1	*ns*
Blood glucose wk 5	210.8	12.8	196.8	6.6	*ns*	176.0	6.2	159.0	5.6	*ns*
Blood glucose wk 6	184.6	17.9	200.4	10.4	*ns*	168.3	6.8	158.6	10.6	*ns*
Blood glucose wk 7	204.3	19.0	182.4	5.2	*ns*	159.9	6.3	140.7	3.5	*ns*
Blood glucose wk 8	193.1	14.4	269.1	28.6	*ns*	168.3	7.0	148.5	4.0	*ns*
Blood glucose wk 9	244.5	30.0	192.3	15.2	*ns*	158.1	4.9	150.5	4.7	*ns*
Blood glucose wk 10	248.7	32.6	184.7	8.8	*ns*	168.2	6.1	151.9	4.8	*ns*
Blood glucose wk 11	283.8	40.3	220.4	17.0	*ns*	167.3	6.3	142.8	2.6	*ns*
Blood glucose wk 12	304.1	46.3	218.5	17.2	*ns*	172.5	5.6	137.2	3.2	*ns*
Blood glucose wk 13	296.6	48.8	242.1	20.5	*ns*	189.7	12.1	143.8	3.0	**
Blood glucose wk 14	281.8	45.1	212.3	18.3	*ns*	201.0	12.4	142.0	6.0	****
Blood glucose wk 15	297.2	44.7	221.9	17.2	*ns*	198.1	14.7	136.5	3.0	****
Blood glucose wk 16	292.9	44.4	218.7	19.7	*ns*	182.3	12.4	133.5	6.3	**
Fasting Blood glucose wk 17	224.3	38.0	241.8	20.6	*ns*	190.0	15.4	146.0	4.9	*
Fat mass wk 3	2.3	0.2	2.4	0.2	*ns*	2.9	0.2	3.5	0.3	*ns*
Fat mass wk 6	8.3	0.5	9.6	0.4	*ns*	9.3	0.4	10.7	0.7	*ns*
Fat mass wk 10	14.5	0.9	16.6	1.1	*ns*	18.3	1.0	19.5	1.2	*ns*
Fat mass wk 15	18.7	1.8	25.4	2.0	****	27.9	1.6	28.3	1.2	*ns*
Lean mass wk 3	11.9	0.5	11.3	0.4	*ns*	11.3	0.3	11.7	0.5	*ns*
Lean mass wk 6	25.6	0.6	26.7	0.5	*ns*	20.4	0.5	22.1	0.3	*ns*
Lean mass wk 10	30.9	0.5	31.5	0.6	*ns*	23.4	0.6	25.8	0.5	*ns*
Lean mass wk 15	33.4	0.6	34.2	0.7	*ns*	25.9	0.6	27.7	0.5	*ns*
Fasting plasma Ins wk 17 (µg/L)	3.0	0.5	18.3	4.0	**	11.7	2.0	7.3	1.6	*ns*
Fasting C-Peptid wk 17 (µg/L)	2.1	0.2	5.5	0.7	***	4.7	0.5	3.0	0.4	*
AUC Blood glucose GTT	78229.2	4783.1	79692.5	3711.5	*ns*	74363.2	2937.7	47859.5	2456.2	***
AUC Blood Glucose ITT	14269.0	3009.5	12994.5	1382.7	*ns*	10543.2	664.4	6983.9	340.7	***

Supplementary Table 7: Phenotyping data from RCS.B6.C3H-*Cdp7*con mice on 60 % HFD. The significance for body weight, blood glucose and body composition were determined by 2-way-ANOVA followed by Bonferroni's multiple comparisons test; an unpaired t-test (two-tailed) was applied for the other traits, *p< 0.05, **p<0.01, ***p<0.001. ns= not significant, wk= week, Ins= insulin, AUC= Area under the curve. Unit for body weight, fat- and lean mass = g, unit for blood glucose: mg/dL. n= 11-13 males and 11-12 females

	RCS.B6.C3H-*Cdp7con* males					RCS.B6.C3H-*Cdp7con* females				
	Cdp7 $^{B6/B6}$		*Cdp7* $^{C3H/C3H}$			*Cdp7* $^{B6/B6}$		*Cdp7* $^{C3H/C3H}$		
Trait	**Mean**	**SEM**	**Mean**	**SEM**	**significance**	**Mean**	**SEM**	**Mean**	**SEM**	**significance**
Body weight wk 3	10.0	0.9	9.8	0.7	*ns*	9.1	0.9	9.3	0.6	*ns*
Body weight wk 4	16.5	1.0	16.0	0.8	*ns*	14.2	0.7	14.1	0.6	*ns*
Body weight wk 5	21.4	0.6	20.2	0.4	*ns*	17.5	0.3	17.2	0.3	*ns*
Body weight wk 6	24.1	0.6	22.2	0.4	*ns*	18.5	0.3	18.3	0.3	*ns*
Body weight wk 7	26.3	0.6	24.0	0.5	*ns*	19.2	0.4	19.3	0.3	*ns*
Body weight wk 8	28.3	0.7	25.5	0.5	*ns*	20.5	0.5	20.2	0.3	*ns*
Body weight wk 9	29.9	0.8	26.7	0.6	*ns*	21.2	0.4	21.0	0.3	*ns*
Body weight wk 10	31.8	0.9	28.0	0.7	*ns*	22.3	0.6	22.1	0.4	*ns*
Body weight wk 11	33.4	1.1	29.2	0.7	*ns*	23.1	0.8	22.8	0.4	*ns*
Body weight wk 12	35.4	1.4	30.6	0.9	*ns*	24.4	1.0	24.1	0.5	*ns*
Body weight wk 13	36.8	1.6	31.8	0.9	*	24.2	1.1	24.7	0.6	*ns*
Body weight wk 14	37.0	1.6	32.3	1.0	*ns*	24.5	1.0	24.9	0.7	*ns*
Body weight wk 15	38.6	1.6	33.9	1.2	*ns*	25.0	1.1	24.9	0.6	*ns*
Body weight wk 16	39.4	1.7	34.1	1.2	*	25.8	1.2	26.1	0.7	*ns*
Body weight wk 17	40.9	1.8	35.7	1.3	*	26.8	1.4	26.8	0.8	*ns*
Body weight wk 18	43.5	1.8	37.3	1.6	**	28.2	1.7	27.7	0.8	*ns*
Body weight wk 19	45.0	1.7	38.1	1.7	***	28.2	1.6	29.4	1.0	*ns*
Body weight wk 20	46.6	1.7	39.0	1.8	****	29.2	1.8	30.7	1.1	*ns*
Blood glucose wk 3	164.3	11.1	154.8	10.6	*ns*	159.2	8.7	154.9	8.1	*ns*
Blood glucose wk 4	226.7	13.0	180.5	9.3	**	188.5	7.9	161.3	11.6	*ns*
Blood glucose wk 5	206.6	13.4	187.9	7.9	*ns*	179.7	7.4	172.7	9.9	*ns*
Blood glucose wk 6	199.9	7.1	195.5	8.6	*ns*	164.4	7.6	159.1	7.7	*ns*
Blood glucose wk 7	197.9	9.8	185.5	9.2	*ns*	166.5	6.6	197.1	11.6	*ns*
Blood glucose wk 8	186.8	12.8	179.8	5.0	*ns*	180.7	7.7	165.4	7.1	*ns*
Blood glucose wk 9	188.1	9.3	166.7	6.0	*ns*	169.1	4.9	155.8	6.4	*ns*
Blood glucose wk 10	167.4	8.4	178.2	5.9	*ns*	163.5	5.6	173.5	7.6	*ns*
Blood glucose wk 11	182.2	4.2	166.2	4.3	*ns*	169.8	6.9	168.0	8.0	*ns*
Blood glucose wk 12	188.9	7.2	161.6	7.5	*ns*	176.6	6.1	167.0	5.3	*ns*
Blood glucose wk 13	172.1	8.5	166.6	6.8	*ns*	169.6	4.2	171.6	8.6	*ns*
Blood glucose wk 14	195.1	7.6	175.5	4.9	*ns*	178.9	5.5	163.9	7.7	*ns*
Blood glucose wk 15	205.2	8.7	190.6	6.8	*ns*	165.8	6.9	160.5	7.8	*ns*
Blood glucose wk 16	193.3	7.4	180.6	7.4	*ns*	168.0	8.2	156.4	5.8	*ns*
Blood glucose wk 17	177.8	10.0	170.7	6.3	*ns*	152.4	6.5	159.1	6.8	*ns*
Blood glucose wk 18	187.4	14.9	174.8	8.3	*ns*	166.1	7.9	153.1	7.1	*ns*
Blood glucose wk 19	191.1	8.6	171.9	8.9	*ns*	158.6	5.4	147.4	5.3	*ns*
Blood glucose wk 20	198.3	5.4	169.5	9.6	*ns*	159.8	5.8	146.4	7.2	*ns*
Fasting Blood glucose wk 21	171.5	10.3	174.0	7.4	*ns*	149.2	9.1	147.8	8.3	*ns*
Fat mass wk3	0.9	0.1	0.7	0.1	ns	0.7	0.1	0.8	0.1	*ns*
Fat mass wk 6	2.1	0.1	1.7	0.1	ns	2.1	0.1	1.9	0.1	*ns*
Fat mass wk 10	5.2	0.7	3.4	0.5	ns	3.0	0.4	2.8	0.3	*ns*
Fat mass wk 15	9.5	1.3	6.4	1.2	**	4.5	0.8	4.4	0.5	*ns*
Lean mass wk 3	8.9	0.8	9.0	0.6	*ns*	8.2	0.7	8.3	0.5	*ns*
Lean mass wk 6	21.4	0.6	19.9	0.3	*ns*	15.4	0.2	15.6	0.3	*ns*
Lean mass wk 10	26.1	0.6	24.0	0.6	*ns*	18.3	0.2	18.0	0.5	*ns*
Lean mass wk 15	28.2	0.7	26.6	0.8	*ns*	19.7	0.2	19.8	0.3	*ns*
Fasting plasma Ins wk 21 (µg/L)	4.5	0.8	1.3	0.3	**	0.4	0.1	0.7	0.2	*ns*
Plasma C-Peptid wk 21 (µg/L)	3.0	0.4	1.0	0.2	*	/	/	/	/	*ns*
Total pancr. Isulin wk21	14.0	0.5	14.5	0.7	*ns*	/	/	/	/	*ns*
AUC Blood glucose GTT	72871.4	3840.9	55554.4	4976.5	**	48247.5	1944.1	43780.2	2201.5	*ns*
AUC Blood glucose ITT	9943.3	598.9	8158.8	422.9	**	6388.8	334.0	5876.6	320.8	*ns*

6.4.2 QTL data

Supplementary Table 8: All significant QTLs (LOD >3) from the N2(NZOxC3H) males. The significance threshold was determined with the help of a 100 permutation test; the 95 %-confidence interval was calculated by Bayesian method. Citrulline, Glutamic acid, Tryptophan, Valine, Carnitine free, Propionylcarnitine, and Glutarylcarntine represent blood metabolites. LOD= logarithm of the odds, FFA= free fatty acids, BMI= Body mass index, Ins= insulin, Chr= Chromosome, cM= Centimorgan, Mb-Pos= Mega base pair position. n= 258 -329

Phenotype	Chr.	Position (cM)	Confidence interval (cM)	Closest SNP-marker (Mb-Pos.)	max. LOD	Week	Mean NZO/NZO	Mean C3H/NZO	Effect size (unit)
Blood glucose	7	12	7_27	37.3	13.3	10	369	247	122 mg/dL
	7	26	28_73	76.7	12.6	10	374	252	122 mg/dL
	15	13	6_17	63.3	6.6	15	409	310	99 mg/dL
	15	36	19_38	63.3	5.5	10	349	272	77 mg/dL
	4	44	38_52	119.0	6.5	20	291	400	109 mg/dL
	5	34	14_43	63.4	6.5	7	293	225	68 mg/dL
	6	52	33_52	139.0	4.9	12	394	312	82 mg/dL
	14	24	17_34	77.5	3.8	9	304	241	63 mg/dL
	18	12	6_18	43.9	4.3	3	164	148	16 mg/dL
	8	11	2_18	41.1	4.3	10	346	279	67 mg/dL
	16	28	7_32	63.8	4.2	10	343	277	67 mg/dL
	3	33	2_49	102.0	3.7	10	328	289	39 mg/dL
	11	22	17_48	82.7	3.1	8	306	250	58 mg/dL
	1	6	0_18	27.3	3.2	8	306	252	54 mg/dL
	17	20	3_28	55.3	3.3	9	305	243	62 mg/dL
Body weight	4	30	23_41	91.0	8.4	19	70.7	64.2	6.5 g
	7	17	7_22	37.3	7.4	17	59.8	65.4	6.4 g
	16	1	0_25	11.5	4.1	6	38.1	36.3	1.8 g
	14	26	6_31	77.5	3.3	6	38	36.3	1.7 g
	3	31	11_46	104.0	3.3	7	42.4	40.7	1.7 g
	10	3	0_15	69.6	3.0	5	32.3	30.8	1.5 g
Lean mass	7	11	4_21	37.3	8.6	15	31.5	33.2	1.7 g
	3	29	17_39	86.2	7.4	6	27	25.6	1.4 g
	10	8	0_14	89.1	5.6	6	26.9	25.6	1.2 g
	2	29	22_44	84.0	4.2	6	26.7	25.6	1.1 g
	16	0	0_26	11.5	3.4	6	26.7	25.7	1.0 g
	6	29	2_39	81.2	3.0	15	31.9	33	1.1 g
Fat mass	14	26	6_32	77.5	4.9	6	10.1	8.9	1.1 g
	4	30	1_40	91.0	4.0	6	10.1	9	1.0 g
	2	25	16_49	84.0	3.2	15	22.8	25.3	2.5 g
BMI	4	36	25_47	91.0	7.1	21	0.46	0.43	0.03 g/cm2
	7	12	3_22	37.3	5.0	21	0.43	0.46	0.03 g/cm2
Lenght	7	9	2_23	37.3	4.6	21	12.2	12.4	0.2 cm
	4	29	12_58	91.0	2.8	21	12.35	12.18	0.17 cm
Liver weight	18	23	14_35	63.0	5.5	21	286	251	345 mg
	5	46	37_53	102.8	3.1	21	255	282	280 mg
Liver triglycerides	18	26	19_31	63.0	13.6	21	46.7	33.9	12.8 µg/mg
Liver glycogen	18	20	4_35	63.0	3.3	21	12.4	17.4	5 µg/mg
Plasma FFA	5	67	56_67	132.9	4.5	21	1.72	1.69	0.03 µg/mg
Refed FFA	4	45	9_64	119.0	3.0	8	1.6	1.9	0.3 mmol/L
Fasting FFA	7	18	7_68	37.3	3.7	8	1.6	1.8	0.2 mmol/L
Plasma Cholesterol	1	58	53_58	172.9	6.7	21	11.0	12.8	1.82 mg/dL
Plasma Ins	7	17	13_25	37.3	4.8	21	6.5	11.3	4.8 µg/L
	4	44	44_62	119.0	4.1	21	10.8	7.2	3.7 µg/L
	6	32	3_52	101.0	3.3	21	8.4	1.2	1.2 µg/L
Fasting plasma Ins	8	12	5_39	41.1	3.9	8	1.5	1.1	0.4 µg/L
Total pancr. Ins	4	45	49_51	119.0	4.2	21	12849	6216	6.3 µg/mg
Citrulline	2	3	0_24	28.7	3.0	10	46.7	43.4	3.32 µmol/L
	6	17	2_50	64.2	3.0	10	46.8	3.17	3.17 µmol/L
Leucine/ Isoleucine	5	36	15_47	82.9	3.6	10	262	260	12 µmol/L
	11	16	2_34	65.5	3.5	10	261	257	4 µmol/L
	10	0	0_27	69.6	3.3	10	263	257	5 µmol/L
Tryptophan	15	6	0_12	48.9	3.9	10	104	89	15 µmol/L
Valine	5	24	15_43	44.8	3.8	10	282	228	54 µmol/L
	11	17	4_37	82.7	3.4	10	279	228	51 µmol/L
	6	2	0_47	28.7	3.2	10	279	228	51 µmol/L
	16	30	2_31	75.1	3.0	10	278	229	49 µmol/L
Carnitine free	7	5	0_12	16.6	7.0	10	24.4	29.1	4.6 µmol/L
	14	27	0_32	77.5	4.8	10	24.9	28.7	3.8 µmol/L
	6	52	15_52	138.5	3.3	10	25.1	28.3	3.2 µmol/L
Propionylcarnitine	7	12	0_25	37.3	3.1	10	0.7	0.9	0.2 µmol/L
Glutarylcarntine	13	29	20_29	74.3	3.3	10	0.1	0.06	0.04 µmol/L

Supplementary Table 9: All significant QTLs (LOD >3) from the N2(NZOxC3H) females. The significance threshold was determined with the help of a 100 permutation test; the 95 %-confidence interval was calculated by Bayesian method. Glutamine, Lysine, Aspartic Acid, Hydroxy-Octadec-1-enoylcarnitine represent blood metabolites. LOD= logarithm of odds, BMI= Body mass index, Chr= Chromosome, cM= Centimorgan, Mb-Pos= Mega base pair position. n=304- 310

Phenotype	Chr.	Position (cM)	Confidence interval (cM)	Closest SNP-marker (Mb-Pos.)	max. LOD	Week	Mean NZO/NZO	Mean C3H/NZO	Effect size (unit)
Blood glucose	7	1	0_7	16.6	6.8	20	214	169	45 mg/dL
	16	4	0_17	11.5	3.6	6	184	172	12 mg/dL
	5	65	52_67	133.0	2.9	10	171	188	17 mg/dL
Body weight	10	7.2	5_11	89.1	9.3	6	32.1	29.5	2.6 g
	4	15	7_26	53.0	6.9	19	62.1	56	6.1 g
	14	23	17_30	63.6	5.2	6	31.8	29.8	2.0 g
	13	29.04	0_29	74.4	4.2	6	31.8	30	1.8 g
	1	9	0_20	46.3	4.0	10	45.2	42.4	2.8 g
	6	20	9_52	64.2	3.9	6	31.7	30	1.7 g
Lean mass	10	6	3_11	89.1	8.4	6	20.3	19.2	1.1 g
	3	7	3_16	54.8	3.8	6	20.2	19.4	0.8 g
	15	0	0_8	32.9	3.5	10	23.2	22.3	0.9 g
	13	0	0_29	16.3	3.1	6	20.1	19.5	0.7 g
	1	18	2_30	46.9	3.0	10	23.1	22.3	0.8 g
Fat mass	4	15	8_25	53.0	7.5	15	28.7	24.7	4.0 g
	14	23	17_32	63.5	6.3	6	10.6	9.2	1.4 g
	10	7.2	3_10	89.1	6.3	10	20.6	17.8	2.8 g
	6	20	5_50	64.2	4.4	6	10.5	9.3	1.2 g
	13	29	0_29	74.3	3.9	6	10.4	9.3	1.1 g
	5	15	3_67	24.9	3.6	6	10.4	9.4	1.0 g
	1	8	0_22	27.3	3.6	10	20.3	18.3	2.0 g
	11	39	6_48	114.0	3.3	6	10.4	9.4	1.0 g
BMI	4	25	10_29	53.0	8.5	21	0.45	0.41	0.04 g/cm^2
Lenght	11	3	0_14	46.7	3.6	21	11.8	12	0.2 cm
Glutamine	12	23	16_38	80.9	4.3	10	0.9	0.7	0.20 µmol/L
Lysine	2	55	5_63	168.0	3.8	10	250.6	223.4	27.2 µmol/L
Aspartic Acid	14	7	0_15	46.7	3.4	10	124.0	148.6	24.6 µmol/L
Hydroxy-Octadec-1-enoylcarnitine	13	20.43	12_28	55.6	3.1	10	0.078	0.044	0.034 µmol/L

6.4.3 KASP SNP Primer for genotyping

Supplementary Table 10: KASP SNP primer for genotyping of the N2(NZOxC3H) population. All primers were purchases from LGC (LGC group, Teddington, United Kingdom). Mb = mega base pairs, A= Adenine, G= Guanine, C=Cytosine, T= Thymine

JAX Stock #	Chromosome	Mb-Position	RS_ID	C3HeB/FeJ	NZO/HlLtJ
01-005230167-M	1	5.2	rs3708040	C	T
01-028127251-N	1	27.8	rs3089881	G	A
01-047362047-M	1	46.9	rs3712347	C	T
01-067230857-N	1	66.6	rs3024048	T	G
01-082250512-N	1	81.4	rs3022821	G	A
01-093273478-N	1	94.7	rs3022828	C	T
01-112993479-M	1	114.2	rs3663366	T	C
01-133333737-M	1	134.4	rs3678662	T	C
01-153183498-M	1	154.1	rs3670558	T	C
01-172244784-N	1	172.9	rs3022854	A	C
01-193173300-M	1	193.6	rs3715125	G	A
02-029164828-M	2	28.7	rs3723307	T	C
02-051174661-M	2	50.5	rs3710476	A	G
02-066991665-M	2	66.1	rs4135996	A	G
02-085004979-M	2	84.0	rs3661740	G	C
02-103071432-M	2	102.1	rs3714595	A	T
02-116033346-M	2	114.9	rs3686811	G	A

JAX Stock #	Chromosome	Mb-Position	RS_ID	C3HeB/FeJ	NZO/HlLtJ
02-131136658-M	2	130.0	rs3662211	A	C
02-149438298-N	2	148.2	rs4223557	A	C
02-169619681-N	2	168.4	rs3024096	G	C
03-035115028-M	3	35.1	rs3700620	T	C
03-055513690-N	3	54.8	rs3023799	C	T
03-074327277-M	3	73.4	rs3724107	T	C
03-087158136-M	3	86.2	rs3688780	C	G
03-104386660-M	3	104.1	rs3688731	T	A
03-121126022-M	3	120.5	rs3687177	C	T
03-137103456-M	3	136.3	rs3668158	A	G
04-032923355-M	4	33.4	rs3706812	T	C
04-051886531-M	4	53.0	rs3726250	T	A
04-071265089-M	4	73.7	rs3722264	A	C
04-088959560-M	4	91.0	rs4136370	A	C
04-101002669-M	4	103.0	rs3672377	G	T
04-117238813-M	4	119.0	rs3715984	A	T
04-135804867-N	4	137.8	rs4224861	T	C
04-150152643-M	4	154.1	rs3693138	A	C
05-005088855-M	5	8.8	rs3724267	T	C
05-023890459-M	5	24.9	rs3664933	G	C
05-043353028-N	5	44.8	rs3023833	C	A
05-062045190-M	5	63.4	rs3666143	A	C
05-082050497-M	5	82.9	rs3705373	A	C
05-099887300-M	5	102.8	rs3663793	T	C
05-117214009-M	5	119.6	rs3723083	G	T
05-130950804-M	5	132.9	rs3665335	C	A
06-028759322-M	6	28.7	rs3706286	C	T
06-048811360-N	6	48.4	rs4225867	T	G
06-064751205-M	6	64.2	rs4136902	G	A
06-082087904-M	6	81.2	rs3660389	G	A
06-101960309-M	6	101.1	rs3719379	T	C
06-121280548-M	6	120.4	rs3710839	G	A
06-138971511-M	6	138.5	rs3712962	T	C
07-011167675-M	7	16.6	rs3675839	T	C
07-026985215-M	7	37.3	rs3724525	G	T
07-039020313-M	7	56.7	rs3680765	G	T
07-058987832-M	7	76.7	rs3693876	A	G
07-072051696-M	7	89.5	rs3701187	T	C
07-093235239-M	7	110.6	rs3706526	C	A
07-109117173-M	7	126.6	rs3670069	C	A
07-129989877-M	7	147.0	rs3700241	G	A
08-021183852-M	8	23.6	rs3691954	A	G
08-039133894-M	8	41.1	rs3664354	A	G
08-055226913-M	8	58.7	rs3717220	A	T
08-076188935-M	8	79.2	rs3658934	T	A
08-095444189-N	8	98.2	rs4227350	T	C
08-117163724-M	8	119.7	rs3686697	A	G
09-089891382-M	9	89.3	rs3709387	A	C
09-103990534-M	9	103.1	rs3679358	C	T
10-028554348-N	10	28.3	rs3023233	A	G
10-070173090-M	10	69.6	rs3687255	G	T
10-089875395-N	10	89.1	rs3089366	C	T
10-107333522-M	10	106.6	rs3654717	T	C
10-128109621-M	10	126.9	rs3676616	T	C

JAX Stock #	Chromosome	Mb-Position	RS_ID	C3HeB/FeJ	NZO/HlLtJ
11-047224208-M	11	46.7	rs3686921	A	C
11-066278669-N	11	65.5	rs3023267	A	T
11-083523677-M	11	82.7	rs3663879	C	G
11-096113981-N	11	95.2	rs3090050	A	G
11-115546745-M	11	114.5	rs3660683	A	G
12-009581325-M	12	9.5	rs3689696	T	G
12-023088024-N	12	29.7	rs3089800	C	T
12-041270227-M	12	48.0	rs3665793	A	G
12-061271925-M	12	67.8	rs3677704	T	A
12-074494300-M	12	80.9	rs3699929	T	G
12-084289638-M	12	91.4	rs3707414	A	C
12-102404294-M	12	109.4	rs3713608	A	C
13-015609597-M	13	16.3	rs3701757	G	A
13-035991657-N	13	36.7	rs3090767	A	G
13-054994059-N	13	55.6	rs4229759	A	G
13-071293388-N	13	74.3	rs3090114	A	G
14-020426806-M	14	26.2	rs3682880	G	A
14-037917554-M	14	46.7	rs3671357	T	C
14-054014360-M	14	63.5	rs3702501	G	C
14-068060767-M	14	77.5	rs3670540	A	C
14-088110939-M	14	97.3	rs3684516	T	A
15-003094890-M	15	3.2	rs3687235	A	G
15-033125499-M	15	33.0	rs3720676	G	A
15-049283927-M	15	48.9	rs3719583	A	C
15-063976267-N	15	63.3	rs3023419	T	A
15-080641980-N	15	79.7	rs4230879	A	G
15-098621793-N	15	97.5	rs3023427	T	C
16-010990227-C	16	11.5	rs4161857	G	C
16-029101273-C	16	29.3	rs4167317	G	C
16-049079612-C	16	49.1	rs4184376	C	T
16-064088849-C	16	63.8	rs4195412	G	A
16-075684315-C	16	75.1	rs4205499	T	C
17-019783711-N	17	20.9	rs3023727	G	T
17-039842179-N	17	41.0	rs3690398	C	T
17-054189177-M	17	55.3	rs3711131	G	A
17-074384915-M	17	75.6	rs3688141	G	A
18-007901098-M	18	8.0	rs3689558	T	C
18-025787392-M	18	25.8	rs3681920	T	C
18-043868444-M	18	43.9	rs3708056	C	A
18-063144592-M	18	63.0	rs3678144	C	T
18-080151519-M	18	79.8	rs3656292	G	A
19-020257763-M	19	20.7	rs3658667	T	C
19-039967462-M	19	40.3	rs4135895	A	G
19-059089086-M	19	59.1	rs3679750	A	G

Supplementary Table 11: KASP SNP primer on chromosome 7 for genotyping of RCS.NZO.C3H-*Cdp7*con. All primers were purchases from LGC (LGC group, Teddington, United Kingdom). Mb = mega base pairs, A= Adenine, G= Guanine, C=Cytosine, T= Thymine

JAX Stock #	Chromosome	Mb-Position	RS_ID	C3HeB/FeJ	NZO/HlLtJ
07-011167675-M	7	16.6	rs3675839	T	C
07-016778161-M	7	25.3	rs3701807	A	G
07-022058953-N	7	30.6	rs4226520	G	A
07-026985215-M	7	37.3	rs3724525	G	T
07-028240185-M	7	38.5	rs3696033	A	C
07-029991530-M	7	47.6	rs3675009	T	C
07-034063244-M	7	51.8	rs3710949	A	G
07-039020313-M	7	56.7	rs3680765	G	T
07-048028246-M	7	65.6	rs3679388	T	G
07-058987832-M	7	76.7	rs3693876	A	G
07-072051696-M	7	89.5	rs3701187	T	C
07-093235239-M	7	110.6	rs3706526	C	A
07-109117173-M	7	126.6	rs3670069	C	A
07-129989877-M	7	147.0	rs3700241	G	A

Supplementary Table 12: KASP SNP primer on chromosome 7 for genotyping of RCS.B6.C3H-*Cdp7*con. All primers were purchases from LGC (LGC group, Teddington, United Kingdom). Mb = mega base pairs, A= Adenine, G= Guanine, C=Cytosine, T= Thymine

JAX Stock #	Chromosome	Mb-Position	RS_ID	C57BL/6J	C3HeB/FeJ
07-016778161-M	7	25.3	rs3701807	G	A
07-026985215-M	7	37.3	rs3724525	T	G
07-028240185-M	7	38.5	rs3696033	C	A
07-029991530-M	7	47.6	rs3675009	C	T
07-034063244-M	7	51.8	rs3710949	G	A
07-041032053-M	7	58.7	rs3720603	G	A
07-048028246-M	7	65.6	rs3679388	G	T
07-053928010-M	7	71.7	rs3717846	T	G
07-067573061-M	7	85.2	rs3713432	A	C
07-082671949-N	7	100.1	rs4226783	C	G
07-102934866-M	7	120.5	rs3680026	A	T

6.4.4. Genes from the haplotype analysis

Supplementary Table 13: Genes located within *Cdp7-prox* revealed from haplotype analysis of the parental strains. All genes mapped to a non-IBD region and harbour at least one polymorphic SNP (Fig. 31)

Position	Gene	Position	Gene	Position	Gene	Position	Gene
27259691	*Numbl*	30186285	*Capns1*	31047497	*Fxyd1*	34938966	*SNORA17*
27271772	*Gm15570*	30196026	*AC149067.1*	31051855	*Fxyd7*	35044748	*Cebpg*
27300174	*Ltbp4*	30221697	*Tbcb*	31059705	*Lgi4*	35076994	*AC149058.1*
27358040	*Gm20479*	30229589	*Polr2i*	31064121	*Fxyd3*	35097092	*5S_rRNA*
27358356	*AC157561.1*	30238987	*Wdr62*	31093762	*Hpn*	35114404	*Cebpa*
27396467	*Spnb4*	30280096	*Thap8*	31117717	*Scn1b*	35181518	*Slc7a10*
27465324	*Blvrb*	30292678	*Clip3*	31130153	*Gramd1a*	35200935	*Lrp3*
27480840	*Sertad3*	30320516	*E130208F15Rik*	31144666	*AC158993.1*	35229769	*AC150683.1*
27483187	*Sertad1*	30321527	*Sdhaf1*	31285724	*Scgb1b2*	35271887	*Gpatch1*
27498211	*Prx*	30351326	*Lrfn3*	33359578	*Scgb2b20*	35329264	*Rhpn2*
27507227	*Gm15541*	30356215	*U2*	33368250	*Scgb1b20*	35387315	*C230052I12Rik*
27520378	*Hipk4*	30408975	*Tyrobp*	33522581	*Scgb1b12*	35397141	*Ccdc123*
27538101	*Pld3*	30414296	*Hcst*	33562261	*Gm12770*	35444123	*Slc7a9*
27582288	*2310022A10Rik*	30417111	*Nfkbid*	33563301	*Gm12771*	35488658	*Tdrd12*
27591679	*Akt2*	30430791	*Aplp1*	33599361	*Scgb2b22-ps*	35542766	*Nudt19*
27649658	*Ttc9b*	30442651	*Kirrel2*	33609665	*Scgb1b22-ps*	35555888	*B230322F03RIK*
27655130	*Map3k10*	30458519	*Nphs1*	33620878	*Scgb2b23-ps*	35574383	*Rgs9bp*
27684399	*C030039L03Rik*	30462175	*Nphs1as*	33630179	*Scgb1b23-ps*	35585629	*Ankrd27*
27726510	*Zfp60*	30488742	*Prodh2*	33648566	*Gm12763*	35636993	*Pdcd5*
27807098	*Zfp626*	30510398	*Gm1082*	33692463	*Rpl23a-ps12*	35680193	*Dpy19l3*
27838295	*Zfp59*	30522568	*Arhgap33*	33732200	*Scgb2b24*	35767368	*Zfp507*
27857569	*Zfp607*	30539220	*BC053749*	33739050	*Scgb1b24*	35767441	*AC120378.1*
27902621	*1700049G17Rik*	30552325	*Hspb6*	33772657	*U7*	35797619	*E130304I02Rik*
27929477	*AC139063.1*	30555517	*Lin37*	33776230	*Gm12782*	36113341	*Gm10166*
27944172	*Gm10651*	30561959	*Psenen*	33803217	*BX537299.1*	36297515	*AC160540.1*
27958850	*Zfp780b*	30563499	*U2af1l4*	33839983	*Gm12768*	37664900	*4930505M18Rik*
27981091	*Zfp850*	30566345	*Tmem149*	33850742	*Scgb2b25-ps*	37955257	*C80913*
27983998	*Gm4636*	30568245	*Gm17104*	33874319	*Gm12757*	38093063	*Ccne1*
27991574	*RP23-73F23.2*	30569170	*Wbp7*	33932263	*Gm12765*	38178218	*1600014C10Rik*
28036862	*Psmc4*	30590677	*Zbtb32*	33943048	*Scgb2b26*	38215671	*Plekhf1*
28066326	*Fcgbp*	30603121	*Upk1a*	33956408	*Scgb1b26-ps*	38257849	*Pop4*
28803031	*Rinl*	30612038	*Cox6b1*	33992015	*Gm12773*	39260840	*RP23-124D10.1*
28803766	*Hnrnpl*	30631387	*Etv2*	33993057	*Gm12755*	39440974	*Gm5590*
28825437	*Ech1*	30640871	*RP23-72M20.2*	34011471	*Scgb2b27*	39444706	*Zfp939*
28832360	*Lgals4*	30644143	*Rbm42*	34016488	*Scgb1b27*	39515757	*Zfp619*
28858871	*Lgals7*	30650745	*AC167978.1*	34033026	*Gm12760*	41027773	*Gm4884*
28876756	*Capn12*	30654015	*Haus5*	34063601	*Gm12779*	41150582	*Gm2128*
28888459	*Actn4*	30670007	*4930479M11Rik*	34090453	*Scgb1b30*	41242360	*Gm9244*
28967586	*Eif3k*	30697663	*2200002J24Rik*	34105866	*Wtip*	41280122	*Gm5592*
28978030	*Map4k1*	30704985	*Gm4883*	34138522	*Uba2*	42573512	*AC102606.1*
29059851	*Ryr1*	30707720	*Atp4a*	34170804	*Gm12778*	42580752	*Gm7221*
29768308	*Mir1964*	30725902	*C630016N16RIK*	34176135	*Gm12783*	42597968	*Gm20434*
29780181	*Zfp30*	30729501	*Tmem147*	34184606	*Pdcd2l*	42604611	*9830147E19Rik*
29811096	*Zfp790*	30737845	*Gapdhs*	34201754	*Gpi1*	42606896	*AC102628.1*
29833651	*Zfp940*	30746598	*Sbsn*	34219771	*BX537302.1*	42655800	*Gm5595*
29853087	*AC156934.1*	30758799	*Dmkn*	34230361	*Gm12758*	42700750	*Gm17067*
29855702	*Gm17199*	30783083	*Krtdap*	34230456	*Gm12762*	42701399	*AC102628.2*
29859994	*Zfp420*	30813478	*Ffar2*	34237106	*4931406P16Rik*	42732331	*Gm18128*
29888442	*Zfp27*	30849461	*Ffar3*	34246053	*Gm6096*	42745722	*Gm6004*
29926091	*Zfp74*	30856001	*Ffar1*	34339765	*Lsm14a*	43291272	*Zfp715*
29953644	*C230062I16Rik*	30865454	*Cd22*	34378679	*Gm12774*	43346734	*Siglec5*
29961106	*Gm10169*	30894194	*Mag*	34384184	*Gm12764*	43383233	*Gm10298*
29978966	*Zfp568*	30919376	*Hamp2*	34433170	*Gm12766*	43406865	*Siglecg*
30033082	*Zfp14*	30937400	*Hamp*	34495825	*Gm12780*	43426309	*LIM2*
30051059	*Zfp82*	30942623	*Usf2*	34542505	*Gm12784*	43437143	*Nkg7*
30072386	*Zfp566*	30956874	*Gm17077*	34634016	*Kctd15*	43439250	*Cldnd2*
30089805	*Zfp260*	30957446	*AC149055.1*	34648216	*Gm12781*	43441424	*Etfb*
30135111	*Zfp382*	30958022	*Lsr*	34661153	*Gm12756*	43459608	*Vsig10l*
30158673	*Zfp146*	30968813	*Fam187b*	34675297	*Chst8*	43470218	*Iglon5*
30165228	*Gm5113*	31027737	*Fxyd5*	34907452	*Pepd*	43498832	*4931406B18Rik*

Position	Gene	Position	Gene	Position	Gene
43557264	*Zfp658*	45088766	*Fcgrt*	45820274	*Grwd1*
43575763	*Zfp719*	45116918	*Mir150*	45832719	*Grin2d*
43603606	*Zfp819*	45123719	*Snord35b*	45872977	*Kdelr1*
43651040	*Ceacam18*	45124974	*Rps11*	45875586	*U4*
43657556	*Siglece*	45125961	*Rpl13a*	45885290	*Syngr4*
43668702	*Ctu1*	45131309	*Flt3l*	45896947	*Tmem143*
43688574	*Klk14*	45140927	*Aldh16a1*	45917603	*Emp3*
43690475	*AC151989.1*	45156119	*Pih1d1*	45919286	*Ccdc114*
43820021	*Klk6*	45160406	*Slc17a7*	45971385	*Abcc6*
43876176	*Klk4*	45172731	*Gm581*	46028699	*Nomo1*
43928831	*Klk15*	45176750	*Pth2*	46093779	*Kcnj11*
43940034	*Klk1b7-ps*	45183716	*Ccdc155*	46107235	*Abcc8*
43946315	*Klk1b8*	45202659	*Dkkl1*	46193465	*Ush1c*
43983359	*Klk1b9*	45216588	*Tead2*		
43992574	*Klk1b11*	45236933	*Cd37*		
44008680	*Klk1b26*	45273667	*1700039E15Rik*		
44047295	*Klk1b27*	45299650	*Trpm4*		
44195259	*Klk1b3*	45321121	*Rpl14-ps1*		
44331759	*Shank1*	45337531	*Hrc*		
44355243	*1700008O03Rik*	45343360	*Ppfia3*		
44384121	*Syt3*	45368219	*Lin7b*		
44424092	*Lrrc4b*	45376328	*Snrnp70*		
44460958	*Aspdh*	45384101	*SNORA67*		
44467487	*Josd2*	45401579	*Kcna7*		
44485126	*Emc10*	45412179	*Ntf5*		
44501598	*Fam71e1*	45414099	*Lhb*		
44501823	*Mybpc2*	45425041	*Ruvbl2*		
44521239	*Spib*	45430023	*Gys1*		
44530309	*Pold1*	45458545	*Ftl1*		
44550345	*Nr1h2*	45462855	*AC151602.1*		
44567649	*Napsa*	45467290	*Bax*		
44580844	*Gm15396*	45476484	*Dhdh*		
44601139	*Myh14*	45493701	*Nucb1*		
44602093	*Kcnc3*	45517245	*Tulp2*		
44681889	*2310016G11Rik*	45518115	*Ppp1r15a*		
44703868	*Izumo2*	45528763	*Plekha4*		
44726629	*Zfp473*	45554274	*Gm16022*		
44744433	*Vrk3*	45554945	*Hsd17b14*		
44807603	*Atf5*	45567335	*Bcat2*		
44812025	*Il4i1*	45567869	*0610005C13Rik*		
44816222	*Nup62*	45608941	*Fgf21*		
44841467	*Tbc1d17*	45612777	*Fut1*		
44849782	*Akt1s1*	45621668	*Izumo1*		
44855453	*Pnkp*	45628661	*Rasip1*		
44863428	*Ptov1*	45629493	*Gm16047*		
44875022	*Med25*	45638257	*Mamstr*		
44891125	*Fuz*	45646584	*Fut2*		
44900420	*Ap2a1*	45672705	*Sec1*		
44939036	*Tsks*	45679570	*Ntn5*		
44954702	*Cpt1c*	45694864	*Car11*		
44971137	*Prmt1*	45704116	*Dbp*		
44987899	*Gm15545*	45710235	*Sphk2*		
44992393	*Bcl2l12*	45712191	*Rpl18*		
44997731	*Irf3*	45718596	*Fam83e*		
45005922	*Scaf1*	45725191	*Spaca4*		
45016775	*Rras*	45730122	*Sult2b1*		
45023228	*Prr12*	45743365	*Metazoa_SRP*		
45051187	*Prrg2*	45778837	*Lmtk3*		
45062699	*Nosip*	45801691	*Cyth2*		
45083666	*Rcn3*	45816857	*Kcnj14*		

6.5 Additional Figures

6.5.1 Genome wide LOD-score plots from the male N2(NZOxC3H) population

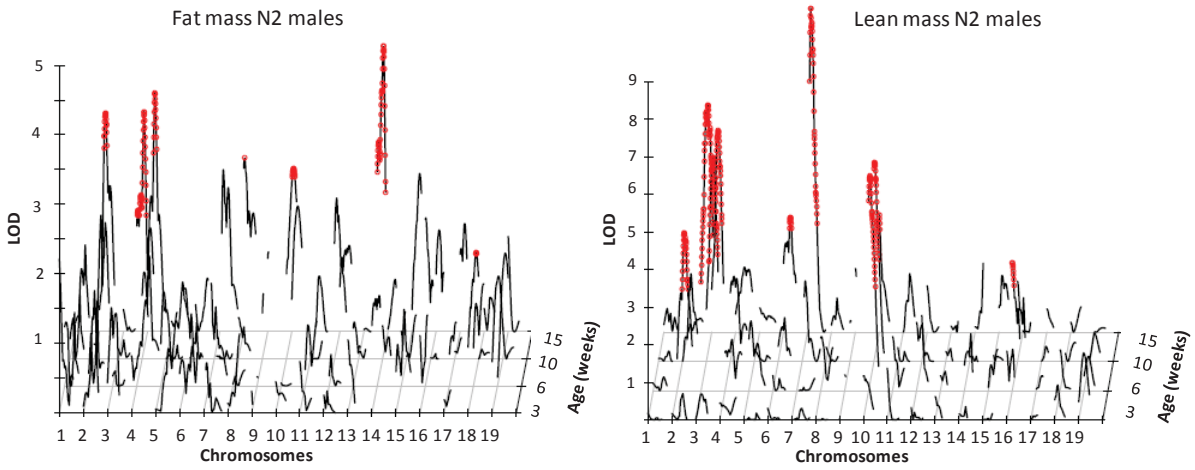

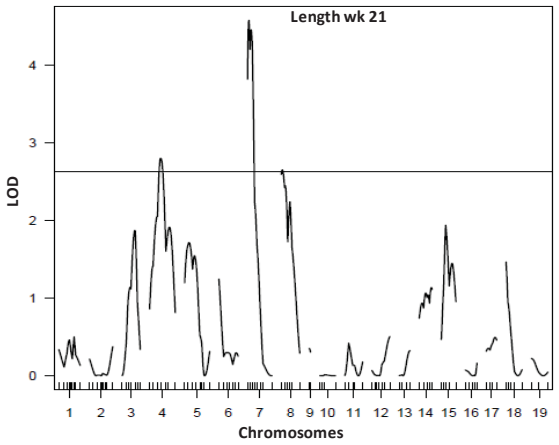

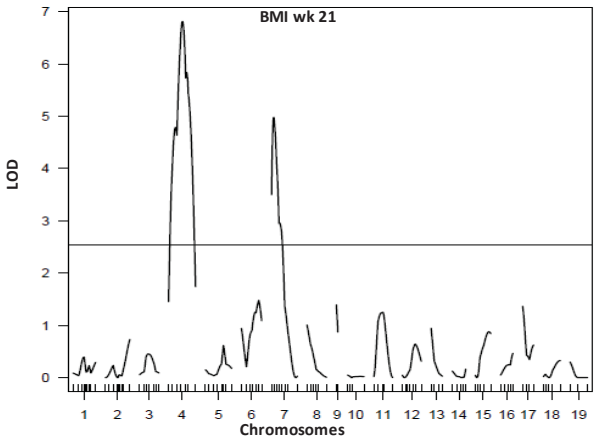

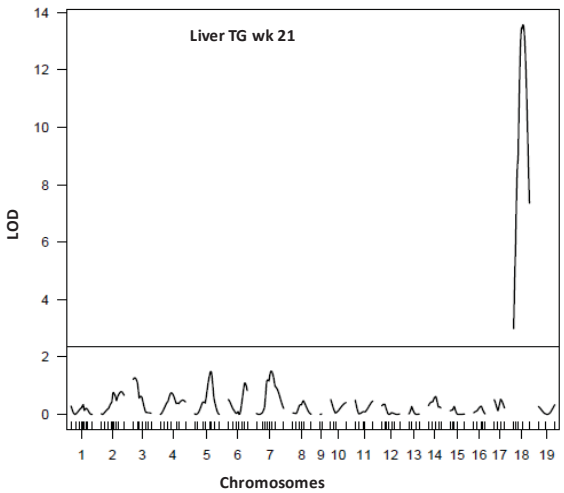

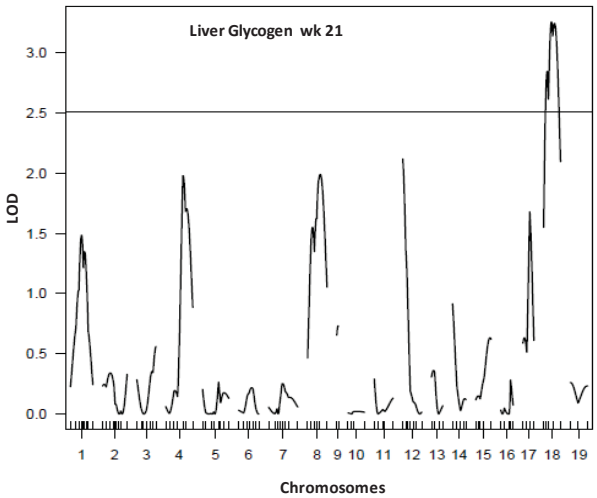

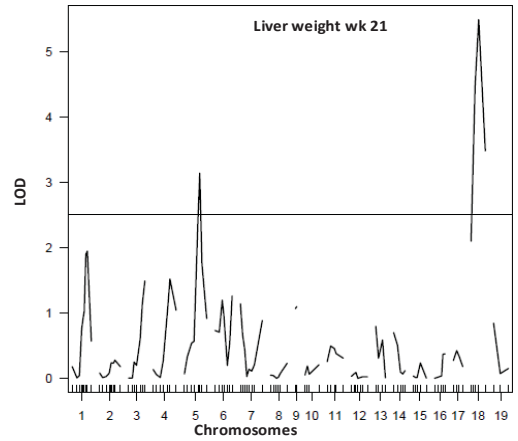
Liver weight wk 21
LOD
Chromosomes

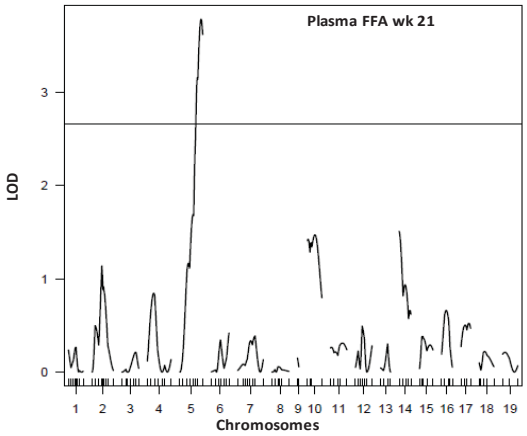
Plasma FFA wk 21
LOD
Chromosomes

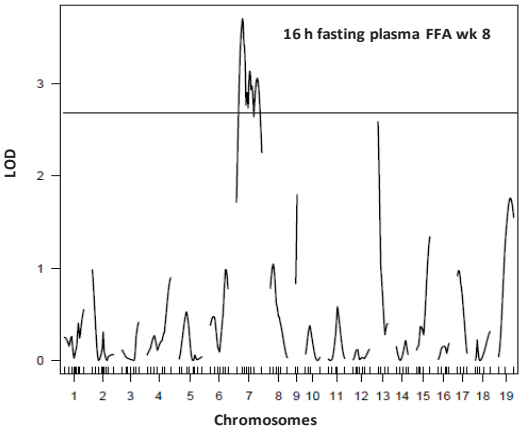
16 h fasting plasma FFA wk 8
LOD
Chromosomes

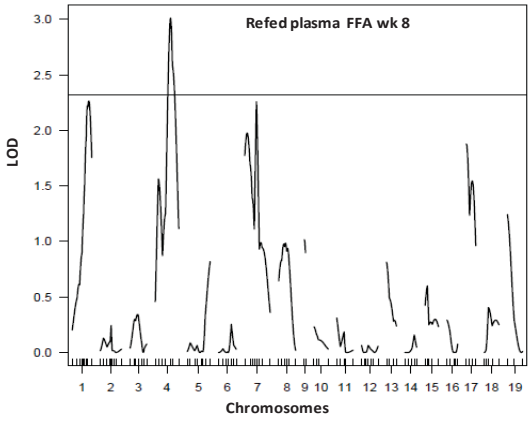
Refed plasma FFA wk 8
LOD
Chromosomes

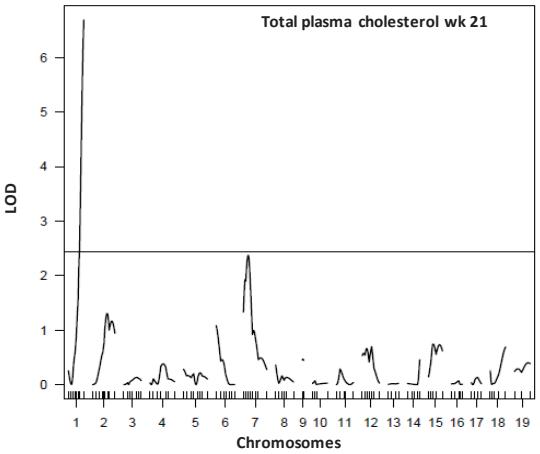
Total plasma cholesterol wk 21
LOD
Chromosomes

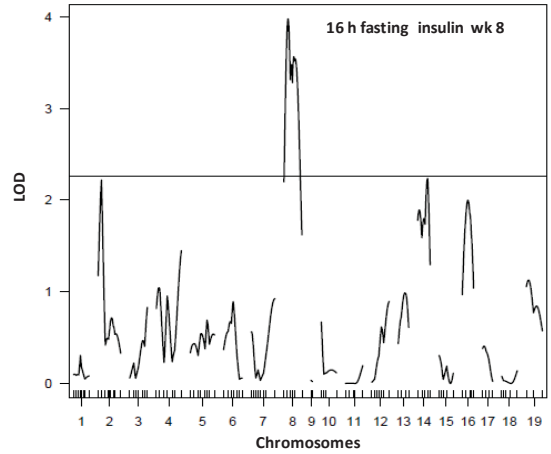
16 h fasting insulin wk 8
LOD
Chromosomes

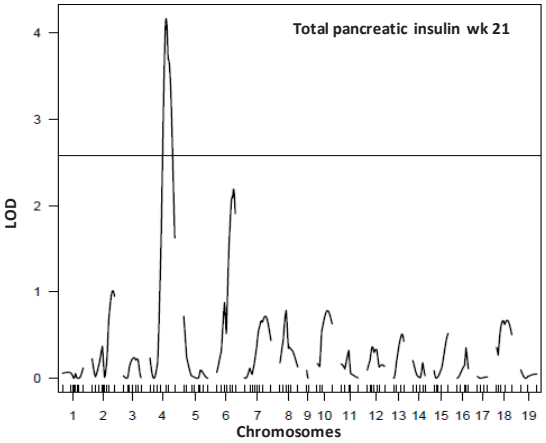
Total pancreatic insulin wk 21
LOD
Chromosomes

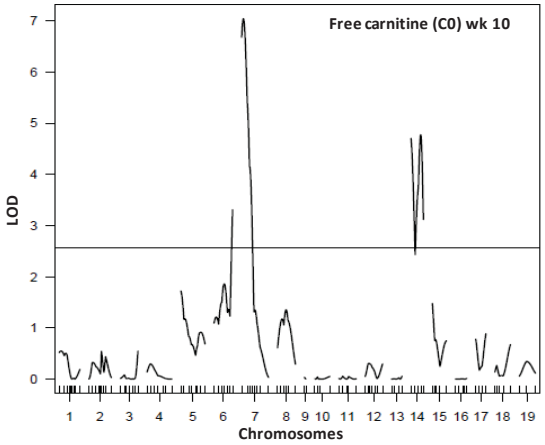
Free carnitine (C0) wk 10
LOD
Chromosomes

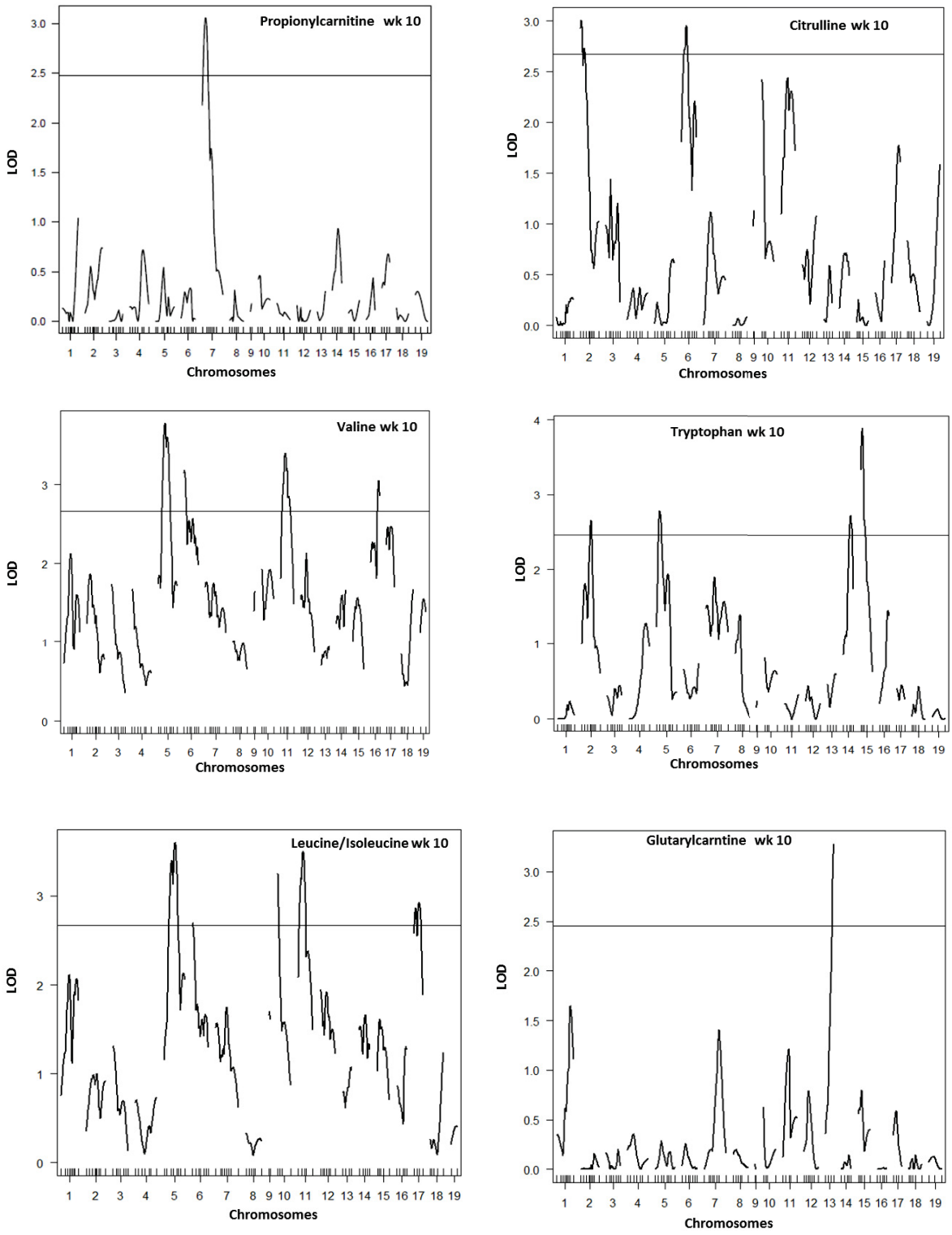

Supplementary Figure 1: Genome-wide logarithm of the odds (LOD) scores distributions for all significant QTLs from the N2(NZOxC3H) males. The respective traits are displayed in on top of each diagram. The analysis was assessed with R/qtl using a 100 permutation test to determine the significance threshold ($p< 0.05$), indicated in red or with the horizontal line. Detailed information for each QTL is shown in Suppl. Tab. 8.

6.5.2 Genome wide LOD-score plots from the female N2(NZOxC3H) population

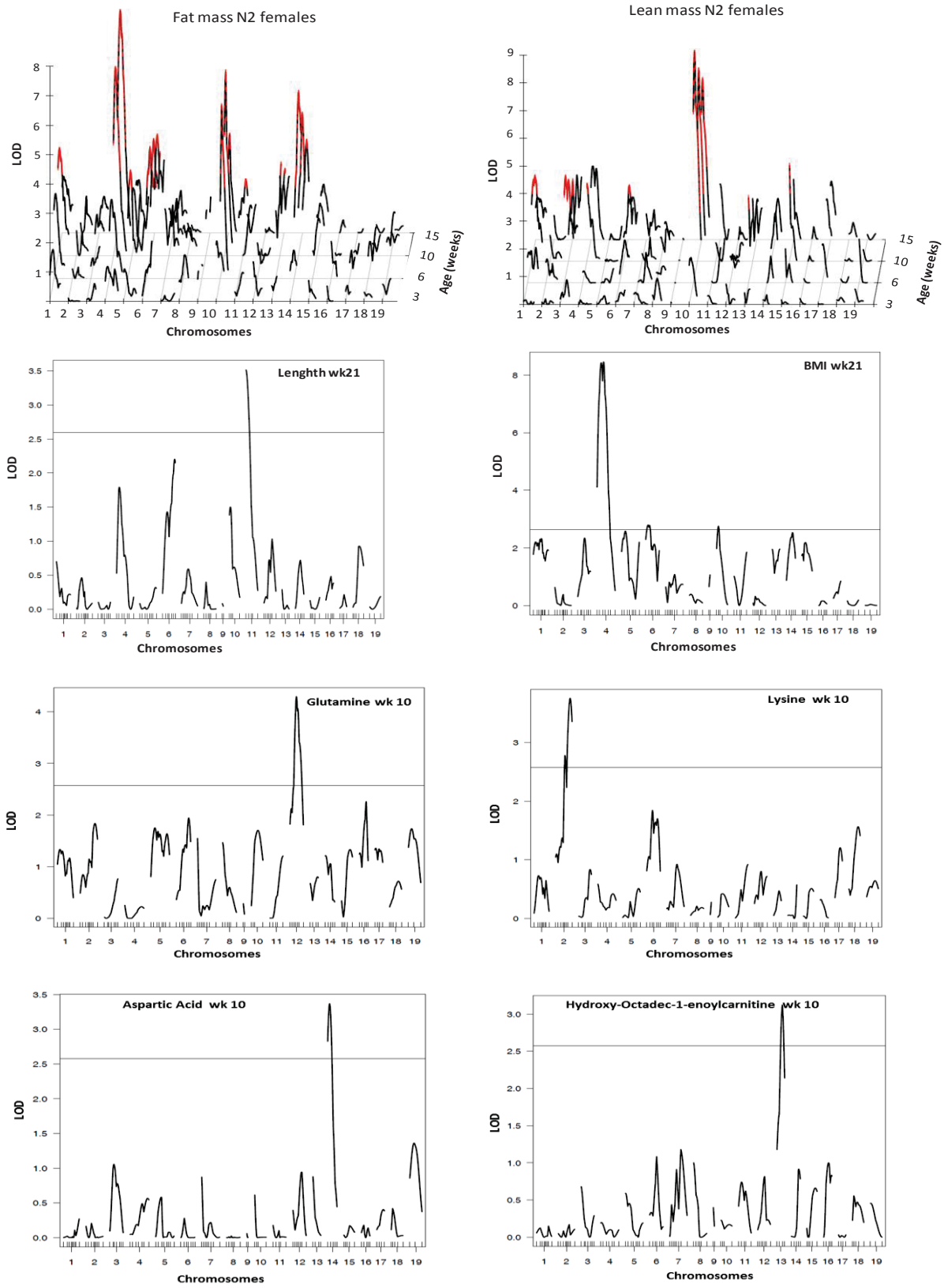

Supplementary Figure 2: Genome-wide logarithm of the odds (LOD) scores distributions for all significant QTLs from the N2(NZOxC3H) females. The respective traits are displayed in on top of each diagram. The analysis was assessed with R/qtl using a 100 permutation test to determine the significance threshold ($p<0.05$), indicated in red or with the horizontal line. Detailed information for each QTL is shown in Suppl. Tab. 9.

6.5.3 Genome wide LOD-score plots for all eQTLs from the male N2(NZOxC3H) population

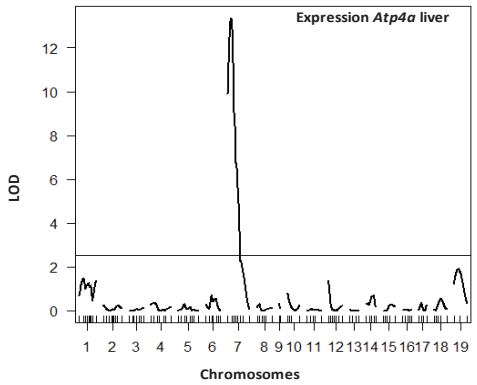

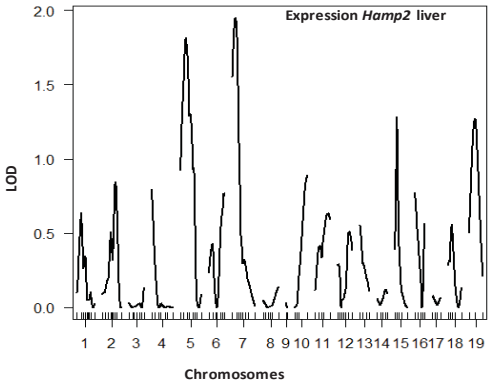

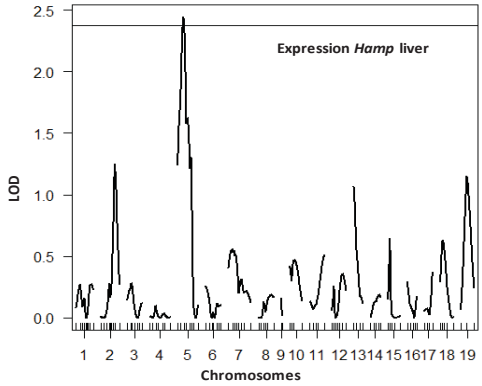

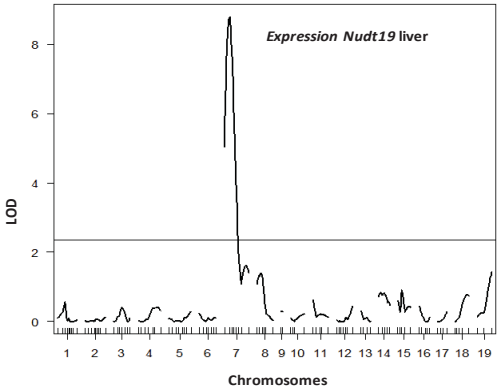

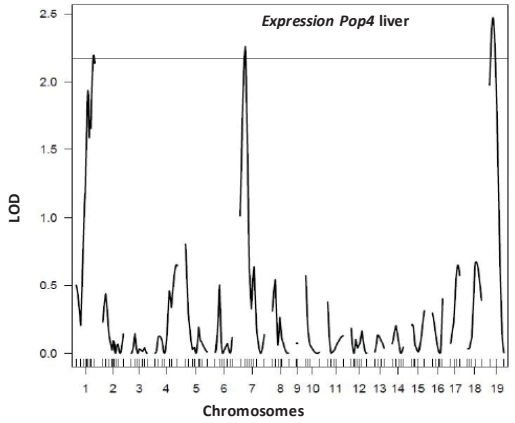

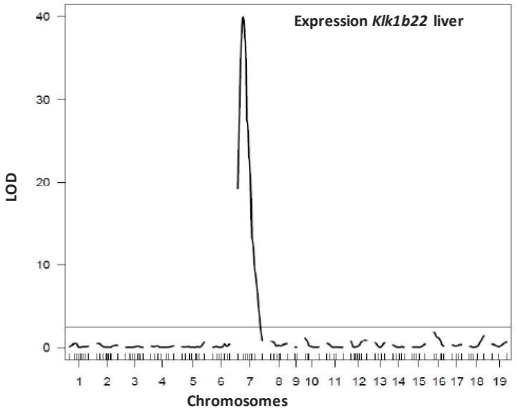

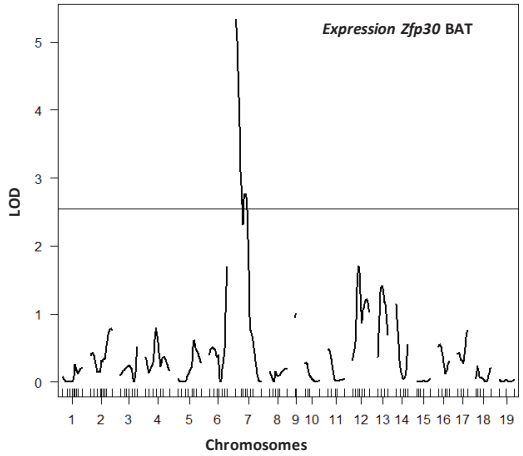

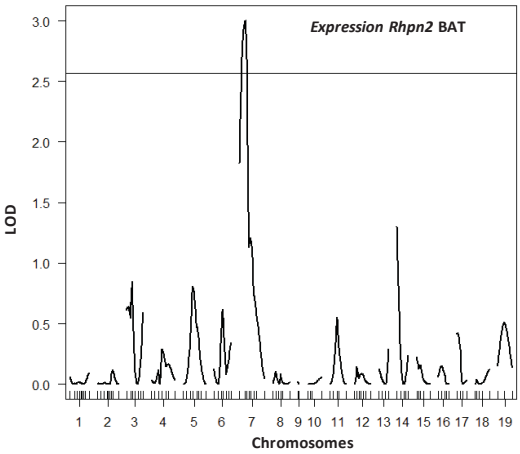

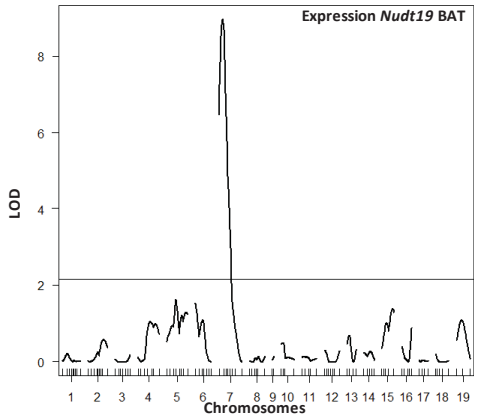
Expression *Nudt19* BAT
LOD
Chromosomes

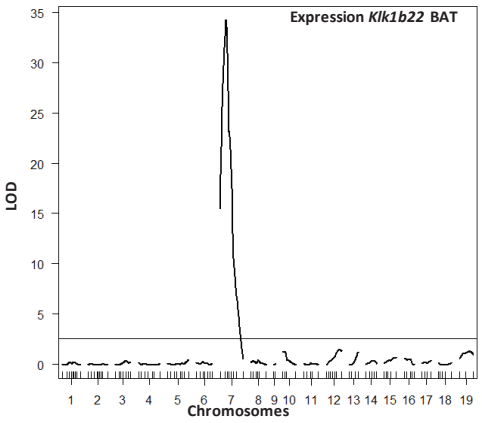
Expression *Klk1b22* BAT
LOD
Chromosomes

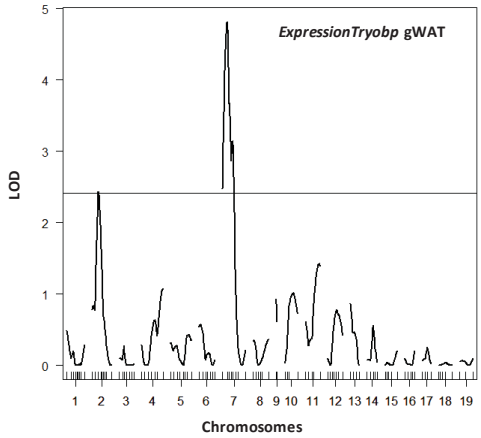
ExpressionTryobp gWAT
LOD
Chromosomes

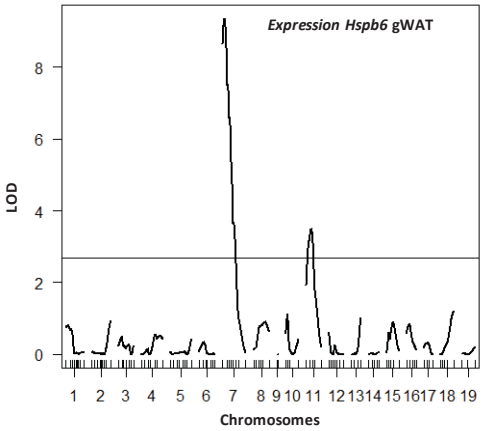
Expression Hspb6 gWAT
LOD
Chromosomes

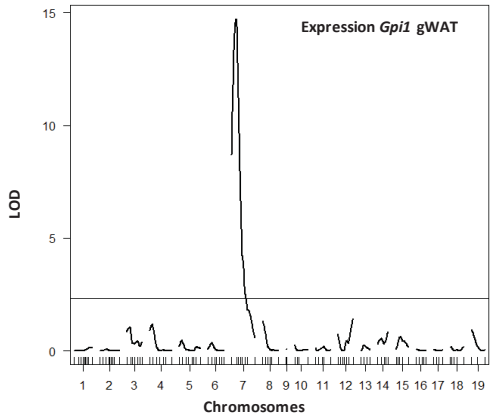
Expression *Gpi1* gWAT
LOD
Chromosomes

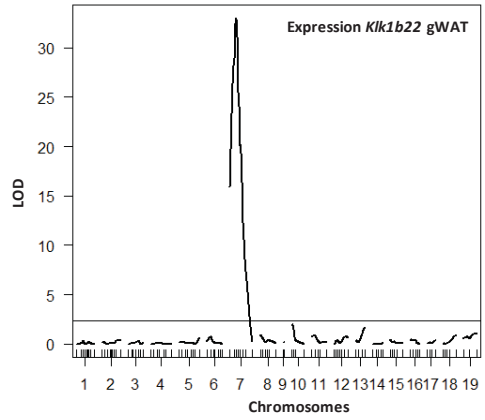
Expression *Klk1b22* gWAT
LOD
Chromosomes

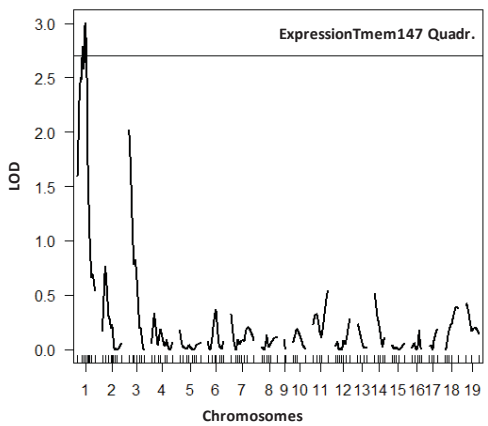
ExpressionTmem147 Quadr.
LOD
Chromosomes

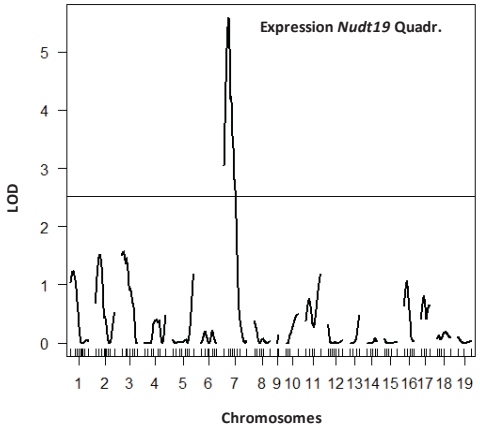
Expression *Nudt19* Quadr.
LOD
Chromosomes

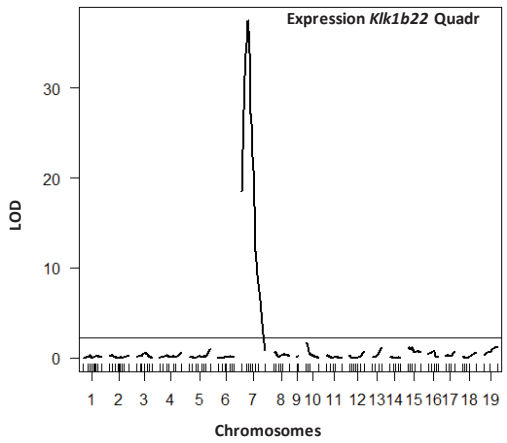

Supplementary Figure 3: Genome-wide logarithm of the odds (LOD) scores distribution for all analysed eQTLs from the N2(NZOxC3H) males. The respective genes and tissue is displayed in on top of each diagram. The analysis was assessed with R/qtl using a 100 permutation test to determine the significance threshold ($p<0.05$), indicated in with the horizontal line. Detailed information for each eQTL is shown in Table 20.

6.5.4 LOD score distributions for multiple QTLs on chromosomes 4, 7, 15 and 18

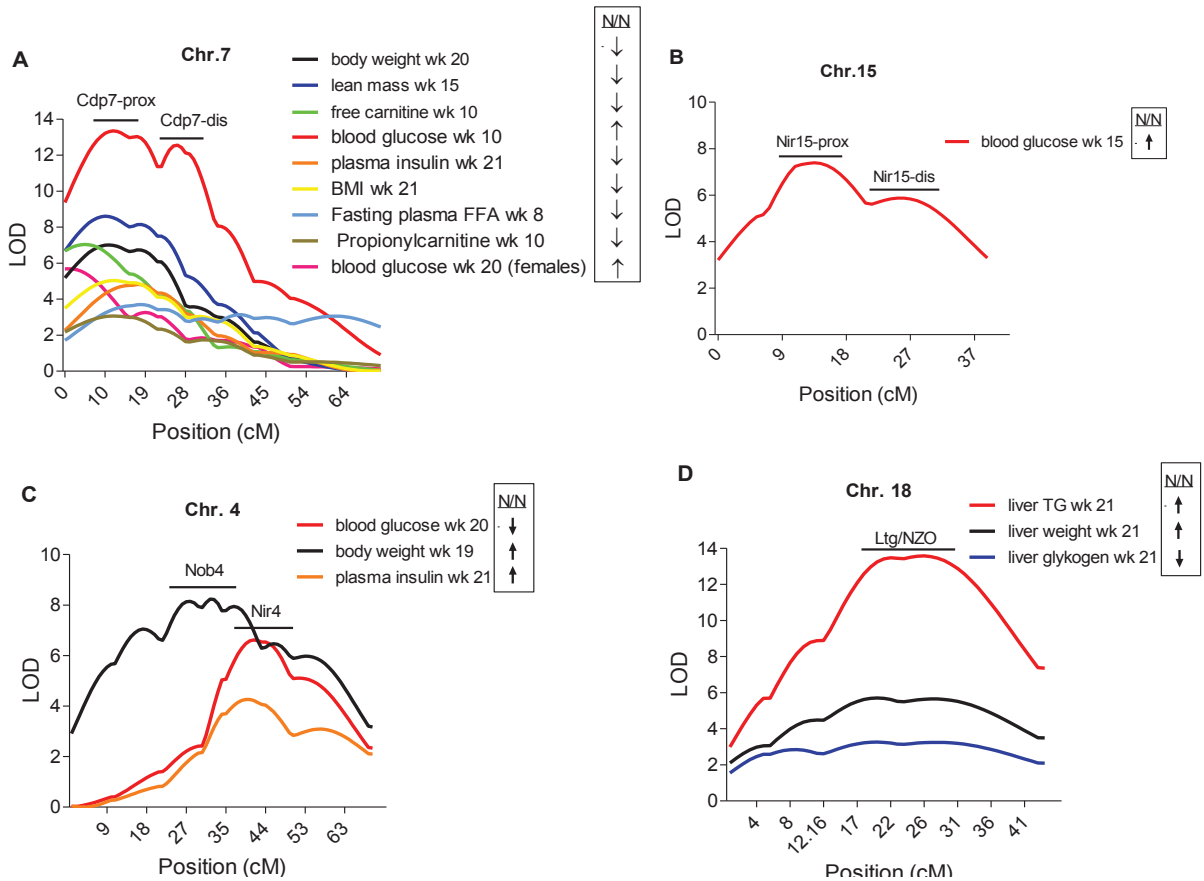

Supplementary Figure 4: Genome-wide logarithm of the odds (LOD) scores distribution for all significant QTLs (LOD > 3) on chromosomes 4, 7, 15 and 18. The QTL names are displayed at the respective position on top of the LOD score curve. The analysis was assessed with R/qtl using a 100 permutation test to determine the significance threshold. The genotypic effects for the different traits are indicated with the arrows. LOD= logarithm of the odds, BMI= body mass index, TG= triglycerides, wk= week, Chr.= chromosome. Cdp7-prox= C3H diabetes protector on proximal Chr.7, Cdp7-dis= C3H diabetes protector on distal Chr.7, Nir15-prox= NZO insulin resistance on proximal Chr. 15, Nir15-dis= NZO insulin resistance on distal Chr. 15, Nob4= NZO obesity on Chr. 4, Nir4= NZO insulin resistance on Chr. 4, Ltg/NZO= NZO liver triglycerides on Chr. 18.

6.5.5 Correlation analysis of mRNA levels with blood glucose, insulin and body weight in N2(NZOxC3H) males

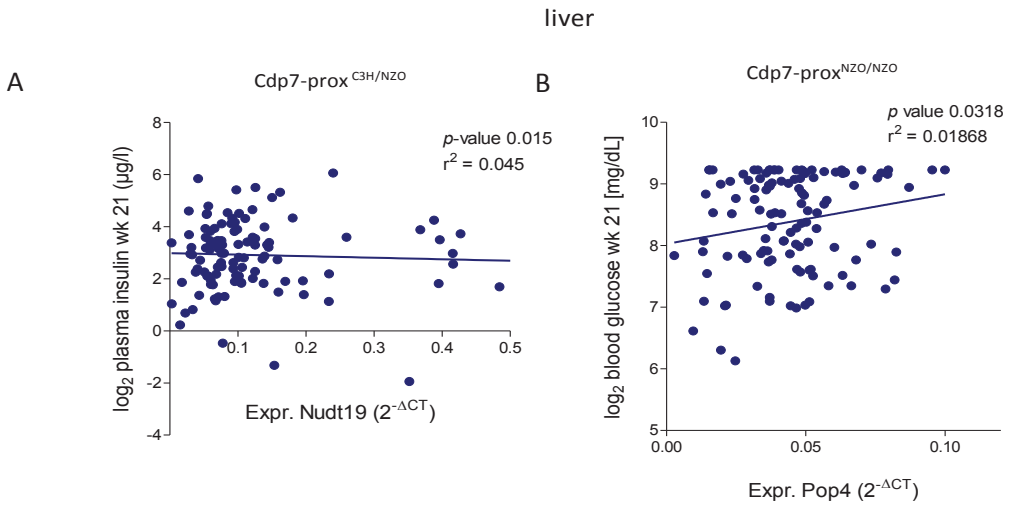

Supplementary Figure 5: Significant genotype-dependent correlations between mRNA levels of candidate genes from the liver with metabolic traits associated with *Cdp7-prox* in N2(NZOxC3H) males. Expression of *Nudt19* significantly correlated with plasma insulin levels in Cdp7-prox$^{C3H/NZO}$ mice (A), whereas mRNA levels of *Pop4* correlated with blood glucose levels in Cdp7prox$^{NZO/NZO}$ mice (B). Dots represent single animals. The correlation was calculated by linear regression: coefficient of determination; r^2 =1: 100% correlation; r^2 =0: no correlation; wk: weeks, Expr.= Expression

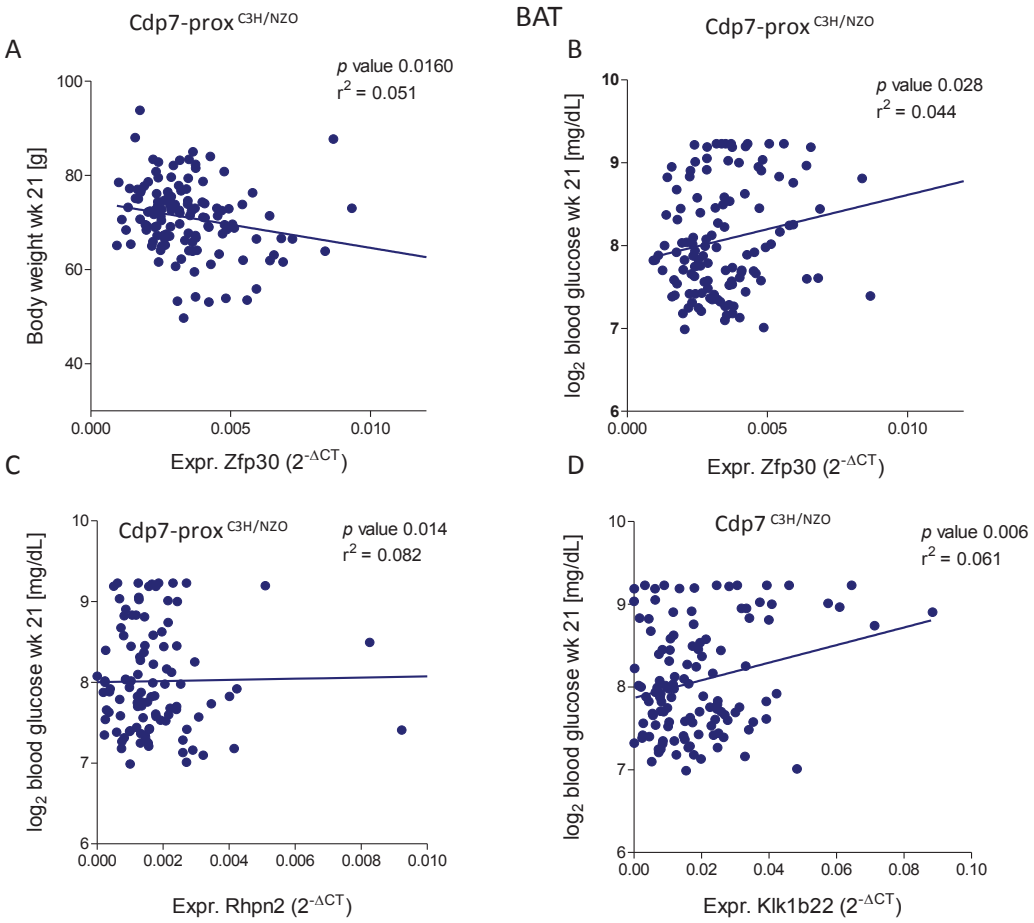

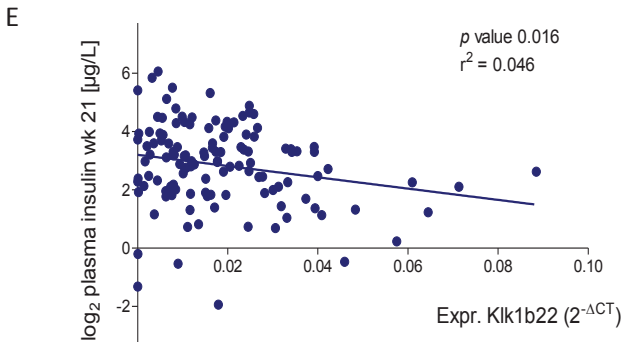

Supplementary Figure 6: Significant genotype-dependent correlations between mRNA levels of candidate genes from the BAT with metabolic traits associated with *Cdp7-prox* in N2(NZOxC3H) males. Expression of *Zfp30* significantly correlated with body weight (A) and blood glucose levels (B). mRNA levels of *Rhpn2* (C) and *Klkb22* (D) both correlated with blood glucose levels, expression of *Klk1b22* further correlated with plasma insulin levels (D). All correlations were exclusively observed in Cdp7-prox$^{C3H/NZO}$ mice. The correlation was calculated by linear regression: coefficient of determination; r^2 =1: 100% correlation; r^2 =0: no correlation; wk: weeks, Expr.= Expression

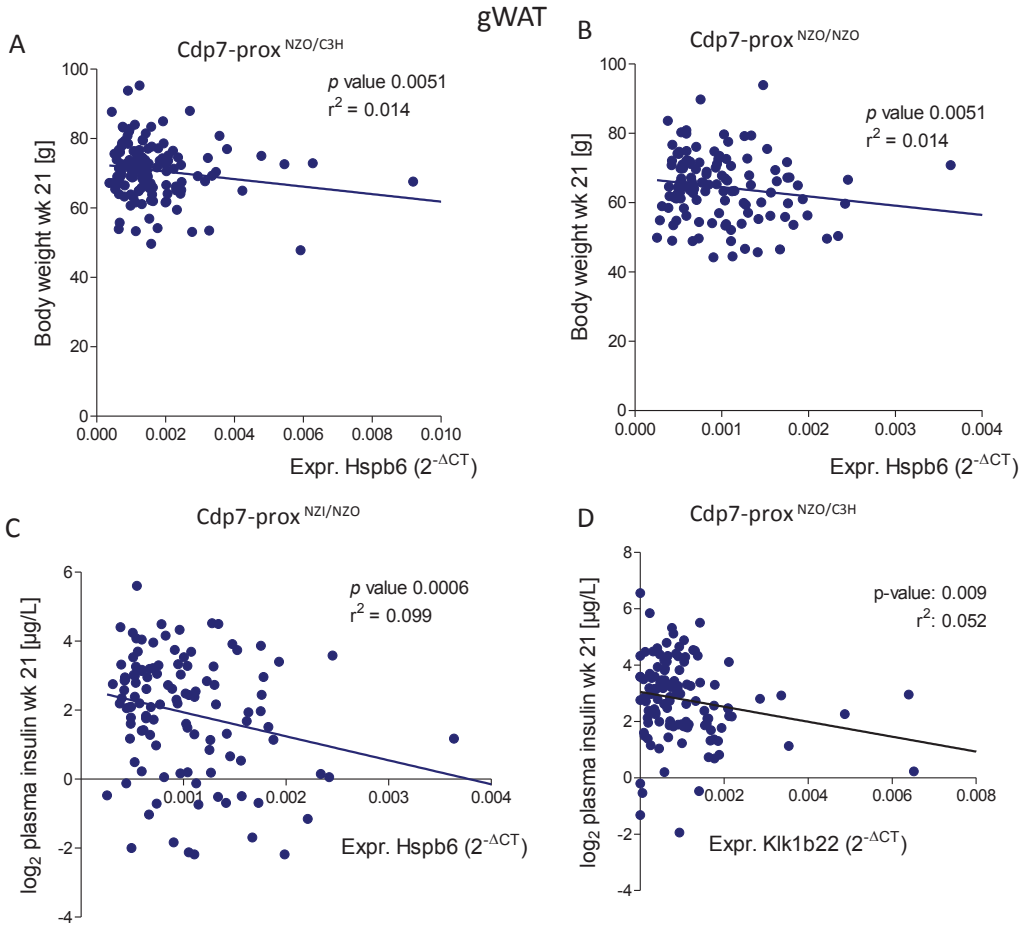

Supplementary Figure 7: Significant genotype-dependent correlations between mRNA levels of candidate genes from the gWAT with metabolic traits associated with *Cdp7-prox* in N2(NZOxC3H) males. Expression of *Hspb6* correlated with body weight in *Cdp7-prox*$^{NZO/C3H}$- (A) as well as in *Cdp7-prox*$^{NZO/NZO}$ animals (B), whereas a correlation of *Hspb6* expression with plasma insulin levels was exclusively observed in *Cdp7-prox*$^{NZO/NZO}$ mice (C). mRNA levels of *Klk1b22* correlated with plasma insulin levels in heterozygous mice (D). The correlation was calculated by linear regression: coefficient of determination; r^2 =1: 100 % correlation; r^2 =0: no correlation; wk: weeks, Expr.= Expression

6.6 List of Abbreviations

2200002J24Rik	*RIKEN cDNA 2200002J24 gene*
a.u.	Arbitrary units
Ackn4	*Actinin alpha 4*
Actb	*Beta actin*
ANOVA	Analysis of variance
approx.	Approximately
Atp4a	*Gastric Hydrogen-potassium exchanging ATPase alpha*
AUC	Area under the curve
B230322F03Rik	*RIKEN cDNA B230322F03 gene*
B6	C57BL/6J
BAT	Brown adipose tissue
BCA	Bicinchonic acid
BCAA	branched-chain amino acids
BMI	Body mass index
Bp	Base pairs
BSA	Bovine serum albumin
C3H	C3HeB/FeJ mouse
cDNA	Complementary DNA
Cdp7-dis	C3H diabetes protector on distal chromosome 7
Cdp7-prox	C3H diabetes protector on proximal chromosome 7
Chr.	Chromosome
cM	Centimorgan
CMRL	Connaught Medical Research Laboratories
CO_2	Carbon dioxide
CoA	Coenzym A
con	Consomic
Cox7a1	*Cytochrome c oxidase subunit VIIa 1*
cDNA	Complementary Desoxyribo nucleic acid
C-peptide	Connecting-peptide
cpm	Counts per minute
Cpt	*Carnitin palmitoyl transferase*
Ct	Cycle threshold
DDZ	Deutsches Diabetes Zentrum Düsseldorf (German Diabetes Cener)
DMEM	Dulbecco's Modified Eagles Medium
DMSO	Dimethylsulfoxide
DNA	Desoxyribo nucleic acid
dNTP	Desoxyribo nucleotide triphosphate
e.g.	Latin: *exempli gratia* – for example
e.i.	Latin: *id est* – that is
EDL	Extensor digitorum longus
EDTA	Ethylene diamine tetra acetate
EdU	5-ethynyl-2'-deoxyuridine
EGTA	Ethylene glycol-bis(aminoethylether)-N,N,N',N'-tetra acetate
ELISA	Enzyme-linked immuno sorbent assay
eQTL	Expression QTL

et al.	Latin: *et alia* - and others
F1	First filial generation
F2	Second filial generation (Intercross)
FAO	Fatty acid β-oxidation
FCCP	Carbonyl cyanide-4-(trifluoromethoxy)phenylhydrazone
FFA	Free fatty acids
Fig.	Figure
Fwd	Forward
Fxyd3	*FXYD domain-containing ion transport regulator 3*
g	Gravity
GFP	Green fluorescent protein
GIR	Glucose infusion rate
Gpi1	*Glucose phosphate isomerase 1*
GSIS	Glucose-stimulated insulin secretion
GTT	Glucose tolerance test
GWAs	Genome-wide association study
gWAT	white adiopose tissue
h	Hour
Hamp	*Hepcidin antimicrobial peptide*
Hamp2	*Hepcidin antimicrobial peptide 2*
HbA1c	Glycated hemoglobin A1c
HFD	High-fat diet
Hspb6	*Heat shock protein, alpha-crystallin-related, B6*
Hz	Hertz
i.p.	Intraperitoneal
IBD	Identity by descent
Ifi202b	*interferon activated gene 202B*
Ins	Insulin
ITT	Insulin tolerance test
KASP	Kompetitive Allele Specific PCR
kcal	Kilo calories
Kcnk6	*Potassium inwardly-rectifying channel, subfamily K, member 6*
Klk1	*Kallikrein 1*
Klk1b22	*Kallikrein 1-related peptidase b22*
Klk1b4	*Kallikrein 1-related pepidase b4*
Klk1b5	*Kallikrein 1-related peptidase b5*
KRH	Krebs-Ringer-HEPES
LOD	Logarithm of the odds
max.	Maximal
Mb	Mega base pairs
Min	Minute
MIN6	Mouse insulinoma cell line
MODY	Maturity-onset diabetes of the young
mRNA	Messenger RNA
n	Number
N2	Backcross
Nir15-dis	NZO insulin resistance on distal chromosome 15

Nir15-prox	NZO insulin resistance on proximal chromosome 15
Nir4	NZO insulin resistance on distal chromosome 4
NMR	Nuclear magnetic resonance
Nob4	*NZO obesity on chromosome 4*
ns	Not significant
Nudt19	*Nudix (nucleoside diphosphate linked moiety X)-type motif 19*
NZB	New Zealand black
NZO	New Zealand obese
OGTT	Oral glucose tolerance test
Pop4	*Processing of precursor 4*
Pos	Position
qPCR	Quantitative polymerase chain reaction
QTL	Quantitative trait locus
Quadr.	Quadriceps
r^2	Coefficient of determination
rcf	Relative centrifugal force
RCS	Recombinant congenic strain
Rev	Reverse
Rhpn2	*Rhophilin, Rho GTPase binding protein 2*
RNA	Ribonucleic acid
RT	Room temperature
SAT	Subcutanous adipose tissue
sec	Seconds
SEM	Standard error of the mean
siRNA	Small interfering RNA
SNP	single nucleotide polymorphism
Spint2	*Serine protease inhibitor, Kunitz type 2*
Suppl.	Supplementary
T1DM	Type 1 diabetes mellitus
T2DM	Type 2 diabetes mellitus
TA	Tibialis anterior
Tab.	Table
Tbc1d1	*TBC1 domain family, member 1*
Tbp	*TATA box binding protein*
TCA	Tricarboxylic acid cycle
TG	Triglycerides
Tmem147	*Transmembrane protein 147*
tRNA	Transfer RNA
Tyrobp	*TYRO protein tyrosine kinase binding protein*
Vs.	Versus
WHO	World health organization
wk	Week
Zfp30	*Zinc finger protein 30*
Zfp420	*Zinc finger protein 420*
Zfp69	*Zinc finger protein 69*
Zfp715	*Zinc finger protein 715*
Zfp940	*Zinc finger protein 940*

Acknowledgements

First of all, I would like to express my gratitude to my supervisor Prof. Dr. Hadi Al-Hasani for giving me the opportunity to work on this exciting topic in an excellently equipped lab. Also thank you Hadi for your great supervision and that you always took your time to discuss with me the project. Your support and enthusiasm for this project motivated me a lot, many thanks!

Also I would like to kindly thank Prof. Dr. Michael Feldbrügge for taking over the co-supervising for this work.

Furthermore, I would like to thank Dr. Alexandra Chadt for constructive suggestions and continuous support throughout the years. Thank you Alex for always being available and all your help!

My special thanks further go to all (former) members of the "QTL-crew". In particular I would like to thank Sandra Lebek, for excellently introducing me into the methodology of the mouse work and to the theoretical background. Thank you Sandra for giving me such a comfortable start and for the great four years together. I also would like to offer my special thanks to Delsi Altenhofen for the great teamwork, I am very happy that you joined our group. Thank you Delsi for helping with the experiments, and also for the nice time outside the lab! Moreover, I would like to kindly thank all students that greatly contributed to the progress of this work: Miriam Weyers, Mareike Damen, Yvonne Schulte, Janek Masuch, Angela Pelligra, Che Yang and Sarah Görigk. It was a pleasure to supervise you in the lab, many thanks for your support! Also thank you Sarah, for proofreading this thesis! Angela and Janek, I further would like to thank you for assisting us after your theses with the everlasting genotyping of the mice. I further want to acknowledge Anja Wagner, Alona Weker and Jan Henning for assisting in this project. You all did a great job!

I would like to express my very great appreciation to Angelika Horrighs and Anette Kurowski for the great technical support, in particular in the animal facility. I want to thank Annette Schober for introducing me into the cell culture and for permanent support in the lab, I really felt sad when you were leaving us. I am very thankful to Lothar Bohne for executing the cell size measurements. I also would like to thank the other technical assistants Antonia Osmers, Ilka Römer, Heidrum Podini, Dagmar Grittner, Birgit Knobloch, Andrea Cramer, and our apprentice Carina Heitmann for always being accessible and for helping in all kinds of organizational or experimental issues. Also, I wish to acknowledge the great work of the animal care taker team, in particular Peter Herdt, for perfectly organizing the animal breeding and the great collaboration. I am further grateful to Nicole Krause for helping with all kinds of administrative issues throughout the years.

Also I want to express my gratitude to Dr. Birgit Knebel for conducting the microarray analysis and to Axel Rasche from the Max Planck Institute for Molecular Genetics in Berlin for the statistical assessment of the data.

I further wish to acknowledge Dr. Jürgen Weiß, Kay Jeruschke and Carmen Weidlich for their support in the histology unit.

I am also very grateful to my other colleagues Dr. Sameneh Mafakheri, Dr. Dhiraj Kabra, Dr. Oleksiy Klymenko, Dr. Torben Stermann, Christian Binsch, Tim Benninghoff, Christian de Wendt, Christian Springer, and Matthias Dille, for their huge helpfulness and for many amusing conservations throughout the years. Also thank you Torben for helping with the islet- and the pancreas preparations. And thank you Tim, for showing me the FAO assay. I also would like to thank all other members from the working group “Pathobiochemistry” for the comfortable atmosphere and overall helpfulness!

Furthermore, I want to thank our cooperation group “Department of Experimental Diabetology” from Annette Schürmann in Potsdam. Special thanks go to Markus Jähnert for teaching the QTL-analysis and to Anne Kamitz and Nicole Hallahan for the good cooperation.

I also want to express my appreciation to Prof. Dr. Ralph Burkhardt and Prof. Dr. Uta Ceglarek from the University Hospital Leipzig for analyzing the metabolites.

Finally, I want to express my very profound gratitude to my family and my friends for continuous moral support throughout my thesis. My special thanks goes to my partner Sebastian, for his endless support and understanding. This gave me a lot of strength, thank you so much!

Eidesstattliche Erklärung

Ich versichere an Eides Statt, dass die Dissertation von mir selbständig und ohne unzulässige fremde Hilfe unter Beachtung der „Grundsätze zur Sicherung guter wissenschaftlicher Praxis an der Heinrich-Heine-Universität Düsseldorf“ erstellt worden ist.

Ferner versichere ich, dass ich bisher noch keinen Promotionsversuch unternommen habe. Die Arbeit wurde bisher an keiner anderen Hochschule eingereicht.

Düsseldorf, den _____ _____

(Tanja Schallschmidt)